Behaviour of Infilled Rehabilitation System with Composites for Steel Pipe

By

Md Shamsuddoha

A dissertation submitted for the award of

DOCTOR OF PHILOSOPHY

Supervisory Team

Dr Mainul Islam
Prof. Thiru Aravinthan
Dr Allan Manalo
Prof. Alan Kin-tak Lau

Faculty of Health, Engineering & Sciences
UNIVERSITY OF SOUTHERN QUEENSLAND

2014

Abstract

Fibre-reinforced polymer-based composites are found effective and suitable for steel pipe repairs because of their unique advantages such as high strength, lightweight, non-corrosive, and fast and easy to handle. In this study, the behaviour of a new type of composite repair system for steel pipelines underwater, which is the grouted composite sleeve, was investigated. This type of repair system relies on the effective transfer of stresses from the steel pipe to the encircling composite sleeve through the grout infill. Research was therefore necessary in optimising the material and geometric properties of each component of this system in order to have a better understanding on its overall behaviour and its effectiveness in repairing steel pipelines.

An experimental study on the mechanical, thermal and shrinkage properties of five epoxy-based grouts commonly used for structural repair was conducted. Three grouts have compressive strength of more than 80 MPa and total shrinkages of only 2.77%, which were deemed applicable for structural repair of steel pipelines. Moreover, the glass transition temperature of these grouts ranges from 50 to 90^{o}C. The inclusion of coarse filler significantly increased the modulus and compressive strength, and reduced the shrinkage, but also reduced the tensile strength. There was considerable reduction in mechanical properties due to hot-wet conditioning at 70^{o}C. This is because of the plasticisation and weakening of the aggregate matrix debonding at a temperature close to the glass transition temperature.

The glass fibre – vinyl ester composites considered in this study have strength and modulus suitable for sleeve in the grouted sleeve repair system. The tensile strength, modulus and interlaminar shear strength of this composite was 427 MPa, 25 GPa and 30 MPa, respectively and its glass transition temperature was 110^{o}C. It absorbed only 0.22% of moisture after hot-wet conditioning of 3000 hours. More importantly, there was almost no change in the modulus and it retained sufficient tensile and interlaminar shear strength needed for a composite sleeve repair system even after exposure to moisture and elevated temperature of 80°C. The glass transition temperature decreased to 97°C after conditioning and reached saturation indicating that, the composite was suitable for pipeline repair in continuous service at higher temperature.

A finite element analysis using a simplified 2D model was conducted to determine the effect of critical parameters on the behaviour of a grouted composite sleeve repair system. Grout modulus and thickness, and sleeve thickness were considered for the analysis. The results of the analyses indicated that the thinner and higher modulus grouts are more effective to transfer load from the steel to the sleeve than the thicker and lower modulus grouts. Similarly, a thicker sleeve reduced the level of stresses and strains in all the components of the repair. Based on the results of the analysis, it was recommended that a grout thickness of 20 mm with a modulus of at least 5 GPa was appropriate for an effective grouted repair system and for practical application.

A full-scale 3D analysis was carried out to determine the effectiveness of the repair system for steel pipelines with a range of localised metal loss. The results of the analyses indicated that the modulus of the infill grout governs the load transfer

between the steel and the sleeve, but the tensile strength governs the functionality of the system. The cracking of the grout resulted in a significant increase in the stress level in the steel pipeline and composite sleeve. The repair system using grout with a higher tensile strength provided a higher pipe capacity by utilising the plasticity of the steel, while the grout with a lower tensile strength cracks even before yielding of the yielding at a low applied internal pressure. Moreover, a thicker sleeve provided higher capacity in the repaired pipe, and both the carbon and glass fibre composites were found effective for composite sleeve repair system. Most importantly, it was determined that the considered grouted composite sleeve repair system can effectively reinstate the capacity of the pipelines with a localised defect of up to 70% metal loss.

An improved understanding on the behaviour of the grouted composite sleeve repair system for pipeline with metal loss was achieved in this study, providing a base knowledge from which further research could continue. The results obtained provided important information on the optimal material properties of the infill grout and the composite sleeve for an effective repair system and the effect of different operating conditions on the overall behaviour of the repaired steel pipelines. These results are very valuable and will help researchers, engineers and stakeholders to consider the actual application and implementation of this new composite system in repairing steel pipelines.

Certification of dissertation

I certify that the ideas, experimental work, results, analysis and conclusions reported in this dissertation are entirely my own effort, except where otherwise acknowledged. I also certify that the work is original and has not been previously submitted for any award, except where otherwise acknowledged.

---------- / /

Md Shamsuddoha

Endorsement by Supervisors:

---------- / /

---------- / /

---------- / /

Publications arising from the research

During the research process, a number of papers have been published, based on the work presented in this thesis. They are listed here for reference.

Publication in the Referred Journals:

1. **Shamsuddoha M**, Islam MM, Aravinthan T, Manalo A, Lau KT. Effectiveness of using fibre-reinforced polymer composites for underwater steel pipeline repairs. Composite Structures. 2013;100:40-54. http://dx.doi.org/10.1016/j.compstruct.2012.12.019
2. **Shamsuddoha M**, Islam MM, Aravinthan T, Manalo A, Lau KT. Characterisation of mechanical and thermal properties of epoxy grouts for composite repair of steel pipelines. Materials & Design. 2013;52:315-327. http://dx.doi.org/10.1016/j.matdes.2013.05.068
3. **Shamsuddoha M**, Manalo A, Islam MM, Aravinthan T, Lau KT. Effect of grout properties on infilled fibre-reinforced composite repairs for steel pipelines. International Journal of Pressure Vessels and Piping. (Under review)
4. **Shamsuddoha M**, Islam MM, Aravinthan T, Manalo A, Djukic LP. Effect of hot-wet conditioning on the mechanical and thermal properties of epoxy grouts for steel pipeline repair. Journal of Materials in Civil Engineering. (Under Review)

Publication at International Conferences:

1. **Shamsuddoha M**, Islam MM, Aravinthan T, Manalo A, Lau K-t. Fibre Composites for High Pressure Pipeline Repairs, in-air and subsea - An Overview. In: *The Third Asia-Pacific Conference on FRP Structures (APFIS 2012)*, Hokkaido University, Japan, 2-4 February 2012.
2. **Shamsuddoha M**, Islam MM, Aravinthan T, Manalo AC, Lau K-t. Mechanical properties of epoxy grouts for structural repair. In: *22nd Australasian Conference on the Mechanics of Structures and Materials (ACMSM22)*, Sydney, 11-14 December 2012.
3. **Shamsuddoha M**, Islam MM, Aravinthan T, Manalo A, Lau KT. Cure shrinkage in epoxy grouts for grouted repairs. In: *Fourth International Conference on Smart Materials and Nanotechnology in Engineering*. Gold Coast, Australia: International Society for Optics and Photonics; 2013. p. 87931J-87931J-87937.

Acknowledgements

I wish to express my deepest gratitude and sincerest indebtedness from the core of my heart to my Principal Supervisor, Dr Mainul Islam, for giving me the opportunity to pursue a doctoral study at the University of Southern Queensland (USQ). I am greatly indebted for his constant guidance, generous support and continuous encouragement throughout the process of completing this dissertation. I am also greatly indebted to my Associate Supervisor, Prof. Thiru Aravinthan, for the continuous enthusiastic technical guidance generating from his in-depth knowledge on the topic, which acted as a driving force to carry out the study. I also greatly appreciate the technical inputs of my Associate Supervisor, Dr Allan Manalo, through the training in both experimental and analytical reasoning of the findings, along the process of this study. I would like to acknowledge the contribution of my Associate Supervisor, Prof. Kin-tak Lau, for his technical suggestions that enhanced the content of the dissertation.

I appreciate the academic, financial and technical support of the Faculty of Health, Engineering and Sciences and the Centre of Excellence in Engineered Fibre Composites (CEEFC), which made this research possible.

This study was undertaken as part of P1.3 Deepwater Composites within the Cooperative Research Centre for Advanced Composite Structures (CRC-ACS) research program, established and supported under the Australian Government's Cooperative Research Centres Program. I acknowledge the continuous support from the CRC-ACS, Australia by providing me with the materials and preparing the specimens for this study. The funding for the experimental investigations is also recognised. The supports in material collection, supply and technical feedback from Mr David Elder, Dr Paul Falzon, and Dr Luke Djukic of CRC Australia, and Mr Bruce Cartwright of Pacific ESI are also highly acknowledged.

I am very thankful for the technical and administrative support from Mr. Wayne Crowell, Dr. Francisco Cardona and Mr. Martin Geach of CEEFC. I also appreciate the support and friendship from all the staffs and postgraduate students.

Finally, all praise goes to the Almighty for giving me the ability to complete the work. My earnest appreciation goes to my wife, Sadia, who had always been an encouragement along our time together in well and woe, and let me accomplish many of my desires by sacrificing some of her own. Sadia, along with our son Sadad, inspire me that I can be. I am also indebted to my parents who had always been supportive when I needed it the most. I also appreciate the friendly and supportive Bangladeshi Community in Toowoomba that made our stay enjoyable.

I also acknowledge the supports along this effort from those whom I failed to mention but been a great support when they occurred.

Table of contents

List of figures

List of tables

Notations

D	External diameter of the pipe
d	Depth of the defect
E	Modulus of steel
E_c	Modulus of composite sleeve
E_g	Modulus of grout
E_s	Modulus of steel
t	Thickness of the pipe
t_g	Thickness of the grout
t_c	Thickness of the composite sleeve
w	Minimum width of the defect
L	Length of the pipe
L_{repair}	Length of the repair
l	Axial extent of the defect
l_1	Half of the axial extent of the defect with minimum remaining thickness
l_2	Half of the axial extent of the defect along the transition of the defect
ε_u	Ultimate strain of steel
ε_y	Yield strain of steel
σ_u	Ultimate strength of steel
σ_y	Yield strength of steel
θ	Radial extent of the defect
θ_1	Half of the radial extent of the defect with minimum remaining thickness
θ_2	Half of the radial extent of the defect along the transition of the defect
ϑ	Poisson's ratio
G	Shear modulus

Chapter 1

Introduction

1.1 General

The deterioration of metal pipelines in adverse in-air and underwater conditions results in the development of repair systems that maintain the utility of pipelines. Fibre composite alternatives for pipeline repair have the potential to compete successfully with available conventional metal options. Infilled composite repair is one of the potential solutions for pipelines with metal loss. Infill provides a smooth surface for the encircling reinforcement and transfer loads from the pipeline to the reinforcement. The mechanical and thermal properties of the components of the repair are significant to describe their performance during application. Detailed study of an infilled repair system is also necessary to evaluate the contribution of the repair components and performance under service conditions. This study presents an improved understanding of the behaviour of infilled fibre-reinforced composite repair of steel pipe with metal loss.

1.2 Background

Natural resources like oil and gas constitute the major share of global fossil fuel, which is the dominant source of energy of the world (Fridleifsson 2003). The advancement of human civilization and scarcity of natural resources like oil, natural gases and minerals lead to exploration deeper into the earth's crust and to expand the venture in remote locations; eventually increasing underground, high pressure ashore and subsea drilling activities. Metal pipelines are the most efficient and the safest ways to transport these natural resources over long distances. At present, most of the pipeline systems are predominantly consist of steel pipes, which have high strength, relative simplicity of joints and low cost (Kennedy 1993). However, steel pipes that are laid underwater and underground can go through adverse deterioration in the form of corrosion, crack, dents, wearing, buckling, gouging, spalling, leaks and rupture. The most vulnerable weaknesses of steel pipe are corrosion and metal loss (Francis 1994; Frankel 1998). Steel pipes carrying fluid, oil and gas are considerably susceptible to failure initiated by corrosion and high operating pressure under adverse atmospheric conditions. The severity is high when salt water and sulphur ingress media are present. A general mechanism and initiation of corrosion in a pipe surface in the presence of salt water is shown in Figure 1.1, where hydroxide and chloride ions are contributing to the accelerated corrosion in submerged and sea water conditions (Kopeliovich 2009). Figure 1.2 shows degradation of the protective coating and formation of hydroxide of iron as a result of the corrosion (Green Cleaning Ideas 2011).

A number of studies were carried out to study the corrosion of steel in saltwater and sulphur conditions and its subsequent performance degradations. Cracking resulting from high pH environment and near-neutral pH as in groundwater were also found responsible for stress corrosion (Niu & Cheng 2007). The presence of CO_2 in temperature (40 – 60°C) resulted in considerable corrosion of steel pipe and strong adsorption of sulphide anions blocking the development of a protective oxide film (Pfennig & Kranzmann 2009; Pfennig et al. 2011). Hence, corrosion and

metal loss cause failures in pipelines and their rehabilitation is one of the prime interests of the researchers all over the world.

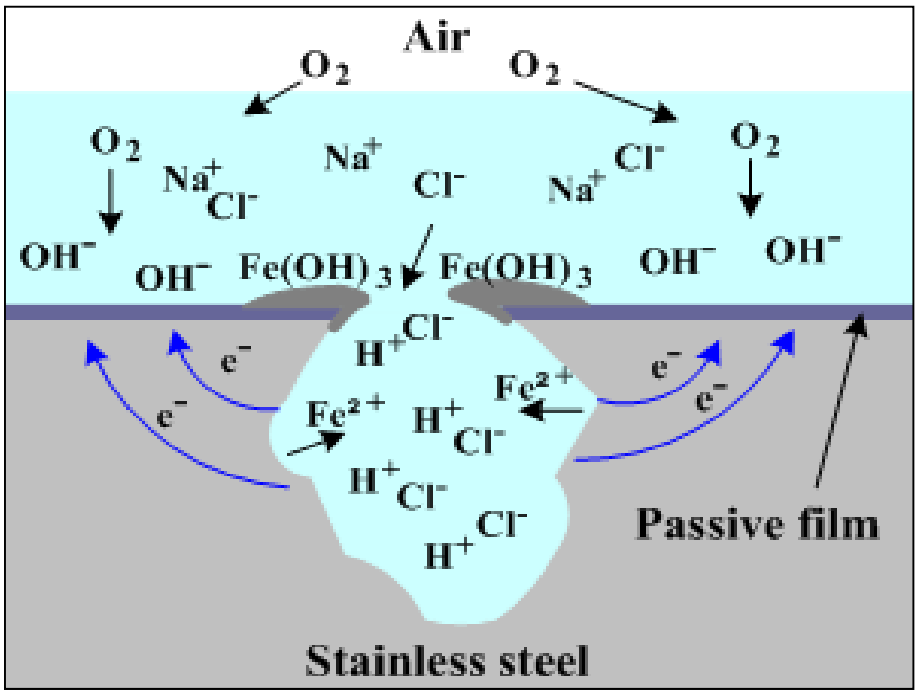

Figure 1.1 **Mechanism of steel corrosion in saline environment (Kopeliovich 2009)**

Figure 1.2 **Corrosion on steel surface in saline environment (Green Cleaning Ideas 2011)**

Traditionally, the most reliable solution for a damaged pipe is to remove the entire pipe or just a localised damaged section and replace it. One can also cover the damage part with a welded steel patch. Welding or clamping of pipelines itself is a cumbersome process, especially in underwater and underground conditions. Conventional repair techniques incorporate external steel clamps that are either

welded or bolted to the outside surface of the pipes. Figure 1.3 shows typical conventional welded steel sleeve repairs (T. D. Williamson Inc 2007).

Unlike onshore pipelines, underwater and buried pipelines are typically designed for self-weight, operating pressure, external pressure and installation effects. Service and safety concerns are dominantly more critical for cases where installation, inspection and maintenance are bulky, costly and time consuming (Kou & Yang 2011). A high pressure metal split sleeve repair is shown in Figure 1.4, where the sleeve is joined by mechanical fastening (PLIDCO Split+Sleeve 2012). Moreover, the cost and technical challenges of rehabilitation and maintenance strategies increase significantly with operating pressure and location of pipe repair. Thus, researchers searched for alternative materials that are relatively lightweight, easily applicable and can be an effective repair solution. Polymers and composites provide a wide range of performances, including rehabilitation of pipelines in the engineering world.

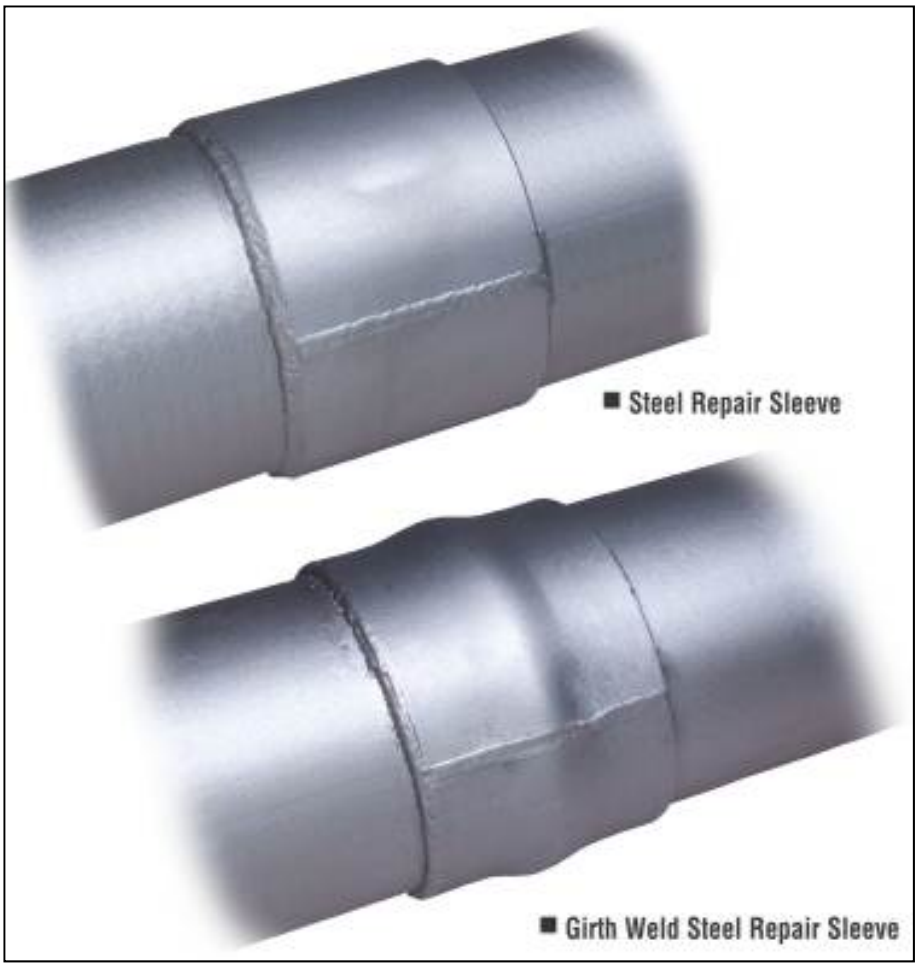

Figure 1.3 **Conventional welded steel repair sleeves (T. D. Williamson Inc 2007)**

Figure 1.4 **PLIDCO Split+Sleeve repair clamp (PLIDCO Split+Sleeve 2012)**

1.3 Composites in pipeline rehabilitation

Fibre composite materials provide excellent advantages over conventional metals in engineering practices for many decades. Fibre-reinforced polymer (FRP) composite is usually made up of polymer/plastic matrix reinforced with fibres (Bakis et al. 2002). The use of fibre-reinforced composites has already been proven effective for the construction and retrofit of filled and hollow in-air, marine and underground cylindrical elements (Cercone & Lockwood 2005; Geraghty et al. 2011; Gibson 2003; Kin-tak & Li-min 2001; Patrick 2004; Sen & Mullins 2007). Fibre-reinforced composites have a high potential for repairing metallic components and tubular pipes. A number of investigations have been carried out in search for strong, durable and cost effective materials for rehabilitating metal pipes laid on underwater and underground. A broad domain of literature is dedicated for identification of defects, monitoring and rehabilitation of steel pipes.

Numerous developments, practices and products are available in this domain, for example: commercially used Clock Spring® (The Clock Spring Company 2011). In addition, the successful application of fibre-reinforced composite materials has been illustrated in the rehabilitation of corroded pipes using hybrid repair (Alexander 2007); rehabilitation of steel tubular structures with CFRP to assess the possibility of rehabilitating tubular steel flexural members with emphasis on underwater applications (Seica & Packer 2007); large scale reinforced plastic pipe production and installation (Gibson et al. 2011; Hille & Romer 2004; Newberry et al. 2008); high performance thermoplastic composite tubes for water depth up to 3000 m (Picard et al. 2007); infilled repair of wooden piles (Lopez-Anido et al. 2005); and feasibility of infilled sleeved repair of pipeline (Palmer-Jones & Paisley 2000). Hence, fibre-reinforced composite and infill materials can be used for repair and rehabilitation. Another recent application of fibre-reinforced composite materials for reinforcing damaged pipelines was reported by Lukács et al. (2010). Based on the experimental and numerical investigations, Lukács et al. suggested that fibre-

reinforced composite materials and the external reinforcing technology can be used for a wide variety of pipe diameters and lengths for both quasi-static and cyclically loaded pipeline sections or pipelines. However, research, development and application of composite in pipelines possess considerable challenge all over the world.

1.4 Challenges of using composites in pipeline repair

The available literature on steel pipe repair has shown that the fibre-reinforced composites can be used effectively for pipe repair. However, the currently used composite repair systems require complex preparation. The application and curing of resin are also difficult to install in limited space or underwater scenario. While half-shell metal repair sleeves have been successfully used in many repair projects, the heavy-weight installation is a major drawback of this system. The combined system of wet lay-up and pre-cured half shell using composites is anticipated to provide a much simpler installation and suitable for axisymmetric repair (Alexander 2007). This system has also the benefit of a wet lay-up in terms of strength potential and improved quality control for the carbon half-shells, as compared to existing layered composite systems. However, effective application of this system can be difficult in case of in-site wet lay-up application in underwater cases. Thus, precured composite without wet lay-up is expected to provide easy installation in field conditions provided, that issues like sleeve joint and load transfer mechanism are addressed.

Considerable research by other researchers has been carried out on the repair of corroded and gouged pipes incorporating fibres and infill. Load transfer mechanism was intensively studied by Duell et al. (2008) and Freire et al. (2007). Both of the studies considered flexible wet lay-up method to regain burst pressure above or near original pipe. Yet, the load transfer mechanism and burst failure patterns were different due to the geometries of corrosion and layer thicknesses adopted. The remaining strength of corroded section depends not only on material but also on flaw geometry (Cunha & Netto 2012). Therefore, the effect of defect geometry on the load transfer mechanism needs to be identified to understand the system behaviour. Perfect axisymmetric defect is certainly rare in field conditions. Localised corrosion can be proven critical in the steel when significant bending occurs in the defect transitions zone under internal pressure. Long axisymmetric type of defect geometry can also be critical for an infilled system where flexural deformation of the steel surface needs to be supported over a longer span than localised corrosion. Oil and gas pipelines are more susceptible to localised corrosions and often need to be analysed based on the orientation and severity for case to case basis.

On the other hand, the contribution of steel is dominant in the elastic zone, where an appropriate factor of safety on yield strength or ultimate tensile strength is often sufficient. However, while repairing pipe with one or more composite layers, the elastic approach may be conservative in determining repair thickness and operating pressure because of the limited understanding on composite repair system behaviour. Previous studies by Duell et al. (2008) and Freire et al. (2007) considered burst pressure as a margin for repair efficiency. Alexander (2007) used pre-cured layered system on axisymmetric metal loss integrating plasticity of the repair components. It is important to investigate the performance of a pre-cured composite repair system along with the contribution of the each component in order to identify

repair efficiency and increase the confidence in using this system to repair steel pipes.

The prospect of infilled fibre-reinforced sleeve is still to be studied for high pressure oil and gas pipelines. A stand-off type of composite repair sleeve was developed in the Centre of Excellence in Engineered Fibre Composites (CEEFC) at the University of Southern Queensland, Toowoomba, Australia (University of Southern Queensland). This repair was successfully used for underwater rehabilitation of piles at the Missingham Bridge in Northern NSW, Australia in 2005 (Heldt et al. 2005). This success presents an ideal opportunity to explore fibre-reinforced composite sleeve in pipeline repair. A proposed schematic illustration of an infilled fibre reinforced sleeve repair is shown in Figure 1.5. Performance requirements of in-fill material for stand-off system are some of the challenges that need to be overcome to make suitable repair for high pressure pipelines.

Heat and moisture is found to affect the potential composite materials for pipeline repair (Carbas et al. 2013; Jiang et al. 2013; Ray 2006). The moisture absorption potentially damage composites resulting in matrix cracks and debonding at the fibre-matrix interface through the diffusion of hydrogen molecules of water to the polymer matrix (Chin et al. 1999; Ellyin & Maser 2004). Hence, the performance of repaired pipelines also depends on the long-term properties of the fibre-reinforced composites and this demands a detailed investigation.

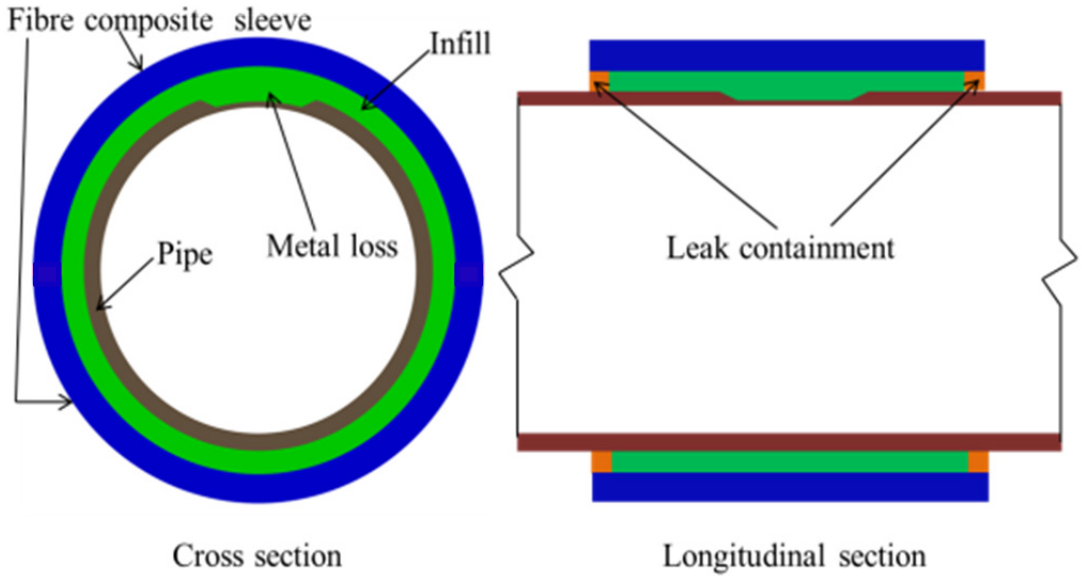

Figure 1.5 Infilled fibre composite split sleeve repair

1.5 Problem statement

Based on the literature review and challenges in the rehabilitation system using composites, the following problems are identified as potential components of investigation for better understanding of the infilled system:

- Infill determines critical performance of the rehabilitation system. Appropriate infills need to be selected, explored and examined for their properties, and determine suitability as a component in the infilled rehabilitation system.

- Potential fibre-composite sleeves need to be selected and properties should to be investigated as reinforcement in the rehabilitation system.
- Thermal and moisture ingress possesses considerable threat for the composite rehabilitation system. Effect of elevated temperature and humid conditions on the components need to be assed for appropriate qualification of the system.
- There is lack of literature on the effect of components properties and repair geometries on the performance of the rehabilitation system. For that reason, a detailed study on the repair effectiveness needs to be carried out for optimum performance.

1.6 Objectives

The aim of this study is to investigate the behaviour of infilled fibre-reinforced composite repair system. Particularly, the objectives of the study can be pointed as follows:

- To characterise the mechanical and thermal properties of infill grout and glass fibre-reinforced composite and to investigate the effect of curing duration on compressive properties as an indication of strength gain.
- To investigate the effect of hot-wet conditioning on mechanical and thermal properties of infill and fibre-reinforced composite of the repair.
- To investigate the behaviour of infilled composite repair system on a pipe with metal loss considering a range of material properties and geometry.
- To simulate the behaviour of a full scale repair and propose a design guideline under internal pressure.

1.7 Scope of the thesis

This study focuses on understanding the behaviour of grouted fibre-reinforced composite repair. No significant material development is conducted and only existing grouts and composite laminate are used for the structural strengthening. Due to intellectual confidentiality, any information related to the chemical composition and microstructure of the grout and composite laminate systems used to develop the composite repair system is not disclosed. However, details of the grouts and composites are provided, where necessary. The attention of the study is focused on the following domains:

- Review of the existing literature on research and developments of composite repair of pipelines.
- Characterisation of the mechanical and thermal properties of epoxy grouts as infill.
- Investigation of the compressive properties of selected epoxy grouts over time to actualise the in situ application of the repair.
- Evaluation of the effect of long-term hot-wet conditioning mechanical and thermal properties of the grouts and glass fibre-reinforced composite as sleeve.
- Parametric finite element (FE) study of the behaviour of a repaired long-flawed steel pipe with 80% wall thinning that is repaired with a range of infill

properties, thickness and sleeve thickness. This determines a suitable range of material properties and geometry.

- Finite element analysis of a full scale repaired steel pipe with different localised metal loss considering suitable infill properties, and using carbon and glass fibre-reinforced composite sleeve properties under internal pressure.
- Investigate the behaviour of the repaired system within the scope of material parameters and identify the governing factors for effective performance of the repair.

A broader investigation approach was undertaken to determine the feasibility of the grouted repair system and to provide a base knowledge on the understanding from which further research could be carried out. However, the following outlines are beyond the scope of this study and considered potential areas of research in the near future.

- Characterisation of carbon fibre-reinforced composite and effect of conditioning on the mechanical and thermal properties.
- Further investigation on the long-term behaviour of the grout systems.
- Evaluation of the behaviour of repaired pipe performance under flexural and axial loading.

1.8 Organization of the thesis

This dissertation represents the investigation of the behaviour of grouted fibre-reinforced composite repair of flawed steel pipe with metal loss. The effects of infill material and fibre-reinforced composite properties along with level of metal loss on the components of infilled repair were investigated. The mechanical and thermal properties of five epoxy grouts as infill, and fibre-reinforced composite as outer sleeve of the repair were characterised. An extensive investigation on the mechanical and thermal properties of the components of the repair under long-term hot-wet conditioning was also carried out to observe the degradation of physical properties. These ranges of properties were used in investigating the behaviour of simplified grouted repair with long flaw pipe using finite element (FE) analysis to optimise the properties of components of the repair. A parametric study on the simulated grouted repair with obtained experimental results on steel pipe with localised defect was carried out to observe the effects of design parameters on the effectiveness of the repair system.

The above mentioned investigation is presented in the several chapters of this thesis. A diminutive description of each chapter is as follows:

- Chapter 1 gives an introduction and objectives of the study. This chapter also highlights the necessity of this study on the grouted sleeve repair of steel pipe. The scope of the study and structure of the thesis are also presented in this chapter.
- Chapter 2 provides a review on the literatures about repair systems using fibre-reinforcement for pipelines. An overview of the properties and potential of possible components of the repair are presented. The researches and developments worldwide on the behaviour of pipeline repair are highlighted.

- Chapter 3 presents the characterisation of the mechanical and thermal properties of epoxy grouts used in this study. The effect of curing duration on the compressive properties of the selected grouts is also presented.
- Chapter 4 illustrates the moisture absorption properties of three best grouts selected from Chapter 3 at elevated temperature. This chapter also describes the effect of hot-wet conditioning on the mechanical and thermal properties of the epoxy grouts.
- Chapter 5 provides effect of hot-wet conditioning on the glass fibre-reinforced composite as potential sleeve of pipeline repair. The effect of elevated temperature on the absorption, mechanical and thermal properties is also investigated.
- Chapter 6 illustrates simplified parametric FE study of a flawed pipe repaired with a combination of infill and sleeve properties. A total of 120 repair combinations of infilled sleeve repair of steel pipe were analysed to investigate the effect of grout thicknesses and sleeve thicknesses and grout modulus on the effectiveness of an infilled repair.
- Chapter 7 presents a 3D simulation of the behaviour of a simulated flawed pipe with localised defect. The effect of level of metal loss, grout properties and sleeve thicknesses on the effectiveness of the repaired pipe is also investigated. Design considerations are also discussed for developing this repair system based on the results.
- Chapter 8 concludes the outcomes of this thesis and recommendations for future works.

1.9 Summary

The growing demand of the steel pipes and associated repairs on metal loss are inevitable over time. In the research and development of repair systems of steel pipes, the use of potential combinations of composites and corrosion geometry demands further attention and detailed study. To better understand the potential of composite, the performance of repair components under internal pressure loading should be studied. Identification of properties of individual components of the repair is necessary to enhance efficiency and reliability of the repair system.

As this work emphasises on the composite repair, recent research, development and practices of composite repair on pipelines are presented in Chapter 2.

Chapter 2

Review of composite repair for steel pipelines

2.1 Introduction

Chapter 1 demonstrated the need to investigate current developments in composite repair, and to identify the challenges and overcome the compatibility issues by optimization of the properties. Adverse environments and mechanical damages in pipes have led to the exploration of different repair options to keep pipes functional. Traditional steel repairs are heavyweight, time consuming and incorporate tedious welding works which restrain their use in pipelines located underground and underwater. As an alternative, fibre-reinforced composite has proven to be an effective repair solution for corroded steel pipelines. The advancement in this new material opens up great opportunities to expand the options for the pipeline industry to rehabilitate and reinstate their pipeline systems using a lightweight, high-strength, fast and easy to handle, and cost effective material system. A substantial body of work has been conducted to assess the use of composite materials for pipeline repair. Most of this work has been focused on assessing the performance of composite and composite-reinforced repair systems without infill. Research and applications publications also exist for the evaluation of infilled fibre-composite repair.

This chapter provides information on the current practices and applications of fibre-reinforced composite materials for the external repair of steel pipelines. It also provides an overview of on-going world-wide advancements in the field of pipeline rehabilitation using fibre-reinforced composites. Furthermore, recent research and developments directed towards making fibre-reinforced composites as an effective alternative material to traditional repair for steel pipes are also presented.

2.2 Repair systems using fibre-reinforced composites

Fibre-reinforced composites have provided the ideal material choice for the rehabilitation of tubular structures because of their lightweight, high strength and stiffness, good corrosion resistance and excellent fatigue properties. Worldwide research and practices show the pursuit to understand the effectiveness and in-depth behaviour of composite repairs. These are summarised in Table 2.1. The literatures and commercial products provide a glimpse of the materials used and the diverse nature of external and internal metal loss scenarios for pipelines or cylindrical structures.

Generally speaking, there are two types of repair systems, Flexible ‘wet lay-up system’ and Pre-cured ‘layered system’, are applied in the repair of defective pipelines (Alexander & Francini 2006). Both repair methods encircle the pipe with a sleeve either flexibly or through stiffer bonded connections. Pipeline repair/rehabilitation systems can be considered under four broad categories : (i) systems that prevent the future progression of corrosion, (ii) repairs that are intended to reinstate the strength of the pipe containing a part wall defect like gouging, (iii) repairs that are designed to enclose the fluid in case of the failure, and (iv) repairs that will restore the strength of the pipe and contain the transported fluid in case of any failure incidence (Palmer-Jones & Paisley 2000). These requirements for

pipeline repair need to be considered in the selection of an appropriate composite repair system.

2.2.1 Flexible wet lay-up system

The flexible overwrap repair system is utilised intensively by the pipe repair industry for onshore repair in the form of overwrapping the steel pipes at even angles or bends for a wide range of pressure applications. This application utilises a resin matrix that is usually uncured during the application and creates a stiff shell after curing. Ehsani (2010) developed and applied a number of repair options utilising both flexible fabric and pre-cured shells. Worth (2005) of Air Logistics published a report that presented a research outcome to validate the Aquawrap® repair system. This report also included the long-term performance data of the repair system with a number of strength and serviceability issues.

Another technology for the flexible wet lay-up system is the Armor Plate® system of Armor Plate Inc. (Alexander & Wilson 2000). This repair system employs an E-glass/epoxy material that is impregnated with different resin systems to address specific environmental conditions such as underwater applications, high temperatures and cold weather. The StrongBack (Integ Pipeline Services 2011) repair system is a water-activated epoxy based and glass fibre-reinforced repair that is claimed to displace water from wet surfaces to create a permanent bond. RES-Q Composite Wrap (T. D. Williamson Inc. 2008) is also an epoxy based carbon fibre-reinforced rehabilitation system for pipe diameter up to 1500 mm. Epoxy cured fibre glass-reinforced PIPEASSURE™ (PETRONAS-CSIRO) system marketed by PETRONAS (Petroliam Nasional Berhad) and Commonwealth Scientific and Industrial Research Organisation (CSIRO) is claimed to be flexible and lightweight, allowing for its application to structures of various shapes and sizes in both underground and underwater conditions. Flexible wrap is also used by Alexander (2007) where circumferentially oriented flexible carbon wrap was selected as the primary load-carrying material due to its relatively high elastic modulus and ability to provide greater reinforcement to the steel carrier pipe than the E-glass material for the same composite thickness. Separate shells were also used in this study to improve flexural and axial capacity. Figure 2.1 shows a typical overwrap repair application that is applied in underwater conditions and was reported by Green (2010).

A composite pipe repair using UV cured vinyl ester matrix for glass fibre wrapping was also studied (Peck et al. 2007; Peck et al. 2004). Results suggested that because of under-curing and non-uniform curing, the capacity for the adhesive to transfer load was reduced, thus compromising the overall strength of the joint and composite piping system. The application of underwater UV curing is a complicated process. Similar to standard heat curing onshore, resin curable in underwater condition is also available commercially. Curing of CFRP wrapped repair was simulated in saltwater conditions by Seica and Packer (2007). Figure 2.2 shows the curing of a fibre-composite repair when submerged in seawater conditions. The results recommended that CFRP-wrapped submerged specimens reached the plastic moment and also exhibited increased ductility and rotation capacity against flexural loading.

Table 2.1 Research, development and practices in fibre-reinforced composite repair of pipes

Year	Country	Reference	Description	Type of application	Level of development
2000	UK	(Mableson et al. 2000)	Glass fibre reinforced repair with vinylester resin on steel pipe	Through wall defect and repair mechanism	R&D
2004	USA	(Peck et al. 2004)	Glass fibre reinforced joint with vinylester resin on composite pipe under UV curing	Pipe joint and curing effects	R&D
2005	USA	(Worth 2005)	Water-activated glass and carbon wrap on metal pipe	External corrosion and mechanical gauge/dent	Applicattion R&D
2007	Brazil	(Freire et al. 2007)	Glass fibre reinforced precured and flexible repairs	External and internal repair with localised flaws with 70% wall thickness	R&D
2007	Canada	(Seica & Packer 2007)	Carbon fibre reinforced flexible system with epoxy resin on steel pipe	Improvement of flexural capacity	R&D
2007	USA	(Alexander 2007)	Glass and carbon fibre hybrid repair on steel pipe	External localised metal loss	R&D
2008	USA	(Duell et al. 2008)	Carbon fibre/epoxy composite wrap with epoxy putty on steel pipe	External axisymmetic and localised flaws with 50% wall thickness	R&D
2009	Brazil	(Mattos et al. 2009)	Glass reinforced flexible wrap with epoxy adhesive on steel pipe	Through-wall localised corrosion	R&D
2009	Libya	(Alshrif et al. 2009)	Glass fibre reinforced wrap and bolted steel clamp repair on steel pipe	Through-wall repair	R&D
2009, 2010	USA	(Ehsani 2009; Ehsani 2010)	Carbon and glass fibre wet layup and cured spiral sleeves on metal and concrete pipes	External and internal repair	Application
2010	Hungary	(Lukács et al. 2010)	Carbon fibre reinforced repair on metal loss and weld defects on steel pipes	External and internal repair	R&D
2011	Canada	(Shouman & Taheri 2011)	Glass epoxy composite repair wrap with epoxy putty on steel pipe	External localised flaws with 80% metal loss	R&D
2011	Malaysia	(Leong et al. 2011)	Glass fibre reinforced overwrap with epoxy resin on steel pipe	External flaws with 80% wall thinning	R&D
-	Malaysia	(PETRONAS-CSIRO)	Epoxy cured glass fabric, which is then cured to form a fibre reinforced composite	External repair of onshore and offshore steel pipe	Application
-	USA	(The Clock Spring Company 2011)	Fibreglass composite sleeve, an adhesive and a filler material on metal pipe	Corrosion or mechanical damage of low-pressure pipe	application
-	USA	(T. D. Williamson Inc. 2008)	Carbon fibre-reinforced flexible system with epoxy resin on metal pipe	Corrosion or mechanical damage	Application
-	USA	(WrapMaster)	Glass fibre reinforced precured spiral sleeve	External blunt and localised metal loss	Application

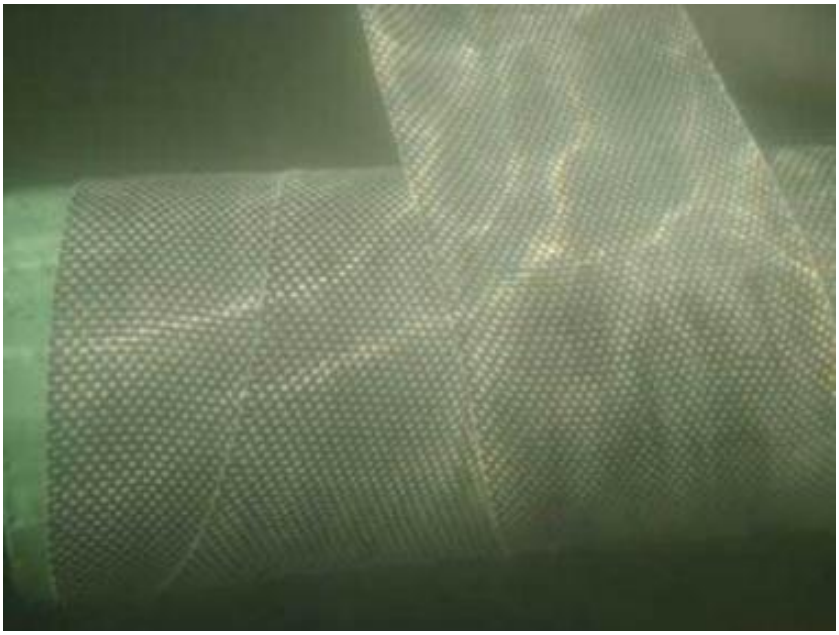

Figure 2.1 **Flexible composite wrapping for underwater repair (Green 2010)**

Figure 2.2 **Flexible CFRP-wrapped specimens being cured under saltwater conditions (Seica & Packer 2007)**

Combination of flexible glass fibre wrap and steel clamps was used by Alshrif et al. (2009) for the rehabilitation of steel pipes. Leong et al. (2011) reported the prospect of flexible wrap repair for offshore pipeline repair. A study by Sciolti et al. (2010) showed that the presence of water affected the thermal and mechanical properties of resins due to plasticization effects. It was evident from this study that there was reduction in glass transition temperatures and associated mechanical properties were also affected by the presence of water, with reductions in stiffness and strength. Thus, in situ curing and washout of resin make the wet-layup system difficult to install in underwater conditions.

The flexible wet lay-up system is suitable for both internal and external repairs. This repair is generally designed for future progression of corrosion and to reinstate the strength of the pipe containing a part wall defect. However, pressure containment is one of the shortcomings of the system. This system is also suited to underground conditions for relatively low to medium pressure applications. However, due to the complex preparation, application and curing of resin for the wet lay-up system, the use of pre-cured spiral sleeve is preferred. The application of the wrap system in a confined space is also very difficult. Thus, the necessity for a composite repair system that requires less complicated installation techniques such as rigid shell sleeve was much needed.

2.2.2 Pre-cured layered system

The pre-cured layered system involves the bonding of pre-cured fibre-reinforced composite materials that are held together with an adhesive applied in the field. Figure 2.3 shows the Clock Spring® repair system intensively used in the pipeline industry (The Clock Spring Company 2011). The WeldWrap™ system is another example of a commercially available layered system (WrapMaster). This type of repair system is a coil of high-strength composite material with a structure that allows it to wrap securely around pipes. The layers of wrap are sealed together with a strong bonding agent. The defect is filled with adhesive filler to assist with support and load transfer prior to their installation. This method of repair is ideal for blunt-type defects. Most medium duty repair technologies are based on this principle. This group of repairs support defects and prevent defect failure through load transfer and restraint (Palmer-Jones & Paisley 2000).

However, repair using these systems is generally limited to straight sections of pipe. A large amount of space is required to apply the layered system on the defected pipe. The underwater application of this system is challenging as it involves in-situ application of adhesive for the layered system. Thus, bonding of layers and their performance along with installation are the major drawbacks of the pre-cured layered system.

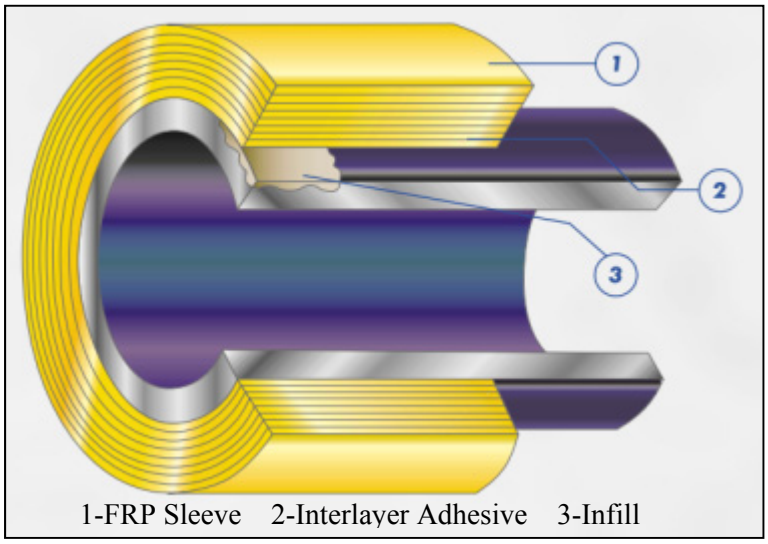

Figure 2.3 Clock Spring® repair (The Clock Spring Company 2011)

2.2.3 Stand-off sleeve

Leak containment of the failed pipe is not fully successful through the previous options and the necessity for an easily applicable solution is still needed. Stand-off sleeve systems provide higher structural integrity than both the flexible lay-up and pre-cured layered systems. Most of the heavy duty repair technologies are based on stand-off rigid shell system. This system can permanently restore the original strength, contains leaks, and supports axial loads. A study by Alexander (2007) showed that carbon half-shells can be effectively used for high pressure pipe repairs. The carbon half shell concept is similar to that of the metal split-sleeve concept used by PLIDCO (PLIDCO Split+Sleeve 2012). The advantage of this system is that it can carry internal pressure, axial tension and bending loads. This repair technique has the potential to be applied in both underground and underwater environments.

In case of material loss, either by corrosion or gouging, infill or cushion is used to ensure a smooth bed for the composite layer. Repaired pipe can bulge outward radially when pressurised. The stand-off sleeve provides a continuous support by the introduced infill layer that minimises the radial deformation and transfers the load from the pipe to the outer shell. At the same time, possible leaks can be contained. Hence, as further improvement to the stand-off clamp repair, the epoxy/grout filled split sleeve system was introduced where two separate parts are mechanically fastened or joined. Figure 2.4 shows a filled sleeve to repair a damaged pipe (AEA Technology Consulting 2001). The principle of this concept largely depends on the performance of the infill. The joining of split sleeves is one of the challenges of this repair, especially in underwater and restricted spaces. Leak containment to confine the fluid under pressure in the system is another challenge that is yet to be addressed for the composite split-sleeve repair system.

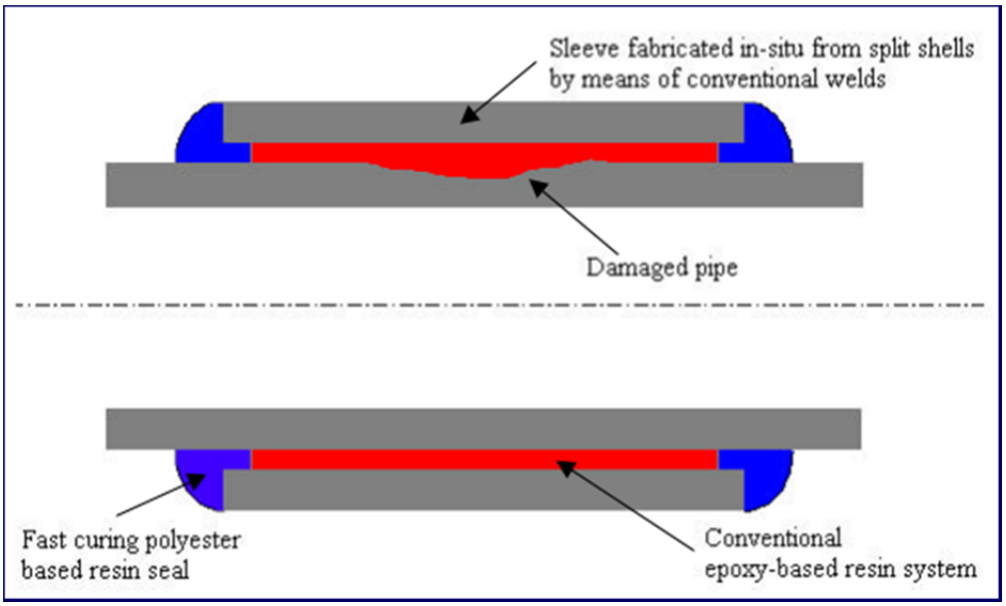

Figure 2.4 **Epoxy filled sleeved repair (AEA Technology Consulting 2001)**

2.3 Component materials for a fibre-reinforced composite repair

The elements of a repair are selected based on the required performance of the composite product under service conditions. The following sections present the

material characteristics of the different components of a composite repair and their performance issues which aim to aid in the selection of appropriate materials for each type of composite repair system and intended application.

2.3.1 Fibre reinforcement

The fibres are the primary load carrying component of composite materials. Fibre orientation determines the directional strength and stiffness for any particular application. The most commonly used reinforcing fibres for composites are glass, carbon, aramid, polyethylene, boron, polyester, nylon and natural fibres. Glass fibres are low cost, easily available and more compatible with resin systems however they have low modulus and more susceptible to fatigue, creep and stress rapture. Carbon fibres exhibit high strength, and stiffness, low density and superior fatigue performance than that of glass fibres (Giancaspro et al. 2010; Ochola et al. 2004; Wonderly et al. 2005). Both glass and carbon fibres absorb water and exhibit lower strength under immersed condition than that under dry condition, but this limitation is more dominant in glass fibres at elevated temperature (Lassila et al. 2002); Ray (2006). However, cost, availability and compatibility are some of the concerns in the applications of carbon fibres. Aramid fibres absorb water and degrade in moisture rich conditions (Sala 2000; Tanaka et al. 2002). (Hausrath & Longobardo 2011) provided a comparative summary of the properties of glass, carbon and aramid fibres which is presented in Table 2.2. The table shows the typical comparison of properties along with the advantages and disadvantages of the fibres most commonly used in pipe rehabilitations.

Table 2.2 Summary of fibre properties (Hausrath & Longobardo 2011)

Property	Glass		Carbon	Aramid
	E-glass	S-2 Glass®	T700SC	K49
Density (gm/cc)	2.58	2.46	1.80	1.45
Tensile strength (MPa)	3445	4890	4900	3000
Tensile modulus (GPa)	72.3	86.9	230	112.4
Comp. strength (MPa)	1080	1600	1570	200
Strain to failure (%)	4.8	5.7	1.5	2.4
CTE (10^{-7}/°C)	54	29	-38	-48.6
Softening point (°C)	846	1056	>350	>150
Advantages	Low cost, easily available and more compatible		Low density, high strength and stiffness, low density and superior fatigue performance	High impact performance, flame resistant and resistant to chemicals
Disadvantages	Low modulus and susceptible to fatigue, creep and stress rapture		High cost, availability and compatibility	Low transverse and compressive strength, susceptible to UV and degrade in moisture

Long term performance of carbon fibre when tested after eight years by The Metropolitan Water District of Southern California (MWD) was found to be satisfactory (Sleeper et al. 2010). This study showed that the modulus was decreased by approximately 16% and the elongation was increased by 12% compared to fresh specimens. Carbon fibres can also withstand higher internal pressure than glass and aramid fibres, as demonstrated in Figure 2.5 where comparison is shown between different fibre reinforcements in terms of maximum circumferential stress against

internal pressure (Toutanji & Dempsey 2001). Natural fibre or hybrids of natural fibre reinforced composites are found to have lower environmental impact compared to glass fibres for some specific applications (Joshi et al. 2004). Yu et al. (2008) reported the use natural fibres in the rehabilitation of underground pipes along with the glass fibre where the application was faster and the strength requirement was also met. In consideration of strength and water absorption issues, the prospects of natural fibres in an underwater scenario are yet to be investigated.

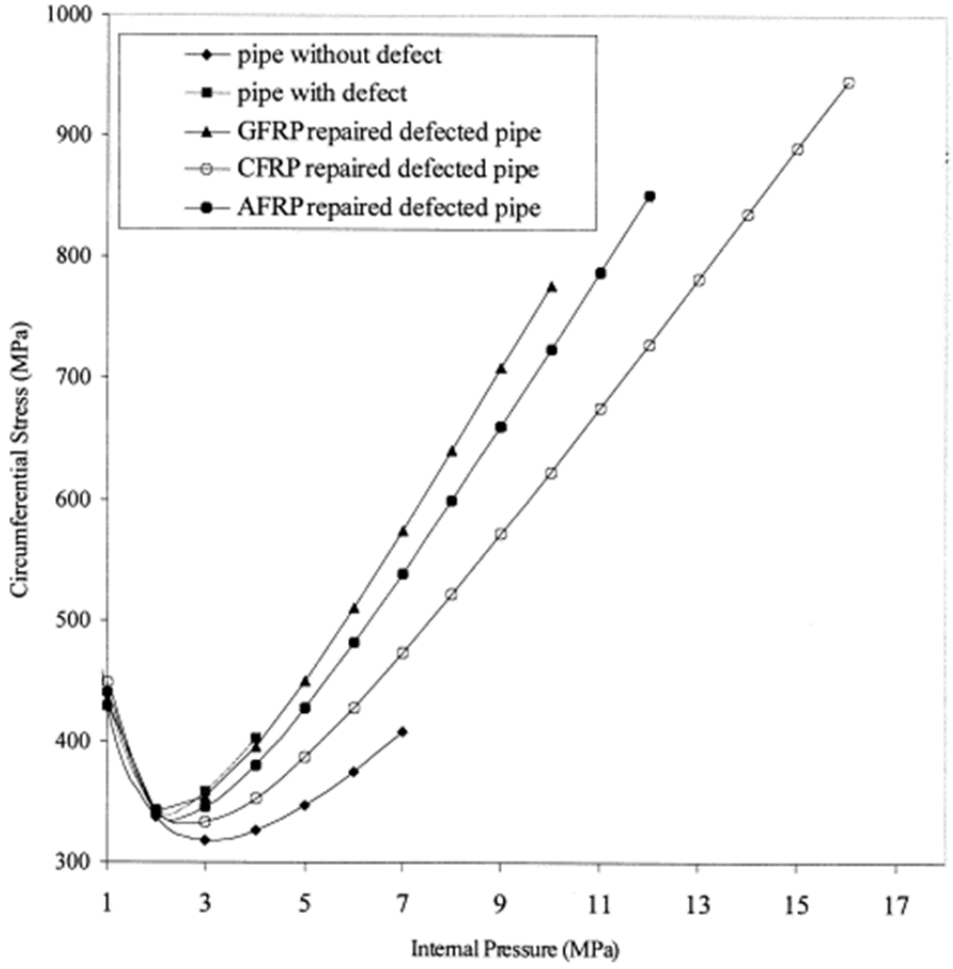

Figure 2.5 Comparison between circumferential stress and internal pressure in the pipe without defect, pipe with defect, and repaired damaged pipes (Toutanji & Dempsey 2001)

Carbon is a very good cathode; hence it is likely to stimulate galvanic corrosion attack on the high alloy metals. Galvanic corrosion resulting from electrochemical coupling of carbon fibres with steel alloys is another mechanism where the design of interfaces, treatment technology, and environmental conditions are must be carefully characterised. A study on carbon fibre reinforced polymer (CFRP) for galvanic corrosion, when carbon and steel are bonded together under a series of conditions, suggested existence of the galvanic corrosion when there is direct contact between a CFRP laminate and steel substrate (Tavakkolizadeh & Saadatmanesh 2001). Since the galvanic corrosion only initiates when there is direct contact between two dissimilar metals in the presence of an electrolyte, measures can be taken to eliminate one or both of these parameters by introducing another composite layer or an infill that is resistant to corrosion.

A hybrid composite system is often utilised to eliminate corrosion when high pressure performance requirements are present. A multilayered hybrid composite sleeve was designed by Alexander (2007), where inner and outer layers of E-glass were introduced to cover circumferential carbon fibres in the reinforcement thus eliminating galvanic corrosion. The inner layer acted to protect the pipe from potential corrosion due to carbon interaction with steel, while the outer layers protected the carbon fibres against potential impact and wear. Alexander (2007) also concluded that the strength provided by the sleeve layout orientation was found to be sufficient in both longitudinally and circumferentially against hoop and flexural loading.

Both glass and carbon fibres are used intensively for pipeline repair. However, selection of certain fibre class and orientation are dependent on the performance requirement of the rehabilitation and the surrounding environmental conditions. Based on the existing literature, glass fibres are suitable for economic in-air repairs that are susceptible to cold-dry conditions. Glass fibres can also be used in underwater conditions provided that the matrix system is protective enough against the surrounding environment. Besides cold-dry conditions, carbon fibres are also suitable for cold-wet and hot-wet environmental conditions and especially for long-life repairs of underground and underwater pipelines where frequent inspection and maintenance are not always feasible, and the higher service life of the structure is expected to offset the additional cost.

2.3.2 Resin matrix

Resin acts as matrix for the fibres. It binds the materials together into a cohesive structural unit and plays a significant role in composite performances. It also protects the reinforcing fibres from adverse environments and provides all the inter-laminar shear strength and resistance against crack propagation and damage. Generally, there are two types of matrix available depending on their behaviour when heated, i.e. thermoplastics and thermosets.

Commonly used thermoplastics are highly aromatic polyketones, polyarylene sulphides, polyamides, polyimides, etc. (Béland 1990). However, due to superior properties compared to thermoplastics, thermosets like epoxy, vinyl ester, polyester and phenol formaldehyde resins are used in most composite applications. A comparative summary of the advantages and disadvantages of common resins in pipeline repair is given in Table 3. The moderately superior thermal stability of epoxies, their excellent bonding properties and their mechanical properties have led to their widespread use as the prime resin in most of the high performance fibre-reinforced composites, especially when carbon fibre is used as reinforcement (Strong 2008). Carbon fibre is commonly produced with a surface treatment and sizing to enhance the bonding performance (Fitzer & Weiss 1987).

A study of the interfacial adhesion in the carbon/epoxy and glass/epoxy composites suggested that adhesion is affected by hygrothermal ageing at higher conditioning temperature and longer exposure time (Ray 2006). However, epoxy resins, along with high strength fibres like carbon, can be used more confidently in repair application than other resins for their anti-corrosive performance and durability even in moist or underwater conditions (Seica & Packer 2007). Considering the importance of pipeline repair and the associated high strength fibre requirement, epoxy resins are the most suitable for both underground and underwater conditions. However, other resins like polyester and vinyl ester can also be used in

in-air applications. The long-term performance of in site-cured resins exposed to moisture and high pressure repair conditions require further research.

Table 2.3 Advantages and disadvantages of resins

Property	Epoxy	Polyester	Vinyl Ester
Advantages	Superior physical and mechanical properties, low cure shrinkage, better adhesion, wide range of adaptability, better compatibility with carbon fibres, good moisture and chemical resistance	Low cost, available and easily applicable	Better strain and strength performance than polyester, low cost
Disadvantages	Higher cost, may possess corrosive contents and may degrade under UV	Moderate strength, low durability, high cure shrinkage, low strain prior to failure and less compatible with carbon fibres	High shrinkage and exothermic temperature during curing, may require post curing, low strain and carbon compatibility than epoxy

2.3.3 Infill

In the construction industry, two types of grout are usually used as infill materials for repair and rehabilitation: cement grout with or without polymer modification and epoxy grout. Both types are used in structural rehabilitation. For example, in the strengthening of the columns and piles, as bonding medium in prestressed members, as binder for soil stabilisation works, for crack repair in the concrete and masonry structures, and as infill in the pipeline repair. Epoxy grouts are recommended over cement grouts for applications requiring high strength, rapid setting, dynamic load bearing, critical alignment, and handling versatility and resistance against aggressive chemical environments (Kneuer & Meyers 1991; Prolongo et al. 2006).

Conventionally, the epoxy resins used in the rehabilitation works are the products of copolymerisation of Bisphenol A and Epichlorohydrin (Mendis 1985). Curing of most of the thermosetting polymers is affected when in contact with water in their uncured phase. By using special curing agents and methods, it is possible to produce systems which are insensitive to wet conditions and are capable of curing under water. This gives the epoxy grouts a wider range of application than cement based, lime based and cement-clay grouts modified with acrylic resin or methyl methacrylate ester polymer. Hence, investigating the properties of the epoxy grouts is crucial in identifying their feasibility for pipeline repair.

Damaged drainage and stormwater discharge systems often use infill grout to fill cracks and form an exterior seal around the pipe (McCullouch 1991). Worldwide, bridges, piers and off-shore platforms that are supported on wood, concrete or steel piles, are often repaired with bonded fibre-reinforced polymer composite shells and sometimes with a grouting/infill for marine environments (Ehsani 2009; Lopez-Anido et al. 2005). These grouts are generally made of epoxy resins. In addition, fillers are used to modify the mechanical, curing and shrinkage properties of the infill (Hamerton 1996).

The fillers can be both metal like aluminium and silver, and/or minerals like alumina and silica of a range of sizes. The layer of infill fills the irregularities or dents of the pipe surface and acts as smooth bed for the encircling sleeve. All the

systems for pipeline repair use a layer of resin "putty" that provides a bed for the fibre-reinforced composite sleeve that is either flexible or rigid. Duell et al. (2008) used a diglycidyl ether of Bisphenol-A (DGEBA) based epoxide cured with an alphatic amine hardener and a silica additive (Modulus 1.74 GPa) to fill the defects on the steel pipe. This investigation used bilinear elastic stress-strain behaviour of the infill, with a 50% drop in modulus after a yield stress of 33.1 MPa. The application of infill with carbon wrap used in this study is shown in Figure 2.6. The results suggested that the failure criterion is reached first for the composite wrap indicating success of filler to transfer load from steel to composite.

A numerical study by Palmer-Jones et al. (2011) showed the feasibility of an epoxy filled repair sleeve system where the grout was treated as an elastic-perfectly plastic material. The stress developed at the grout was found critical for this type of repair. In fact, the larger the defect, the higher the stress generated in the grout. However, possible grout shrinkage and the effects of the different curing conditions of the grout were not taken into account in this analysis.

Mattos et al. (2009) studied an alternative repair using two systems: silicon steel alloy within high molecular weight polymers and oligomers and epoxy resins with aluminium powder. The compressive strength of the above mentioned materials were 56 and 104 MPa, and flexural strengths were 59 and 67 MPa respectively. It was also suggested to apply the above mentioned materials and then to cover using a composite material sleeve to ensure a satisfactory level of structural integrity. Polyester based infill materials were also found to be suitable by Sirimanna et al. (2010; 2011; 2012) for deteriorated piles, and the compressive strength was found within the range of 40 – 90 MPa. The range of properties are also comparable to the properties of the infill used by Duell et al. (2008). Hence, grouts with the compressive strength of 70 – 120 MPa are also expected to provide satisfactory performance as infill in pipe rehabilitation. However, behaviour of the thick infill layer applied to a repair system should be investigated further for incoming load.

Polymers can shrink during curing (Haider et al. 2007; Li et al. 2004; Zarrelli et al. 2002). Resin, when used in thick layers can experience residual stresses and thus affect the load transfer performance. The resin based infill used inside the annulus of the repair is vulnerable to shrinkage. Thus, measures should be taken to avoid excessive shrinkage that can create interlayer separation and cracking of the infill layer. Reduction of shrinkage is achievable by introducing fillers to the resin. An infill layer is also expected to eliminate galvanic corrosion as it lies between the steel and composite layers. Issues like flowability and strength transfer demand additional investigation for better understanding of infill performance.

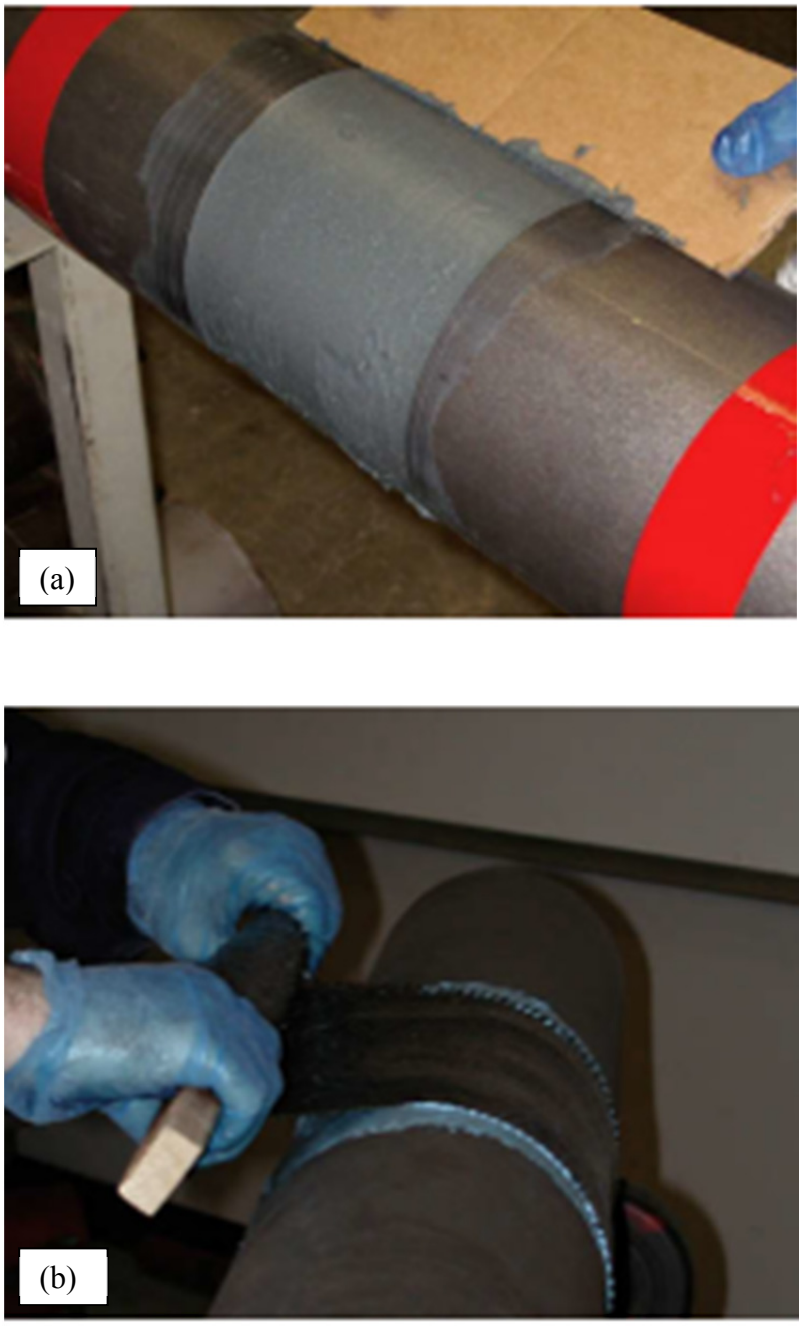

Figure 2.6 **Pipe exterior repair process using infill and flexible wrap (a) Filling defect with putty (b) Wrapping epoxy wetted carbon fabric around the defect (Duell et al. 2008)**

2.4 Considerations for repairing pipes using fibre-reinforced composites

Selection of an appropriate rehabilitation system involves a clear understanding of the nature and extent of the corrosion, and knowledge of the mechanism in which a particular repair system works. Reliable predictions of the effective operation of the repaired pipeline can be obtained through appropriate research and development study prior to field application. Furthermore, the following important factors should be taken into consideration in designing and evaluating the effectiveness of a fibre-reinforced composites system in repairing steel pipes.

2.4.1 Geometry and degree of metal loss

The type of defects in steel pipes is diverse in nature and one single universal solution is difficult to adopt for all the defect types. The pipe defects associated with metal loss are grouped into the three main categories according to the guideline provided by AEA Technology Consulting (AEA Technology Consulting 2001). According to this guideline, the possible damage scenarios of a steel pipe can be (i) the pipe subjected to external metal loss, (ii) the pipe subject to internal metal loss, and (iii) piping components that are leaking. This review is focused on the external corrosion scenario and gouging defects and associated material options and repair considerations.

Naturally occurring corrosion or gouging is difficult to analyse. Researchers often use controlled mechanical gouge or metal loss to replicate the actual scenario. The depth-thickness ratio and angular extension of the corrosion determines the buckling and collapse modes of circular pipes (Jianghong 2006). The guidelines for determining the remaining strength and test pressure requirement can be obtained from ASME B31G (1991). Recommendations are also given by Det Norske Veritas (DNV) (2010) for assessing the corrosion defects of pipes subjected to internal pressure and longitudinal loads. One typical mechanically gouged pipe wall used by Duell et al. (2008) is shown in Figure 2.7 where both the axisymmetric and localised defect length was equal to the diameter of the pipe and radial extension of localised defect was also equal to the diameter. The geometry of gouge chosen to simulate specific repair conditions is often arbitrary and case specific.

The burst model of corroded tubular elements in comparison to other assessment methods were studied where the defect circumferential width had an influence on the failure pressure (Szary 2006). Generally, burst pressure decreased when both circumferential and longitudinal defect extension increased. This process was more influenced by the longitudinal extension. Defects with dimensions greater than 20% of $2a/\pi D$ (non-dimensional circumferential extension) and 20% of $2b/\pi D$ (non-dimensional longitudinal extension) did not decrease the failure pressure any further. Hence, the geometry of the defects and level of metal loss play an important role for internal pressure in a tubular structure.

The critical stress in a corroded pipe is dependent, not only on the material properties, but also on the defect geometry as indicated by Cunha and Netto (2012). They tested forty-one pipe samples of 75 mm nominal diameter with a machined defect up to burst, and 58 FEM simulations were performed modelling the plastic instability of pipes with the hypothesised defects. The tests and simulations comprised shallow (25%), intermediate depth (50%) and deep (75%) defects with short, intermediate and long lengths in steel pipes. The analytical predictions of the instability or burst pressure were consistently within engineering acceptable accuracy.

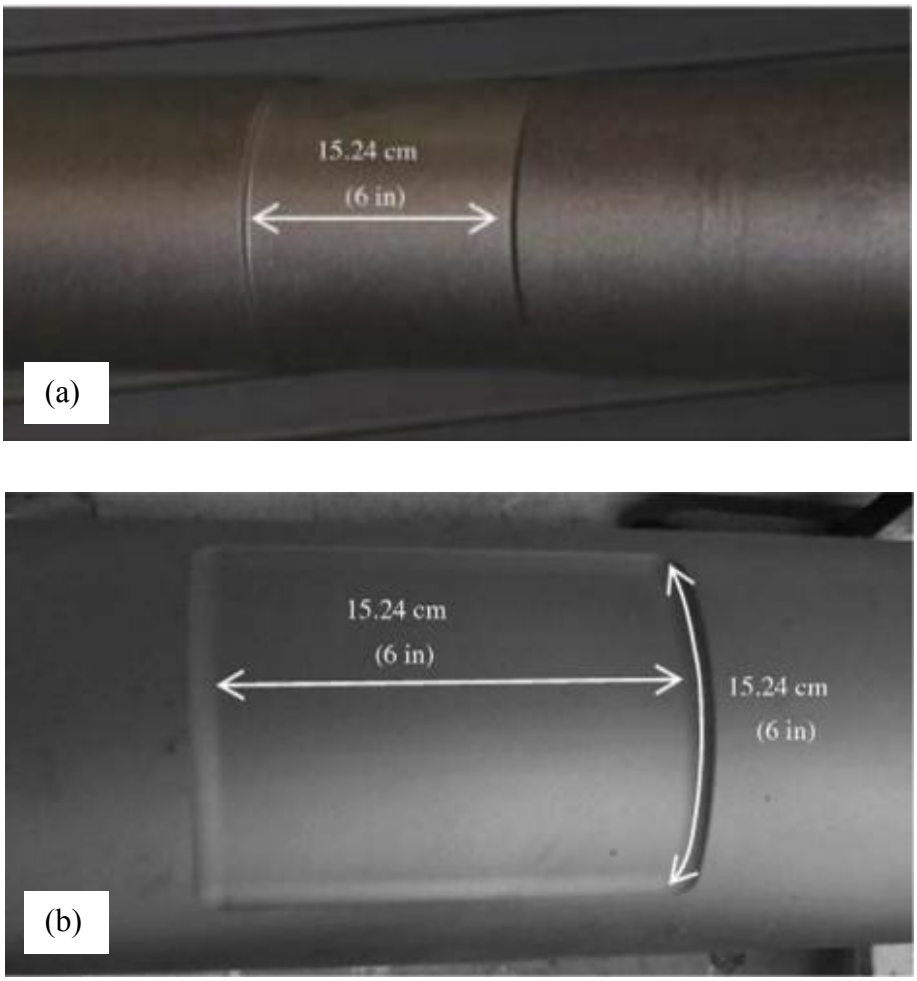

Figure 2.7 **Pipe test vessels with machined defects with a depth of 50% wall thickness (a) axisymmetric defect (b) 6 x 6 patch defect (Duell et al. 2008)**

Cunha and Netto (2012) also concluded that beyond a length that denoted by $\alpha \geq 3.5$ for axisymmetric defect and $\alpha \geq 4.5$ for narrow flaw, could be considered as of infinite length and strength of a pipe with a very long axisymmetric defect is similar to that with reduced thickness. Here, α is a non-dimensional half-length of the defect and depends on material property, defect thickness and pipe section. Figure 2.8 shows how the defect geometry and material property affect the critical stresses in a long narrow defect scenario where x denotes the remaining strength as ratio of critical stress to ultimate tensile strength and y axis denotes strain hardening exponent of the pipe material. The plot showed that a pipe with a long narrow defect is expected to have higher remaining strength than that of an undamaged pipe, with an exception of deep flaw (75%) and low value of hardening exponent (<0.8). Thus, the depth and shape of defect are important parameters to study when considering composite repair on steel pipes. To validate a repair for pipe, one must consider all the cases of geometry (localised and axisymmetric), along with plastic contribution of pipe material.

2.4.2 Surface modification

The effectiveness of fibre-reinforced composite repair systems lies in the bonding strength of the resin between steel and composites. Surface treatment is required to increase the surface energy of the adherents as much as possible to improve bonding. Consequently, a relationship exists between good adhesion and

bond durability (Lees 1989). The application of sand paper and a final rinse with solvent helps create an oil, grease and dirt free surface. Grinding and sandblasting the steel substrate surface, instead of simply hand-sanding the surface, was found to increase the average shear strength by at least 40 percent (Smith 2005).

A number of surface preparation practices are available based on the surrounding environment and level of corrosion. Usually, high pressure cleaning is used to remove surface contamination and fouling organisms that have not yet dried. More rigorous and effective cleaning can be done by hand and power tools. However, blast cleaning is considered to be the best option due to the application of abrasive particles under a compressed air stream. Water jetting or hydro blasting is considered more advantageous than grit blasting as it produces less dust and has less of an impact on the environment. It is the most widely used cleaning technique in the repair industry. Australian standard series AS1627 titled "Metal Finishing-Preparation and Pretreatment of surfaces" provides ten methods for possible surface treatments. The first part of this series, AS1627.0 (1997), summarises the appropriate methods for the preparation of metal surfaces. Part 9 of this series is dedicated to pictorial demonstration that refers to ISO 8501-1:1988 (1988). A cross reference of other recognised standards for surface preparation is given in (Thompson's Welding Services).

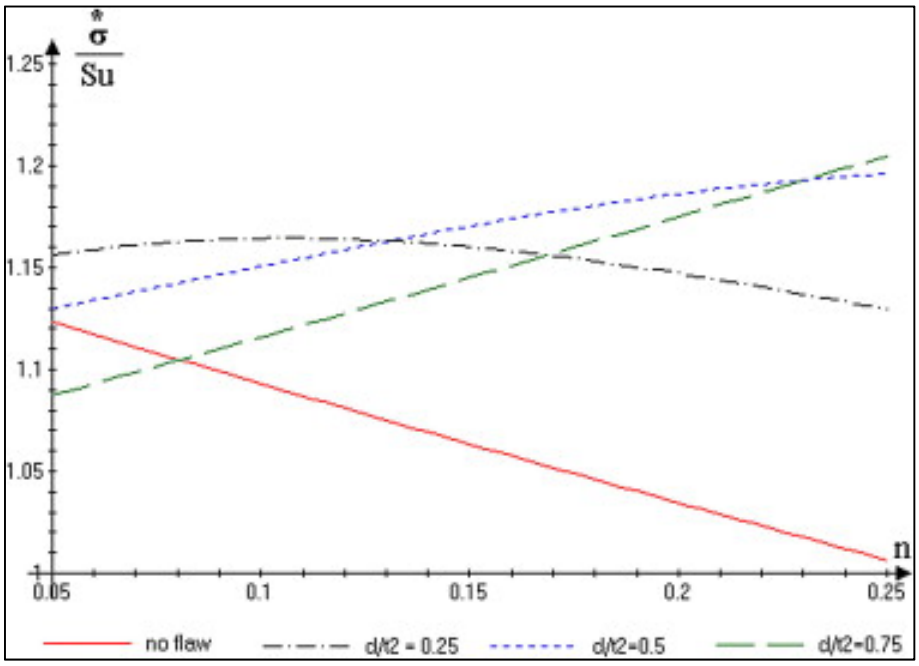

Figure 2.8 Critical hoop stress of long narrow flaws (Cunha & Netto 2012)

As pipe repairs are conducted in close proximity to hydrocarbon atmospheres, any method to mechanically roughen the surface (sandblasting, cutting, grinding) that may produce heat and sparking; must be applied with caution (Mattos et al. 2009). More importantly, a surface preparation technique that promotes good adhesion between steel and composite needs to be investigated for corroded pipes before the application of the repair. Considering the importance of surface bonding, sensitivity and location of repair, water jetting is expected to be the most suitable method for corroded or scaled pipeline surfaces.

2.4.3 Behaviour of repair components

One of the prime concerns of the researchers in the field of pipeline repair is the stress and strain contribution provided by each element of the repair. Based on prior research using strain gauges installed in between different layers, it is clear that variations in strain exist between the different layers (Alexander 2007; Freire et al. 2007).

Shouman and Taheri (2011) investigated the performance of composite repaired pipelines under internal pressure, axial loading and bending force where increased thickness of the wrap could prevent the yielding of the pipe at the defect region; however it did not improve the strength of the pipe in the axial direction. This study also suggested that the repair layer that did not add much to pipe stiffness against bending due to the circumferential alignment of the fibre wrap. Thus, it is necessary to provide axial reinforcement in case of axial and bending loads other than internal pressure.

A study by Freire et al. (2007) suggested that, up to the start of yielding of the pipe defect region, only the elastic pipe stresses actually equilibrated the pressure loading due to the steel's high Young's modulus. After yielding, the composite material started working effectively, carrying an important part of the pressure loading increments. The strain behaviour is shown in Figure 2.9. However, the contribution of the infill materials that occupied the defect (70% of pipe thickness) was not demonstrated in the comparison. Freire at al. also analysed the model with a simple analytical approach to justify the application of the Remaining Strength Factor (RSF) to a pipeline with metal thickness loss that has been repaired with composite sleeves. The analytical results are shown in Figure 2.10. It can be seen that the circumferential strains are distributed in an approximately linear shape along the radial direction even if the internal pressure makes the pipe steel material undergo elastic or plastic behaviour. The result shown in the Figure 2.10 is also comparable to Figure 2.9 and indicates that after the steel has reached its yield point, a larger portion of the pressure load is carried by the outer composite layer.

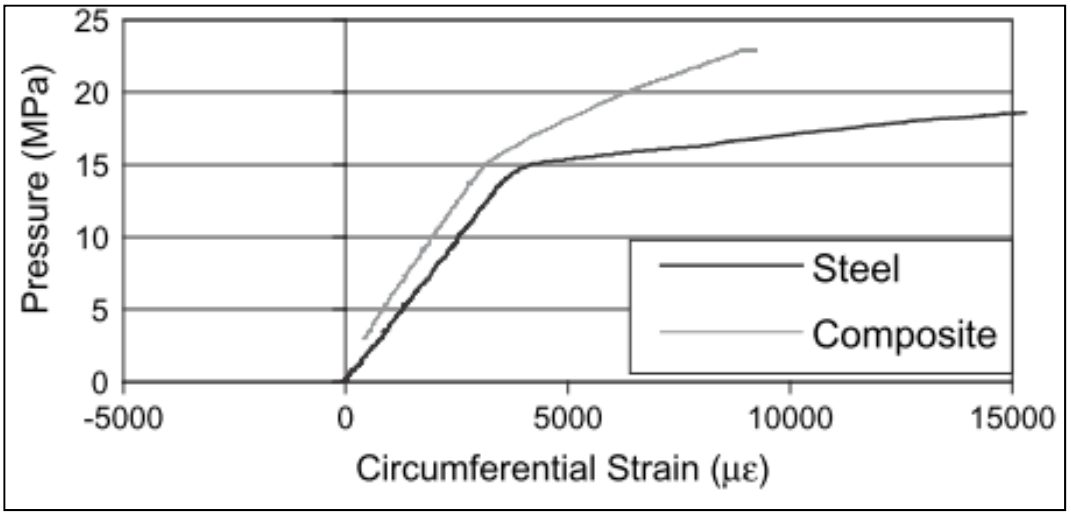

Figure 2.9 **Circumferential strain at the centre of the defects as function of internal pressure (Freire et al. 2007)**

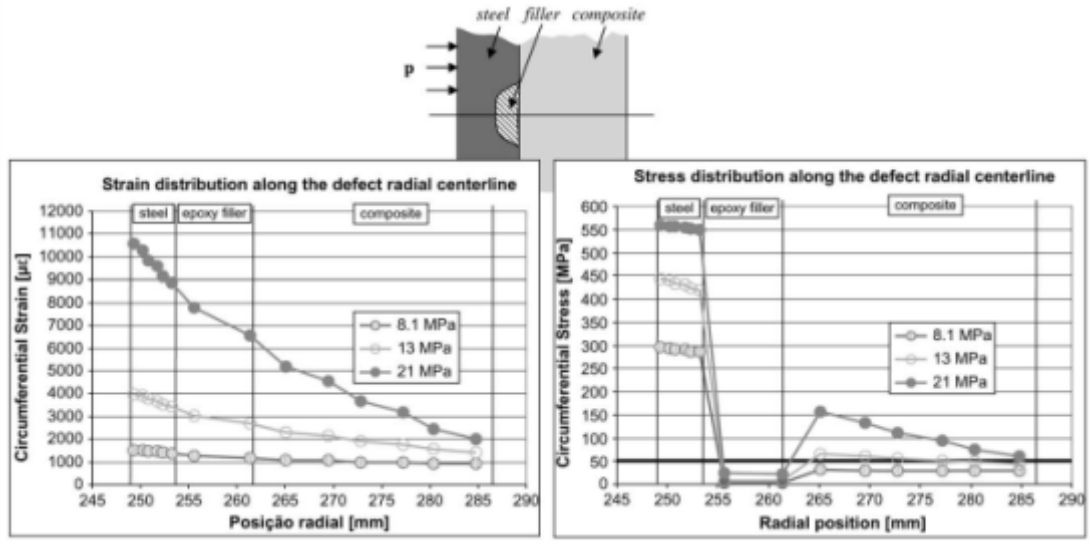

Figure 2.10 **Finite element prediction of strain and stress distributions along the defect radial centreline (Freire et al. 2007)**

Duell et al. (2008) carried out a rigorous study based on both finite element analysis and laboratory experiments. The finite element analysis considered the infill properties. A typical analytical distribution of stress and strain in this study is shown in Figure 2.11. The stress and strain distribution in this figure is applicable for a thin layer of resin that adheres between steel and flexible fibre overwrap. Based on the results of this study, when the repaired vessels were pressurised in monotonic static loading, the vessels burst violently, with the wrap exploding apart and the steel pressure vessel rupturing along a longitudinal crack running the length of the defect region. This failure behaviour is different than the failure pattern observed by Freire et al. (2007), where prior to the steel yielding, the composite material starts to work effectively carrying a significant portion of the load pressure. This makes the systems with larger defects more susceptible to defect or material variations within the composite wrap than the repaired pipes with smaller defect regions, which could result in lower ultimate burst pressures. However, another reason that might be contributing to this failure behaviour was the repair thickness applied for these studies. Thus, experimental and numerical studies containing long narrow to axisymmetric flaw geometries and repair thicknesses in repair scenarios are required to understand the relationship between repair components and failure patterns in fibre-reinforced composite repair in pipeline.

The system used by Alexander (2007) only considered the axisymmetric defect that was filled up by a carbon wrap. Under internal pressure, due to the relative stiffness of the steel in comparison to the composite, during the initial stages of loading, the steel carried a higher percentage of the load. However, as yielding occurred both in the corroded region and the base pipe, a greater percentage of the load was distributed to the composite material. Figure 2.12 shows the strain distribution in the repair system where a limit state design method is adopted to identify the allowable loading limits. This study, however, did not include infill in its repair scenario. This failure pattern is comparable with the study by Freire et al. (2007) thus differing from the failure patterns of Duell et al. (2008) despite both having axisymmetric flaw.

Composite repair can experience long-term degradation especially when subjected to an adverse environment for a long time. The repair and rehabilitation of pipelines in remote locations demand confidence on long-term performance. Composites can be subjected to degradation through creep and water absorption (Farshad & Necola 2004; Keller et al. 2013) and sustainable temperature (Goertzen & Kessler 2007) that can lead to sudden failure prior to reaching its full performance. According to ISO 24817 (2006), the Class 3 type of repair containing produced fluid should be tested for long-term performance. Long-term is defined as greater than or equal to 1000 hours. This standard also suggests testing the system for cyclic loading if the predicted cycle is more than 7000 in its lifetime.

Mattos et al. (2012) carried out burst test and long-term pressure test on a pipe containing a through-thickness defect was repaired with an epoxy system where the repaired pipe burst at a lower pressure due to a mismatch effect between the epoxy patch and pipe materials. The typical failure of the epoxy repaired through wall defected pipe is shown in Figure 2.13. The constant internal pressure was 10.34 MPa at a temperature of 353.15 K (80°C). During the long-term pressure test when the pipe ruptured after six days, sudden pressure peaks more than the static strength (17.2 MPa) were revealed that could be caused by minor temperature variations from the pressure control system. Thus, a proper pressure control device is essential to conduct long-term pressure test in high pressure environments.

The prospect of the through thickness pipe repair approach was analysed in light of fracture mechanics by Mableson et al. (2000). They found that the repair should be sufficient against hoop and axial stresses as well as blister formation under internal pressure. Köpple et al. (2013) also studied through-wall defect repair using composite where both analytical and numerical comparison was presented to characterize the deflection of the repair component. Their study suggested that the deflection generated from bending and shear could be accurately estimated using both analytical and numerical approaches provided that the repair thickness to defect radius ratio is less than 0.5, otherwise the deflection could be overestimated.

Load transfer mechanism also requires further study. Significant degradation of bond properties under axial loading was found when the surfaces were moist (Leong et al. 2009). This study also found that regardless of grouting conditions either wet or dry, failure always occurs at the infill-sleeve interface. The mechanical behaviour of internally pressurised pipes varies considerably with flaw geometries. Load transfer and failure of repair elements are also dependent on corrosion and gouging patterns. The contribution of the repair elements for combinations of flaw geometry in the infilled sleeve system is a gap in the current knowledge and awaits further research. The detailed property identification of infill material is necessary, along with how the properties are going to be compatible with the other repair elements.

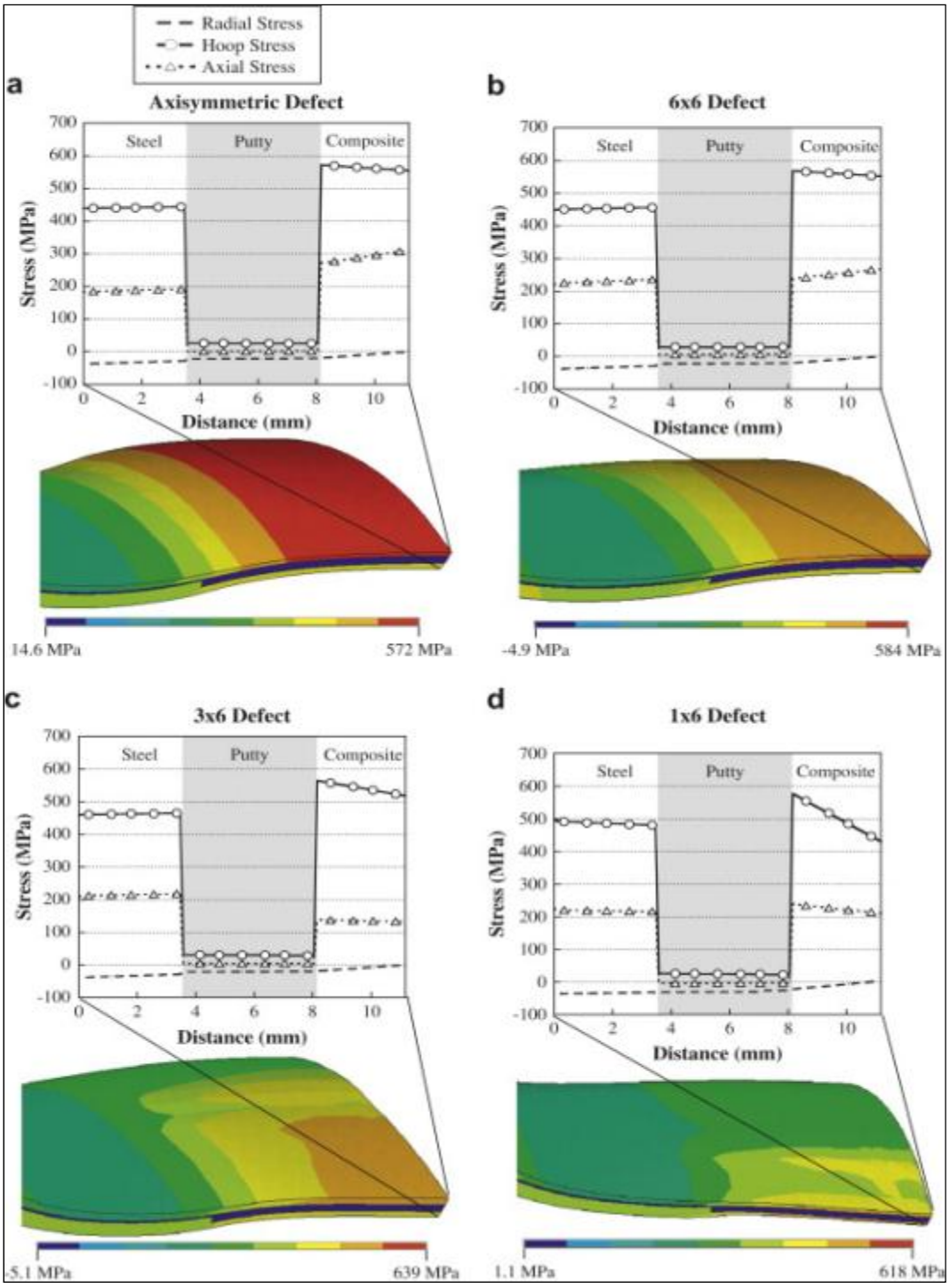

Figure 2.11 FEA predicted radial, hoop, and axial stress at the centre of the 50% wall loss defect from the inside of the pipe wall to the outside of the composite wrap at burst pressure (Duell et al. 2008)

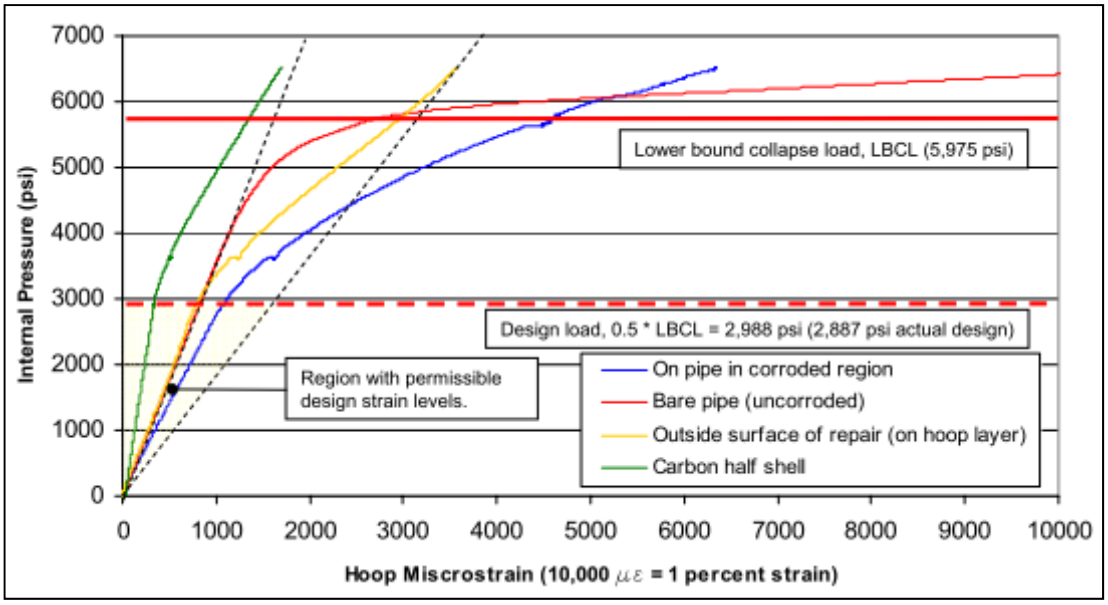

Figure 2.12 **Circumferential strain as a function of internal pressure applied to repair systems (Alexander 2007)**

Figure 2.13 **Failure of epoxy repair (Mattos et al. 2012)**

2.4.4 Current codes and practices

The acceptance of fibre-reinforced composites as an alternative to conventional repair materials is indicated through the recent development of codes and standards. ASTM D2992 (2006) specifies a standard practice for designing fibre glass pipe and fittings. However, the most significant advance in the repair of high pressure and high risk pipelines is the development of the standard by the American Society of Mechanical Engineers Pressure Technology Post Construction

Committee: ASME PCC-2:Part 4 (2006) which is dedicated to the applicability of composite overwrap repairs to pipelines. Part 4 of ASME PCC-2 states, "The composite materials allowed for the Repair System include, but are not limited to, glass, aramid, or carbon fibre reinforcement in a thermoset resin (e.g., polyester, polyurethane, phenolic, vinyl ester, or epoxy) matrix. Fibres shall be continuous." This code allows any ASME compliant metallic pipeline to be repaired with a composite overwrap for all the possible repair scenarios of hoop, axial and leak proofing. The code also includes the ASME metallic pipe plastic (yielding) philosophy in the repair.

ISO 24817 (2006) provides a similar methodology to that of ASME PCC-2 (2006) however, it does not allow pipe yielding and therefore is suitable for non-metallic and/or brittle pipes. ASME PCC-2 standard allows the repair of equipment and piping within the scope of ASME Pressure Technology Codes and Standards, after it has been placed in service. This standard provides three designs of repair options for non-leaking pipes. The options are: (i) pipe allowable stress i.e. includes allowance for original pipe where yielding of the pipe may or may not be included, (ii) repair laminate allowable strains, i.e. excludes allowance of original pipe, and (iii) repair laminate allowable stresses determined by performance testing, i.e. design based on long term performance test data. The pipe allowable stress method does not consider the strain hardening of the steel and remaining pipe material does not reach yield, and remains elastic throughout operation.

Based on realistic case studies and the calculated values of thickness according to the pipe allowable stress method, Alexander (2009) concluded that calculated repair thicknesses were about 2.5 times and 5.5 times greater than the laminate allowable strain and laminate allowable stress by performance testing, respectively. ASME PCC-2 underestimates the repair layer when internal live pressure exists during the installation (Saeed et al. 2012). However, Saeed et al. (2012) assumed that the substrate pipe carried no further load after yielding (elastic – perfectly plastic) and any further load was only carried by the composite. Thus, consideration of post yield strain hardening in the analysis is one of the shortcomings of composite repair that requires attention. Simultaneous studies through numerical analysis and experimental test data are suggested to attain the closest possible behaviour of the repair.

According to ASME Boiler & Pressure Vessel Code Section VIII Division 2 (2007), three analysis methods are available for evaluating protection against plastic collapse while analysing pressure vessels. The methods are: (i) Elastic Stress Analysis Method, (ii) Limit-Load Method and (iii) Elastic-Plastic Stress Analysis Method. Elastic stress analysis method compares the elastic stress analysis results of the structure subjected to certain loading conditions with an associated limiting value. However, for components with a complex geometry, a limit load or elastic-plastic analysis method is recommended. The limit-load method determines a lower bound to the limit load of a structure and applies design factors to the limit load such that the onset of gross plastic collapse will not occur (Biel & Alexander 2005). Since limit analysis addresses the failure modes of ductile rupture and the onset of gross plastic deformation of a structure, the strain in the reinforcing composite material can be obtained after a load has been transferred from the steel carrier structure.

Elastic-plastic stress analysis method, however, considers ultimate stress and perfect plasticity behaviour i.e. non-linear geometry until collapse. This method is

more precise than other methods. The inclusion of a composite into the repair system introduces more than one stress-strain property in the model. Numerical analysis is accepted in both limit-load method and elastic-plastic analysis methods for the complex geometry and material behaviour. In case of repairing a pressure vessel using fibre-composite repair, structural performance of the repair system can be analysed with any of the analysis methods. Alexander (2007) successfully used limit load analysis to assess the performance of composite repair of an offshore riser.

Stress-based design is usually user for repair systems. Material nonlinearity is not addressed in these strength and stiffness based analyses where loading is primarily elastic and a safety factor is introduced to ensure a desired level of confidence. However, when load increases and requires a certain amount of material nonlinearity in the steel (i.e. plasticity) in order to transfer load from the steel to the composite through infill, linear elastic design methods are not useful and may not be acceptable as they are often restrictive and conservative.

2.5 Conclusions

Numerous techniques and material options have been utilised by researchers and commercial end-users. The defect scenarios are different and so are the repair options. It is seen that the performances of the prime components (i.e. external shell, infill and resin binders) currently available, in a shell repair system are already promising. Composite sleeve repair with infill will provide an easily applicable and long-term solution for steel pipelines. However, little work has been carried out to investigate the behaviour of a pre-cured composite shell system with infill. Few studies have been carried out on the effectiveness of infill material to be used in the annulus between damaged pipe and outer shell.

Further research is necessary for identification of suitable infill and fibre-reinforcement properties for repair efficiency. The effect of adverse service condition on the properties is also requires investigation. The stress contributions of repair elements along with infill need to be investigated. Further studies on the subsequent load transfer mechanism among the components of a repair system must be conducted to understand their combined action. A design guideline is also warranted to actualise the simplified performance indication from the material properties and metal loss. These technical issues are pursued in the following chapters in this dissertation.

Infills are subjected to compressive, tensile, flexural, and shear loading, or a combination of these loadings based on their applications, especially when used inside narrow confinements and under high pressure. The properties of infills are also significant to understand the behaviour of the repair system. The properties are also required in the numerical simulation or theoretical prediction of the behaviour of a repair system for an optimum design. With the advancement of high performance composites, new challenges are emerging in finding the infills that can be suitably used in combination with FRP materials to rehabilitate the damaged pipelines. Moreover, an evaluation of the thermal properties of the components of the repair is also important, as polymers exhibit degradation at elevated temperature. It is essential, therefore, to characterise the mechanical and thermal properties of infills to determine their efficiency as infill materials in the repair. In Chapter 3, an investigation into the characterisations of five epoxy grouts is presented.

Chapter 3

Mechanical and thermal properties of epoxy grouts as infill

3.1 Introduction

Composite materials provide an ideal opportunity to rehabilitate existing structures. From the extensive literature, it is evident that polymeric infill have been proven effective for repairing metallic components and tubular pipes. Most repair systems use grout or 'putty' to fill the corroded or gouged section in the pipe and cylindrical sections (Duell et al. 2008). Another development is a stand-off split sleeve that can be used to repair high pressure pipelines (Gibson 2003; Palmer-Jones et al. 2011). In this type of repair system, the annulus between the pipe and the outer sleeve is filled with a suitable infill material ensuring a smooth bed for the composite layer. More importantly, the infill grout refills the damaged profile and provides a continuous support to minimise the outward distortion and transfer the load from the pipe to the fibre-reinforced composite reinforcement. Thus, the effectiveness of these repair systems largely depends on the performance of the grout. In this study, epoxy grouts are investigated. Epoxy grouts are chosen due to their superior mechanical and thermal properties, ease of handling and effectiveness in wet conditions compared to other grouts. The reasons for choosing epoxy grouts over other available grouts were already discussed in Section 2.3.3.

Defective pipelines need to be repaired and brought into service condition as quickly as possible to restore flow with minimum financial loss. However, the time required to gain full functionality of the repair depends on the maturity of the elements of the repair. It is therefore essential to identify the time at which the grout can be considered capable of meeting in-service conditions. Compressive properties are considered as one of the prime evaluating properties in the industry. This chapter also includes a detailed investigation examining the effect of time on the compressive properties of three selected grouts.

From a number of studies it is evident that polymers experience shrinkage during the curing process. Internal stress, volumetric shrinkage and warpage are some of the inevitable issues for polymers during curing (Chekanov et al. 1995; Haider et al. 2007; Wang et al. 2012). Shrinkage during the curing process may result in an uneven finish and separation of the adjoining surfaces, which eventually causes inefficient load transfer. As long as the resin system is liquid, it can accommodate the shrinkage. After a certain time, when polymer has reached a certain degree of polymerisation, it no longer flows to accommodate the shrinkage (Hossain et al. 2009). This is the "post-gel" part of the curing contraction, when the material is getting stronger and exerting forces and, as a result, stress is being produced. This post-gel shrinkage affects the development of stress in polymers (Magniez et al. 2012; Presser & Geiss 2011; Yu et al. 2006; Zarrelli et al. 2002). The resin-based infill used inside the annulus of the repair is vulnerable to shrinkage. Resin, when used in high content can crack from the developed residual stresses, thus affecting load transfer performance. Thus, measures need to be taken to avoid excessive shrinkage that can create interlayer separation and cracking of the infill layer.

In this chapter, five available epoxy grouts were selected based on their application and mechanical properties as reported by their respective manufacturers through their technical data sheets. These grouts were also selected as they have resistance against acids, alkalis and hydrocarbon based fluids, and thus are advantageous for underground and underwater pipeline repair. Thermal along with compressive, tensile, shear and flexural properties of these grouts were determined and their failure behaviour was observed to understand their performances under different loading conditions. The effect of the addition of the fillers on the thermal properties was also determined. Considering the important role of epoxy grouts in structural repair, volumetric analysis was also conducted to characterise the volumetric shrinkage of epoxy grouts with and without additional coarse filler, and to determine the amount of shrinkage contributing to rigid contraction. The effect of coarse filler in the shrinkage performance is also investigated. Finally, these properties were evaluated to determine their suitability as infill for the composite repair of steel pipelines.

3.2 Experimental Methodology

3.2.1 Materials

Five epoxy grouts with different specified compositions of neat resin, hardener and aggregate were mixed in a plastic bucket using an electric hand drill. The grouts were collected from respective distributors and supplied by Cooperative Research Centre for Advanced Composite Structures (CRC-ACS), Australia. The first three grouts had two parts: high viscous resin with fine filler particles which were already included in the resin part, and low viscous hardener. The fourth grout had three parts: viscous epoxy resin, low viscous hardener, and a combination of coarse and fine filler particles. The fifth grout was a modification of the third grout which was mixed with the equal weight of coarse filler. Table 3.1 shows the proportions of various ingredients of the grouts. Due to commercial confidentiality, the grouts investigated in this thesis are named as Grout A, B, C, D and E. Figure 3.1 shows the ingredients of the grouts investigated in this study. Since the aim of this study was to characterise the behaviour of the mechanical properties, chemical analysis of the ingredients were not conducted.

3.2.2 Test program

The test program was divided into two stages. The first stage included the determination of the 7-day compressive, tensile, flexural, shear, and thermal properties of the grouts. Based on the results from the first stage, grouts C, D and E exhibited superior mechanical properties and the effect of curing period on the compressive properties of these grouts were investigated in the second stage. The test was carried out on the 25 mm diameter 25 mm high cylindrical specimens for grouts C, D and E at 1, 3, 7, 14 and 28 days. In addition, the 50 mm diameter 100 mm high cylindrical specimens were tested at 3, 7 and 14 days for grouts C and D to determine the size effects on compressive properties and failure patterns. Further, the 50 mm diameter compressive specimens of grout E were tested at 7 and 28 days.

Table 3.1 Composition of the grouts

Grouts	Part-components	Mixing ratio	Primary constituents[9] (% Weight)			
			Resin[8]	Hardener	Fine aggregate	Coarse aggregate
A	Resin with fine filler[1]: Hardener	3.4:1.0[6]	22.75 (45.04)	11.46 (22.65)	65.79 (32.31)	-
B	Resin with fine filler[2]: Hardener	3.4:1.0[6]	23.50 (46.92)	11.02 (21.47)	65.49 (31.60)	-
C	Resin with fine filler[3]: Hardener	4.0:1.0[6]	27.37 (49.35)	9.52 (20.00)	63.11 (30.65)	-
D	Resin: Hardener: Coarse filler[4]	2.4:1.0:12.0[7]	15.58 (26.12)	6.49 (13.35)	77.92 (60.52)	
E	[(Resin with fine filler[3]: Hardener): Coarse filler[5]]	[(4.0:1.0)[6]:1.0[7]]	13.66 (27.60)	4.76 (11.19)	31.55 (17.14)	50.03 (44.06)

[1]0.06 – 350 µm, [2]0.05 – 90.0 µm, [3]0.05 – 300.0 µm, [4]0.45 µm – 2.36 mm, [5]45 µm – 2.36 mm, [6]By volume, [7]By weight, [8]Bisphenol A and/or F epoxy resin, [9]Values in the parenthesis are % volume

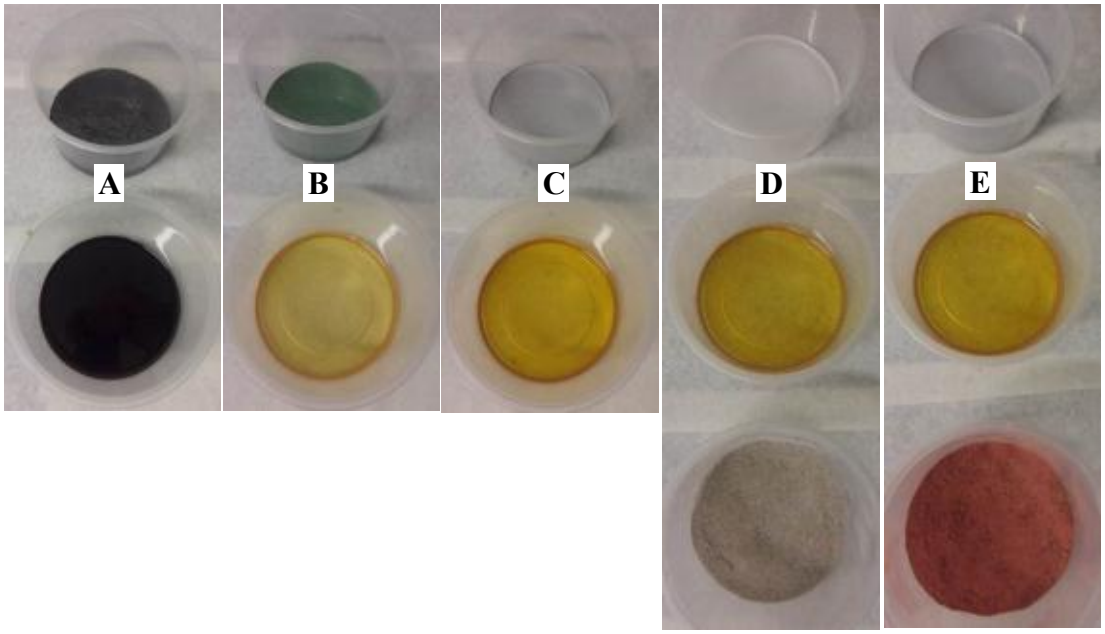

Figure 3.1 Ingredients of the grouts

3.2.3 Specimen preparation and test set up

3.2.3.1 Mechanical tests

Freshly mixed grouts were poured into the designated moulds. The specimens were removed from the moulds after 24 hours, and cured in a controlled environment at 23ºC for 7 days prior to testing. The specimens were cut and polished to the required dimensions. Compressive, tensile, flexural, shear and thermal properties of the grouts were determined after 7 days of curing. Table 3.2 summarises the details of tests conducted on the prepared specimens. Relevant standards and practices are also shown in the table.

All the mechanical characterisation tests other than the 50 mm diameter cylindrical compressive specimens were carried out using a 100 kN MTS hydraulic testing machine. Due to the requirement of higher capacity before yielding, the 50 mm diameter cylindrical compressive specimens were tested using a 2000 kN SANS

servo-hydraulic compression testing machine. The compressive strain was measured from the crosshead displacement and initial height of the specimen. Figure 3.2 shows the mechanical testing of the prepared specimens. A laser extensometer was used to measure the strain data. The effective span length in-between the end supports for flexural test was 230 mm. V-notched shear specimens with a notched width of 12 mm at the middle were tested using Wyoming shear testing fixture.

Table 3.2 Summary of test details

Tests	Standards/Methods	N	Dimensions	Geometry	Loading rate
Compressive	ASTM C579 (2001)	5	25x25 mm 50x100 mm	Cylinder	1.3 mm/min
Tensile	ASTM D638 (2010)	6	10x10 mm	Dog bone	1.0 mm/min
Flexure	ASTM C580 (2002)	6	250x25x25 mm	Prismatic	3.0 min/min
Shear	ASTM D5379 (1998)	5	76x20x10 mm	V-notched	1.3 mm/min
DMA	ASTM E1640 (2009)	3	60 x 12 x 5 mm	Prismatic	1°C/min

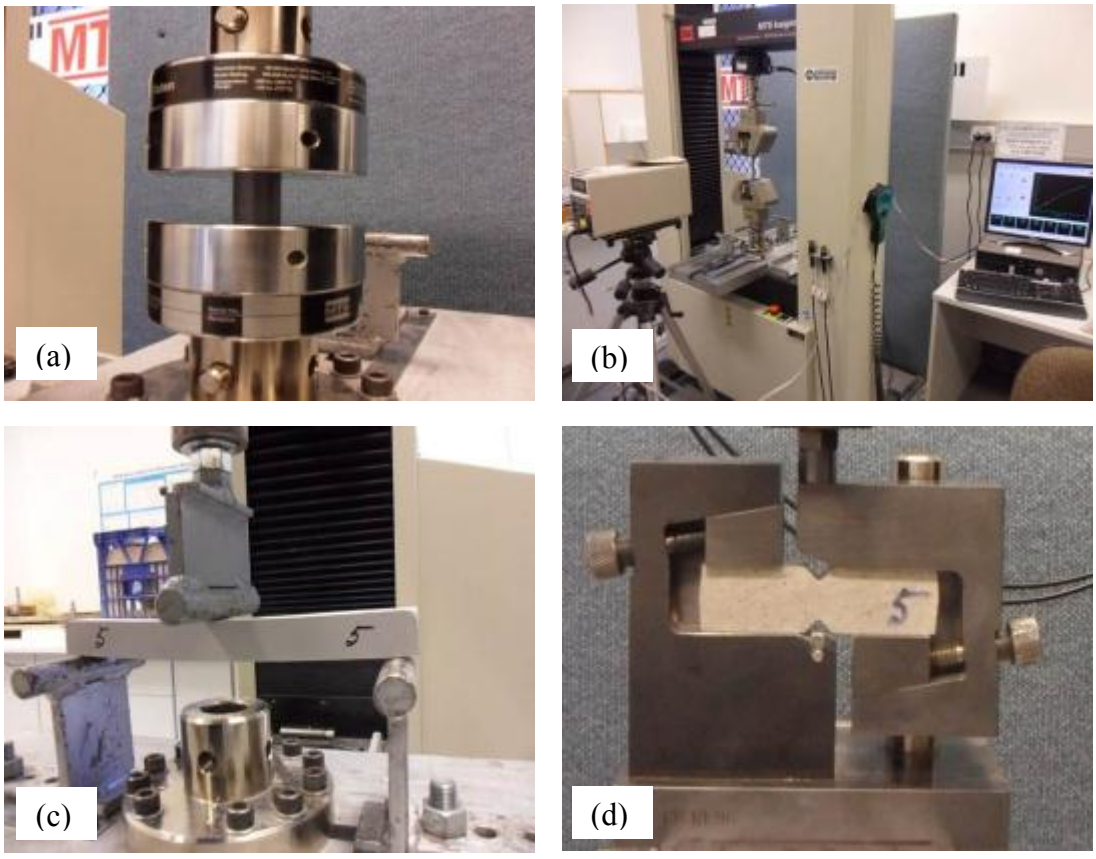

Figure 3.2 Mechanical tests of the grouts; (a) compressive, (b) tensile, (c) flexural and (d) shear

3.2.3.2 Thermal analysis

Dynamic Mechanical Analysis (DMA) and Modulated Differential Scanning Calorimetry (MDSC) methods were used to determine the glass transition temperatures of the grouts at 7 days. The dynamic mechanical analyser used to carry out the dynamic test was a calibrated DMA Q800 with Universal Analysis 2000 V5.1 Build 92 manufactured by TA Instruments. Rectangular specimens with nominal dimensions of 60 mm long, 12 mm wide and 4 mm thick were prepared for the DMA analysis. The specimens were clamped in the three-point bending fixture

of the DMA apparatus and were tested according to ASTM E1640 (2009). The heating rate was 1ºC/min up to 180ºC. On the other hand, a calibrated DSC Q100 with Universal Analysis 2000 V8.1 Build 261 software manufactured by TA Instruments was used for the dynamic analysis. Dry nitrogen gas at 80 ml/min was used during the experiments to purge the DSC cell. Samples between 25-40 mg were enclosed in the standard DSC aluminium sample pans. Dynamic scans were performed at a heating rate of 10ºC/min from 35-150ºC.

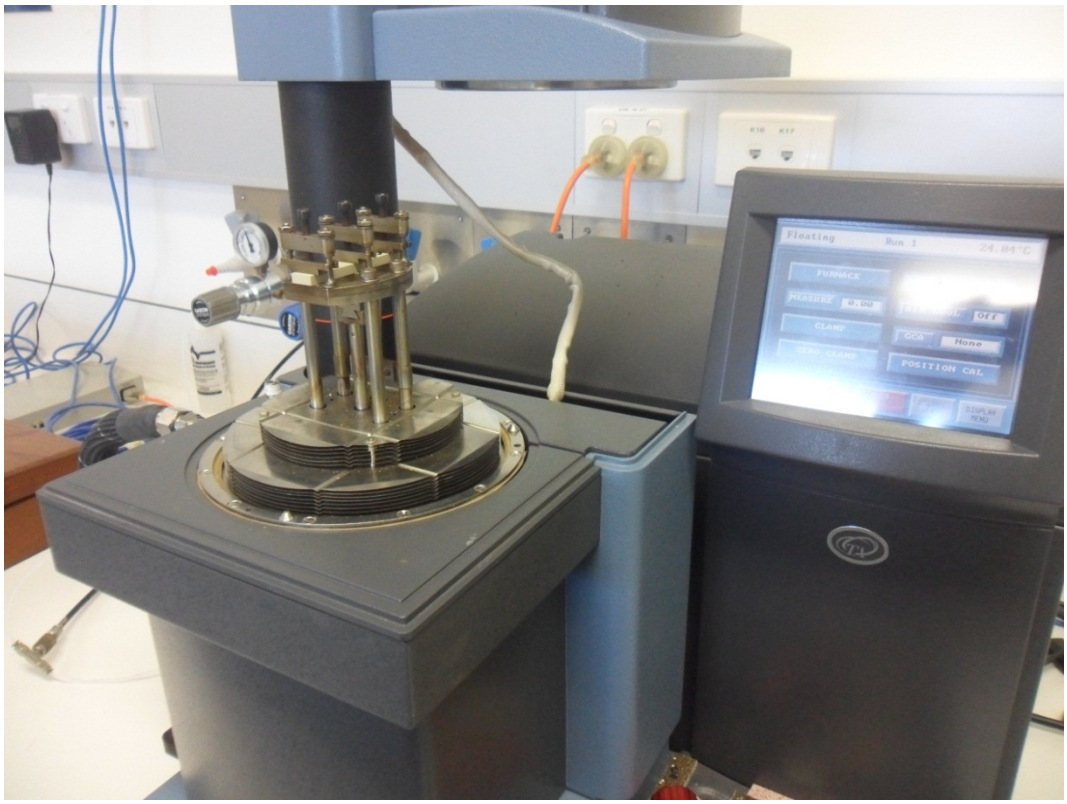

Figure 3.3 DMA specimens mounted on test machines

3.2.3.3 Volumetric analysis

Based on the mechanical properties of the grouts, two grouts C and E were selected for volumetric investigation. Mechanical and thermal properties of these grouts were found adequate for structural repair of pipelines. Besides, grout C and E are chosen as representatives of fine-filled and coarse-filled system, respectively. It is to be noted that grout E was obtained by introducing coarse filler in grout C. Volumetric analysis was thus carried out on these two grouts to investigate the improvement in the volumetric shrinkage due to addition of coarse filler. Test detail of volumetric analysis is discussed in Appendix A.

3.3 Experimental results and discussion

3.3.1 Compressive properties

A summary of the test results of the grouts is given in Table 3.3. The lowest strength and stiffness are found for grout A. This is expected as grout A has the lowest resin content among grouts A, B and C. The yield and ultimate compressive strengths of grouts A are found to be 52 and 67 MPa, respectively. Also it can be seen from the table that grout E exhibited the highest compressive strength and

stiffness among the investigated grouts despite having the lowest resin content. The ultimate compressive strength and modulus of grout E are found to be 120 MPa and 11 GPa, respectively. Grout E has the highest filler content compared to all other grouts. Thus grout E including coarse filler gain the advantage of achieving higher strength and modulus than that of other grouts.

Table 3.3 Summary of the 7-day compressive properties

Grouts	Yield strength (MPa)	Modulus of elasticity (GPa)	Strain at yield stress (10^{-2} mm/mm)	Ultimate strength (MPa)	Strain at ultimate strength (10^{-2} mm/mm)
A	52.03 (0.18)*	1.70 (0.49)	5.62 (0.45)	67.31 (0.32)	26.55 (0.29)
B	65.86 (1.38)	3.44 (0.33)	3.23 (0.30)	74.01 (0.81)	22.63 (0.79)
C	106.14 (1.35)	5.57 (0.13)	3.43 (0.15)	106.14 (1.35)	3.43 (0.15)
D	100.90 (1.29)	7.01 (2.17)	2.30 (0.23)	100.90 (1.29)	2.30 (0.23)
E	119.53 (3.48)	10.99 (0.69)	1.87 (0.10)	119.53 (3.48)	1.87 (0.10)

*Values in the parenthesis are standard deviation

3.3.1.1 Stress-strain behaviour

Figure 3.4 shows the typical compressive stress-strain behaviour of the tested grouts tested after 7 days. The stress-strain plot suggests that the grouts show two distinct patterns when loaded under uni-axial compression. The behaviour of grouts A and B are found to be different compared to C, D and E grouts. The compressive specimens of grouts A and B show an elastic behaviour followed by a plastic deformation. Grouts A and B exhibit peak stresses at the plastic zone. The stress-strain behaviour in compression specimens of grout C fall beyond the yield stress. However, the stress of grouts D and E in the post-yield region fall suddenly when compared to the compression specimens of grout C. The yield stresses of grouts C, D and E are the maximum strengths indicated through the decline of stress beyond the yield stress. The stress remains almost constant after reaching the yield stress and is followed by prolonged linear ascent towards failure for the compression specimens of grout A. The stress in the compressive specimens of grout B drops after yield stress and then rises linearly towards peak stress. No distinct brittle-ductile transitions are observed in the compressive specimens of grouts A, B and C. The maximum stresses are observed at around 27 and 23% strain for the A and B grouts, respectively. From the plots, the yield strains of grouts A, B and C are found to be about 6%, 3% and 3%, respectively. The yield strains of grouts D and E are found to be within the range of 2 to 3%. This behaviour of grouts A, B and C indicates the fundamental characteristics of the typical compressive stress-strain behaviour of polymers (Jang & Jo 1999; Siviour et al. 2005). Compressive stress-strain behaviour was characterised by Chen et al. (2002) into five stages: linearly elastic, non-linearly elastic, yield-like behaviour, strain softening, and nearly perfect plastic flow. The behaviour of grouts A and B follow the first four stages. However, the stress increases with strain rather than the expected perfect plastic flow. This post-strain hardening phenomenon of polymers is also reported in (Littell et al. 2008b; Siviour et al. 2005). The possible reasons for this strain hardening under compression are described later in Section 3.3.1.2. The stress-strain relationship of grout C is similar to the ideal behaviour shown by the fine filled epoxy resin where the stress descends after yield stress (Chow 1991). Similarly, the post-yield descending relationship is

also found apparently similar to the polyester based filler materials (Sirimanna et al. 2012). Grouts D and E, which contain coarse filler, show compressive stress-strain behaviour similar to polymer concretes rather than that of polymers (Vipulanandan & Paul 1990).

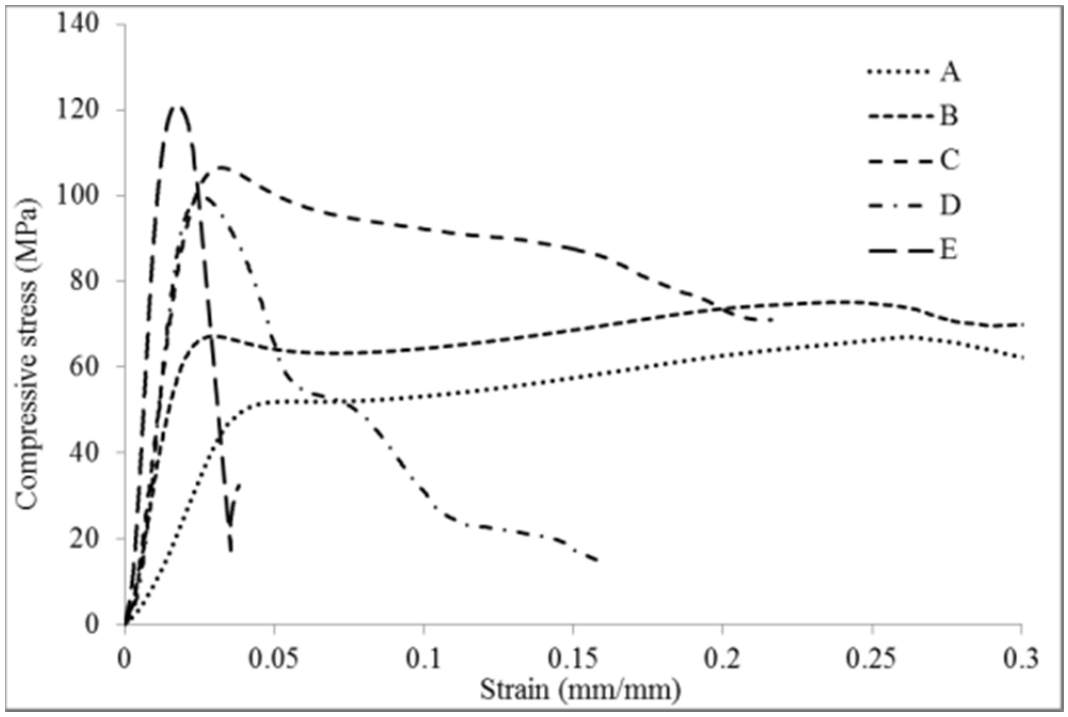

Figure 3.4 **Typical stress-strain behaviour of 7-day compressive specimens**

3.3.1.2 Failure mechanism

Figure 3.5 demonstrates the failure patterns of grouts A, B, C, D and E under uni-axial compression. Under compression, grouts A and B exhibit considerable circumferential bulging after the initial elastic behaviour. The radial deformation is less in grout C. There is no significant lateral expansion in grouts D and E. This behaviour can also be observed in the stress-strain curve in Figure 3.4, where there is no significant post-yield hardening in grouts C, D and E. The bulging continues until failure which is initiated by vertical cracks at the peripherally expanded specimens. The bulging starts after the linear elastic zone. From the stress-strain and failure behaviour, it is evident that grouts A, B and C form internal cracks during yield stress.

The post-yield behaviour of the specimens of grouts A and B under compression is dominated by bulging beyond axial yield strain and finally the specimens split into pieces. Since, the lateral deformations are larger during the failure of the specimens; it is reasonable to presume that the yield strength prior to elastic zone of grouts A and B as a design parameter in applications, where cracking of the infill layer is not expected. During both the post-yield elastic softening and elastic hardening of grouts A and B, bulging continues without visible cracks. However, the visible cracks in the outer periphery of grouts A, B and C occur prior to maximum stresses. In the cases of grouts A and B, these outer vertical cracks occur in the transition period between post-yield hardening and peak stress prior to failure. Interweaved randomly oriented micro cracks were observed in grouts C, D and E prior to formation of large cracks.

Figure 3.5 shows that grouts A, B and C form cup-and-cone beneath the outer shell which has been separated during the nonlinear elastic deformation. It is obvious that the frictional force between the platens and the specimen surfaces creates a horizontal compressive force, eventually forming cones at the ends. The wedges in the compression specimens form at an angle of about 45º with the vertical axis for grouts A, B and C. Although, the orientation of cracks in the outer shell of in grouts A and B are vertical, the initiation of these cracks in grout C are not vertical (about 45º inclined) at the mid-height of the specimens which is demonstrated in Figure 3.5c. The formation of wedges and the separation of the outer shell is more visible in grouts A and B than it is in grout C. The ultimate failure pattern of grouts D and E is randomly oriented and followed by a sudden split sound prior to the yield/peak stress. The stress-strain behaviour of grouts A and B exhibit post-yield hardening beyond 5% strain. This behaviour is due to the meeting of the failure wedges (cup-and-cone formed) caused by continuous loading for up to a prolonged strain. Another reason for the hardening is the axial resistance provided by the outer shells that is separated from the internal wedges.

3.3.2 Tensile properties

Table 3.4 provides the summary of the strength and modulus of the investigated grouts in tension, flexure, shear as well as their thermal properties at 7 days. It can be seen from the table that the tensile strength of the investigated grouts is between 11 and 32 MPa and the tensile modulus is between 3 and 17 GPa. Grout C exhibited the highest tensile strength of 32 MPa. Although the strength and resin content in grouts D and E are less than that of grout C, higher tensile moduli are obtained in grout D and E with values of about 15 and 17 GPa which are about three times higher than that of grout C. Hence the inclusion of filler has resulted in an increment of stiffness in grouts D and E.

3.3.2.1 Stress-strain behaviour

The comparison of the typical stress-strain behaviour from each type of the grout is shown in Figure 3.6. Two distinct stress-strain behaviours are observed. Grouts A, B and C show a relatively prolonged ductile deformation under tensile load with grout C exhibiting the highest strength among these grouts. This behaviour may be due to the fine filler in the grout matrix. Grouts D and E have moderate strength and the specimens have failed at lower strains than that of grouts A, B and C. All the grouts failed due to splitting, which is perpendicular to the length. It is evident that the inclusion of coarse filler has contributed to the reduction of the tensile strength of grouts D and E.

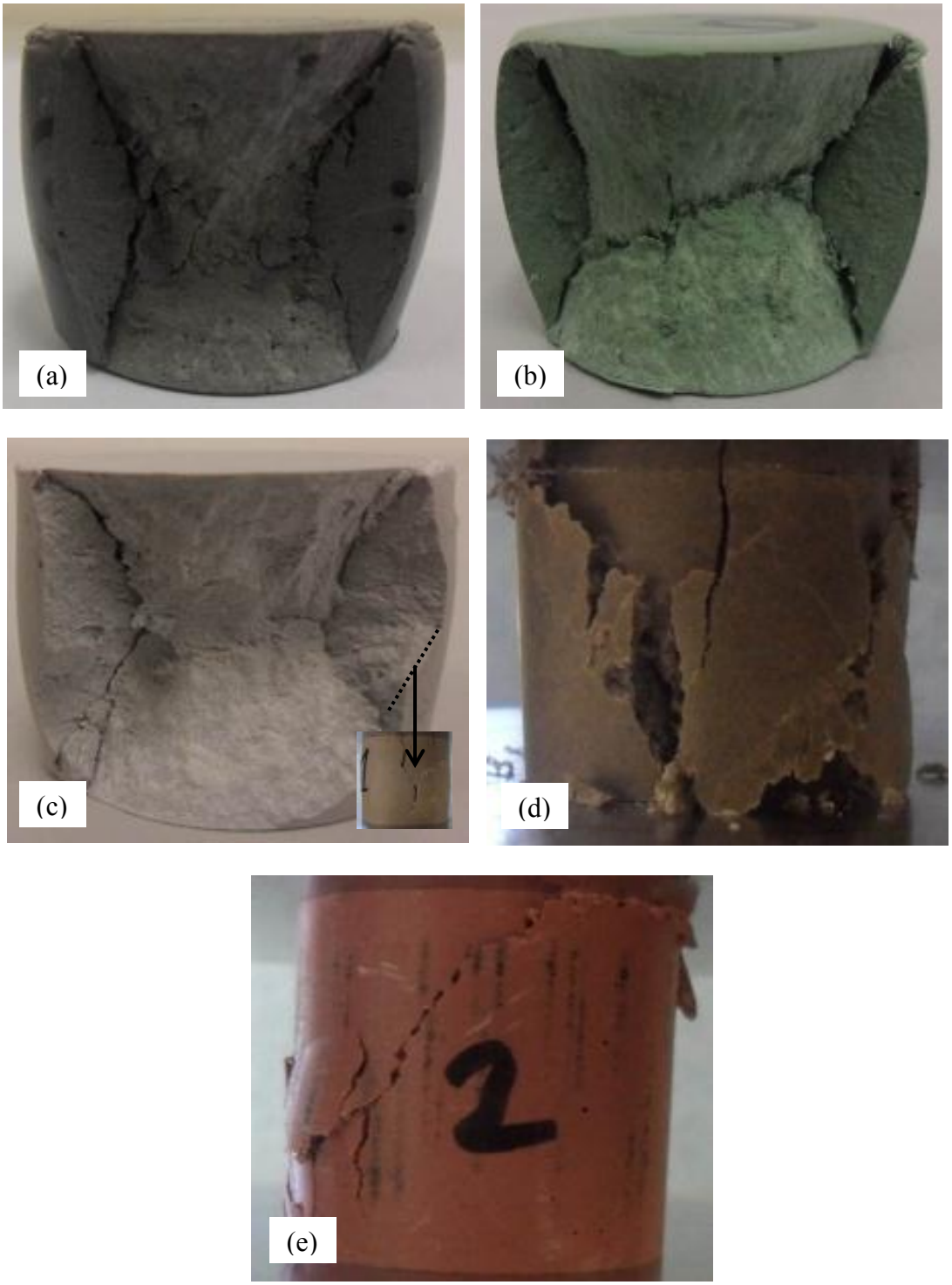

Figure 3.5 **Failure patterns of grouts under compression; (a) grout A, (b) grout B, (c) grout C, (d) grout D and (e) grout E**

Table 3.4 Summary of 7-day tensile, flexure, shear and thermal properties

Properties			Grouts				
			A	B	C	D	E
Tensile	Tensile strength (MPa)		11.27 (2.66)*	23.67 (1.08)	31.97 (3.45)	21.20 (1.56)	19.14 (0.84)
	Tensile modulus (GPa)		3.25 (0.53)	3.63 (0.11)	4.90 (0.81)	14.76 (1.99)	16.52 (4.68)
Flexural	Flexural strength (MPa)		27.43 (3.99)	40.61 (2.39)	53.04 (1.62)	34.60 (2.20)	34.87 (2.59)
	Flexural modulus (GPa)		3.76 (0.54)	3.52 (0.23)	6.15 (0.24)	13.02 (0.74)	12.81 (0.71)
Shear	Shear Strength (MPa)		13.37 (0.94)	21.83 (0.80)	29.97 (1.88)	25.29 (0.79)	28.18 (1.85)
Glass transition	DMA (°C)	T_g	38	40	59	60	53
		T_t	60	62	83	85	90
	DSC (°C)		43	58	59	60	60

*Values in the parenthesis are standard deviations

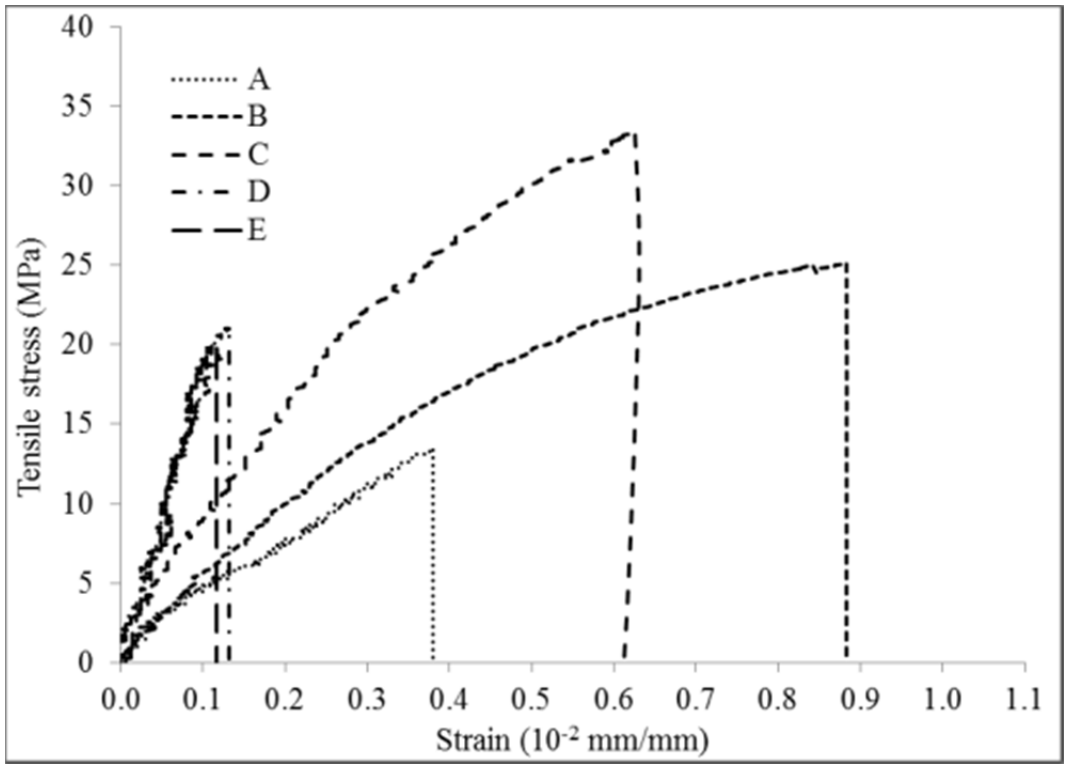

Figure 3.6 Typical stress-strain behaviour of tensile specimens

3.3.2.2 Failure mechanism

The failure pattern of tensile specimens of grouts A, B and C is comparable and exhibit smooth texture on the cracked surface. Figure 3.7 shows the typical failure surfaces of the tensile specimens. Failure surface of grout B shown in the figure represents grouts A, B and C. The cracked surfaces of both grouts D and E show that the matrix failure occurs through the aggregates. The action of the coarse filler in the resin matrix can be described in two different ways. The first possibility is that the aggregate is strong enough to provide sufficient resistance against failure where the failure occurs at the interfaces of the resin matrix and the aggregate, provided the matrix is also stronger than the interfacial bonding energy. The second possibility is that the aggregate is weaker than both the resin matrix and the interfacial bond. These options were discussed in Suwanprateeb (2000) for fine calcium carbonate in a polyethylene composite. Hence, it is evident that the interfacial bond is stronger than the resin matrix, and eventually, the resin matrix is stronger than the aggregates. This behaviour justifies the reduction of strength in the tensile specimens, especially in grout E. The coarse aggregate is acting as filler rather than reinforcement. Due to the reduction of content in the total volume, the major contribution of strength which comes from the resin matrix is also reduced. Similarly, relative ductility that is seen in grouts A, B and C which comes from the resin is also reduced. Hence, the stiffness has increased in the coarse filled grouts. Figure 3.7 demonstrates the voids that were trapped in the cured grouts. This also results in relatively higher standard deviations for the modulus values in grouts D and E. The coarse filler is often recommended to improve the curing and shrinkage performances in the grouts necessary for structural repair.

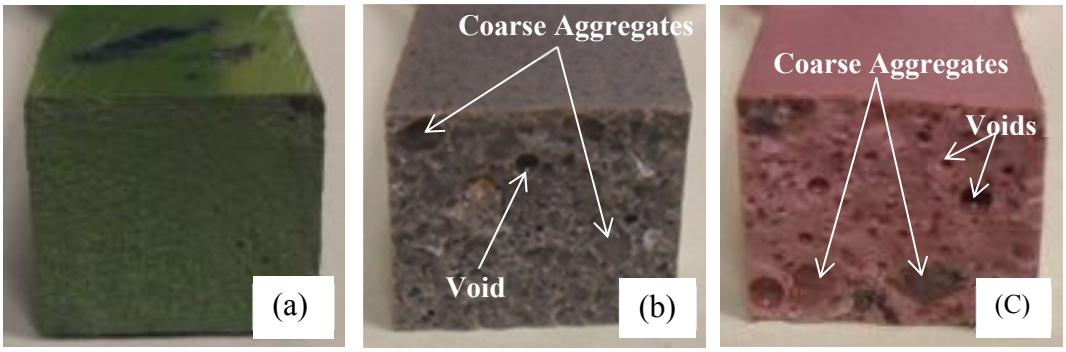

Figure 3.7 **Typical failure surface of tensile specimens; (a) grout B, (b) grout D and (c) grout E**

3.3.3 Flexural properties

Figure 3.8 shows a typical comparison of the load-deflection behaviour of the grouts in flexure. All the grouts show linear elastic load-deflection behaviour prior to failure. The flexural behaviour of the grouts is relatively comparable to their respective tensile behaviour. The load-deflection behaviour of grouts D and E show lower strength as well as lower deflection than that of other grouts. As an example, grout E shows about 1.5 times lower flexural loading than that of grout C, whereas the deflection reduces by about 3 times. This indicates brittleness of grouts D and E due to the inclusion of coarse aggregate. As shown in Table 3.4, grout C has the highest flexural strength while grout E's strength is 34% lower than grout C due to the addition of coarse filler. The flexural stiffness of grouts D and E is found to be about 13 GPa.

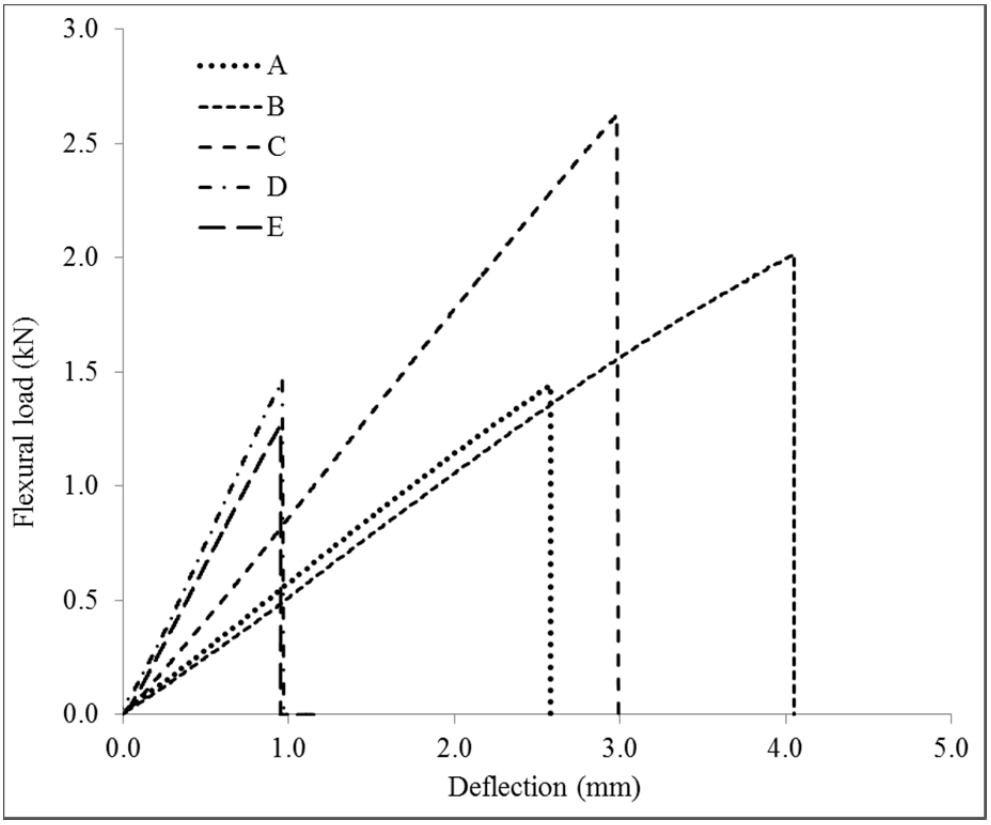

Figure 3.8 **Typical flexural load-deflection behaviour**

The typical failure patterns of the flexural specimens of the grouts are shown in Figure 3.9. All specimens fail in a brittle manner. In grouts D and E, the crack formations are almost vertical and perpendicular to the length of the specimens. However, the cracks deviate from its tension zone alignment when they propagate towards the compression zone for grouts A, B and C. From the flexural strength it can be correlated that the deviation of crack line and formation of compression wedge was more evident with the increment of flexural capacity. Clearly defined compression wedge is formed in grout C. Also, the inspection of the cracked surface suggests that the failure of the resin matrix propagates through the aggregates. This behaviour is also comparable to the tensile behaviour discussed earlier. Figure 3.10 shows the relationships between the direct tensile and flexural tensile properties of the grouts indicating a comparable trend in these properties. Higher direct tensile properties of the grouts result in correspondingly higher flexural properties. This comparability indicates that the flexural failure in the specimens is governed by tension which is also evident from the initiation of cracks in the tension zone.

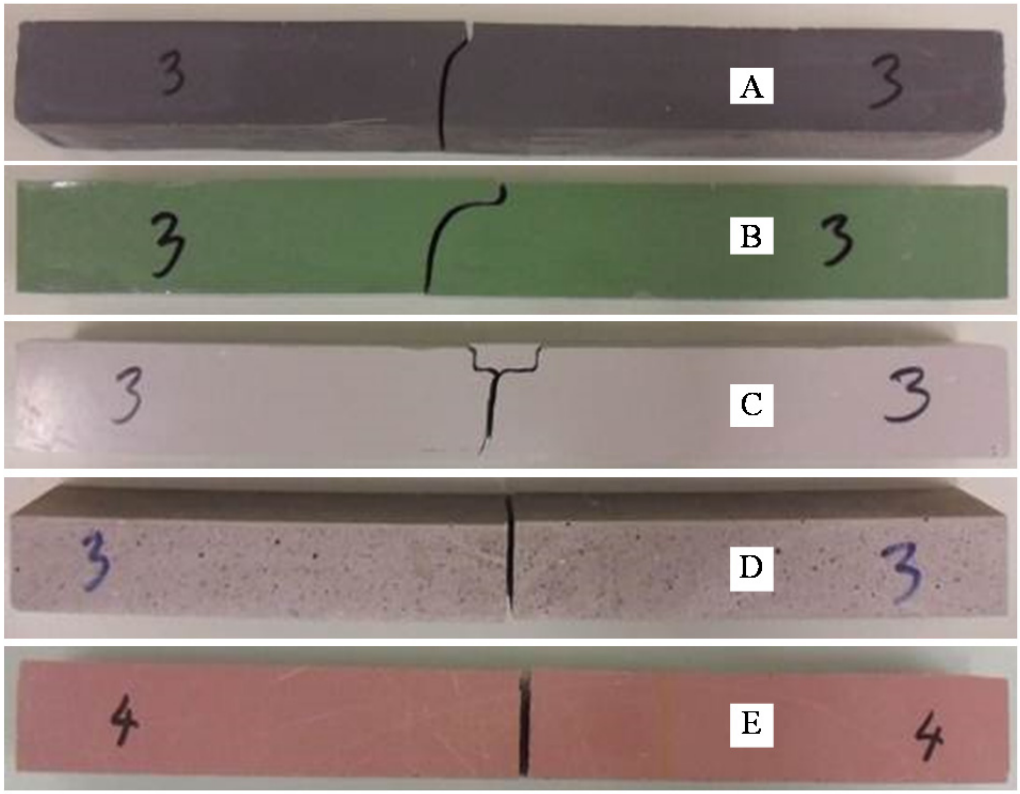

Figure 3.9 Typical failure of the flexural specimens

3.3.4 Shear properties

Table 3.4 shows that the shear strength of grouts A, B, C, D, and E are 13, 22, 30, 25, and 28 MPa, respectively. Figure 3.12a shows the relative comparison of load and crosshead displacement of the grout under shear loading. The failure occurs suddenly after the peak load with no prior warning. Figure 3.12b shows the typical crack generation in shear specimens. The failure is composed of two diagonal cracks and a failure wedge in between the cracks. The direction of the cracks is within the ranges between 30-40º. One crack runs from the top of the bottom notch diagonally towards the top plane surface and the second crack runs almost parallel from bottom

of the top notch towards the bottom plane surface forming a shear wedge. A combination of shear and tensile failure was also observed in epoxy resin specimens where the higher inclination with the vertical axis was related to dominance of shear failure (Araki et al. 2005). Hence, it is evident that the failure in the grouts is governed by a combination of shear and tension rather than pure shear.

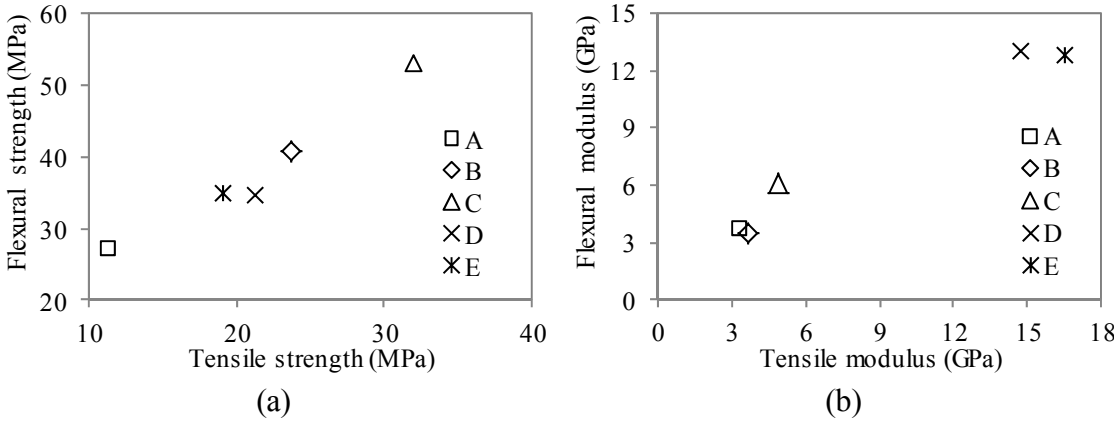

Figure 3.10 **Relationship between 7-day; (a) flexural and tensile strength, and (b) flexural and tensile modulus**

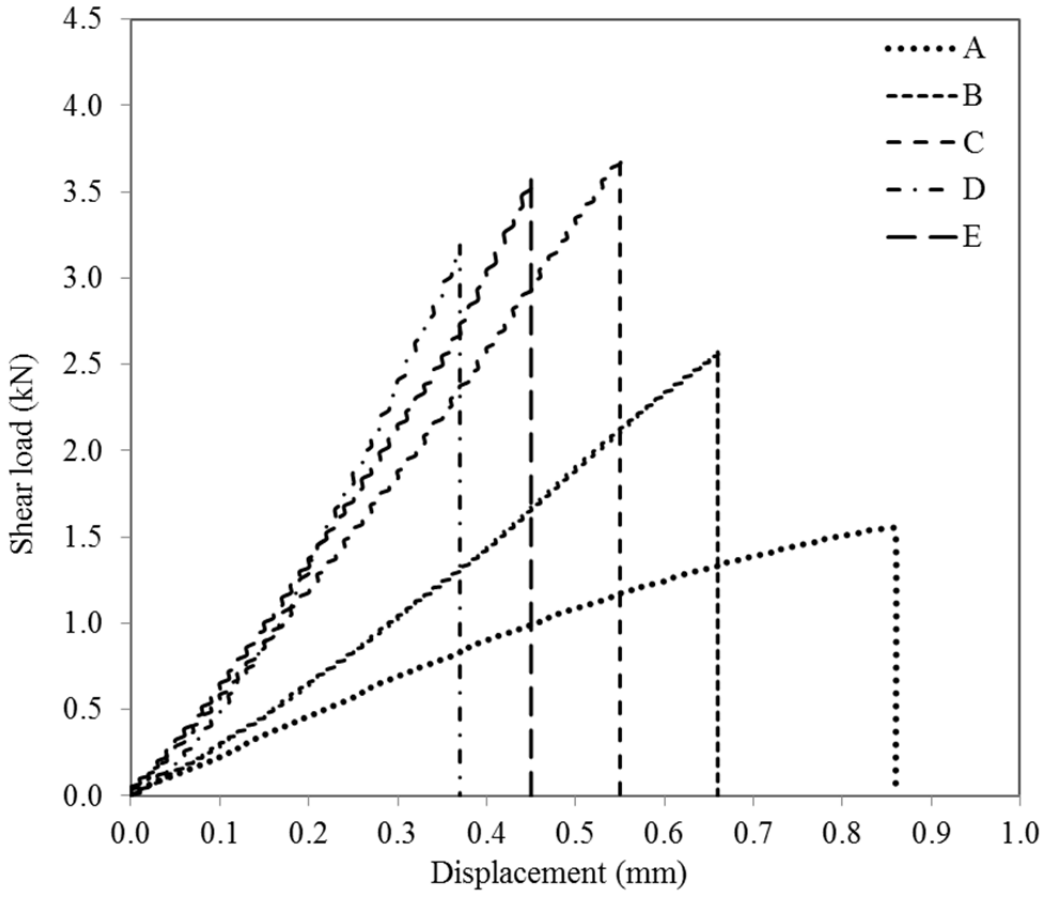

Figure 3.11 **Typical load-displacement behaviour of shear specimens**

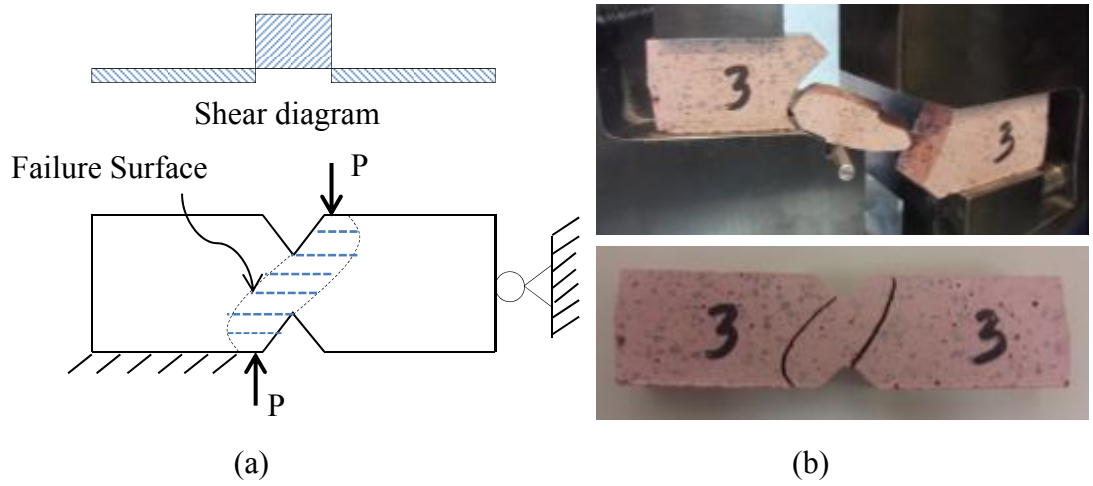

Figure 3.12 **Typical shear specimens under loading; (a) shear behaviour and (b) failure in the shear specimens**

3.3.5 Thermal properties

Thermoplastics and thermosets undergo molecular changes under elevated temperature. These changes become evident through physical changes. The temperature that causes transition in the polymer from a glassy state to a rubbery state is the glass transition temperature (T_g). DSC measures the change in heat flow, whereas DMA measures the change in modulus in the specimen under continuously increasing temperature. The glass transition obtained from DSC analysis suggests a consistent lower T_g value than DMA results as indicated in the existing literature (Lee & Park 2010). Table 3.4 provides the summary of the glass transition temperatures of the grouts. Since DMA is considered to be the most sensitive method to determine glass transition for a filled thermoset matrix (Wolfrum et al. 2000), it is suitable to consider the glass transition from DMA method for pipeline repair.

Tangent of the phase angle is the ratio of dissipated energy to stored energy and is called tan delta (tan δ). The tan delta signals were used by both Li et al. (2000) and Goertzen & Kessler (2007) to determine thermal properties for the epoxy adhesive and the components of pipeline repair, respectively. ISO/TS 24817 (2006) refers to ASTM E1640 (2009) which suggests that glass transition temperature can be obtained from either transition of storage modulus (T_g), or peak of loss modulus (T_l), or peak of tan δ (T_t). In this study, T_g and T_l are presented since these values provide the extremes of glass transition range.

A superposition of the storage modulus, loss modulus and tan δ is shown in Figure 3.13. From this plot it can be seen that the storage modulus inflexion provides lower T_g than both the loss modulus and tan δ peaks. This behaviour is also comparable to Goertzen and Kessler (2007). Figure 3.14 shows storage modulus signals of the grouts against temperature. The T_g values of the grouts range from 38 – 60°C. The highest value of T_g is found to be 60°C for grout D. The T_g value of grout E is found to be 53°C which is about 6°C less than grout C. A comparative plot of the tan δ signals with temperature of the grouts is shown in Figure 3.15. The highest value of T_t is observed in grout E with a value of 90ºC which is about 6ºC higher than the T_t of grout C. Hence, the reduction of resin content in grout E does not reduce its glass transition temperature.

According to ASME PCC-2 (2006), the service temperatures of a repair component for non-leaking and leaking pipes should not be 20 and 30ºC less than the glass transition temperature (T_t), respectively. Hence, grouts C, D and E are deemed suitable in applications where the required service temperatures are 50 – 60ºC and 60 – 70ºC, respectively for the leaking and non-leaking pipe repairs when tan δ signal is considered.

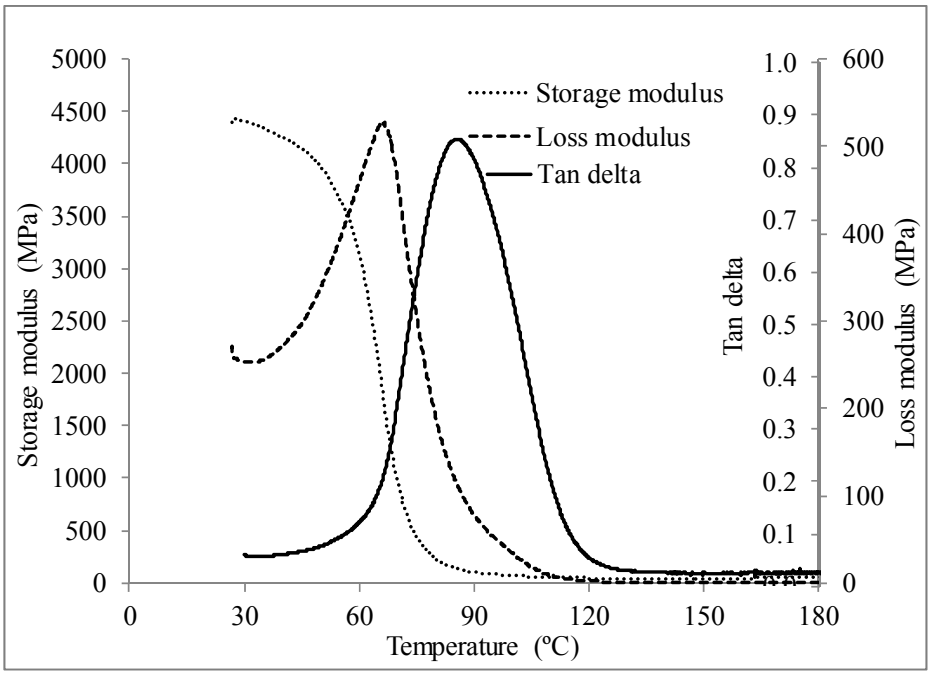

Figure 3.13 **Typical 7-day DMA signals plots for the grouts**

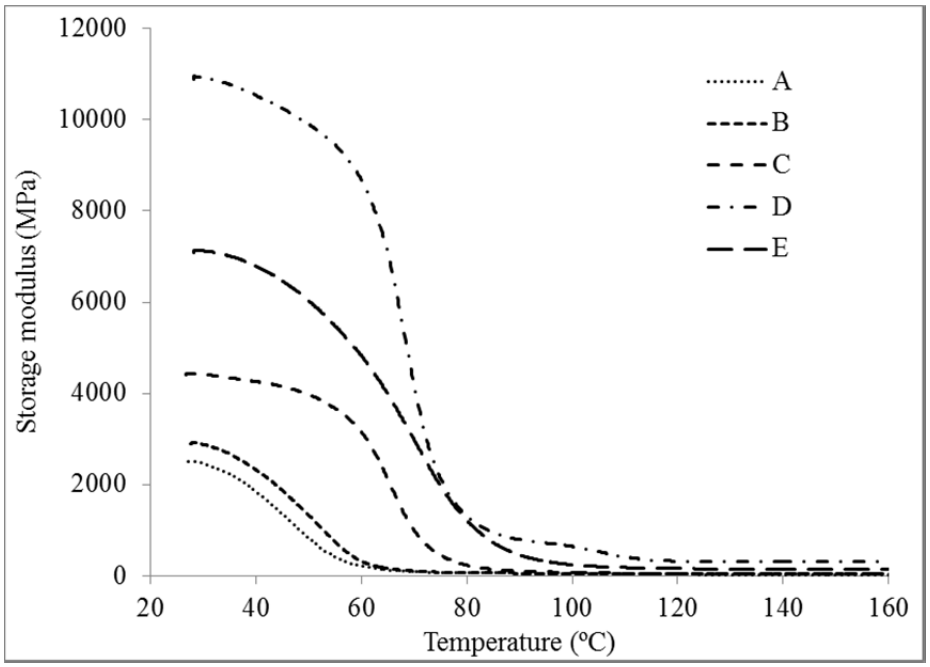

Figure 3.14 **Storage modulus plot of the grouts to determine T_g**

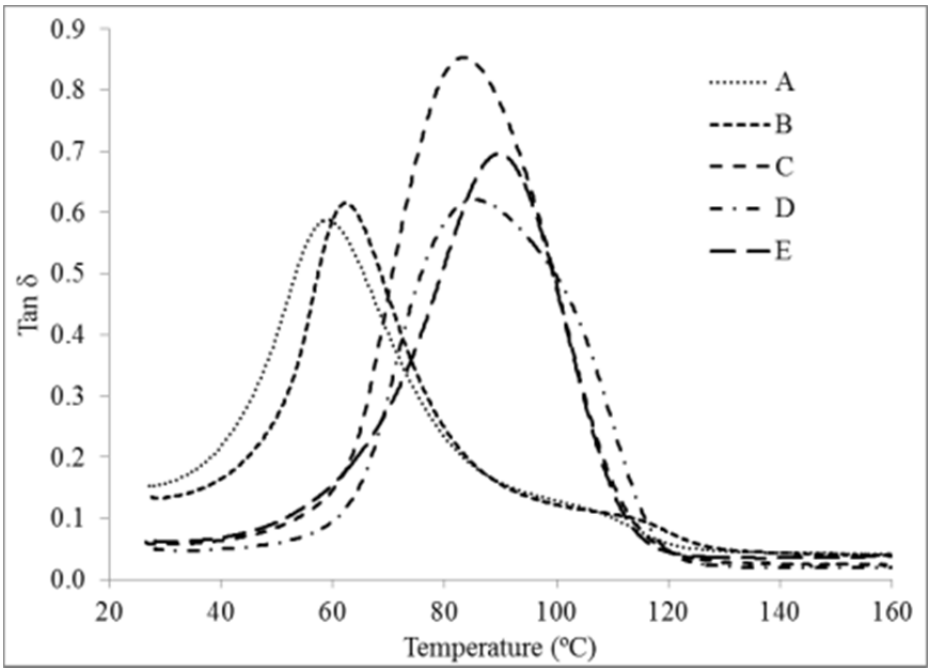

Figure 3.15 Tan δ plot of the grouts to determine T_t

3.3.6 Shrinkage properties

A fine-filled grout system was modified using coarse filler. Shrinkage properties of the epoxy grouts were investigated. Details of the results are given in Appendix A.

The maximum volumetric shrinkages exhibited by Grouts A and B over a 28 day period are about 2.77% and 1.09%, respectively. Most of the shrinkage occurs within the first 24 hours of mixing. The grouts achieve more than 80% and 90% of the 28-day shrinkage, over 1 and 7 days, respectively.

Grout C exhibited shorter gel time than that of grout E. Grout E underwent less volumetric shrinkage after gel time than that of grout C. The filled system exhibited higher reduction in post-gel shrinkage with a value more than 60% when compared to overall shrinkage on 28 days.

The filled grout experienced less shrinkage, and hence is expected to reduce the post cure stress and crack development. However, in the case of a mass grout pour in a confined space, gel time can be shorter. Hence, the effect of thickness and surrounding confinement behaviour of epoxy grouts should be considered for in-situ structural applications.

3.3.7 Behaviour with time

Among the investigated five grouts, the mechanical and thermal properties of grouts C, D and E are found to be higher than that of grouts A and B. Compressive properties were used in this study to investigate time dependency. Hence, grouts C, D and E were selected to identify their compressive behaviour over the 28 day period.

3.3.7.1 Effect of curing period

A summary of the compressive test results for the 25 mm diameter and 50 mm diameter cylindrical specimens of grouts C, D and E tested over 28 days are

given in Table 3.5. The compressive strength, modulus and yield strain are presented in the table. The compressive strength values of the grouts presented are the maximum compressive strength before failure of the specimens. The yield strain values are the peak strains for all the results other than 1-day strain of grout C where yield strain and peak strain are different. The average 1-, 3-, 7-, and 14-day compressive strengths of the 25 mm diameter specimens of grout C are about 36%, 78%, 85%, and 93% of its 28-day strength, respectively. Moreover, the average 1-, 3-, 7-, and 14-day moduli are about 13%, 79%, 95%, and 96% of its 28-day modulus, respectively. The relationships between the strength and stiffness along with time of the 25 mm diameter and 50 mm diameter compression specimens of grout C with time are shown in Figure 3.16 and Figure 3.17, respectively. Despite having lower stiffness at day 1, the specimens of grout C gained considerably higher stiffness within 3 to 7 days of curing. Grout C gained 36% of its 28-day compressive strength in day-1 and increased gradually over time.

The relationships between strength and stiffness of the 25 mm diameter and 50 mm diameter compression specimens of grout D with time are shown in Figure 3.18 and Figure 3.19, respectively. The 1-, 3-, 7-, and 14-day compressive strengths of grout D of the 25 mm diameter specimens are about 58%, 83%, 92%, and 93% of the 28-day compressive strengths, respectively. Moreover, the 1-, 3-, 7-, and 14-day moduli are about 41%, 65%, 73%, and 93% of the 28-day modulus, respectively. The strength gain in the early days (1 and 3 days) of grout D is higher (58% and 83%) than that of the stiffness (41% and 65%) in those periods.

Figure 3.20 and Figure 3.21 show the variations in the strength and modulus, respectively for grout E over time. The 1-, 3-, 7-, and 14-day compressive strengths of the 25 mm diameter specimens are 29%, 87%, 93%, and 96% of its 28-day compressive strength, respectively. Moreover, the 1-, 3-, 7-, and 14-day compressive modulus are about 18%, 87%, 98%, and 99% of the 28-day moduli, respectively. However, despite of having 29% and 18% of its 28-day strength and stiffness in day 1, respectively, grout E gains considerably much of its strength (87% and 93%) and stiffness (87% and 98%) within 3-7 days of curing.

Table 3.5 Summary of compression test results over different curing periods

Grouts	N	Parameters	1-day	3-day		7-day		14-day		28-day	
			25 mm	25 mm	50 mm	25 mm	50 mm	25 mm	50 mm	25 mm	50 mm
C	5	Yield Strength (MPa)	44.70 (0.42)*	97.36 (3.36)	101.18 (0.55)	106.14 (1.35)	114.19 (3.21)	116.53 (1.88)	116.78 (1.42)	125.44 (0.97)	-
		Modulus (GPa)	0.73 (0.16)	4.65 (0.57)	5.93 (0.22)	5.57 (0.13)	6.67 (0.37)	5.63 (0.57	6.93 (0.11)	5.87 (0.42)	-
		Yield Strain (x10^{-2} mm/mm)	2.36 (0.69[#])	3.69 (0.25)	3.25 (0.22)	3.43 (0.15)	3.10 (0.11)	3.35 (0.22)	3.21 (0.16)	3.68 (0.09)	
D	5	Yield Strength (MPa)	64.07 (2.11)	91.46 (2.02)	92.88 (1.96)	100.90 (1.29)	97.61 (2.63)	102.33 (0.80)	106.27 (0.73)	109.66 (2.95)	-
		Modulus (GPa)	4.01 (0.95)	6.26 (1.12)	8.60 (0.76)	7.01 (2.17)	8.61 (1.13)	8.95 (0.89)	11.75 (1.00)	9.68 (1.01)	-
		Yield Strain (x10^{-2} mm/mm)	3.20 (0.60)	2.54 (0.39)	2.01 (0.18)	2.30 (0.23)	2.11 (0.14)	2.06 (0.18)	1.65 (0.10)	2.12 (0.24)	-
E	5	Peak Strength (MPa)	37.86 (1.32)	112.06 (2.04)	-	119.53 (3.48)	120.06 (3.57)	123.26 (2.99)	-	128.59 (2.48)	126.48 (1.10)
		Modulus (GPa)	2.03 (0.19)	9.72 (0.52)	-	10.99 (0.69)	11.85 (0.15)	11.17 (1.01)	-	11.24 (0.57)	13.64 (0.82)
		Yield Strain (x10^{-2} mm/mm)	5.92 (0.50)	2.00 (0.05)	-	1.87 (0.10)	1.89 (0.07)	2.00 (0.22)	-	1.91 (0.05)	1.72 (0.19)

* Values in the parenthesis are standard deviations, [#]Peak strain = 34.46 (1.01) x10^{-2} mm/mm

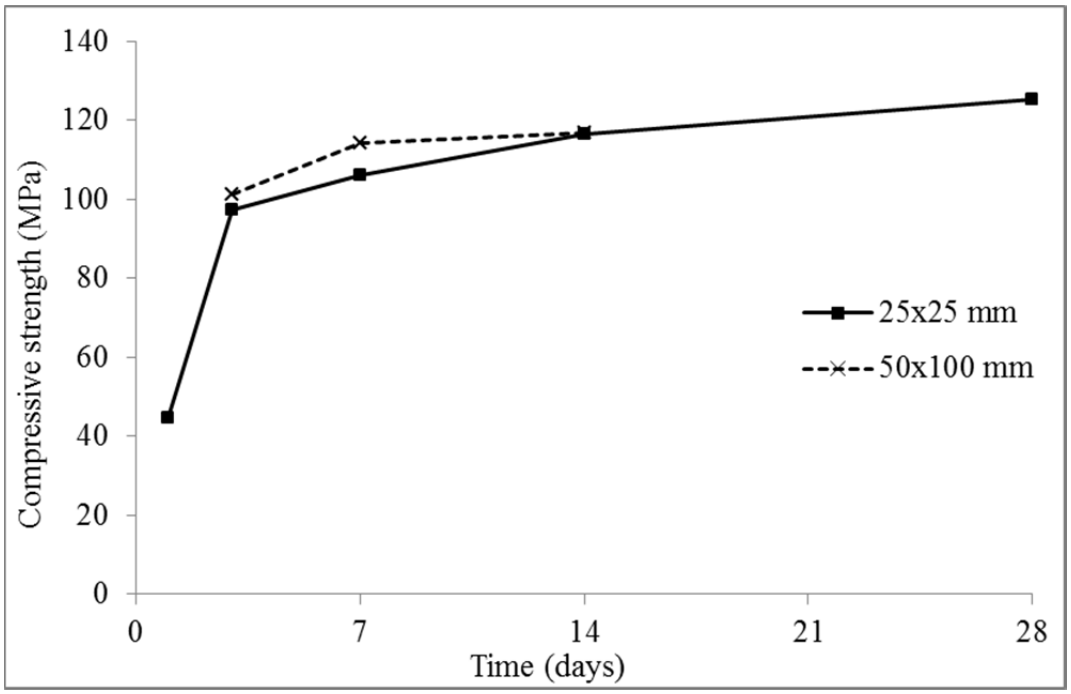

Figure 3.16 **Effect of curing period over compressive strength of grout C**

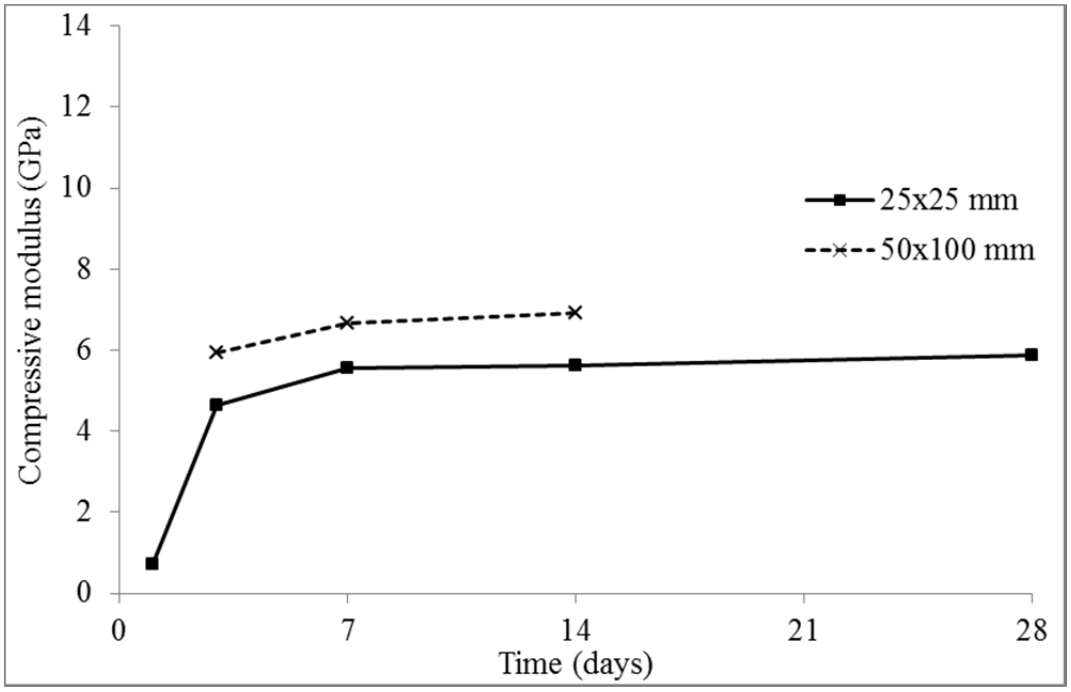

Figure 3.17 **Effect of curing period over compressive modulus of grout C**

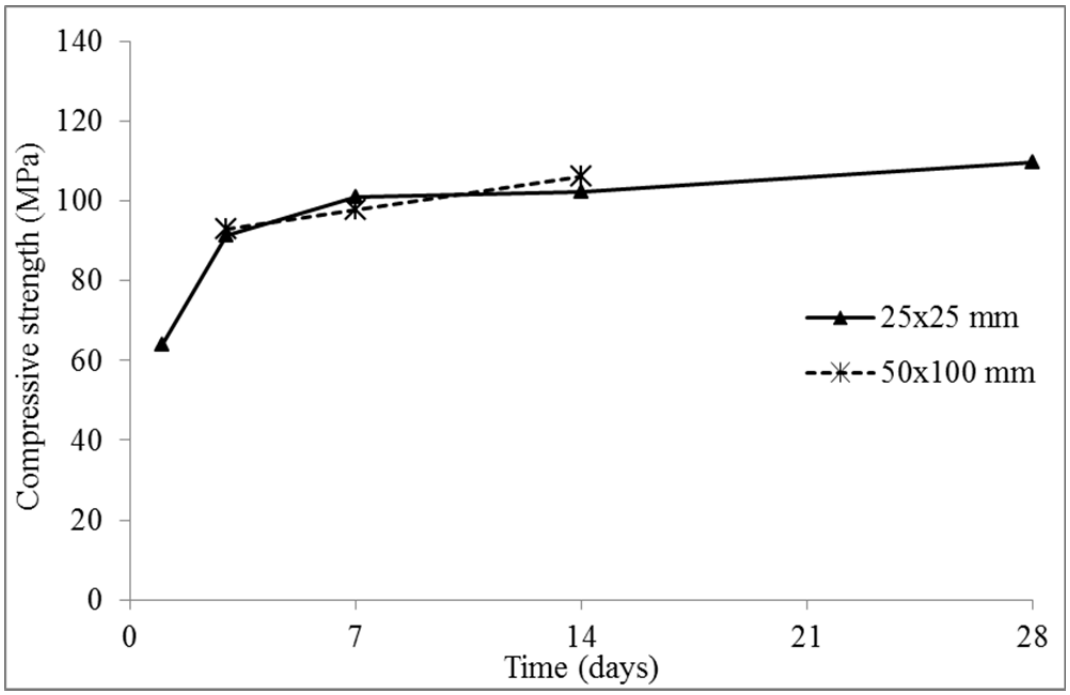

Figure 3.18 **Effect of curing period over compressive strength of grout D**

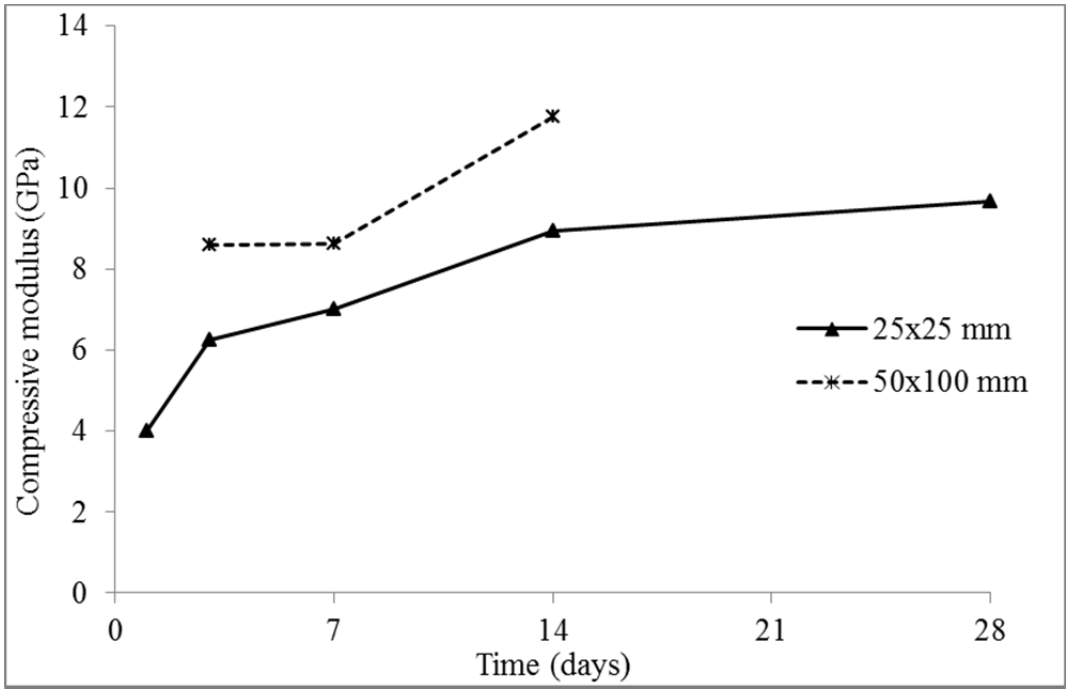

Figure 3.19 **Effect of curing period over compressive modulus of grout D**

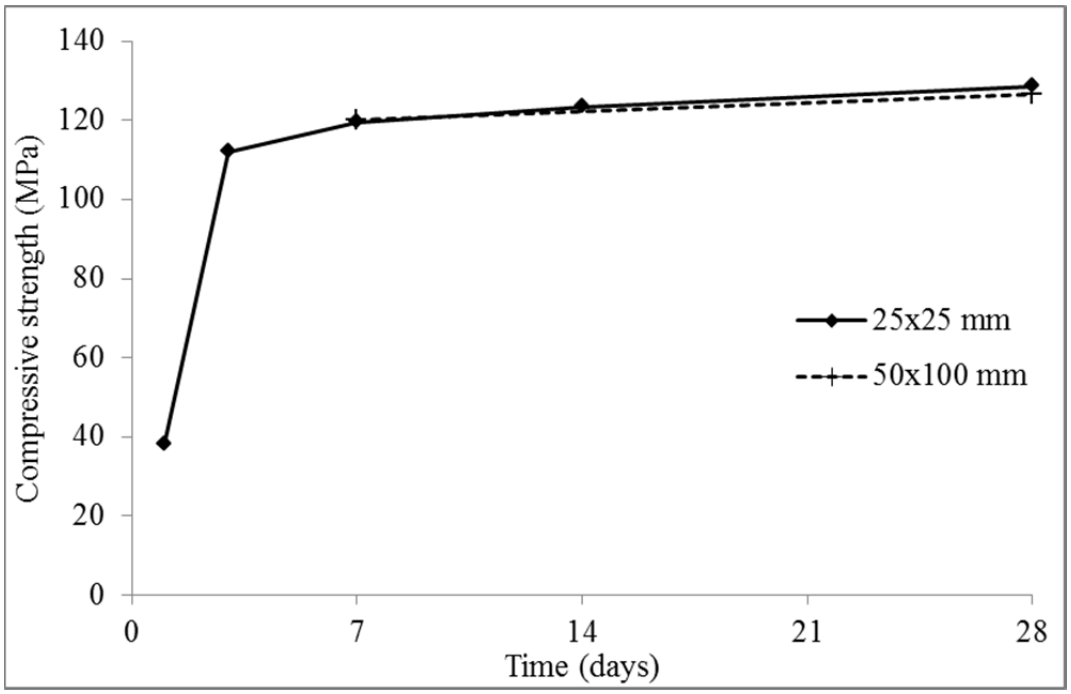

Figure 3.20 **Effect of curing period over compressive strength of grout E**

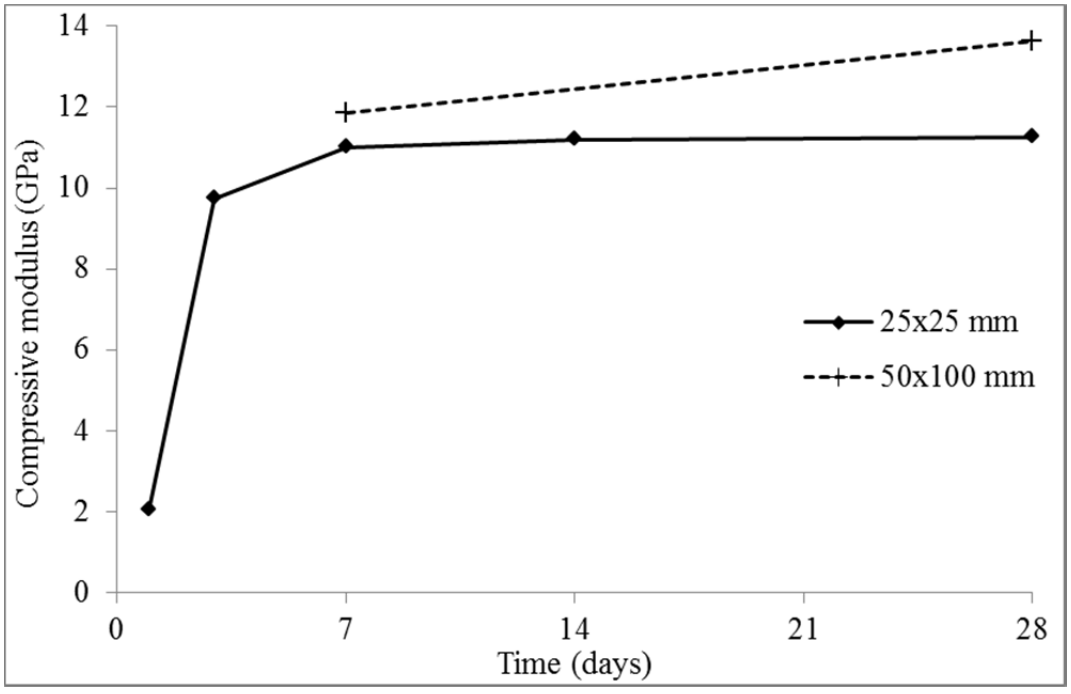

Figure 3.21 **Effect of curing period over compressive modulus of grout E**

A comparison of stress-strain relationships over the durations is shown in Figure 3.22 to Figure 3.24, where a typical behaviour from each of the test duration is plotted. At day 1, grout C exhibits plastic deformation until the maximum loading after the initial elastic deformation. The 3-, 7-, 14-, and 28-day specimens of grout C demonstrate initial elastic deformation until the yield stress and then the stress drops with the formation of cracks. This stress-strain relationship is usually observed in polymer concretes, which is discussed earlier in Section 3.3.1.1. Unlike grout C, the 1-day specimens of grout D shows initial elastic stress-strain behaviour and

subsequent decreasing stress prior to yielding (as seen from Figure 3.23). The typical stress-strain behaviour of grouts D and E over time show that their post-yield failure is sudden and the yield strains are lower than that of grout C. The development of strength of polymer concrete was studied by Vipulanandan and Paul (1993) where the development of strength exhibited a similar trend for polyester based polymer concrete which is comparable to the behaviour of grouts D and E.

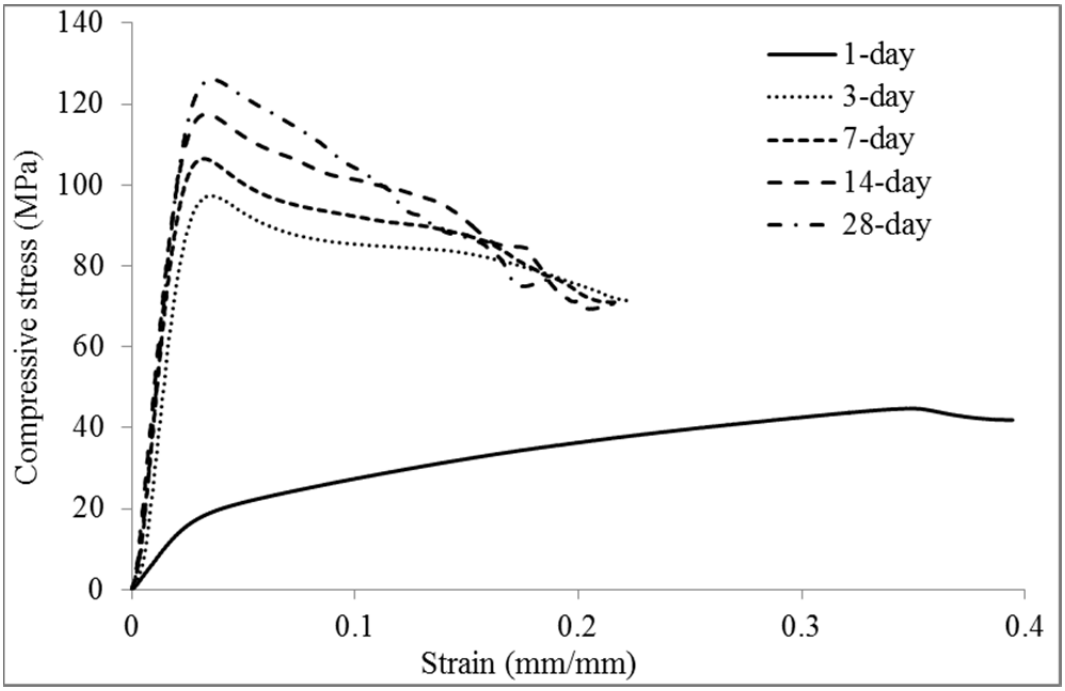

Figure 3.22 **Typical compressive stress-strain relationship of grout C**

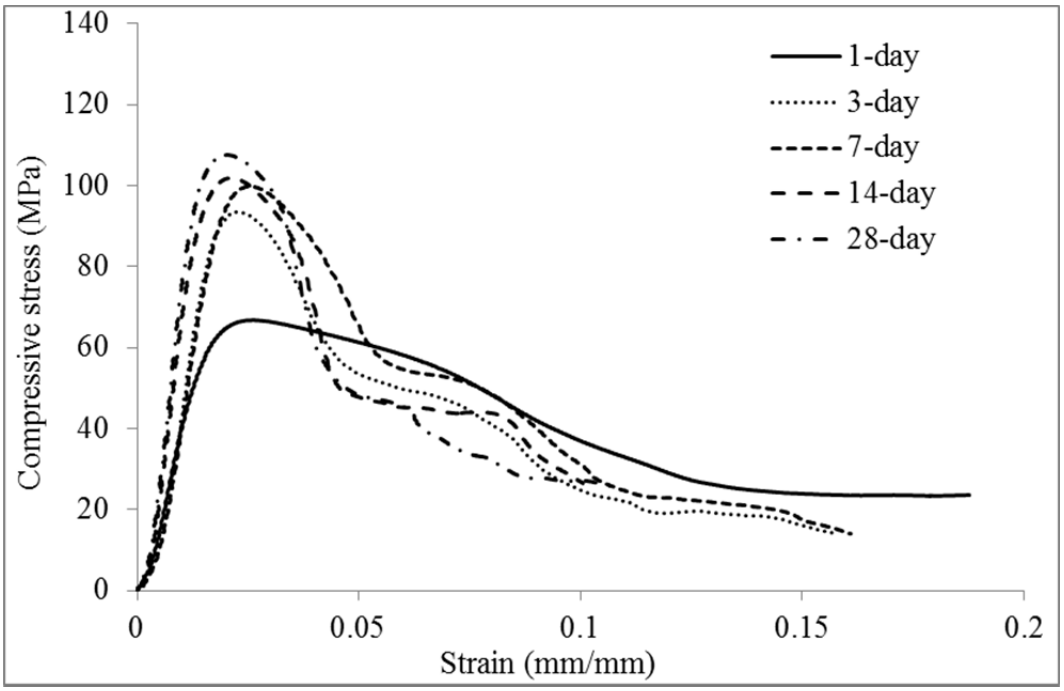

Figure 3.23 **Typical compressive stress-strain relationship of grout D**

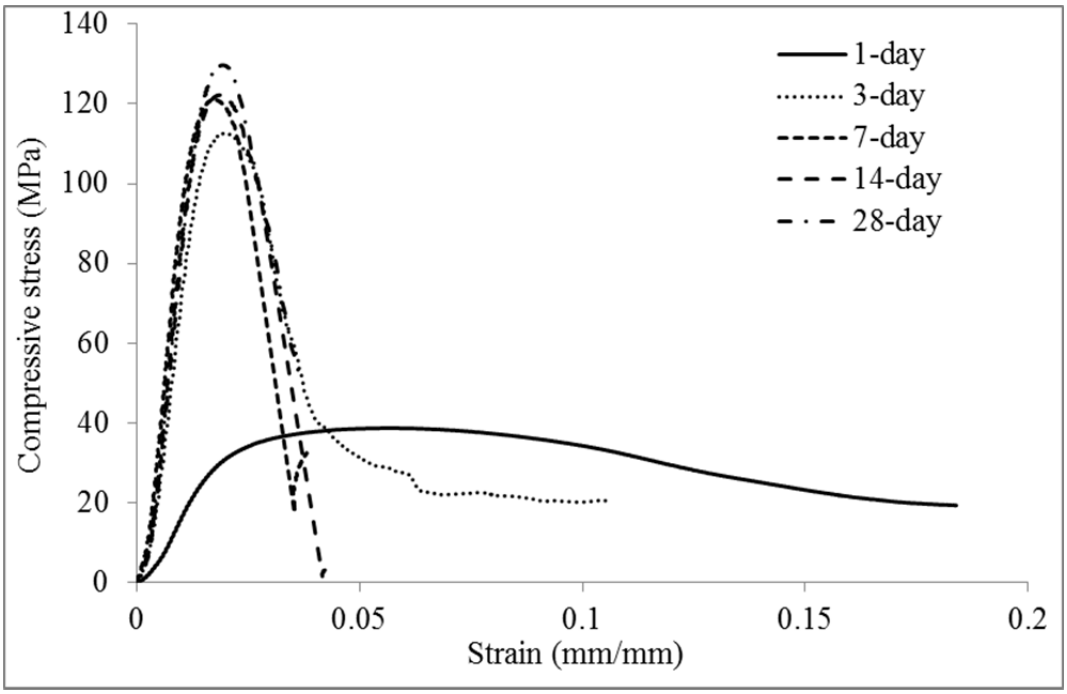

Figure 3.24 Typical compressive stress-strain relationship of grout E

3.3.7.2 Effect of curing period on failure mechanism

Typical failures of the 25 mm and 50 mm diameter specimens of grout C are shown in Figure 3.25 and Figure 3.26, respectively. The failure is initiated with circumferential bulging for all specimens of grout C up to 28 days. However, there is a gradual reduction in bulging with the extended curing duration. Split cracks are observed at the periphery of the specimens which is initiated with outward bulging primarily at the middle of the specimens. Internal cup-and-cone failures are observed for the 1-, 3-, 7-, and 14-day specimens of grout C, when the external spilt layers of the specimens were removed. The internal crack distribution is similar to Figure 3.5c. The 28-day specimens show a combination of vertical and diagonal cracks which end up forming columnar segments; not necessarily total split failure which can be seen in Figure 3.25e. The diagonal separation exhibited by the 28-day specimens of grout C is a typical failure in concrete cylinders and is also observed in grouts D and E, and is discussed later in this section. The external split failure is also observed in the 50 mm diameter specimens of grout C as shown in Figure 3.26.

Figure 3.27 to Figure 3.30 show the typical failure patterns of the compression specimens of grout D and E, respectively over time. The failures in the 25 mm diameter specimens of grouts D and E initiated with the randomly oriented cracks when tested at day 1. However, 1-day specimens of grout E do not break down to fragments indicating a lower rate of curing (still-soft) than that of grouts C and D. No distinct direction of the crack propagation is observed at day 1 for specimens D and E. Finally, the specimens split down to columnar fragments. All the 3-, 7-, 14-, and 28-day specimens along with all the 50 mm diameter specimen of grouts D and E show either a cone-type, or a single shear plane, rupture prior to failure. It can be seen from the 3 to 28 day specimens D and E that when a cone forms, the wedge splits the remaining cylinder. In the case of a shear failure, diagonal cracks open further through the sliding along the shear plane. In some cases, for example Figure 3.28b, the shear plane is extended throughout the

transverse corners of the specimen. The failure in the 14- and 28-day specimens of grout E is sudden and produces a crushing sound. The failure pattern of the compressive specimens of grouts D and E are comparable to the failure of the filled polymer for pile rehabilitation (Sirimanna et al. 2010).

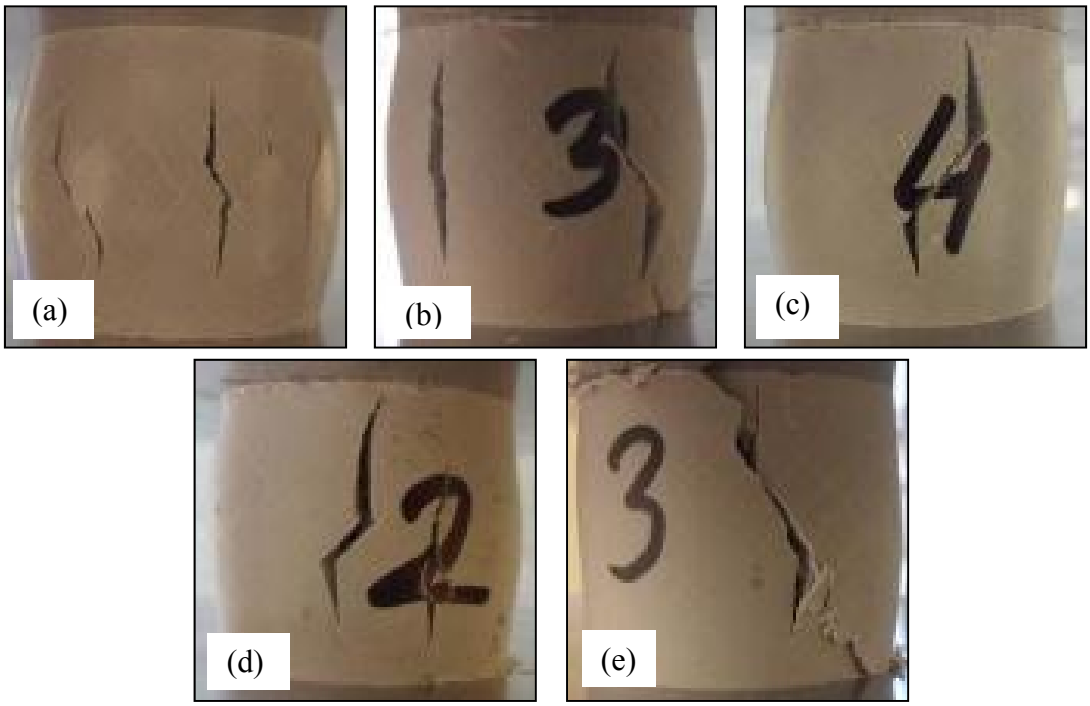

Figure 3.25 **Effect of curing age on compressive failures of the 25 mm specimens of grout C; (a) 1-day, (b) 3-day, (c) 7-day, (d) 14-day and (e) 28-day**

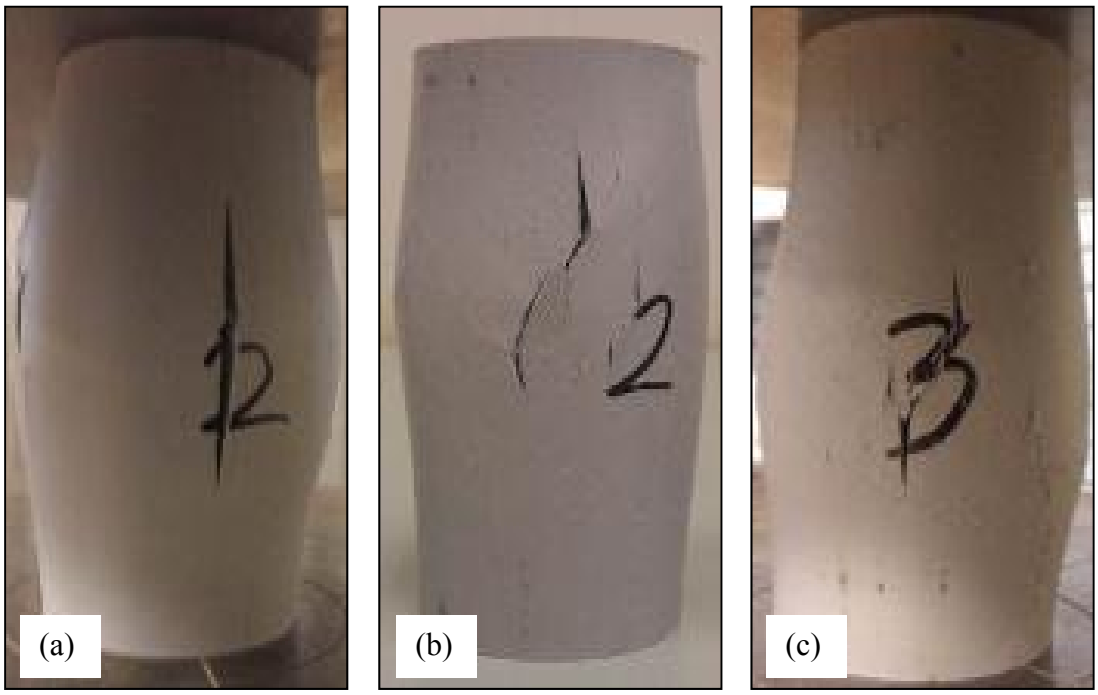

Figure 3.26 **Effect of curing age on compressive failures of the 50 mm specimens of grout C; (a) 3-day, (b) 7-day and (c) 14-day**

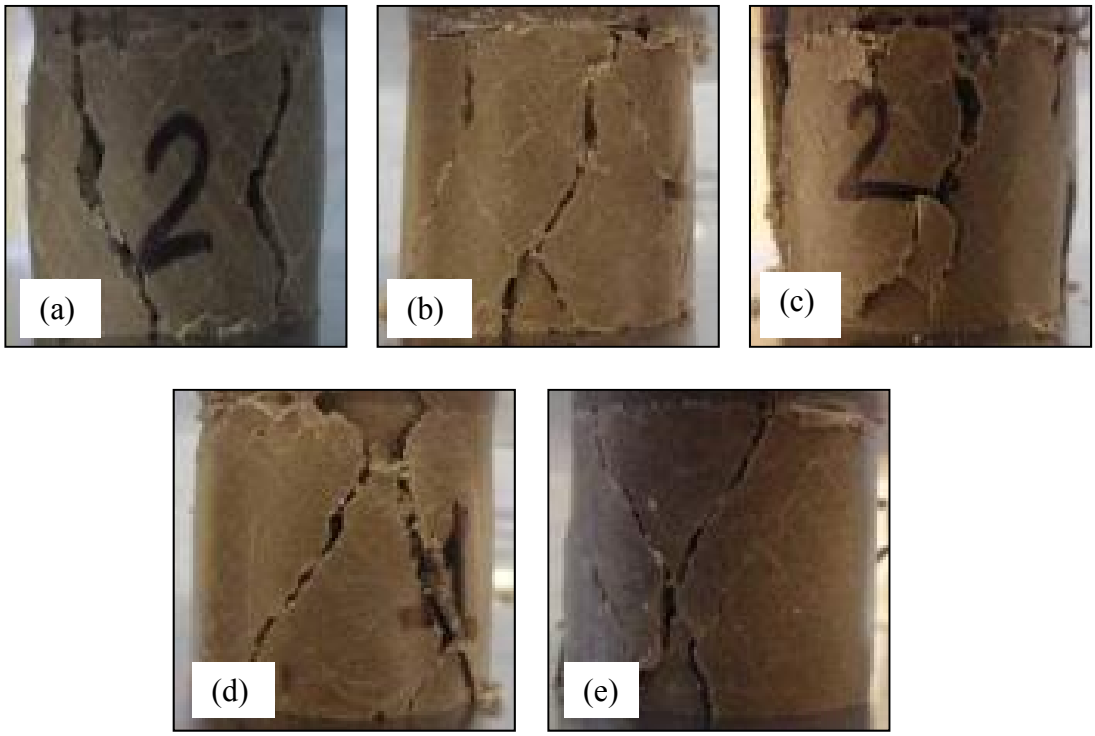

Figure 3.27 **Effect of curing age on compressive failures of the 25 mm specimens of grout D; (a) 1-day, (b) 3-day, (c) 7-day, (d) 14-day and (e) 28-day**

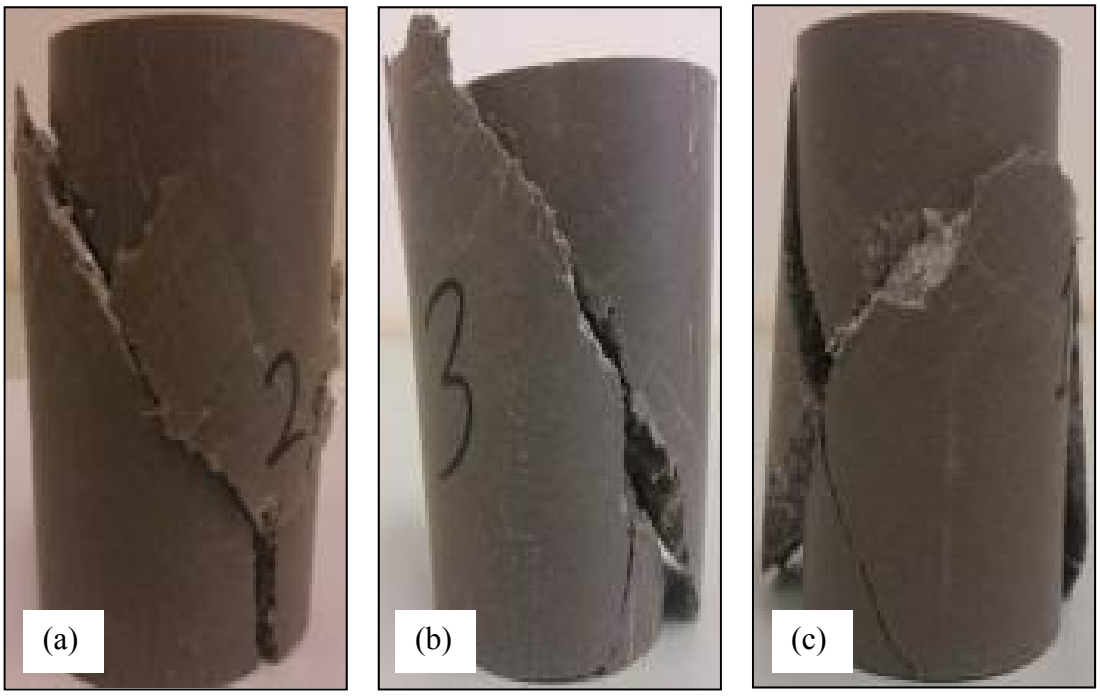

Figure 3.28 **Effect of curing age on compressive failures of 50 mm specimens of grout D; (a) 3-day, (b) 7-day and (c) 14-day**

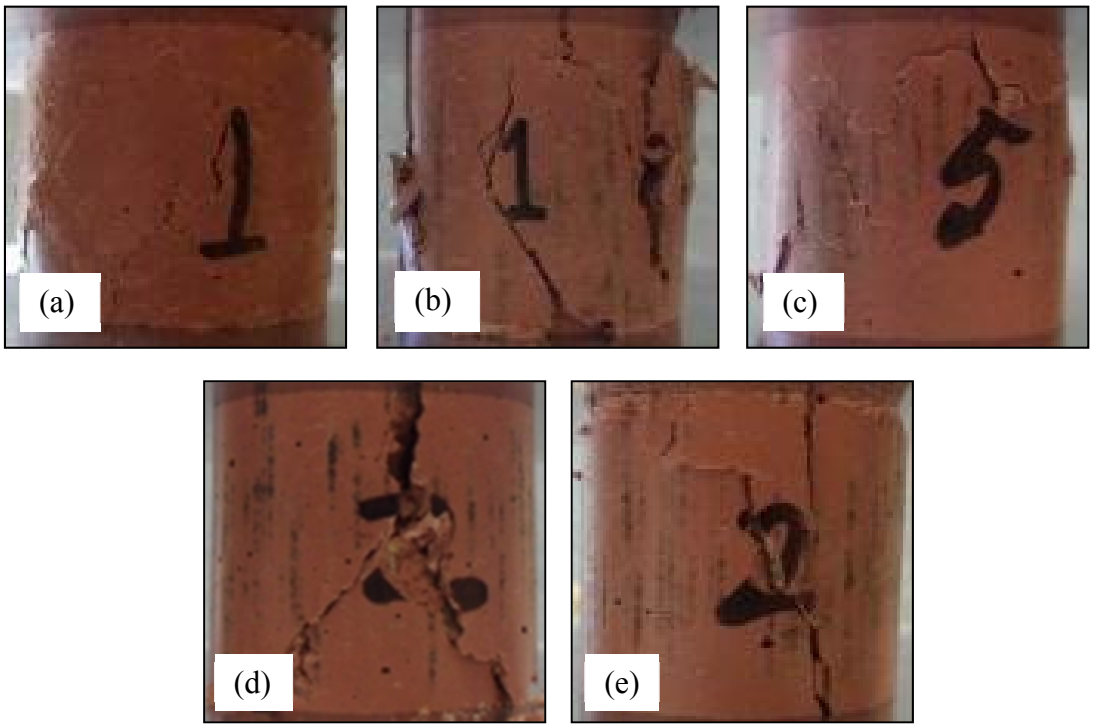

Figure 3.29 **Effect of curing age on compressive failures of the 25 mm specimens of grout E; (a) 1-day, (b) 3-day, (c) 7-day, (d) 14-day and (e) 28-day**

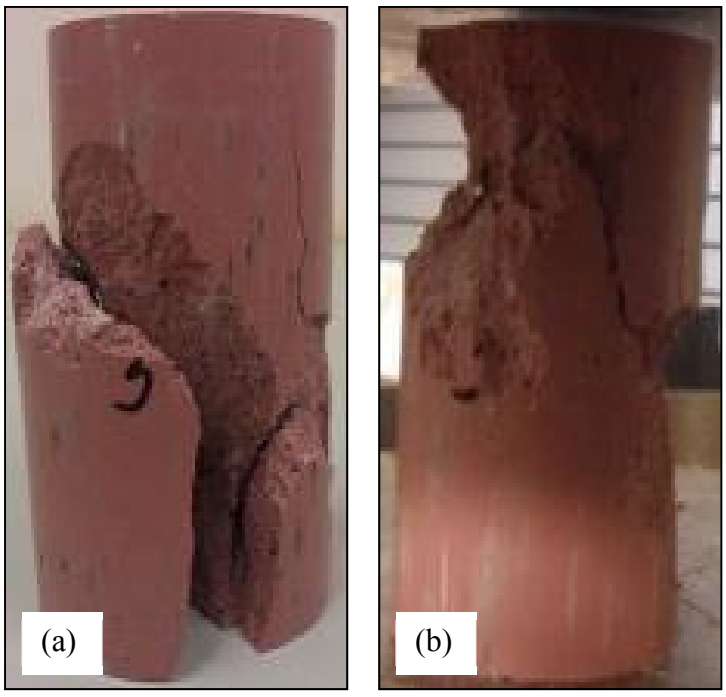

Figure 3.30 **Effect of curing age on compressive failures of the 50 mm specimens of grout E; (a) 7-day and (b) 28-day**

3.3.7.3 Effect of specimen size

Figure 3.16 to Figure 3.21 provide a comparison of strength and stiffness between the 25 mm and 50 mm diameter specimens. The compressive strengths of the 25 mm diameter compression specimens of grout C are found to be about 4, 7, and 0.2% lower than the 50 mm diameter specimens at 3, 7, and 14 days,

respectively. Similarly, the modulus values are found to be 22%, 17%, and 19% lower for the 25 mm diameter specimens than that of the 50 mm diameter specimens when compared on 3, 7, and 14 days, respectively. The average compressive strengths of the 25 mm diameter specimens of grout D are about 1.53 and 4% lower than the 50 mm diameter specimens at 3 and 14 days, respectively. However, the average strength for the 25 mm diameter specimens of grout D is about 3% higher than the 50 mm diameter specimens at 7 days. The moduli of grout D are about 27%, 19%, and 24% lower for the 25 mm diameter specimens than that of the 50 mm diameter specimens at 3, 7 and 14 days, respectively.

The average compressive strength of the 25 mm diameter specimens of grout E is found to be around 0.4% lower than the compressive strength of the 50 mm diameter specimens measured at 7 days. Whereas, the average 28-day compressive strength of the 25 mm diameter specimens is about 2% higher than that of the 50 mm diameter specimens. The average 7- and 28-day compressive moduli of the 25 mm diameter specimens of grout E are about 7% and 18% lower, respectively than that of the 50 mm diameter specimens.

The aim to include the 50 mm diameter specimens in this study was to validate the test results of the 25 mm diameter specimens and to study the effect of height-diameter ratio on the compressive properties. Kim et al. (1999) provided statistically determined relationship to consider the effect of the specimen size on the strength of concrete. The relationship is more suitable for the cylindrical concrete specimens with diameter range of 75 – 150 mm. According to the relationship, the compressive strength decreases with decreasing height-diameter ratio for the above mentioned cylinders. The authors also suggested that the height-to-diameter ratio of 1.0 might create certain irregularity in the prediction due to the effects of confinement and energy release zone. This relationship is also comparable to ASTM C 39 (2001) where a reduction factor of 0.87 is specified for height-to-diameter ratio of 1.0. Although the current study does not include concrete, it is expected that the strength will be lower for the 25 mm diameter specimens than that of the 50 mm diameter specimens. Hence, the deviation of the compressive strength that is found within the range of +7.05% to -1.67% is reasonable. However, the differences in the modulus values are found for the 25 mm diameter and 50 mm diameter specimens for grouts C, D and E for the tested days. Differences in the yield strains also observed as seen from Table 3.5.

3.3.7.4 Effect of specimen size on failure mechanism

The typical formation of initial dislocation of the surfaces in both the 25 mm diameter and 50 mm diameter compression specimens of grout C is shown in Figure 3.31a. This type of crack growth was also observed in epoxy adhesives under uniaxial compression which was studied by Asp et al. (1996), where cracks extended in various directions from some certain points creating star-like profiles. The formation of stress induced cracks in the outer surface of the specimens is comparable to the effects of microscopic fracture and failure leading towards macroscopic failure under compression loading (Horii & Nemat-Nasser 1985).

The typical internal failure in a 50 mm diameter specimen is shown in Figure 3.31b. The formation of inclined cracks in the outer periphery of the 25 mm diameter specimens are also observed in the 50 mm diameter specimens of grout C. The failure in the 50 mm diameter specimens is the combination of cup-and-cone on one side and split on the other side. The difference in failure pattern in the 25 mm

diameter and 50 mm diameter specimens may occur due to the height-to-diameter ratio. Due to the height-to-weight ratio of 1.0, the cones formed in the 25 mm diameter specimens of grout C are almost in contact with each other. Prior to bulging, the outer layer of the specimen starts separating from the formed cone. Thus, the failure is more governed by crushing. The load platens at the ends of the outer shell start to push down the separating shell and an outward radial bulging is observed. During the bulging under compression and associated friction from the adjacent cones, the outer shell acts as a confinement to the inner volume of the specimen. The shell itself experiences cracks under the stress induced by compressive loading, outward bending and circumferential strain. Overall, the descending branch of the stress-strain curve of the compressive specimens of grout C is less steep than that of grouts D and E. This indicates that the increased post-peak contribution in the fracture energy by the outer shell and crushed wedges.

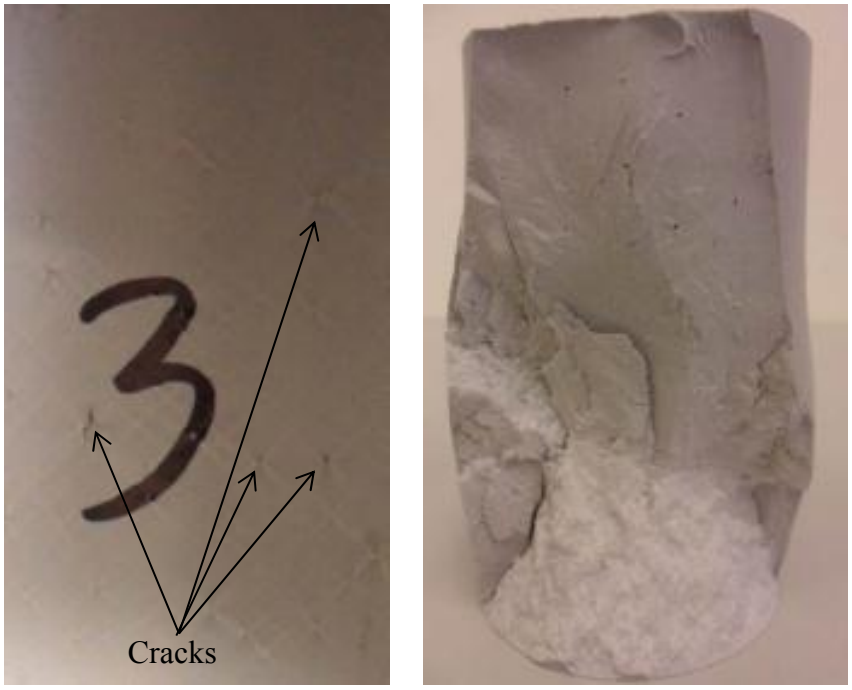

Figure 3.31 **Typical failure behaviour in the 50 mm grout C specimens; (a) initiation of crack formation, and (b) failure pattern**

During testing, the bulging in the outer periphery is observed at the middle of the specimens. However, Figure 3.26 shows that the vertical position of the circumferential bulging is not located exactly at the vertical centre of the compression specimens of grout C. Due to the action of lateral sliding after the post yield deformation, the sideway expansions are not perfectly horizontal. The height-to-diameter ratio for the 50 mm diameter compression specimens is 2.0, which led to the formation of a localised damage band in the middle of the compression specimens. This failure in the specimen has occurred due to cracking rather than crushing. The cracks in the damage band cause swelling in the middle of the specimens. The weaker central part of the specimen allows the upper and bottom fragments of the specimen to slide on each other following a suitable inclined plane. Hence, the lateral expansions shown in Figure 3.26 are slightly inclined from horizontal. Due to the sliding in the two fragments and the expansion of internal cracks, the outer shell of the 50 mm diameter specimen tends to split vertically.

Because of the friction from the load platen, the outer shell forms a cone at one end of the specimen. After the separation of one end, the remaining of the shell split up from the core. The tensile strength of grout C is found to be higher than that of grouts D and E and was discussed earlier in the chapter. Grout C has a higher resin-to-filler content than that of grouts D and E. Hence, it is believed that the cohesion of the specimen may play a governing role in the resistance against failure during the post-peak region of the compression specimens of grout C.

The stress-strain relationship of grout E shows that the stress drops down just after the peak stress. It should be noted by the appearance, that the 25 mm diameter specimens exhibit relatively more broken fragments than those in the 50 mm diameter specimens. Such fragmentation may occur due to the size effect of the 25 mm diameter specimens and in some cases due to slightly extended crushing prior to termination of the testing. The 50 mm diameter specimens produce large cones or shear wedge segments which separate without crushing each other, or the segments are strong enough to crush the obstructing fragments. However, due to the lower height-to-diameter ratio, the segments of the 25 mm diameter specimens crush further when broken fragments touch the platens during the post-peak loading.

3.3.7.5 Effect of coarse filler

Figure 3.32 and Figure 3.33 show the comparison of the strength and modulus, respectively between grouts C and E, when the 25 mm diameter cylindrical specimens are tested over time. The 1-day compressive strength of grout E is about 15% less than that of grout C. However, the 3-, 7-, 14-, and 28-day c strength of grout E are found to be about 15, 13, 6, and 3% higher, respectively than that of grout C. The increase in stiffness due to inclusion of coarse filler is more noticeable for all the test durations. The 1-, 3-, 7-, 14-, and 28-day strength grout E are found to be around 178%, 109%, 97%, 98% and 92% higher than that of grout C, respectively. In case of 50 mm diameter specimens, the compressive strength and modulus of grout E are found to be 5% and 78% higher than that of grout C. Hence, the inclusion of coarse filler by about 44% by volume (in addition to about 17% fine filler) has contributed to almost two times increase in the stiffness.

The behaviour of grout E is also similar to grout D in terms of post-yield stress-strain relation. Grout D contains about 78% (by weight) filler which is also reflected in the stiffness values. The stiffness of grout D for all curing periods is higher than that of grout C except for the 1-day stiffness. Golestaneh et al. (2010) reported that a higher compressive strength with an epoxy resin and a blend of fine and coarse filler can be achieved by adding only fine or coarse filler to polymer concrete. The improvement in strength using blend of fine and coarse filler was also reported by Kang and Hussin (2008), where brittleness was reduced by optimising the filler contents. The drastic fall in the stress-strain curve of grouts D and E in Figure 3.23 and Figure 3.24, indicate the sudden failure and increasing brittleness due to the addition of coarse aggregate.

3.4 Evaluation of epoxy grouts for pipeline repair

According to Mendis (1985), all the tested grouts having a compressive strength of more than about 40 MPa have the potential to be used in crack repairs. Table 3.6 shows the relevant mechanical properties suggested for a range of repair and rehabilitation works. Based on their properties, grouts C, D and E have the potential to be used in the structural rehabilitations as their compressive strengths are

more than 80 MPa. Furthermore, a high performance grout with the compressive strength of 85 MPa is suitable for rehabilitating fatigue-damaged tubular joints (Thandavamoorthy et al. 2001). Thus, epoxy grouts with compressive strength within this range have the potential for use in the composite repair of steel pipelines. It follows that grouts C, D and E are suitable for this application.

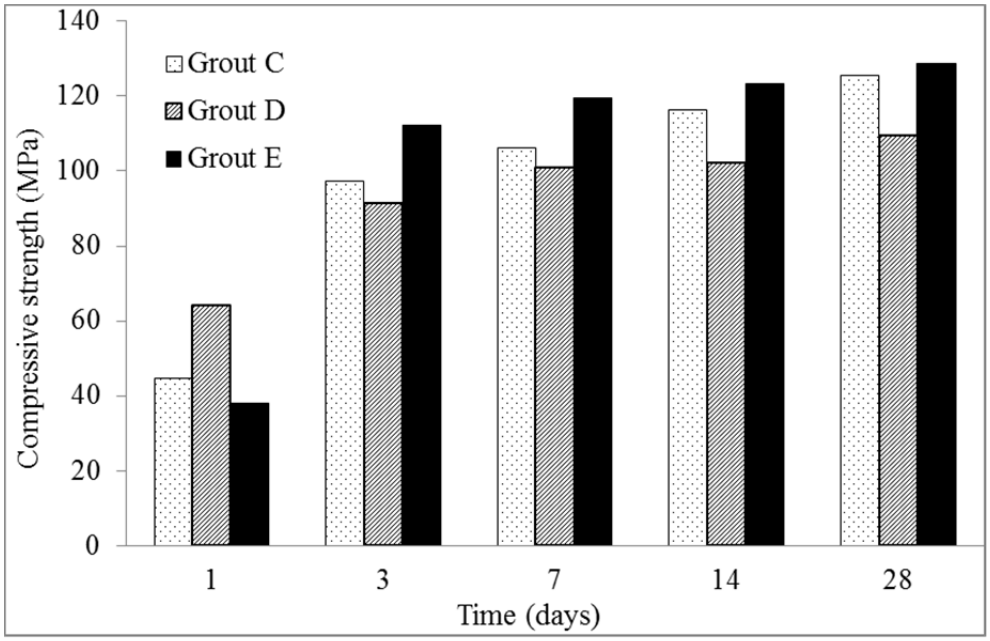

Figure 3.32 **Effect of coarse filler on strength of grouts C, D and E over different curing periods**

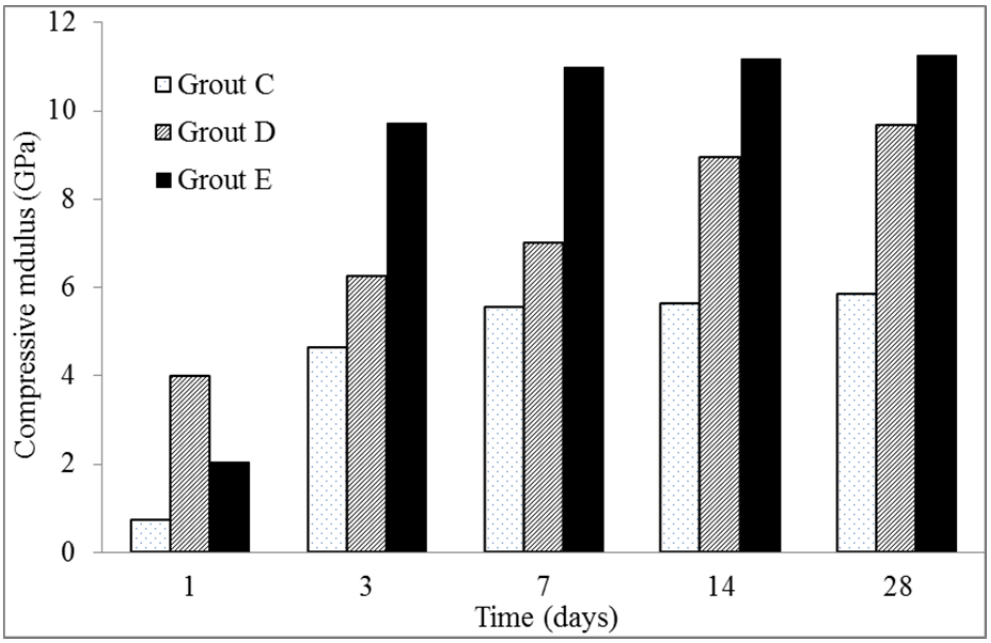

Figure 3.33 **Effect of coarse filler on stiffness of grouts C, D and E over different curing periods**

A technical insight into an epoxy-grouted hot tap fittings technology for pipeline repair was described by Vu et al. (2011), where the compressive, tensile, and flexural strengths specified in that article were 75, 23, and 50 MPa, respectively. Duell et al. (2008) used an epoxy based grout and epoxy wetted flexible carbon wrap to repair pipes which had undergone 50% thickness losses on the asymmetric and

localised defects. In that study, both numerical and experimental results showed that the grout would be subjected to a compressive strength of about 33 MPa when the system is at a pressure of 44 MPa. In the simulation, they used bilinear elastic stress-strain behaviour with an initial modulus of 1.74 GPa and post-yield modulus of 0.87 GPa (50% of initial modulus) to predict the repair performance. Hence, the yield stress and strain found for the tested grouts were higher than the putty used in this study and were sufficient against compressive loading from the internal pressure.

Although, the stress-strain behaviour of grouts C, D and E are not similar to the bilinear behaviour of the mentioned epoxy grout, the grouts are expected to provide sufficient support to the thicker grout infill in the annulus between the outer sleeve and steel pipe of the repaired pipe. Mattos et al. (2009) investigated with an alternative repair system using two grout systems: silicon steel alloy filled polymers and oligomers, and epoxy resins with aluminium powder. The compressive strengths of the above mentioned materials were 56 and 104 MPa, respectively. As a further development of the previous repair application, the burst tests and long-term pressure tests were carried out on the pipe containing a through-thickness defect that was repaired with the same epoxy system (Mattos et al. 2012). The constant internal pressure applied during the long term testing was 10.34 MPa. Thus, the investigated grouts C, D and E have the potential to be used on the similar type of repairs in terms of the compressive performance.

Table 3.6 Typical properties of epoxy grout for repair and rehabilitation (Mendis 1985)

Applications	Compressive Strength (MPa)	Tensile Strength (MPa)	Bond Strength (MPa)
Bonding dissimilar materials	-	10-55	7-35
Concrete crack repair	41-97	14-55	14-35
Structural rehabilitation	83-97	28-48	28-41
Foundation and heavy machinery applications	≥ 97	-	15-28

The tensile and flexural loads are one of the governing forces in pipe repair. The dominant force in pipe repair is circumferential load which acts as a tensile stress along the hoop direction in the components of the repaired section. The corroded pipe and the adjacent grout can be subjected to flexural stresses. According to the range of the properties suggested in Table 3.6, the tensile strength of grout C is sufficient for the structural repair. However, the requirements of the properties in a composite repair system are subjected to a range of defect geometries and loading conditions. Since the grout in the repair system is enclosed in between the composite sleeve and the pipe, the combination of the stresses in the elements should be investigated further. The bonding property of the grout is another parameter which is important for grouted repair as shown in Table 3.6. However, the bonding between the interface of the grout and pipe, and grout and fibre-reinforced composite shell is one of the challenges yet to be investigated. Besides, polymers experience shrinkage when poured in thick annulus. Inter-layer stress or separation can be experienced which may affect the effectiveness of the grouts. Thus, inter-layer bonding and shrinkage of the grouts must be investigated prior to selection of the suitable grouts.

3.5 Conclusions

In this chapter, five epoxy grouts were tested to characterise their mechanical and thermal behaviour at 7 days to investigate their feasibility as infill grout for composite repair of a steel pipeline. Based on the properties, three of these grouts were selected and their compressive properties were further investigated over 28 days. The following conclusions can be drawn from the results of this study:

- The compressive strength and modulus of the five epoxy grouts range from 50 – 120 MPa and 1.7 – 11.0 MPa, respectively. The tensile, flexural and shear strength of the grouts range from 11 – 32, 27 – 53, and 13 – 30 MPa, respectively. The tensile and flexural stiffness of the grouts are found to be within the range of 3 – 17 GPa, and 4 – 13 GPa, respectively.
- Glass transition temperatures of grouts A and B are about 40ºC and 60ºC considering storage modulus and tan δ, respectively. Grout C, D and E provide a glass transition range of 50 – 60ºC and 80 – 90ºC considering storage modulus and tan δ, respectively.
- The compressive behaviour of grouts A and B are similar to the polymers. Grout C exhibits polymeric characteristics in the early days of curing. However, 28 days cured grout C and the coarse aggregate filled grouts D and E exhibit behaviour comparable to polymer concrete. Grouts C, D and E gained more than 90% of the 28-day compressive strength and stiffness within 7 days of curing.
- The mechanical and thermal properties of grouts C, D and E are found to be superior to grouts A and B. The higher resin content of grout C results in higher tensile and flexural strength. Despite having low resin content, grouts D and E have higher compressive properties along with tensile and flexural stiffness.
- The inclusion of coarse filler in grout C results in about two and three times increase in the compressive and tensile modulus, respectively. There is about a 13% increase in the compressive strength whereas the tensile strength decreases by about 34% at 7 days.
- The inclusion of coarse filler in grout C results in the reduction of the volumetric shrinkage by about 2.5 times over 28 days. The post-gel shrinkage also decreases due to the slow curing rate indicated by longer gel time.

The mechanical, thermal and shrinkage properties of five epoxy grouts are identified in this chapter. These properties will aid an understanding of the behaviour of the grouts in the repair scenarios. However, three grouts: C, D and E are selected based on the properties found in this chapter. Further analysis on the properties of these grouts needs to be carried out to observe the suitability of the properties of the grouts in in-situ applications. In Chapter 4, these three grouts will be used for further investigation of moisture uptake properties and associated effects on these properties.

Chapter 4

Properties of grouts under hot-wet conditioning

4.1 Introduction

A structure is designed and constructed for a certain lifetime. This lifetime is based on its constituent materials, level of quality control, surrounding environment and accidental loads experienced during service. Inevitably, many structures undergo rehabilitation due to the deterioration they experience over time. The defects must be addressed with reliable rehabilitation systems using appropriate materials. Often, advanced composite materials offer substantially enhanced mechanical, durability and constructability-related properties essential for durable repair of the deteriorated structure.

Oil and gas pipes are particularly susceptible to failure initiated by corrosion due to their high operating pressure under adverse atmospheric conditions. According to ASME PCC-2 (2006), the service temperature of a repair component for non-leaking and leaking pipes should not be 20°C and 30°C less than the glass transition temperature, respectively. Elevated temperature is found to affect the physical properties of epoxy polymers (Carbas et al. 2013; Littell et al. 2008a). Epoxy mortar was also found to degrade under raised temperature (Kelsey & Biswas 1993). An epoxy system was also found susceptible to moisture ingress (Vanlandingham et al. 1999). Hence, the effect of elevated temperature and moisture on the component of repair should be studied.

The work presented in this chapter was carried out to observe the effect of hot-wet conditioning on the mechanical and thermal properties of grout materials contained within the grouted sleeve repair resembling elevated temperature at underwater conditions. Five epoxy grouts were tested for mechanical and thermal properties in Chapter 3. Among these five grouts, three grouts were selected due to their suitable mechanical and thermal properties which were determined for as manufactured grouts specimens tested at 23°C. The compressive strength and modulus of these three epoxy grouts: C, D and E were found to be 106 – 120 MPa and 5.6 – 11.0 MPa, respectively. The tensile strength and modulus of the grouts ranged from 19 – 32 MPa and 4.9 – 16.5 GPa, respectively. Having identified these properties, this study goes on to investigate three grouts under hot-wet conditioning at elevated temperature. Compressive, tensile, shear, flexural and thermal properties of these grouts were determined and their failure behaviour was observed to understand their performances in different loading conditions under elevated temperature and underwater conditioning. The results of the study provide suitability of the glass transition temperature of the grouts adopted to identify the suitability of the 1000 hours conditioning as representative of “long-term” conditioning and serviceability limits according to ISO/TS 24817 (2006), which is a standard used for qualification of polymer matrix composite repair materials.

4.2 Experimental methodology

4.2.1 Materials

Three epoxy grouts with different specified compositions of neat resin, hardener and aggregate were selected based on their mechanical and thermal properties at ambient temperature. The selected grouts are C, D and E. The mix ratios were given in Table 3.1 in Section 3.2.1.

4.2.2 Specimen preparation

The mixing and specimens preparation process is similar to that described in the previous chapter and discussed in Section 3.2.3. Figure 4.1 shows the mixing of typical grout E and preparation of grout specimens before hot-wet conditioning. The specimens were cut and polished to the required dimensions. Table 3.2 summarises the details of specimen dimensions and tests conducted on the prepared specimens. The specimens were removed from the moulds after 24 hours and cured in a controlled environment at 23ºC for 7 days prior to hot-wet conditioning.

4.2.3 Hot wet conditioning

As shown in Figure 4.2, the grouts were conditioned in a temperature controlled bath containing tap water. The conditioning was carried out at the laboratory facilities by CRC-ACS, Australia. 1000 hours of conditioning was selected to conform to the long-term durability criteria suggested by ISO/TS 24817 (2006). ASTM E1640 (2009) provides a number of methods to determine glass transition temperature. Glass transition can be obtained from storage modulus (T_g), loss modulus (T_l) and tan δ (T_t). An investigation on the thermal properties of these unconditioned grouts suggested a T_g range of 53 – 60°C, and T_t range of 83 – 90°C for the above mentioned grouts in Chapter 3.

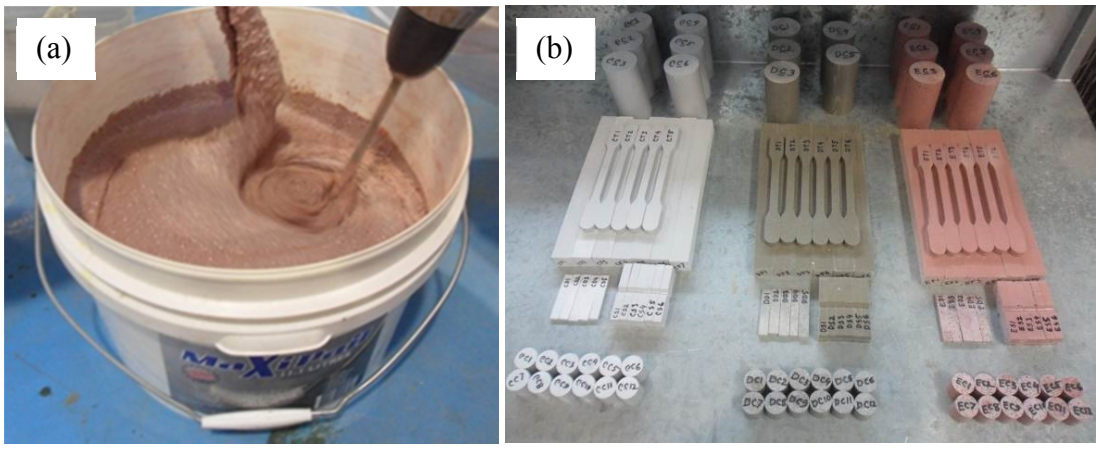

Figure 4.1 **Preparation of specimens; (a) mixing of the grouts, and (b) grout specimens for hot-wet conditioning**

According to ISO/TS 24817 (2006), the service temperature of a repair component for non-leaking and leaking pipes should not be 20°C and 30°C less than the glass transition temperature, respectively. The non-leaking defect type is limited within the substrate and not expected to become through-wall within the lifetime of the repair, and is also defined as Type A. On the other hand, leaking defect type is a through-wall defect requiring sealing and structural reinforcement, and is termed as Type B. In this study, T_t is taken as the glass transition temperature ceiling for leaking and non-leaking conditions. Therefore, 70°C is considered for hot-wet

conditioning and 65°C is considered for mechanical testing, which is around the range of 20 – 30°C less than the T_t of the unconditioned grouts. Absorption measurements were taken using Adam PW254 scales accurate to 0.1 mg for weighing of the specimens less than 250 g, and scales accurate to 1 mg for higher than 250 g. The moisture absorption was measured weekly.

4.2.4 Test set up

4.2.4.1 Mechanical testing

The compressive, tensile, flexural, shear and thermal properties of the grouts were determined after 1000 hours of hot-wet conditioning. Table 3.2 provides details of the tests for the grouts and composites. Relevant standards and practices are also shown in the table. All the mechanical characterisation tests were carried out following the similar instrument as discussed in Section 3.2.3. Figure 4.3 shows the elevated temperature at which the tests were conducted and typical mechanical testing of the prepared specimens. The unconditioned specimens were preheated in an oven at 65°C for at least 30 minutes while the hot-wet conditioned specimens were preheated in a water bath placed in an oven for at least 30 minutes prior to being placed into the temperature chamber. The test started once the chamber temperature reached 65°C and was maintained for 10 minutes.

Figure 4.2 Grout specimens being conditioned at the water bath

4.2.4.2 Thermal analysis

Dynamic Mechanical Analysis (DMA) was used to determine the glass transition temperatures of the conditioned grouts. Table 3.2 shows the details of the rectangular specimens with nominal dimensions and the test method for thermal analysis. The glass transition temperature is determined using a method similar to that discussed in Section 3.2.3 and Section 4.2.3. The test set up for the DMA specimen is shown in Figure 3.3.

4.3 Results

4.3.1 Moisture absorption properties

Hot-wet conditioning results in a mild change in colour on the surface of the grouts. The most notable physical change that occurs on the surface of the grout during the absorption process is the formation of blisters on the surface of grout E which is shown in Figure 4.4.

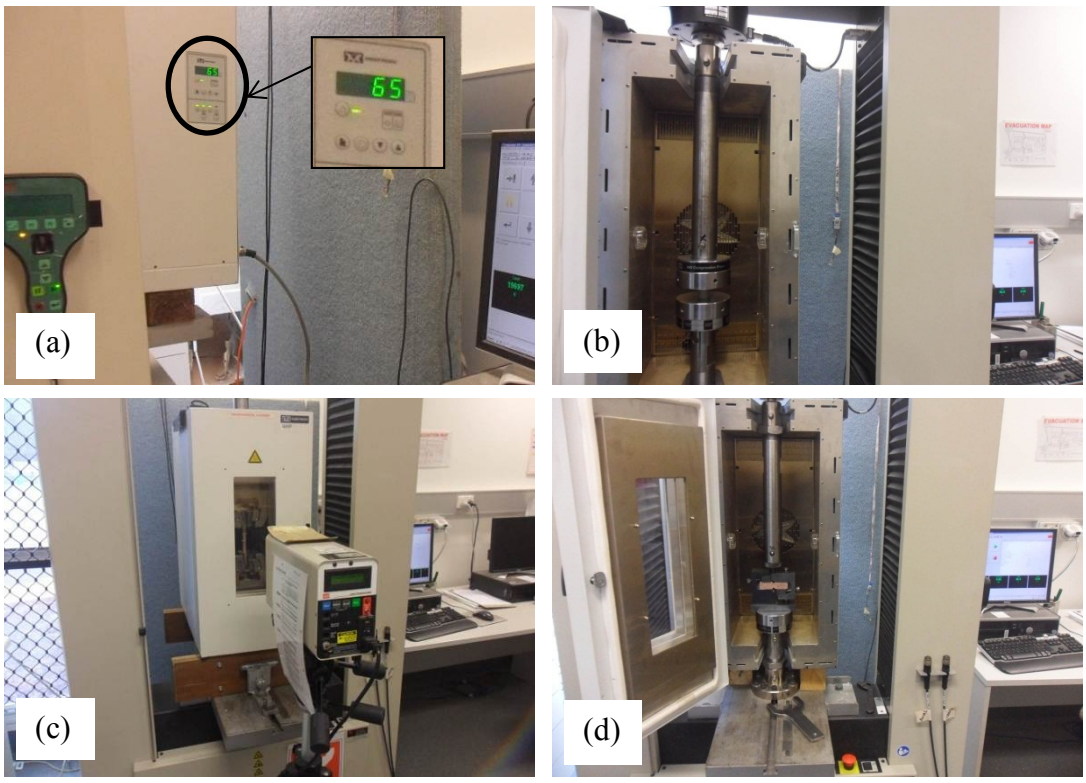

Figure 4.3 **Mechanical tests of the grouts; (a) elevated temperature, (b) compressive, (c) tensile at elevated temperature, and (d) shear**

Figure 4.5 to Figure 4.7 show the normalised moisture absorption trend of the grouts over the 42 day conditioning period. Moisture content is presented against immersion time in hours. The 50 mm diameter cylindrical specimens absorbed less moisture than that of 25 mm specimens. The highest absorption is observed for the 5 mm DMA specimens that are the thinnest of all type of specimens. Normalised absorption of the specimens with similar minimum dimension shows a comparatively similar trend in all the grouts.

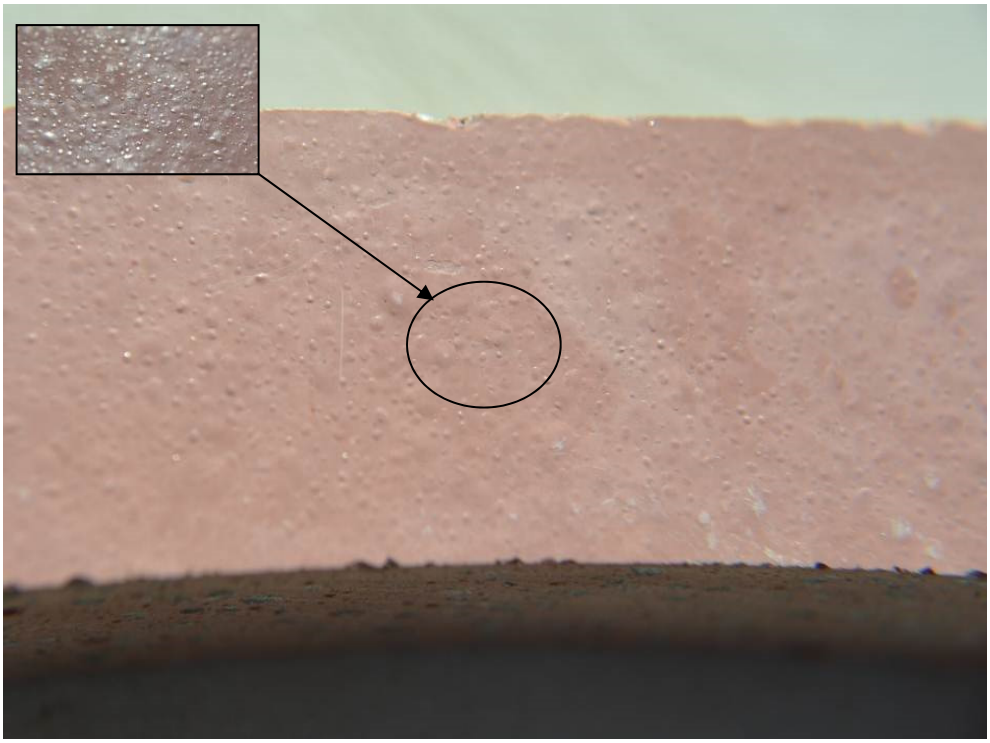

Figure 4.4 **Formation of blisters on the surface of grout E due to hot-wet conditioning**

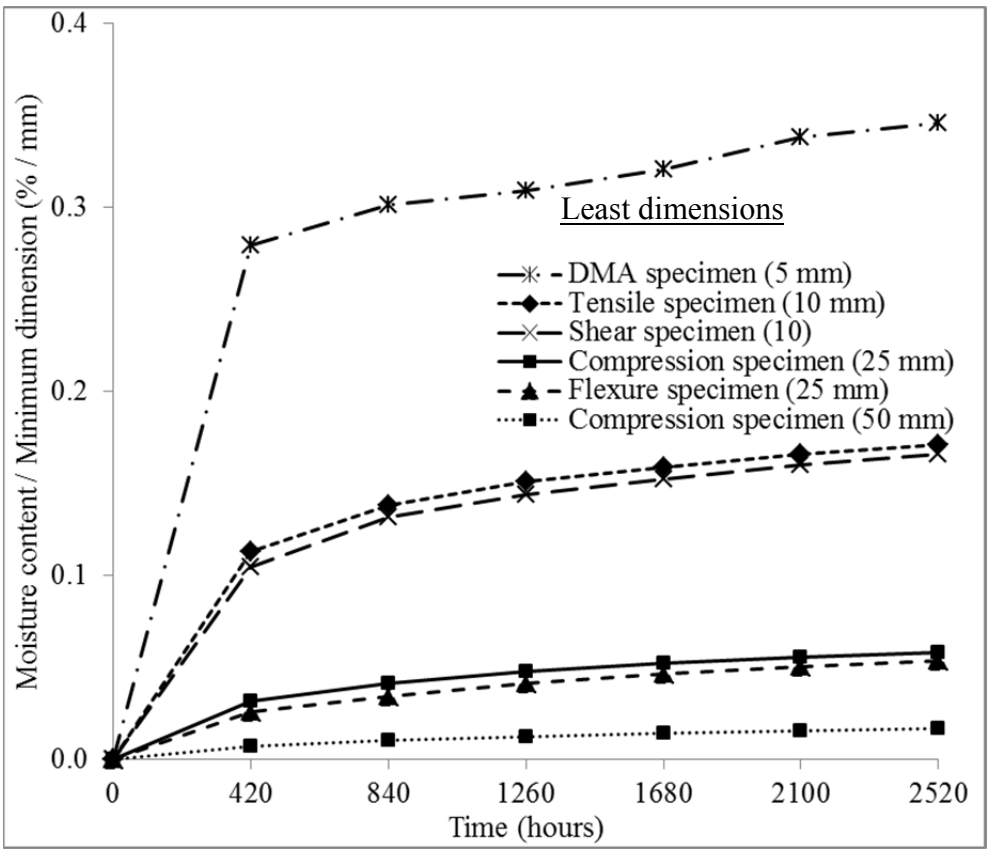

Figure 4.5 **Normalised moisture absorption of grout C**

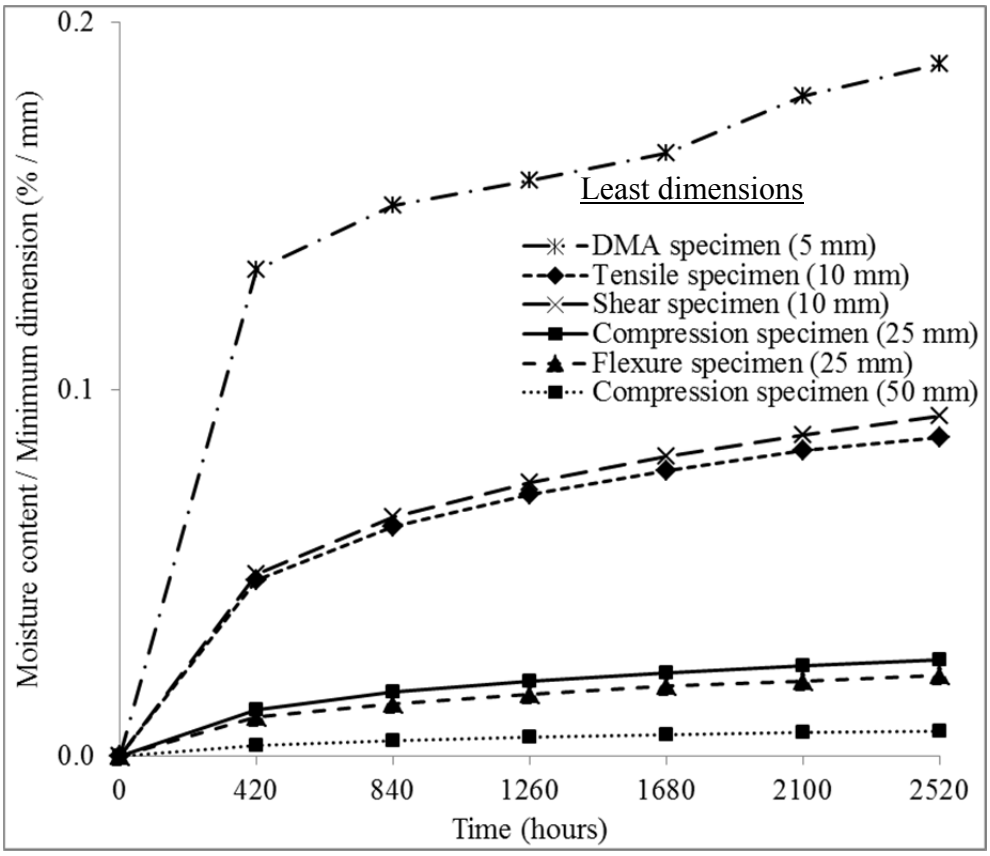

Figure 4.6 **Normalised moisture absorption of grout D**

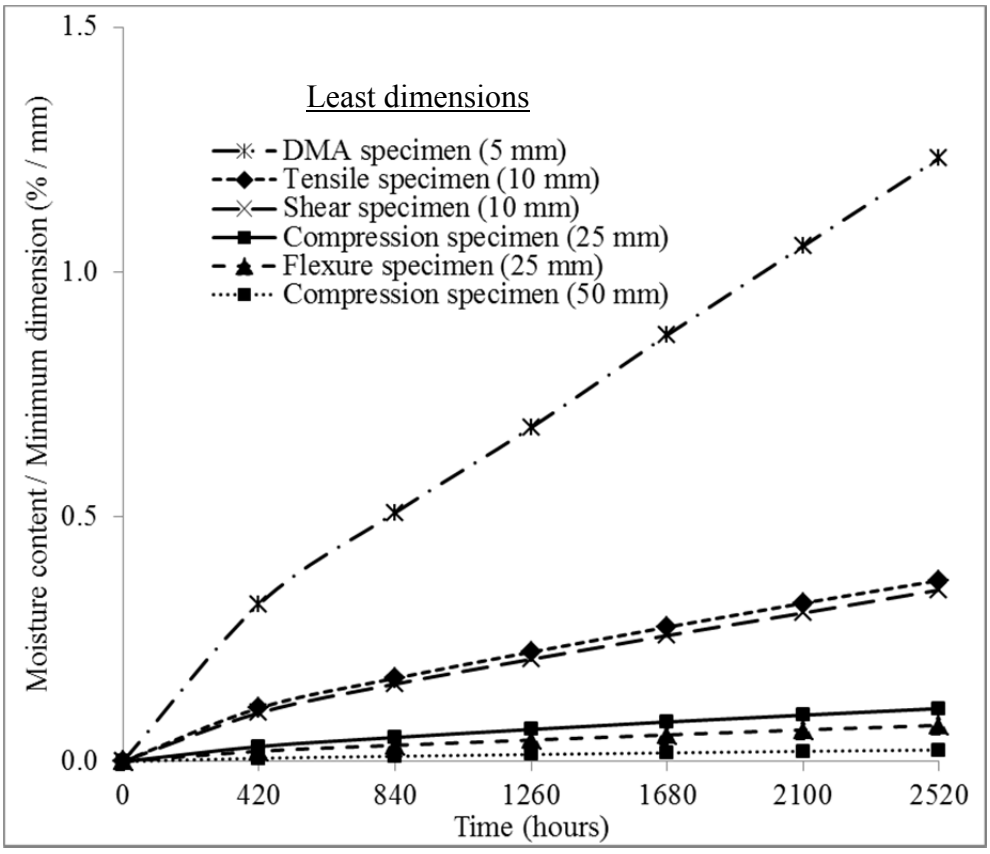

Figure 4.7 **Normalised moisture absorption of grout E**

When the moisture absorption of the grouts is compared, the highest absorption is observed for grout E with a value of 1% to 6% after 42 days. Studies on epoxy-modified concrete suggested about 6% moisture absorption which may vary depending on resin content (Aggarwal et al. 2007; Lixin et al. 2004). The lowest absorption is found for grout D with values ranging from 0.3% to 0.9%. The trend of the moisture content of the grouts suggests that the absorption rate is the highest during the first 7 days (420 hours) and decreased thereafter for grouts C and D, whereas the absorption increased with time for grout E.

4.3.2 Mechanical properties

The mechanical and thermal properties of the grouts which are tested at 65°C after 1000 hours of hot-wet conditioning at 65°C are given in Table 4.1. The details of the results were discussed later in this section.

4.3.2.1 Compressive properties

The maximum strengths are found to be 93 MPa, 29 MPa and 45 MPa for grouts C, D and E, respectively. Compressive moduli of the grouts are found to be 0.42 GPa, 0.57 GPa and 0.56 GPa for grouts C, D and E, respectively. From the plots, the yield strain of the 25 mm specimens of grouts C, D and E are about 32, 8 and 11%, respectively. The maximum strengths of the 50 mm specimens are found to be 81 MPa, 50 MPa and 49 MPa for grouts C, D and E, respectively. The moduli for the 50 mm specimen of grouts C, D and E value at about 0.33 GPa, 3.33 GPa and 3 GPa, respectively. Hence, the compressive strength of 50 mm grout C specimens is reduced by about 13% and modulus reduced by about 22% than that of 25 mm specimens. Whereas, the compressive strength and modulus of the 50 mm specimens of grouts D and E increased by about 72% and 7%, respectively than that of 25 mm specimens. Moreover, the modulus of the 50 mm specimen of grout E is about 34% higher than that of the 25 mm specimen.

Figure 4.8 shows the typical compressive stress-strain behaviour of the tested grouts. The 25 mm compressive specimens of the grouts show an elastic behaviour followed by yield stresses. It can be seen that Grout D is an exception to the other grouts indicating initial non-linearity at the beginning of the loading. For this reason, modulus was calculated within strain of 0.1 to 0.2 for this stress-strain relation due to the stable gradient in this region. Figure 4.9 shows the compressive stress-strain behaviour of the 50 mm specimens. The 50 mm compressive specimens of grouts C, D and E do not exhibit post yield hardening.

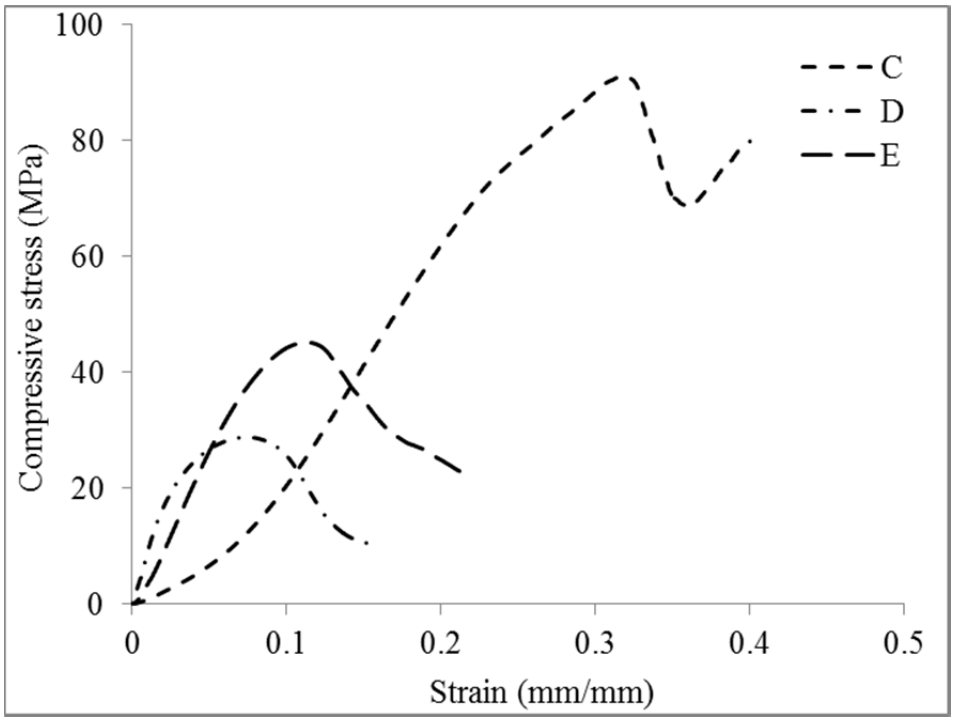

Figure 4.8 **Typical stress-strain behaviour of the 25 mm compressive specimens of grouts**

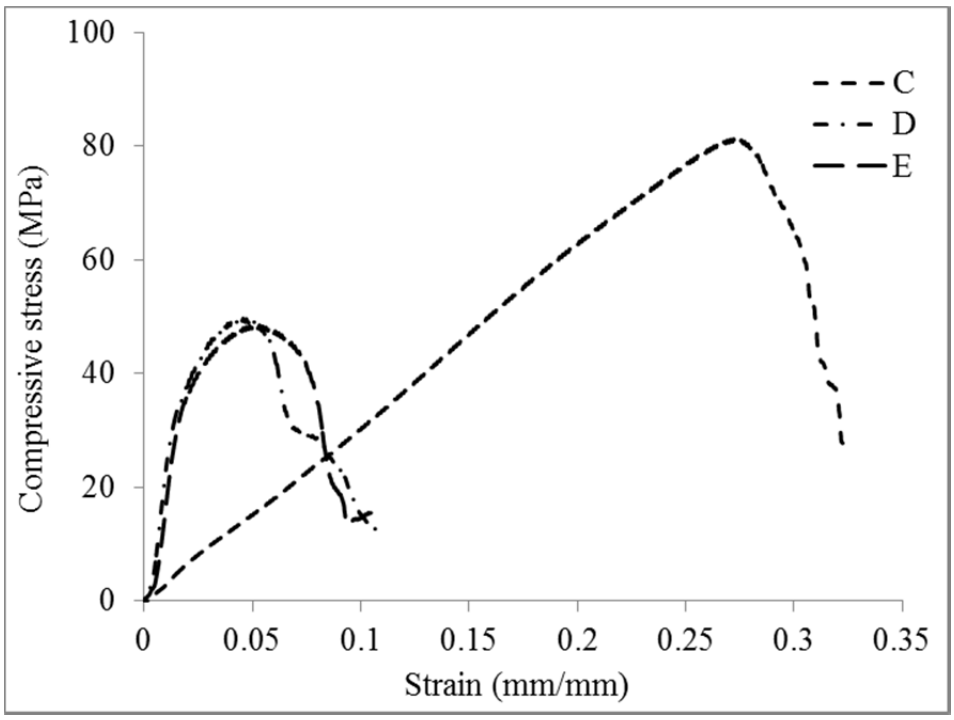

Figure 4.9 **Typical stress-strain behaviour of the 50 mm compressive specimens of grouts**

Properties of grouts under hot-wet conditioning

Table 4.1 Summary of mechanical properties of grout subjected to hot-wet conditioning

Properties		C		D		E	
		25 mm	50 mm	25 mm	50 mm	25 mm	50 mm
Compressive	Compressive strength (MPa)	93.10 (2.47)*	81.34 (3.38	28.9 (3.55)	49.77 (6.90)	45.23 (1.85	48.54 (1.46)
	Compressive modulus (GPa)	0.418 (0.030)	0.327 (0.017	0.570 (0.204)	3.327 (1.26)	0.559 (0.024	3.012 (0.251)
	Strain at peak stress (mm/mm)	0.318 (0.004)	0.272 (0.004	0.075 (0.003)	0.048 (0.005)	0.111 (0.004	0.052 (0.003)
Tensile	Tensile strength (MPa)	12.22 (1.26)		1.66 (0.124)		1.29 (0.111)	
	Tensile modulus (GPa)	0.381 (0.075)		0.161 (0.005)		0.029 (0.004)	
	Strain at peak stress (%)	3.05 (0.71)		2.16 (0.25)		6.44 (0.62)	
Flexural	Flexural strength (MPa)	8.71 (0.36)		18.68 (0.70)		12.76 (0.54)	
	Flexural modulus (GPa)	0.120 (0.013)		0.529 (0.038)		0.203 (0.007)	
Shear	Shear strength (MPa)	10.24 (0.78)		3.36 (0.42)		6.29 (0.87)	

*Values in the parenthesis are standard deviations

Figure 4.10 demonstrates the typical failure patterns of the 25 mm specimens of grouts C, D and E under uni-axial compression. Under compression, grouts C exhibits circumferential bulging after the initial elastic behaviour. The bulging continues until failure which is initiated by vertical cracks at the peripherally expanded specimens. The bulging starts after the linear elastic zone. There in minor lateral expansion in grouts D and E. This behaviour can also be observed in the stress-strain curve in Figure 4.8, where there is no post-yield hardening in grouts C, D and E. However, there is increment of stress for the 25 mm specimen of grout C after yield strain. This is due to the meeting of the failure wedges caused by continuous loading for up to a prolonged strain which can be seen from Figure 4.10a and Figure 4.11a.

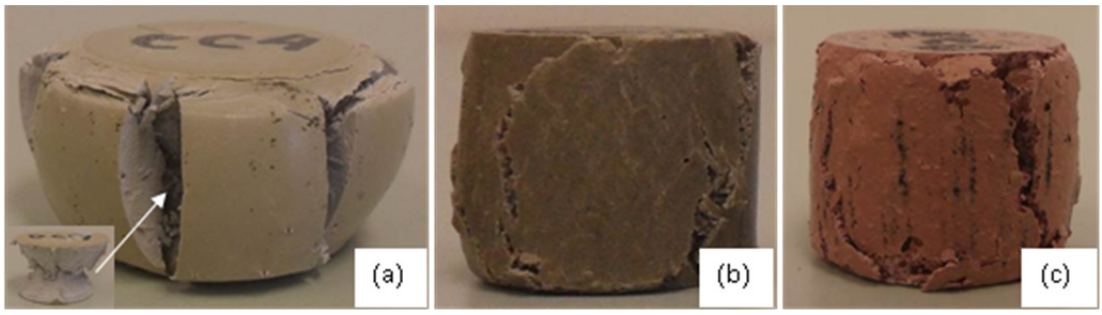

Figure 4.10 **Typical failure patterns of 25 mm cylindrical specimens under compression; (a) grout C, (b) grout D and (c) grout E**

Another reason for the hardening is the axial resistance provided by the outer shells that is separated from the internal wedges. With the formation of the cup-and-cone, it is obvious that the frictional force between the platens and the specimen surfaces creates a horizontal compressive force and eventually forms cones at the ends. The wedges in the compression specimens form at an angle of about 45º with the vertical axis for both 25 mm and 50 mm specimens of grout C. The orientation of cracks in the outer shell of grout C is vertical. The cracks in the 25 mm specimens of grouts D and E are randomly oriented with no visible wedge. This can be seen from Figure 4.10b and Figure 4.10c.

From the stress-strain and failure behaviour, it is evident that the 25 mm specimens of grouts D and E form internal cracks near the yield stress. The ultimate failure pattern of the 50 mm specimens of grouts D and E is randomly oriented and followed by the yield/peak stress as shown in Figure 4.11b and Figure 4.11c. The failure wedges of the 50 mm specimens are larger than the 25 mm specimens. The minor cracks form at the middle height of the specimens followed by the failure wedges to push one another towards failure.

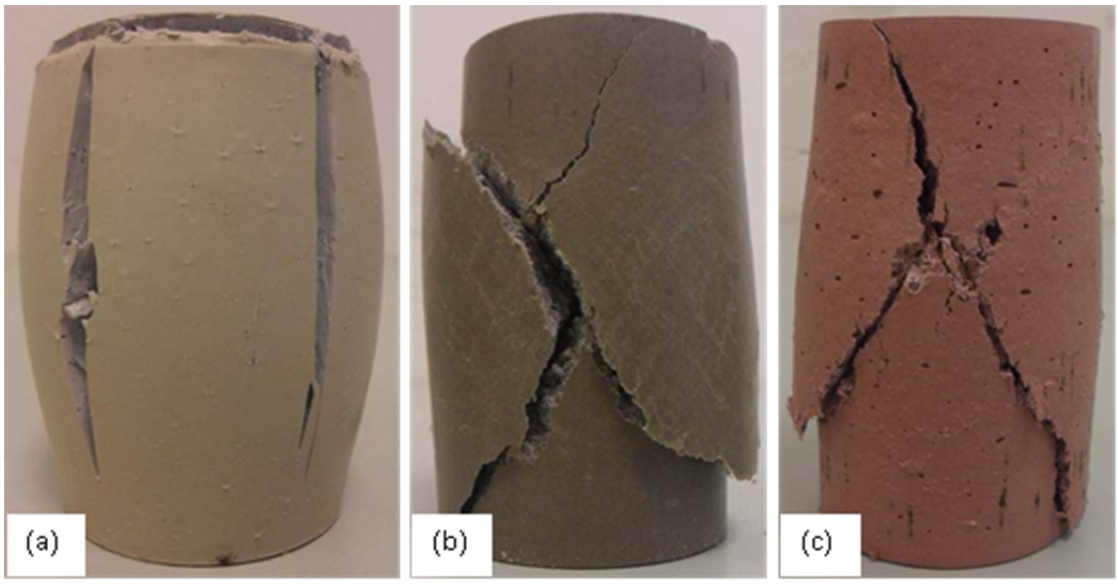

Figure 4.11 **Typical failure patterns of 50 mm cylindrical specimens under compression; (a) grout C, (b) grout D and (c) grout E**

4.3.2.2 Tensile properties

Table 4.1 provides a summary of the tensile strength and modulus of the investigated grouts in tension. From the table it can be seen that the highest tensile strength and stiffness of the investigated grouts are found for grout C with a value of 12 MPa and 0.38 GPa, respectively. The lowest tensile strength and modulus are found for grout E with a value of 1.29 MPa and 0.03 GPa, respectively. Hence, the tensile strength and stiffness of Grout D are reduced by about 10 times and 13 times, respectively compared to grout E. The tensile strength and stiffness of grout D are 1.66 MPa and 0.16 GPa, respectively.

The comparison of the typical stress-strain behaviour from each type of the grout is shown in Figure 4.12. Two distinct stress-strain relations are observed. Grout C shows a linear stress-strain relation exhibiting the highest strength compared to grouts D and E. Although grout C contains a fine filler in the grout matrix, this behaviour may be due to the elevated temperature which reduces the stiffness and hot-wet conditioning which then reduces the glass transition temperature discussed later in Section 0. The highest failure strain is observed in grout E.

Figure 4.13 shows the typical failure pattern of the tensile specimens. The formation of a crack in grout C is sudden and a splitting sound is heard. Failures in grouts D and E progress slowly compared to grout C and are not perfectly perpendicular to the length or straight along the thickness.

Figure 4.14 exhibits the failure surfaces of the grouts. The failure of tensile specimens of grout C exhibits smooth texture. The failure pattern of D and E is comparable. Figure 4.14 also demonstrates the voids that were trapped in the cured grouts and failure of interface bonding. It can be seen that the failure occurred in between the aggregate filler and matrix interface.

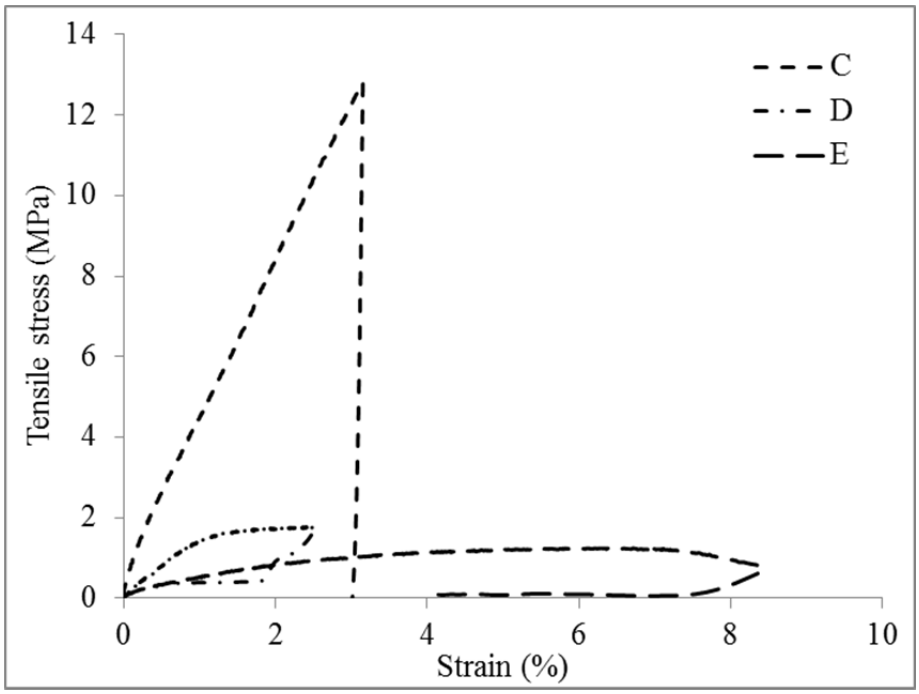

Figure 4.12 **Typical tensile stress-strain behaviour of the grouts**

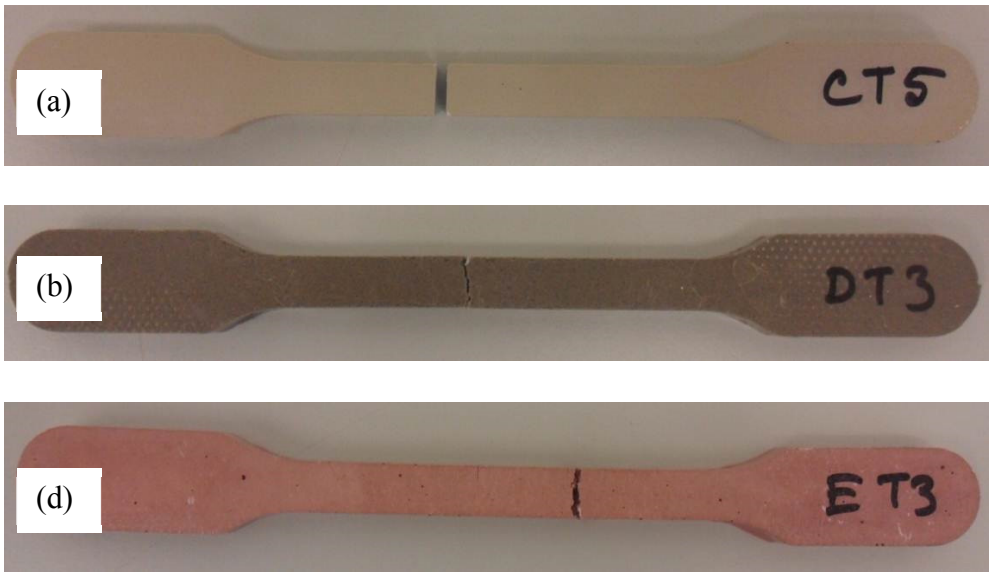

Figure 4.13 **Typical failure pattern of tensile specimens; (a) grout C, (b) grout D and (c) grout E**

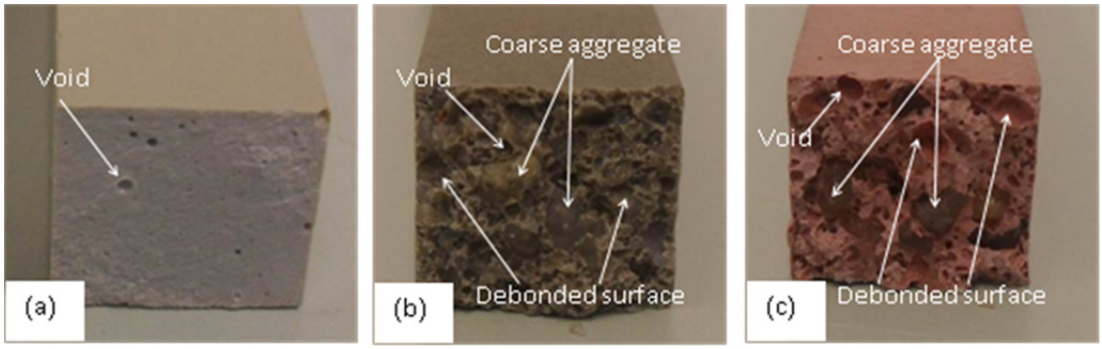

Figure 4.14 **Typical failure surface of tensile specimens; (a) grout C, (b) grout D and (c) grout E**

4.3.2.3 Flexural properties

Table 4.1 shows a typical comparison of the load-deflection behaviour of the grouts in flexure. All the grouts show linear elastic load-deflection behaviour prior to failure. The load-deflection behaviour of grouts D and E show low strength and higher deflection than that of other grouts. As shown in Table 4.1, despite having lower tensile strength, grout D has the highest flexural strength and stiffness with a value of 19 MPa and 0.53 GPa, respectively. The lowest strength and stiffness of grout C are found to be 9 MPa and 0.12 GPa, respectively. The strength and stiffness of grout E is found 1.5 times and 1.7 times higher than that of grout C.

The typical failure patterns of the flexural specimens of the grouts are shown in Figure 4.15. All specimens fail over a prolonged period, with clearly visible crack formation. The crack formations are almost vertical and perpendicular to the length of the specimens. Compression wedges are not found during failure. Furthermore, the inspection of the cracked surface suggests that the failure of the resin matrix propagates through the resin matrix, and interface of the resin and aggregate. This behaviour is also comparable to the tensile behaviour discussed in Section 4.3.2.2.

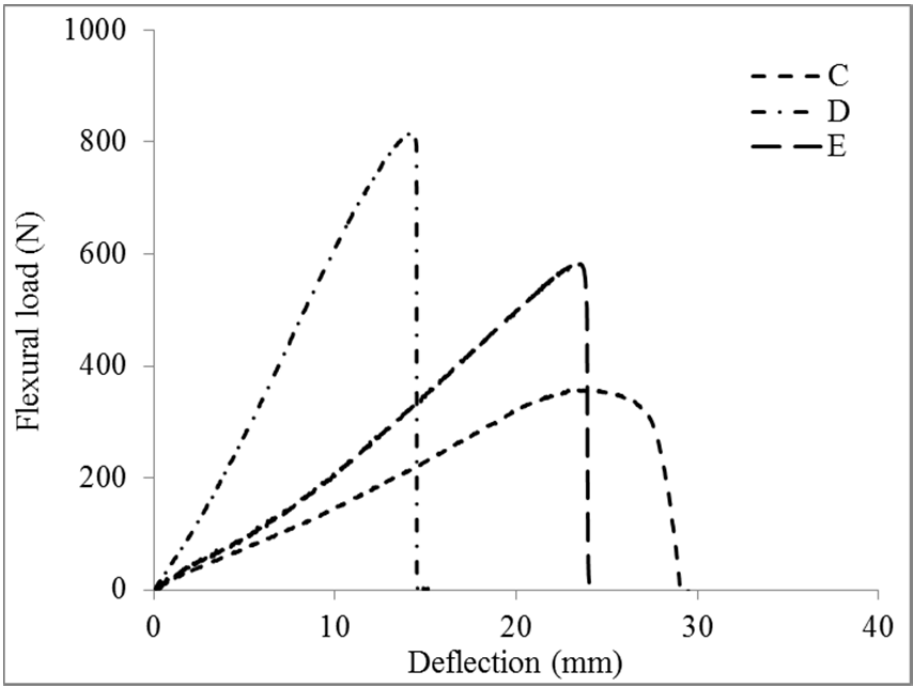

Figure 4.15 Typical flexural load-deflection behaviour

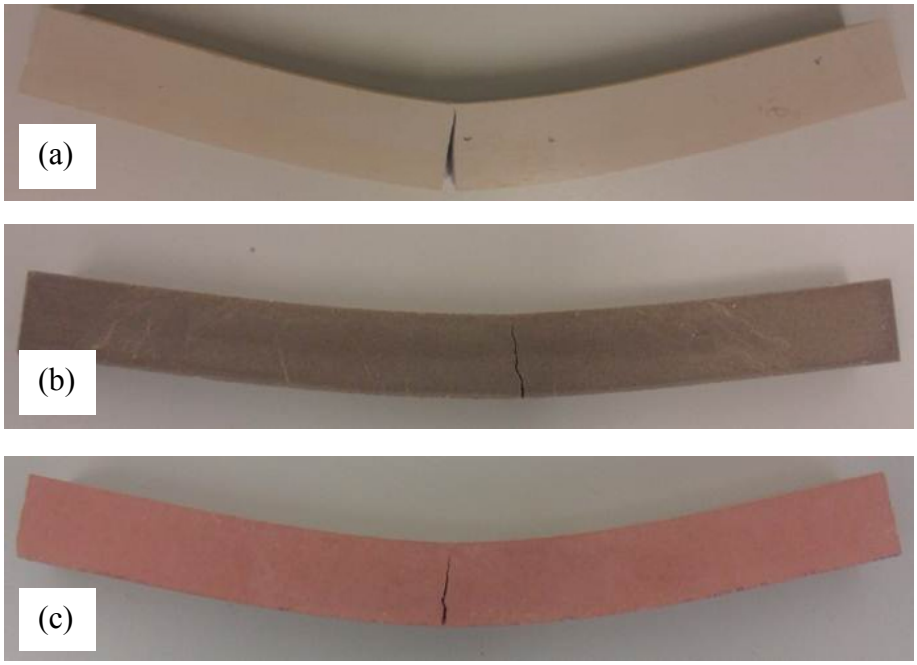

Figure 4.16 Typical flexural failure of the specimens; (a) grout C, (b) grout D and (c) grout E

4.3.2.4 Shear properties

Table 4.1 shows that the shear strength of grouts C, D and E are 10, 3 and 6 MPa, respectively. Figure 4.17 shows the relative comparison of load and crosshead displacement of the grout under shear loading. Grout C exhibits higher strength with comparatively straight load-displacement behaviour compared to other grouts. Due to the inclusion of filler, grout E provides lower strength compared to grout C. Figure 4.18 shows the typical crack generation in shear specimens. The failure occurs gradually after the peak load. The failure of grout C is composed of two diagonal cracks and a failure wedge between the cracks.

4.3.3 Thermal properties

Figure 4.17 provides a summary of the glass transition temperatures of the grouts. Since DMA is considered to be the most sensitive method for determining glass transition temperature for a filled thermoset matrix (Wolfrum et al. 2000), it is appropriate to consider the glass transition temperature from the DMA method for pipeline repair. ISO/TS 24817 (2006) refers to ASTM E1640 (2009) which suggests that glass transition temperature be obtained from either transition of storage modulus (T_g), or peak of loss modulus (T_l), or peak of tan δ (T_t). Storage modulus inflexion provides a lower glass transition than both the loss modulus and tan δ peaks. This behaviour is also comparable to Goertzen & Kessler (2007).

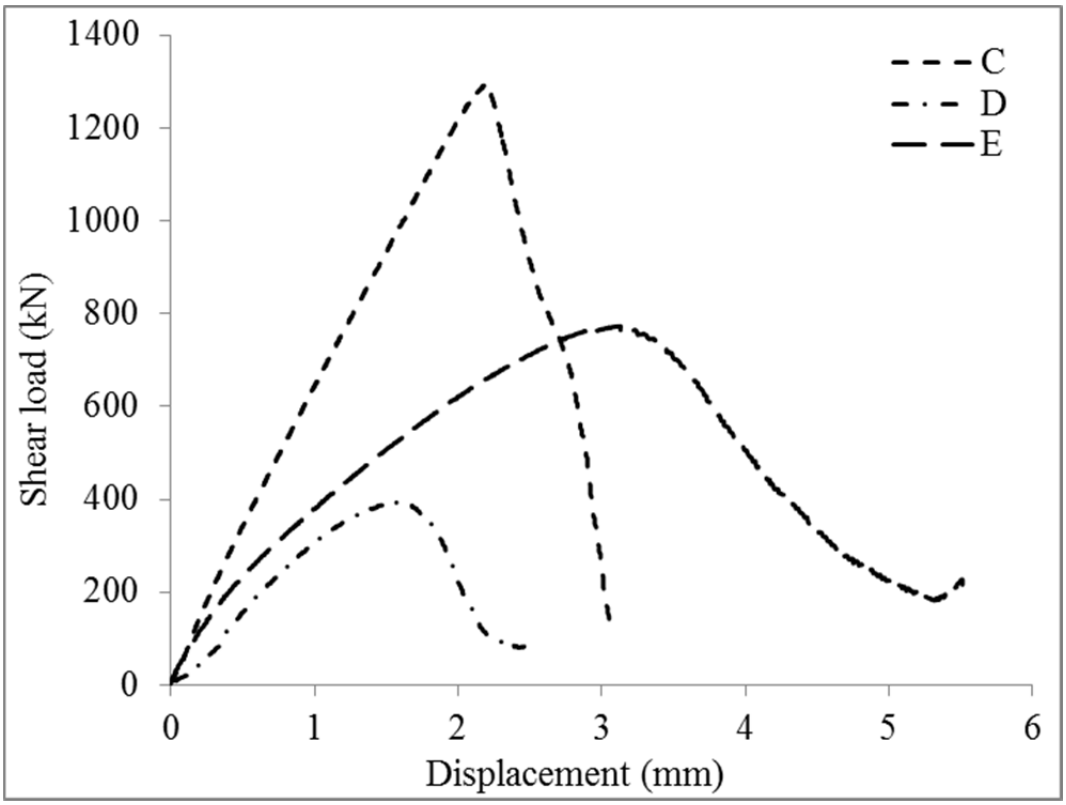

Figure 4.17 **Typical shear load-displacement behaviour**

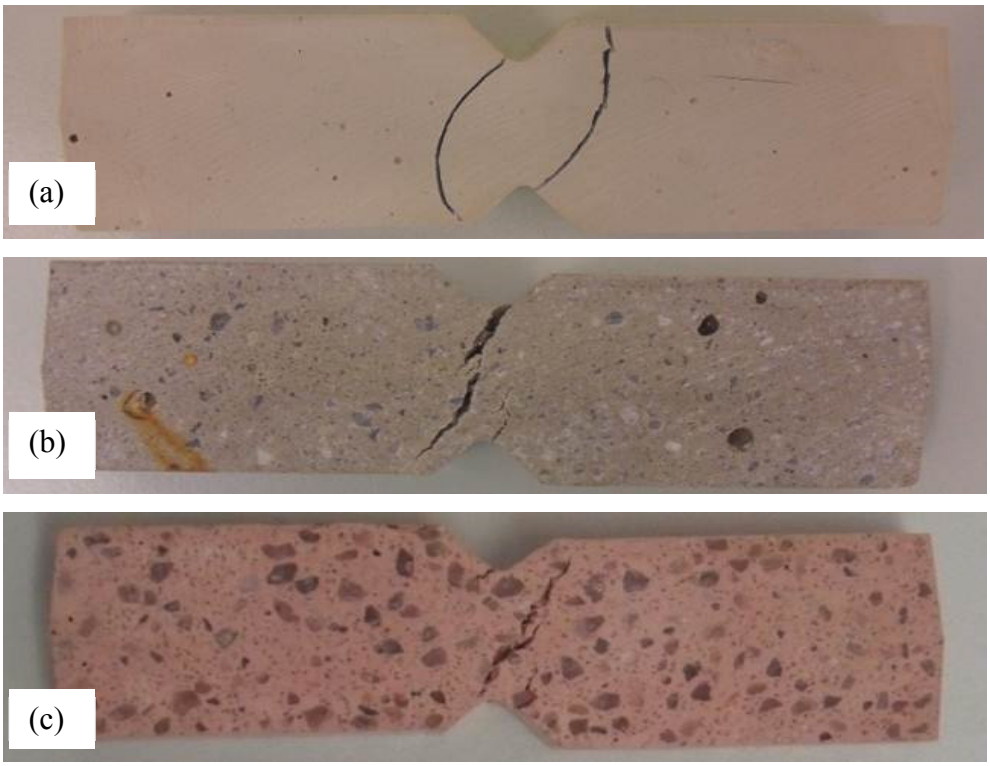

Figure 4.18 **Typical failure pattern of the shear specimens; (a) grout C, (b) grout D and (c) grout E**

Table 4.2 Summary of glass temperature of the conditioned grouts

Properties		C	D	E
Glass transition	T_g (°C)	39	38	42
	T_t (°C)	67	59	69

A superposition of the storage modulus and tan δ is shown in Figure 4.19 and Figure 4.20. The highest value of tan δ peak was observed in grout E with a value of 69ºC which is about 2ºC higher than that of grout C. Hence, the reduction of resin content in grout E does not significantly reduce its glass transition temperature. The range of T_g and T_t range between 39 – 42ºC, and 59 – 69ºC, respectively. However, as the storage modulus was recorded from the room temperature, the tangent of the initial storage modulus could not be drawn. Hence, a horizontal line is considered as the initial tangent line which intersects with another tangent line drawn from the decreasing storage onset to determine the T_g.

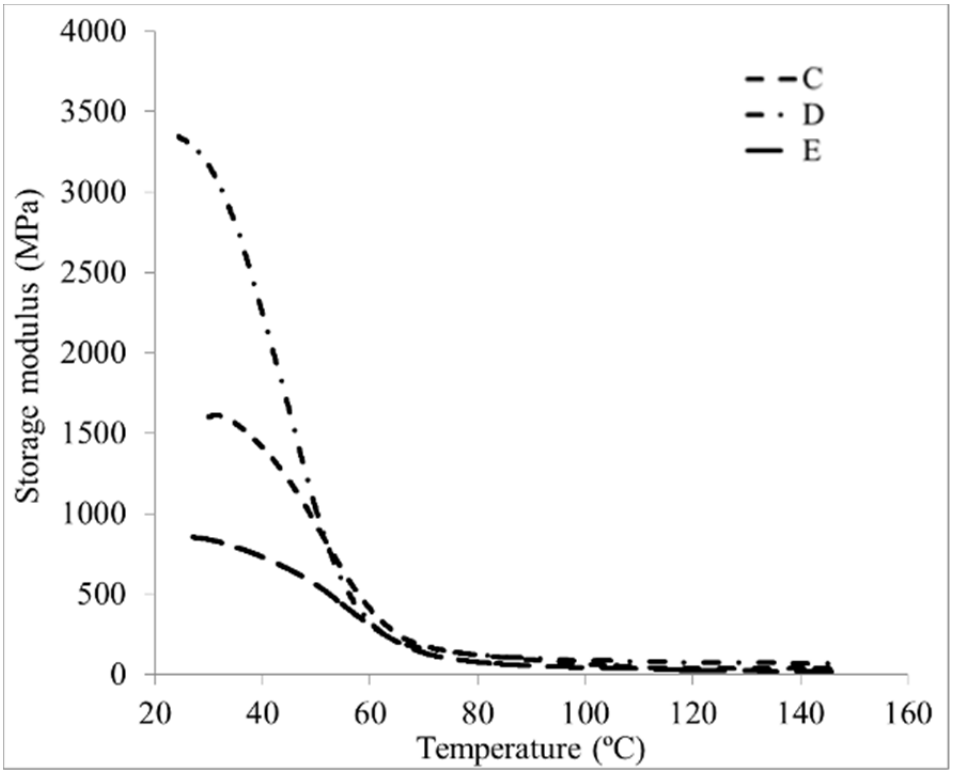

Figure 4.19 Storage modulus vs temperature plot of hot-wet conditioned grouts

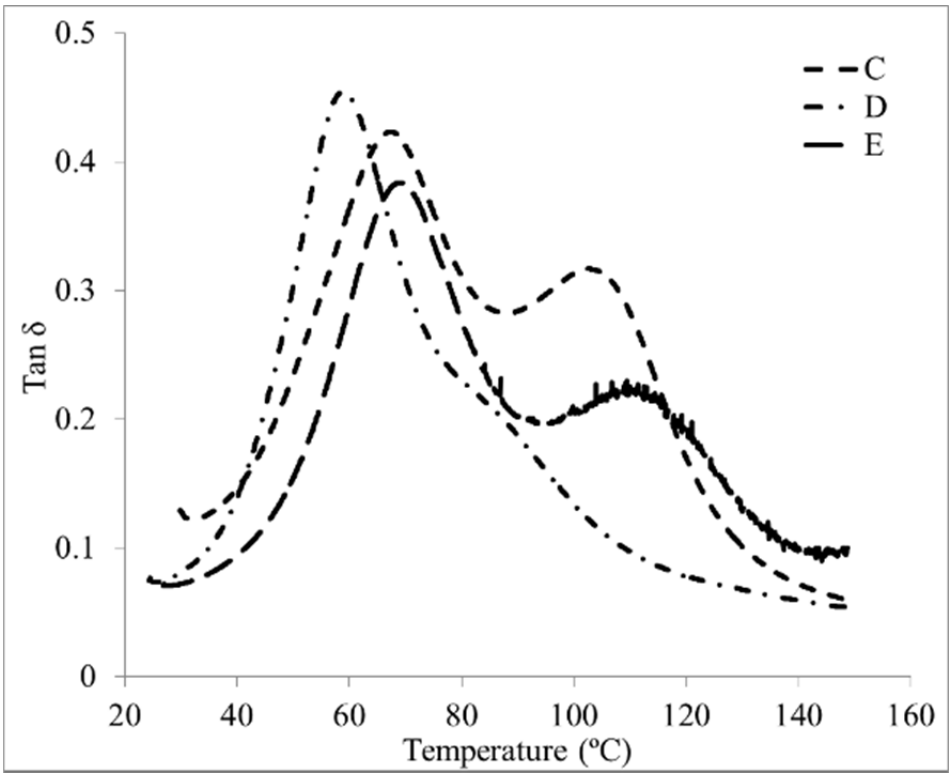

Figure 4.20 **Tan δ vs temperature plot of grouts of hot-wet conditioned grouts**

4.4 Discussion

4.4.1 Effect of specimen size on moisture absorption

Higher absorption is observed in grout E as seen from Figure 4.5 to Figure 4.7. From the composite of the grouts investigated in this chapter, it can be seen that grout E contains the lowest resin content. The reasons is that lower resin content is related to higher moisture absorption in epoxy modified mortar (Aggarwal et al. 2007). The comparatively higher absorption of the thinner specimens at the beginning of conditioning (420 hours) suggests that these specimens are susceptible to greater initial absorption than that of the thicker specimens. A summary of the maximum absorption rate of the grouts is shown in Figure 4.21. Grout E eventually experiences the highest reduction in mechanical properties. The failure surface shows that grout E contains more void the other grouts. This contributed to the increased moisture uptake underwater. The absorption trend of grouts C and D is similar to the absorption trend found on epoxy-modified concrete absorption properties (Jupiter et al. 2010). However, the absorption trend of grout E is increasing at an exponential rate for the test period considered. This behaviour is comparable to Non-Fickian Sigmoidal diffusion pattern (Crank 1975). Hence, grout E is more prone to mass uptake under hot-wet conditioning. It is to be noted that the absorption trend of grout E indicates that the mass uptake rate decreases over time. This implies that the absorption rate for grout E is expected to decrease at a time beyond the test period considered.

The effect of the least dimension on moisture uptake of the grouts is presented in Figure 4.22 to Figure 4.24. It is evident from the plots that the thicker the specimen, the lower the absorption rate. It is to be noted that specimens with comparable least dimensions exhibit similar nominal moisture intake. This implies

that the least dimension is critical since moisture penetration along a smaller thickness, or least dimension, provides a higher wetted volume than that of a thicker specimen.

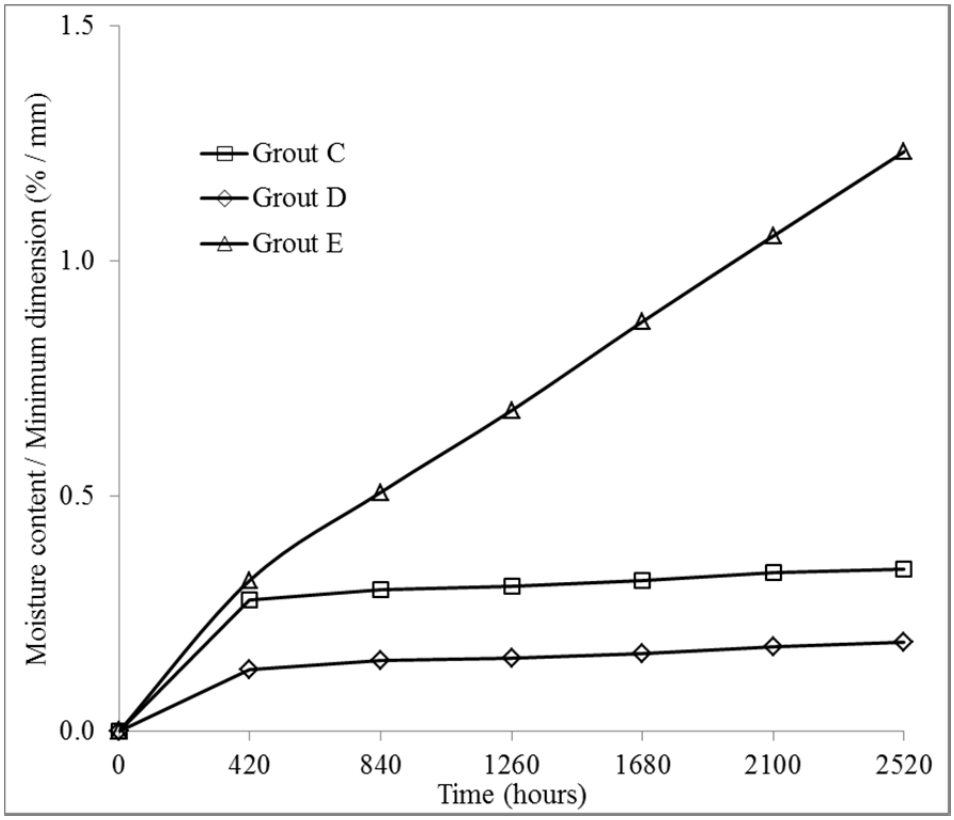

Figure 4.21 **Maximum moisture uptake of the grouts**

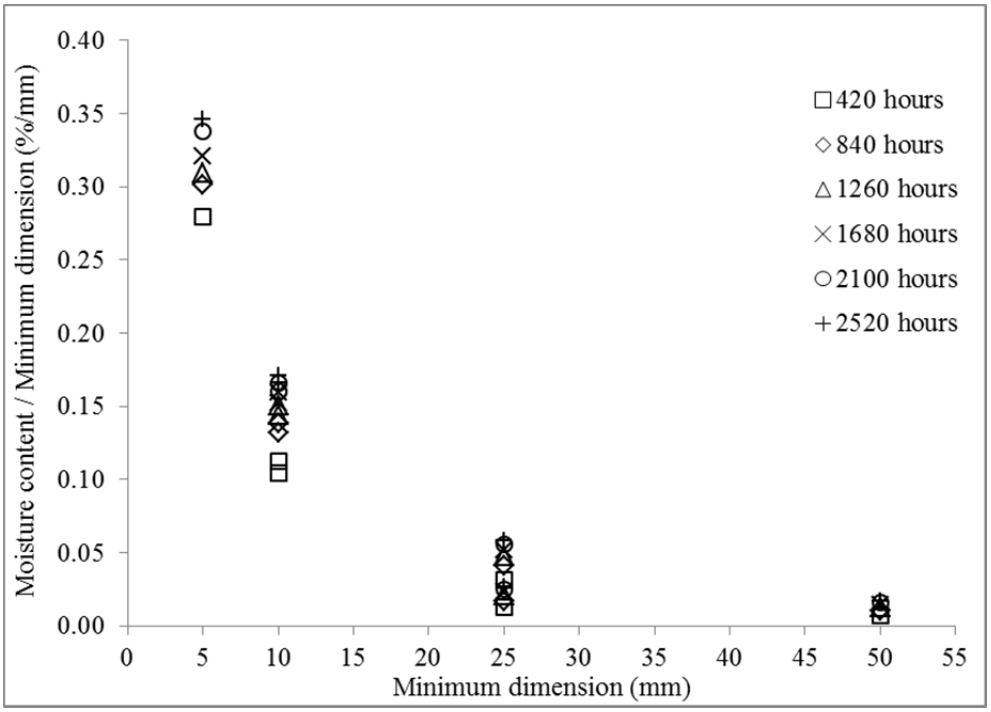

Figure 4.22 **Effect of minimum specimen size on nominal moisture absorption of grout C**

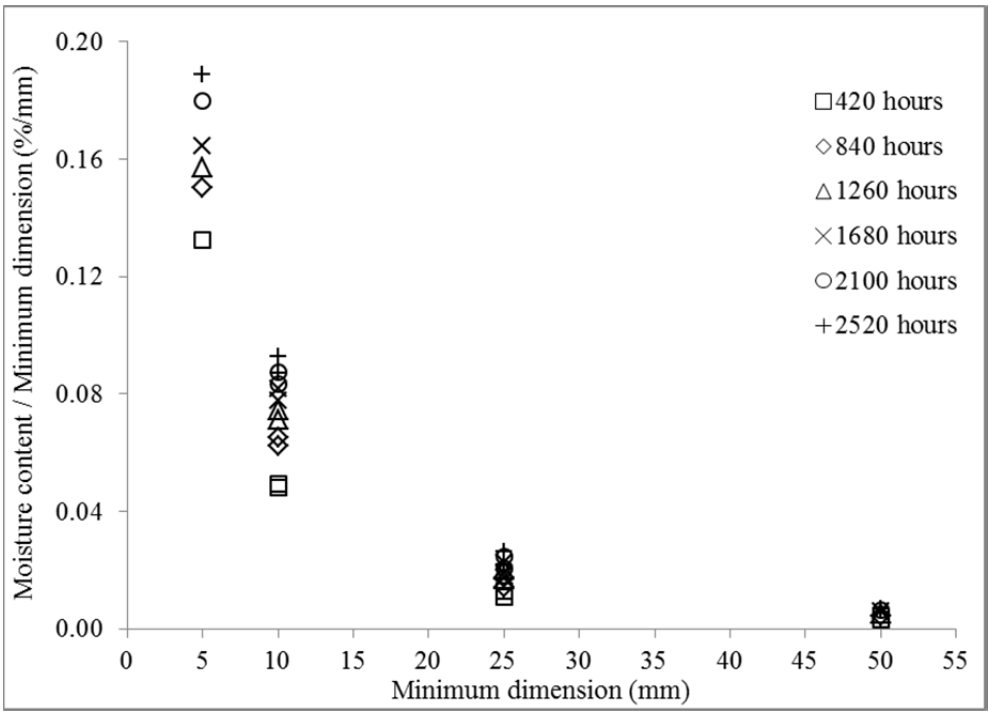

Figure 4.23 **Effect of minimum specimen size on nominal moisture absorption of grout D**

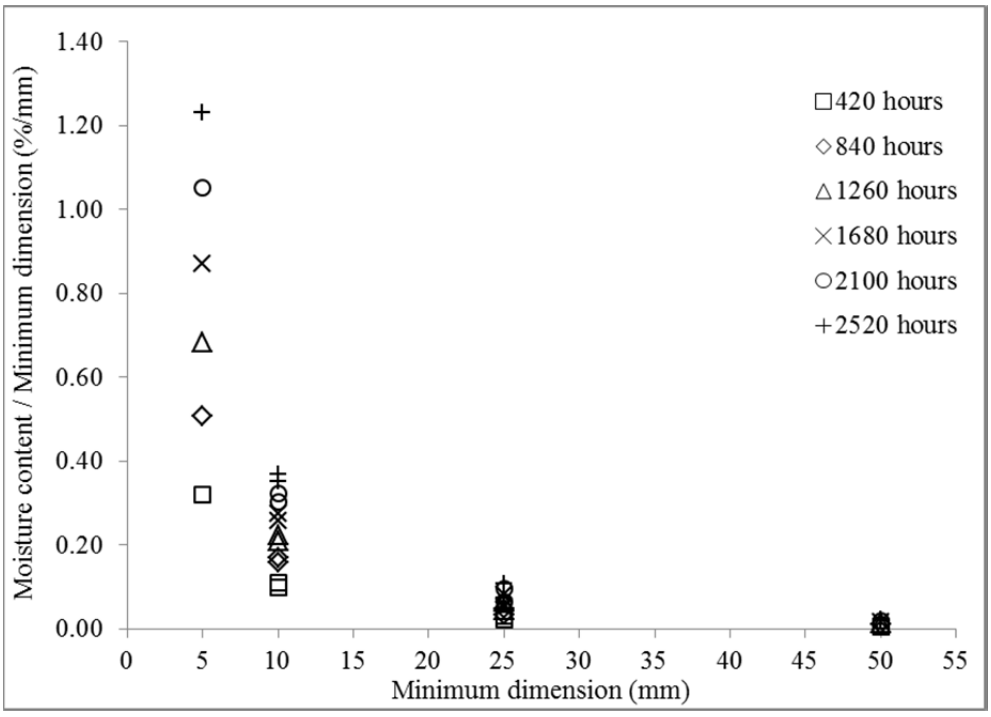

Figure 4.24 **Effect of minimum specimen size on nominal moisture absorption of grout E**

4.4.2 Effect of conditioning on mechanical properties

Table 4.3 provides a summary of the percentage reduction of the hot-wet conditioned grouts. The comparison is drawn with the mechanical and thermal properties of the similar grouts cured at 23°C for 7 days and tested at room temperature. These properties of the grouts are retrieved from Chapter 3. The comparison suggests considerable reduction of properties of the hot-wet conditioned

grouts. The dominant reduction occurs in the stiffness of the grouts. Tensile and flexural moduli of the hot-wet conditioned grout decrease by more than 90% compared to unconditioned grouts. However, compressive moduli of the 50 mm specimens of grouts D and E decrease by about 61 – 75%. This may happen due to the thicker diameter which may be affected less than in the 25 mm specimens. The tensile strength of grouts D and E are also reduced by more than 90%.

The compressive strength (Section 4.3.2.1) of the 25 mm specimens of grout C reduced to half when conditioned at 70°C and tested at 65°C, compared to as-manufactured specimens tested at room temperature. The reduction in compressive strength is higher in the coarse aggregate filled grouts (D and E) than that of the fine filled system. Hence, coarse filled system is more susceptible to degradation under hot-wet conditioning. Grouts D and E, which contain coarse filler, show that the compressive stress-strain curves fall after the yield/maximum stress. The failure strains of the 50 mm specimens are found to be higher than that of the 25 mm specimens. The highest reduction of strain is found for grout E where the 50 mm specimens exhibited about half the failure strain of that of the 25 mm specimen. This happens due to the localised crack formation at the middle, as shown in Figure 4.11. This phenomenon is also observed for the unconditioned 50 mm specimens at room temperature (Section 3.3.7.4).

The flexural properties of grout C are found to be lower than that of grout D and E, whereas the tensile properties of grout C are found higher (as shown in Table 4.1 and Figure 4.12). This behaviour is opposite to the comparative trend of direct tensile and flexural properties indicated in Chapter 3. This is due to the fact that conditioned grout specimens soften due to the action of elevated temperature. Hence, a tensile crack forms at the bottom when loaded. Since the crack is formed at the fibre, the top of the specimen goes through compression. Grout C has the highest resin / filler ratio among the grouts and provides lower resistance due to softening of the resin in the matrix.

Table 4.3 Summary of reduction of the mechanical properties

Properties		% Reduction compared to unconditioned specimens cured for 7 days at 23°C					
		C		D		E	
		25 mm	50 mm	25 mm	50 mm	25 mm	50 mm
Compressive	Compressive strength	12.3	28.8	71.4	49.0	62.2	59.6
	Compressive modulus	92.5	95.1	91.9	61.4	94.9	74.6
Tensile	Tensile strength	61.8		92.2		93.3	
	Tensile modulus	92.2		98.9		99.8	
Flexural	Flexural strength	83.6		43.8		63.4	
	Flexural modulus	98.0		95.9		98.4	
Shear	Shear strength	65.8		86.7		77.7	

Grouts D and E show relatively prolonged ductile deformation under tensile load (Section 4.3.2.2) compared to grout C. It is evident that the inclusion of coarse filler has contributed to the reduction of tensile strength as well as modulus when tested at elevated temperature conditions. It can be seen, from the cracked surfaces of both grouts D and E that the failure occurs in the matrix as shown in Figure 4.14. The action of coarse filler in the resin matrix can be described in two different ways (Suwanprateeb 2000). The first possibility is that the aggregate is strong enough to provide sufficient resistance against failure where the failure occurs thorough the resin matrix and the aggregate, provided the matrix is also stronger than the interface

bonding energy. The second possibility is that the individual aggregate strength is lower than both the resin matrix and the interface bond. From a detailed magnified view of grout E, shown in Figure 4.25, aggregates do not split due to tensile force. It can also be seen that debonding of aggregate and matrix is smooth indicating that interfacial bonding between aggregate and matrix is weaker than the particle strength of the aggregate. Again, since the matrix itself splits, the resin matrix is weaker than the aggregate particle strength. This behaviour is opposite to the tensile behaviour found from the study on these grouts in Chapter 3. This implies that hot-wet conditioning reduces the strength of the matrix-grout interface in each of the grouts.

From the shear test results presented in Section 4.3.2.4, the direction of the shear cracks was within the range of 30 – 45º. One crack runs from the top of the bottom notch diagonally towards the top plane surface, and the second crack runs almost parallel from the bottom of the top notch towards the bottom plane surface forming a shear wedge. The combination of shear and tensile failure was also observed in epoxy resin specimens where the higher inclination with vertical axis was related to the dominance of shear failure (Araki et al. 2005). However, failure in grouts D and E are more governed by shear where one failure plane is formed close to the notch. Hence, it is evident that the failure in grouts D and E is governed primarily by shear.

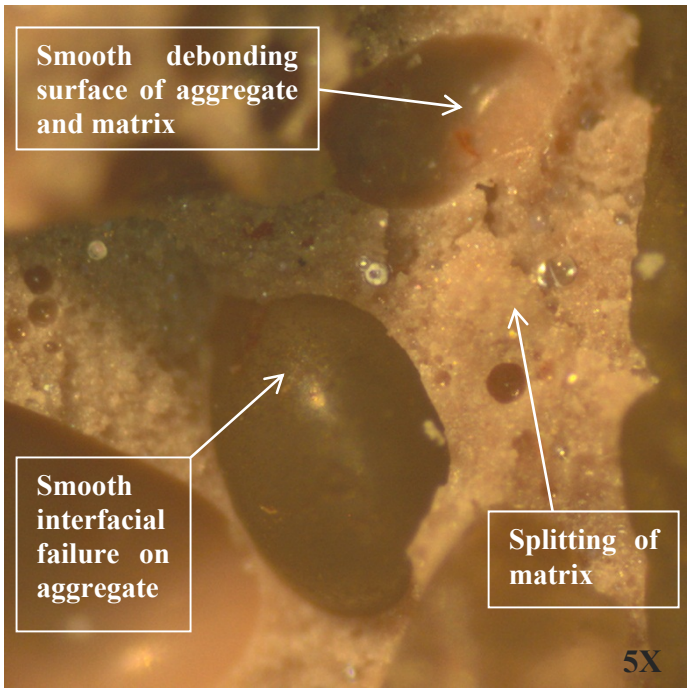

Figure 4.25 **Typical magnified failure surface of tensile specimen of grout E**

4.4.3 Effect on thermal properties

The T_g of the conditioned grouts C, D and E are found to be about 39ºC, 38ºC and 42ºC, respectively. In contrast, T_t is measured at 67ºC, 59ºC and 69ºC, for grouts C, D and E, respectively. The investigation on the thermal properties of these grouts without conditioning in Chapter 3, suggested that the T_g of these grouts ranged from 50 – 60ºC. This implies that hot-wet conditioning reduced the glass transition temperature of the grouts. Epoxy resin is found to experience a reduction in glass transition temperature (Zhou & Lucas 1999). Hence, it is expected that glass transition is reduced in epoxy grout due to conditioning. The mechanical properties

are affected by the hot submerged condition (70ºC) and elevated temperature testing at 65ºC, which is above their glass transition temperature as determined by the storage modulus. According to ASME PCC-2 (2006) and ISO/TS 24817 (2006), the service temperature of a repair component for non-leaking (Type A) and leaking (Type B) pipes should not be 20ºC and 30ºC less than the as manufactured glass transition temperature, respectively. From the results presented in Section 4.3.3, it is evident that the appropriate glass transition assignment approach used here, taking the onset of decline in the storage modulus, is more a conservative approach than taking the peak of the Tan δ curve (T_t). Furthermore, T_g is shown to reduce by approximately 20°C after hot-wet conditioning which justifies the 20 – 30°C temperature buffer. Hence, for the purposes of pipeline repair and rehabilitation, a conservative approach for taking the onset of decline in the storage modulus for glass transition temperature assignment is suggested. Future study of the long-term behaviour considering a range of temperatures is recommended, which is beyond the scope of the study.

4.5 Conclusions

Three grouts were tested for mechanical and thermal properties. The grouts were hot-wet conditioned for 1000 hours at 70°C to observe the effect of elevated temperature hot/wet conditioning resembling an underwater service pipeline environment. Compressive, tensile, flexural, shear and glass transition properties were determined. The following conclusions can be drawn from the results:

- The highest absorption is observed for grout E with a value of 1% to 6% after 2520 hours. The lowest absorption is found for grout D with values ranging from 0.3% to 0.9%. An accelerated absorption is found for the thinner specimens than that of thicker specimens.

- Aggregate filled grout experiences much more reduction in compressive properties than that of fine filled grout due to hot-wet conditioning. About 62% reduction of compressive strength is found compared to unconditioned specimens for 25 mm specimens of grout E when cured underwater at elevated temperature. More than 90% of the modulus is found to be reduced due to elevated temperature moist curing for the 25 mm specimens compared to the unconditioned specimens. However, the 50 mm specimens of grouts D and E experiences less reduction (more than 60 – 75%) in strength and modulus than that of grout C when compared with the conditioned specimens.

- The lowest tensile strength and modulus are found for grout E with a value of 1.3 MPa and 0.03 GPa, respectively for the conditioned specimens. The highest tensile strength and modulus are found for grout C with a value of 12 MPa and 0.38 GPa, respectively. Tensile strength and modulus decrease by more than 90% than that of unconditioned specimens except the strength of grout C which reduced by about 62%.

- The highest flexural strength is found to be 19 MPa for grout D which is about 44% less than that of the unconditioned specimens. The

lowest flexural strength is found to be 9 MPa for grout C which is reduced by about 84% of the unconditioned grout. More than 95% of the flexural modulus of the grouts is reduced due to hot-wet conditioning. The shear strength of grouts C, D and E are found to be 10 MPa, 3.4 MPa and 6.3 MPa, respectively which are reduced by about 66%, 87% and 78%, respectively of the unconditioned grout.

- The hot-wet conditioning reduces the glass transition temperature and results in a reduction in potential operating temperature. The reduction of strength and stiffness is due to the reduction of the glass transition temperature below and close to the elevated temperature used for hot-wet conditioning in this study.

The grouted repair system consists of infill grout and fibre-reinforced composite. Chapter 5 provides an investigation of the mechanical and thermal properties of a glass/vinyl ester composite sleeve of the grouted as sleeve repair. The effect of hot-wet conditioning of the properties is also analysed.

Chapter 5

Properties of glass fibre – vinyl ester composite as sleeve

5.1 Introduction

The prospect of fibre-reinforced composite as a reinforcement of pipeline repair is already been established (Shamsuddoha et al. 2013). The grouted sleeve system is made up of infill and a reinforcement sleeve. Details of the grout properties were tested in Chapter 3 and Chapter 4. It is, therefore, necessary to determine the physical properties of the composite materials as a sleeve. This chapter discusses the behaviour of a fibre-reinforced composite material under tensile, shear properties along with thermal properties.

A composite repair system is now being designed for both in-air and underwater conditions with elevated temperature (Djukic et al. 2013). However, polymeric composites are vulnerable to heat and moisture when operating in harsh service conditions as they absorb moisture in humid environments (Jiang et al. 2013; Ray 2006). The moisture sorption during environmental exposure is considered an indication of potential damage from matrix cracks and debonding at the fibre-matrix interface through the diffusion of hydrogen molecules of water to the polymer matrix (Chin et al. 1999; Ellyin & Maser 2004). The ingress of moisture may cause lowered damage tolerance and structural durability (Aniskevich et al. 2012; Engindeniz & Zureick 2008; McBagonluri et al. 2000). Hence, the performance and the structural integrity of repaired pipelines depend on the long-term properties of the fibre-reinforced composites and this demands a detailed investigation.

This chapter investigates the effect of hot-wet conditioning on the mechanical and thermal properties of glass fibre reinforced composites resembling a composite repair system for steel pipelines subjected to elevated temperature and in underwater condition. Glass fibre - vinyl ester composite laminates were manufactured and then tensile, shear and thermal properties were determined in both unconditioned and conditioned states. The experiments were chosen based on the requirements of 1000 hours of conditioning according to ISO/TS 24817 (2006), which is a standard for the qualification of composite repairs.

5.2 Experimental methodology

5.2.1 Materials

Fibre-reinforced composites made up of vinyl ester resin and E-glass fibres were used in this study. The materials used for this study were supplied, prepared and conditioned by CRC-ACS, Australia. CRC-ACS also supported the study by preparing the test plans of this study. The fibre reinforcement was a 1216 gsm 0/90 biaxial glass fibre non-crimp fabric (NCF) consisting of 567 gsm warp yarns and 638 gsm weft yarns stitched together by 11 gsm polyester yarns. The fibre content was 71% by weight determined from the burn-off experiments according to ASTM D 3171 (1999). The fibre stacking is shown in Figure 5.1.

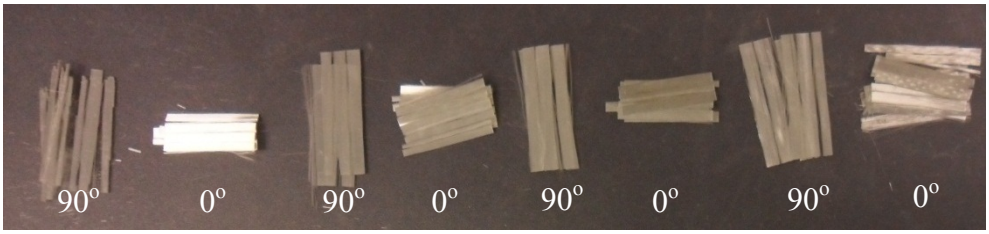

Figure 5.1 Stacking orientation of glass fibre / vinyl ester composite

5.2.2 Specimen preparation

All panels were manufactured via a vacuum bag resin infusion (VBRI) process and were post-cured in an oven at a temperature of 80°C for 12 hours. The laminate specimens were prepared to characterise their role as sleeve in a composite of the repair system.

5.2.2.1 Tensile specimens

The longitudinal tension (LT) and transverse tension (TT) coupons were prepared in accordance with ASTM D3039 (2008). A 600 mm x 600 mm panel of $[0/90]_4$ configurations was laid up; the four plies are stacked together with no reflection about the centreline with respect to the thickness. The LT specimens were cut along the 0° direction of the panel while the TT specimens were cut along the 90° direction. The tensile coupons were 250 mm long by 25 mm wide, with an average thickness of 3.6 mm (0.9 mm per ply).

5.2.2.2 Shear specimens

The interlaminate shear specimens were prepared in accordance with ASTM D 5379 (1998). A composite block with a laminate configuration of $[0]_{90}$ was manufactured with a thickness of approximately 80 mm. The block was then cut into a thickness of 4.5 mm and machined into 76 mm long and 20 mm wide specimens. A V-notch was machined centrally in both sides. The specimens were prepared such that the intended shear plane between the V-notches would result in a shear failure through the thickness of the laminate. A pair of bonded strain gauges oriented in +45° and -45° was attached to the specimen to measure the shear strain. The strain gauges were sealed using flexible silicon glue protecting the circuit from the ingress of moisture during the hot-wet conditioning. This sealant was only used to cover the area directly surrounding the gauges, leaving the other side of the specimen exposed to the water.

5.2.2.3 Glass transition temperature specimens

The glass transition temperature coupons were prepared in accordance with ASTM E 1640 (2009). These specimens were cut from the same panel prepared for the tensile coupons. The coupons were 60 mm long by 12 mm wide, with an average thickness of 3.6 mm (0.9 mm per ply).

5.2.3 Hot-wet conditioning

The specimens were conditioned in a temperature controlled bath containing tap water, as shown in Figure 5.2. A hot-wet conditioning duration of 1000 hours was used for all mechanical test specimens, as well as T_g specimens. This duration was selected in accordance with the time defined in ISO/TS 24817 (2006) as being representative of long-term conditioning. Another set of specimens for longitudinal

tensile and shear tests were hot-wet conditioned for 3000 hours to attain saturation of the specimens. The specimens were assessed for saturation as per ASTM D 5229 (2010). The mass measurements were taken using the Adam PW254 scales with an accuracy of 0.1 mg at every 7 days. The glass transition temperature was determined following the procedure described in ASTM E 1640 (2009). From the results, the T_g of the composite is found to be 110°C which is presented later in Section 5.3.3. The HWC temperature was chosen to be 80°C for two reasons: (i) this is the highest service temperature allowed for the composite material as per ISO/TS 24817 (2006), and (ii) moisture uptake is faster at a higher temperature compared to a lower. According to ASME PCC-2 (2006) and ISO/TS 24817 (2006), the maximum service temperature of a repair component for non-leaking (Type A) and leaking (Type B) pipes should be 20°C and 30°C lower than the glass transition temperature, respectively. Therefore, 80°C is considered for hot-wet conditioning and mechanical testing, which is about 30°C less than the T_g of the unconditioned specimens.

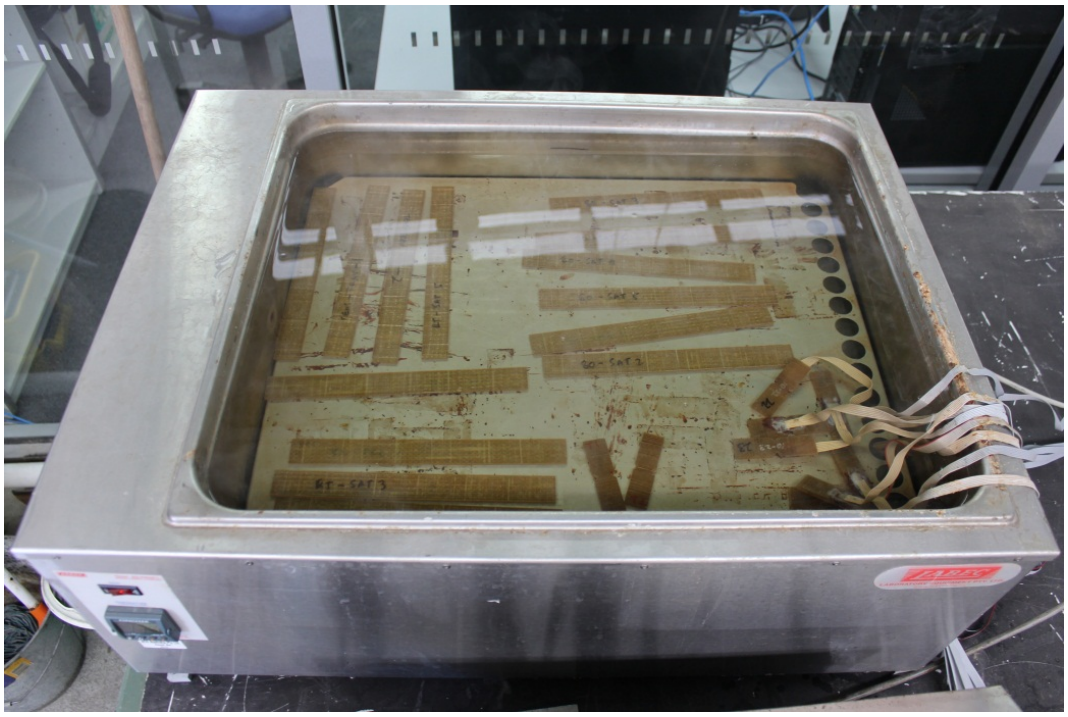

Figure 5.2 Specimens being conditioned at the water bath

5.2.4 Test details

The mechanical and thermal properties of the unconditioned and hot-wet conditioned composites were determined at room temperature (RT) and at an elevated temperature (80°C). Since the TT specimens have lower mechanical properties than the LT specimens, the TT specimens were considered more critical and investigated for further study to determine the effect of hot-wet conditioning. The conditioned specimens were immersed and conditioned for 1000 hours (~42 days) and 3000 hours (~126 days) before testing. It is seen from the previous chapter that thinner specimens are susceptible to higher absorption compared to thicker ones. The DMA rectangular specimens were conditioned and weighed over the 3000 hours conditioning to observe the time required to achieve saturation. The test matrix and test conditions are presented in Table 5.1. Tensile and shear as well as thermal properties were determined for as-manufactured (AM) and hot-wet conditioned (HWC – 1000 and HWC – 3000) specimens.

Table 5.1 Test summary

Specimen type	ID	Test Temp. (°C)	Standards/Methods	N	Loading rate
Tensile, LT	AM	RT 80	ASTM D3039 (2008)	5	2 mm/min
Tensile, TT	AM	RT 80			
	HWC – 1000	RT 80			
	HWC – 3000	RT 80			
Shear, S	AM	RT 80	ASTM D 5379 (1998)	5	1.3 mm/min
	HWC – 1000	RT 80			
	HWC – 3000	RT 80			
Glass transition temperature	AM HWC – 1000 HWC – 3000	RT to 150 RT to 150 RT to 150	ASTM E 1640 (2009)	3	1°C/min

5.2.4.1 Mechanical tests

Table 5.1 provides with the details of the tests for the composite. Relevant standards and practices are also shown in the Table. Geometries of the specimens were presented earlier in Section 5.2.2. All the mechanical characterisation tests were carried out following the same instrument as discussed in Section 3.2.3. Figure 5.3 shows the set-up and equipment used for testing elevated temperature. The preheating of the specimens was carried out at 80°C which is similar to the temperature discussed in Section 4.2.4.

During tensile testing, a biaxial extensometer was placed centrally across the specimen to measure the strain in both longitudinal and transverse directions. The strain in the through-thickness direction of the specimens was not measured. Once the strain reached 3000 με, the tests were halted, and the extensometer removed. The test was then resumed without any strain measurement. The tensile modulus and Poisson's ratio were calculated from the stress-strain curve using the Chord Method between the strain of 1000 and 3000 με. The V-notched (Iosipescu) shear specimens were tested using a Wyoming shear testing fixture. Two gauges were placed on the outer surface of the laminate and on the specimen surface oriented in the +45° and -45° directions. The shear modulus was calculated from the stress-strain curve between the strain of 1500 and 2500 με. A pair of bonded strain gauges was used to take measurements. The strain gauges were sealed using flexible silicon glue for protecting the circuit from the ingress of moisture at elevated temperatures. This is shown in Figure 5.12(a). This sealant was only present on one side of each specimen, and only covered the area directly surrounding the gauges. The other side of each specimen was exposed to the water.

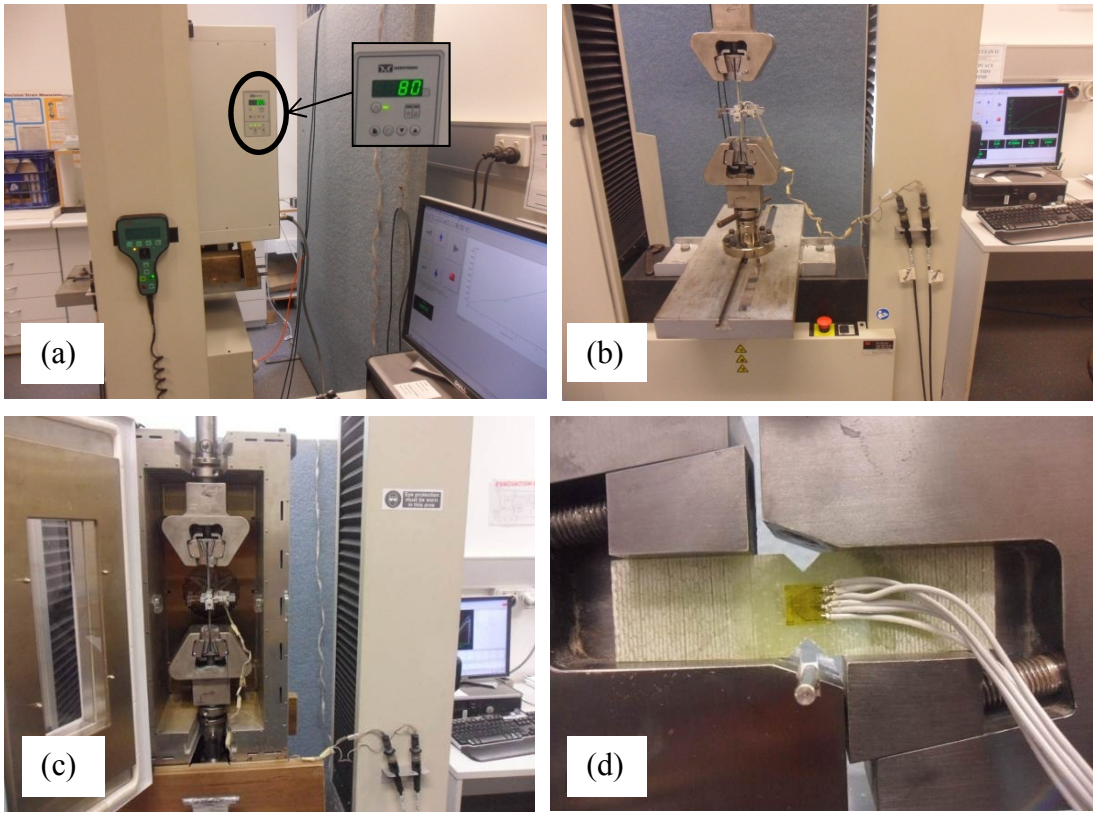

Figure 5.3 **Mechanical tests of the composite; (a) elevated temperature, (b) laminate tensile, (c) laminate tensile at elevated temperature, and (d) shear**

5.2.4.2 Thermal analysis

Dynamic Mechanical Analysis (DMA) was used to determine the glass transition temperatures of the composites which were conditioned under water at elevated temperature. The thermal analysis was carried out similar to that described earlier in Chapter 4. As discussed in Section 5.2.3, T_g value is used as ceiling value for hot-wet conditioning and testing. However, the highest possible glass transition value, T_t is also determined for extended understanding of the effect of hot-wet conditioning on thermal properties.

5.3 Experimental results and observations

5.3.1 Moisture absorption

Figure 5.4 shows the moisture absorption of the T_g specimen over 3000 hours of conditioning. The percentage moisture content and mass change are presented against immersion time. The highest moisture content is found to be about 0.22% which is reached within 672 hours (28 days). Study on glass fibre - vinyl ester composite conditioned at normal and saline water at a range of temperature of 15 – 80°C showed that the composite absorbed moisture by about 0.5% - 1.1% due to the existence of double bonds resulted from free radical polymerisation of the reactive styrene diluent and the unsaturated groups (Fraga et al. 2003; Kootsookos & Mouritz 2004; Zhang et al. 2000). ASTM D 5229 (2010) suggests an average moisture content of the material changes by less than 0.01% within the span of the reference time period, 1 week, as an indication of equilibrium. The moisture content is found to reach equilibrium at 1008 hours.

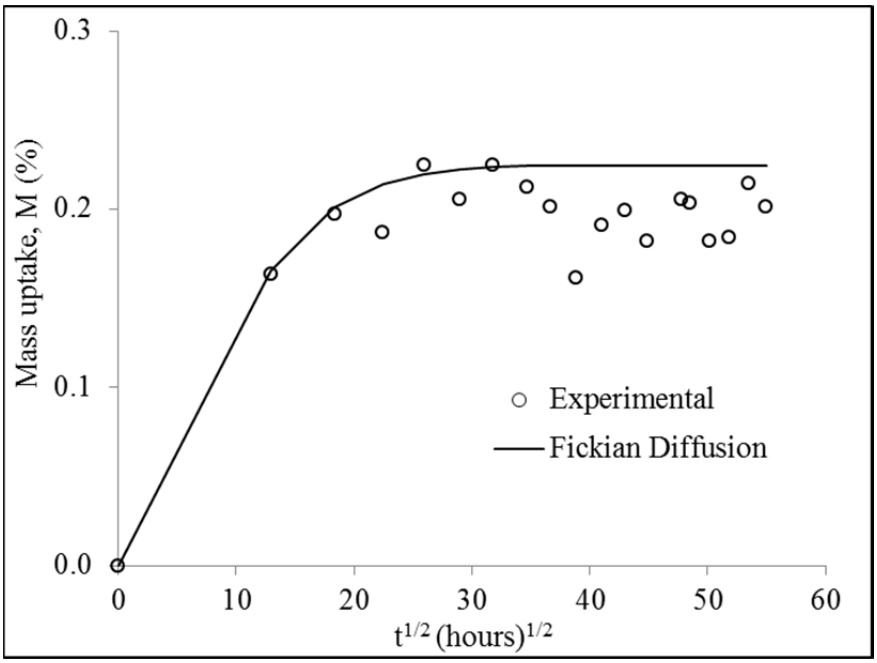

Figure 5.4 Moisture uptake of glass fibre - vinyl ester composite

5.3.2 Mechanical properties

Table 5.2 summarises the mechanical properties of both the unconditioned and conditioned glass fibre – reinforced vinyl ester composites at room and elevated temperatures with the figures in bracket as the standard deviations. The results are described in the following chapter.

Table 5.2 Summary of mechanical and thermal properties of composite

Properties		AM		HWC		HWC – Saturated	
				1000 hours		3000 hours	
		RT	80°C	RT	80°C	RT	80°C
LT	Strength (MPa)	427.1 (16.4)	395.9 (11.2)	186.7 (7.9)	147.5 (11.2)	153.2 (3.38)	127.7 (8.92)
	Modulus (GPa)	24.6 (0.1)	23.0 (0.5)	23.2 (0.7)	23.2 (0.8)	20.7 (0.30)	22.3 (0.53)
	Poisson's ratio	0.126 (0.010)	0.238 (0.018)	0.113 (0.010)	0.089 (0.020)	0.076 (0.007)	0.104 (0.012)
TT	Strength (MPa)	501.6 (15.3)	438.6 (23.3)	-	-	-	-
	Modulus (GPa)	28.0 (0.2)	26.7 (0.3)	-	-	-	-
	Poisson's ratio	0.133 (0.013)	0.203 (0.059)	-	-	-	-
S	Shear strength (MPa)	30.0 (2.6)	18.8 (4.1)	10.2 (1.8)	7.4 (2.9)	9.2 (1.9)	6.7 (2.7)
	Shear modulus (GPa)	4.15 (0.10)	3.13 (0.19)	3.27* (0.16)	5.58** (N/A)	4.55** (N/A)	***
	Failure strain (με)	8008 (515)	7120 (1457)	2919* (468)	1373** (N/A)	1823** (N/A)	***
Tg (°C)		110 (1.2)		97 (1.7)		101 (0.6)	
Tt (°C)		128 (0.3)		113 (0.5)		115 (0.4)	

* Only 2 readings used to calculate average, where failure occurred along notched shear plane
** Only 1 reading used, where failure occurred along notched shear plane
*** Results neglected since failure occurred near the test fixture supports

5.3.2.1 Laminate tensile properties

The tensile strength, modulus and Poisson's ratio of the unconditioned specimens along the longitudinal direction (LT) are 502 MPa, 28 GPa and 0.133, respectively while along the transverse direction (TT) are 427 MPa, 25 GPa and 0.126, respectively. Being the direction of lower properties, the TT specimens are conditioned and analysed in the remainder of this chapter. After hot-wet conditioning, the tensile strength, modulus and Poisson's ratio of the TT specimens are reduced to 187 MPa, 23 GPa and 0.113, respectively when tested at RT. When

tested at 80°C, this further reduced to 148 MPa, 23 GPa and 0.089, respectively. On the other hand, the HWC – 3000 specimens have tensile strength of 153 MPa when tested at RT but reduced to 128 MPa when tested at 80°C. However, tensile modulus of HWC – 3000 specimen is around 21 MPa when tested in both RT and at 80°C.

Figure 5.5 to Figure 5.6 show the typical load-extension behaviour of the transverse AM, HWC – 1000 and HWC – 3000 laminates. The behaviour is linear to failure with small disturbances seen at approximately 2 mm cross-head extension due to the disengagement of the extensometers. However, the AM specimens show abrupt change near the peak load as indicated by the sudden drop in the load-extension line due to the initiation of failure in the specimens.

The typical failure modes for the unconditioned specimens are shown in Figure 5.7. The failure of the unconditioned AM specimens for both RT and elevated temperature are similar. The longitudinal failures are progressive indicating partial tear of fibres near the grip and finally total collapse of the laminate releasing a cluster of fibre fragments as seen from Figure 5.7. This type of failure was also reported for glass fibre reinforced composites (Torabizadeh & Fereidoon 2013; Wonderly et al. 2005). The crack covers the entire gauge area where matrix cracking and fibre pull out are also observed. However, the damage area in the transverse specimens was more limited compared to than that of the LT specimens (Figure 5.7b).

The typical failure of the transverse HWC-1000 and HWC-3000 specimens is shown in Figure 5.8. The failure pattern of the specimens tested at room temperature and elevated temperature is similar. The failure occurred suddenly with a smaller damaged area compared to unconditioned specimens. Small amount of fibre-matrix debonding is observed for both the HWC-1000 and HWC-3000 specimens. The dominant failure of the unconditioned specimens occurred at or within 5 mm of the grip which can be defined as failure "Type A" according to ASTM D3039 (2008).

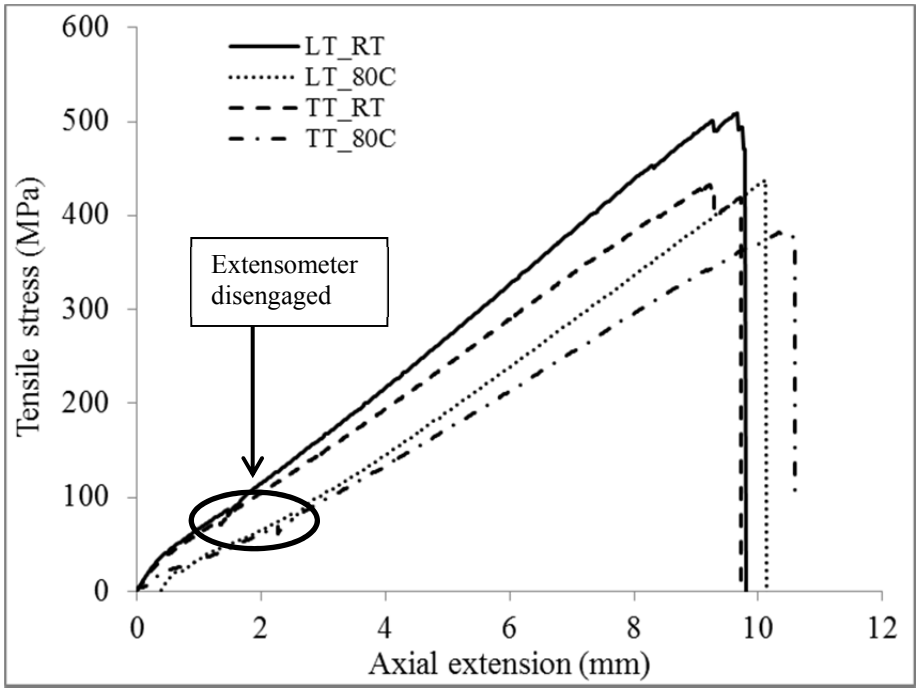

Figure 5.5 **Typical stress-extension behaviour of the AM laminate tensile specimens**

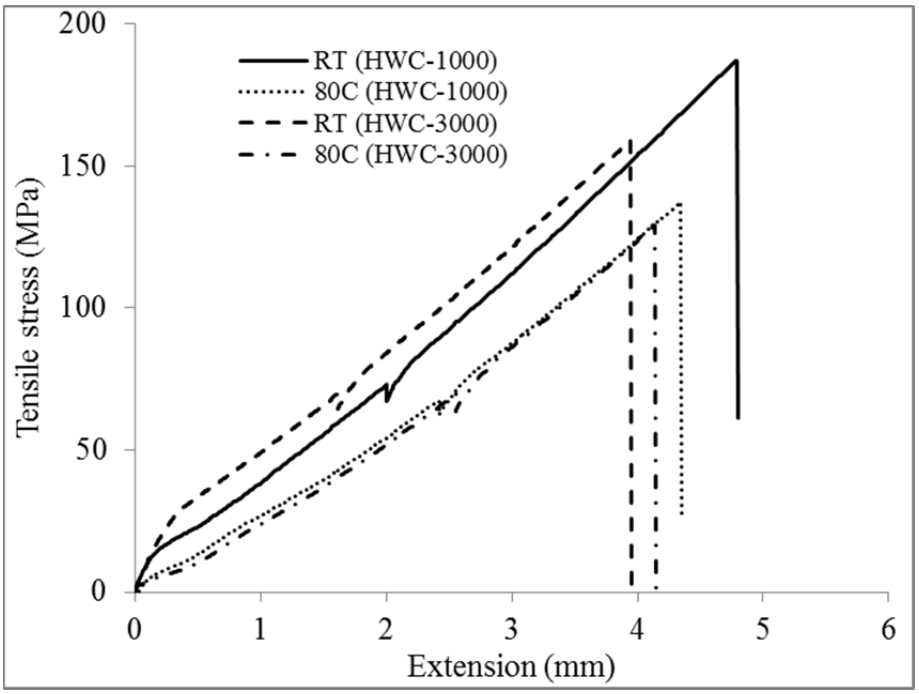

Figure 5.6 **Typical stress-extension behaviour of conditioned laminate tensile LT specimens**

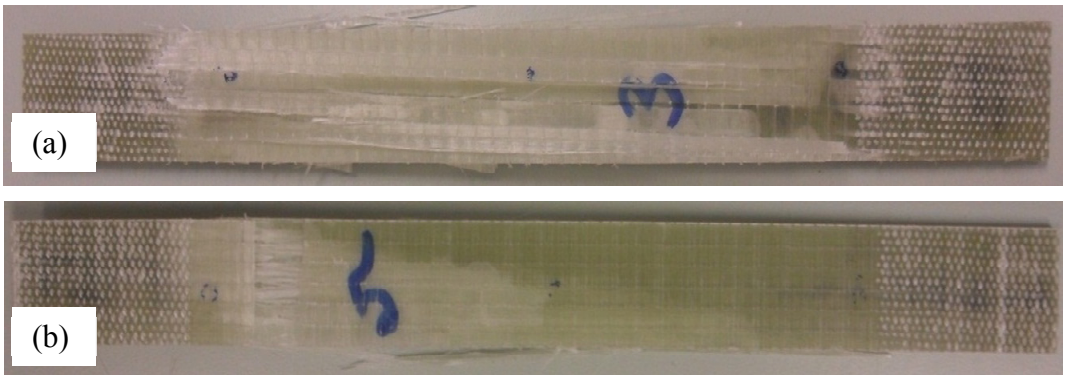

Figure 5.7 **Typical tensile failure pattern of unconditioned AM laminate specimens; (a) LT, (b) TT**

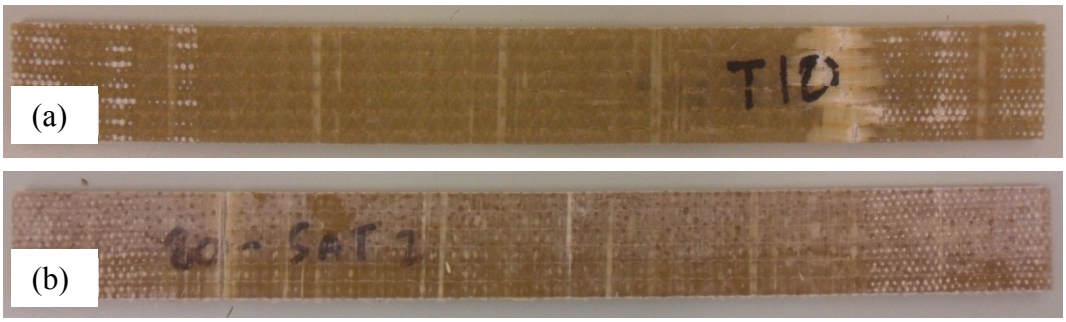

Figure 5.8 **Typical tensile failure pattern of conditioned LT laminate specimens; (a) HWC – 1000 specimens, (b) HWC –3000 specimens**

5.3.2.2 Interlaminate shear properties

Table 5.2 summarises the shear properties of the composite. The shear strength and modulus of the unconditioned AM specimens are around 30 MPa and 4.2 GPa, respectively when tested at RT and are reduced by about 37% and 25%, respectively when tested at 80°C. On the other hand, the strength of the HWC –

1000 specimens is 10 MPa when tested at RT and is reduced by 28% when tested at 80°C while the stiffness is at 3.3 GPa when tested at RT but increases by 71% when tested at 80°C. The strength of the HWC – 3000 specimens is 9 MPa when tested at RT but is reduced to about 7 MPa when tested at 80°C with the stiffness almost the same.

The typical shear stress-strain behaviour of the AM, HWC – 1000 and HWC – 3000 specimens is shown in Figure 5.9 and Figure 5.10. The stress-strain relation of the unconditioned and conditioned specimens is almost linearly elastic up to failure. The reduction of strain with the increase of stress at the end of the stress-strain plots near the failure of the specimens indicates that either one or two of the strain gauges at this instance is no longer functioning, which is considered as the failure of the specimens and the termination of data collection. The peak shear stress of specimens tested at room temperature is higher than that when tested at elevated temperature. The failure strain of the AM specimens is around 8000με.

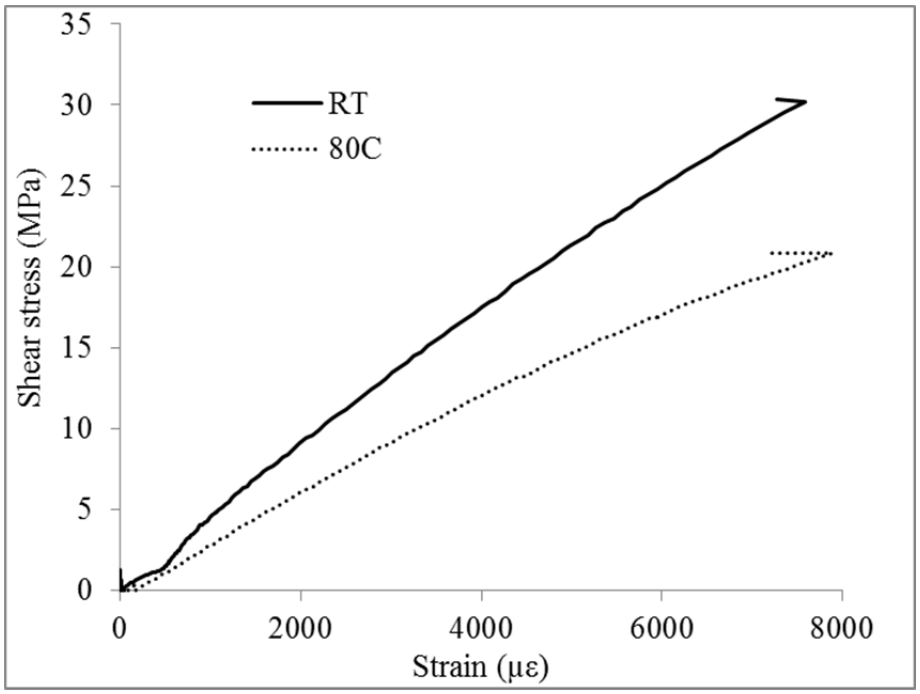

Figure 5.9 **Typical stress-strain behaviour of unconditioned AM shear specimens**

Figure 5.11a shows failed shear specimens in the test fixture. Figure 5.11b presents the typical failure pattern of the shear specimens at RT and 80°C. It can be seen that the cracks start at the root of the notches in the AM specimens and progress along the shear plane up to the root on the bottom of the notches. After the peak load, the failure is sudden and results in complete separation of the specimen. Failure of the conditioned specimens tested at both RT and 80°C is comparable. Figure 5.12 show the typical failure pattern of the HWC – 1000 and HWC – 3000 shear specimens. The cracks primarily occur near at the notches. However, sometimes there are two approximately systematic cracks in HWC – 1000 and HWC – 3000 specimens located immediately adjacent to the tips of the applied load.

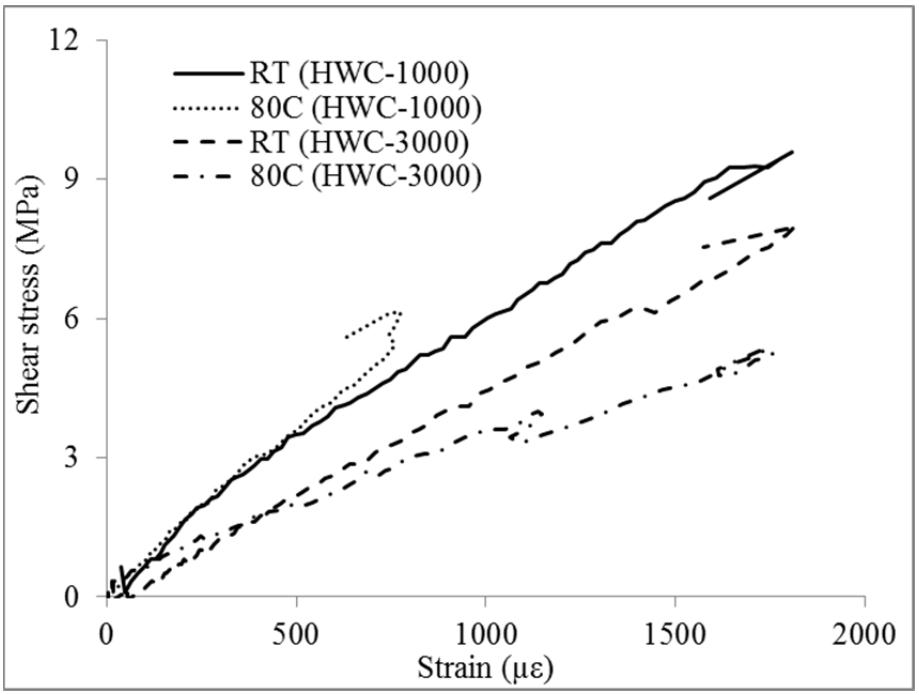

Figure 5.10 **Typical stress-strain behaviour of the conditioned shear specimens**

While testing the conditioned specimens, it was found that failures initiated along the shear plane (Figure 5.12), and also near the test fixture supports away from the intended shear plane as seen in Figure 5.12a. Failure of the composite away from the intended shear plane may be the result of the flexible sealant applied to the strain gauges to protect them from moisture-induced damage across the conditioning period. For all specimens, shear strength was calculated using the area across the notch, even when the failure occurred near the test fixture supports. In these cases the shear plane can be considered to have strength in excess of the stated individual values. However, the average shear modulus and failure strain presented in Table 5.2 are calculated only from specimens that failed along the shear plane between the notches.

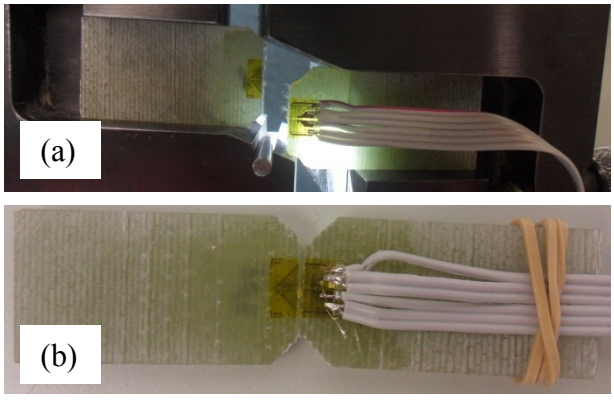

Figure 5.11 **Typical failure pattern of unconditioned AM shear specimens; (a) failure during testing and (b) typical failure plane**

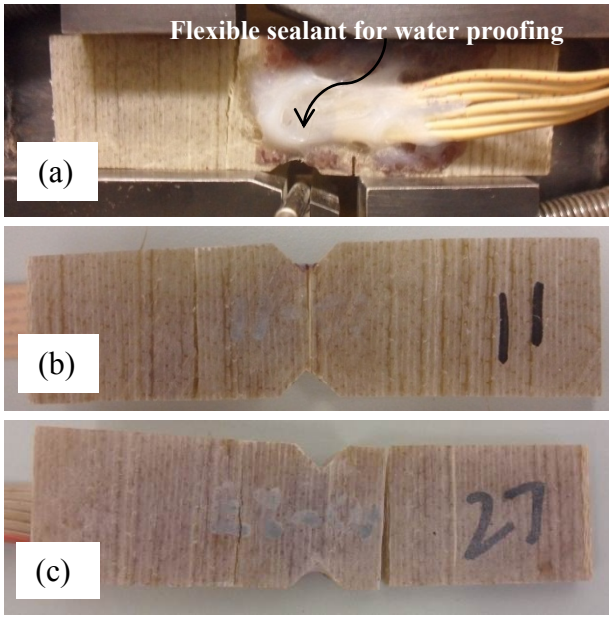

Figure 5.12 **Typical failure pattern of conditioned shear specimens; (a) failure during testing, (b) HWC – 1000 specimens tested and (c) HWC – 3000 specimens**

5.3.3 Thermal properties

Figure 5.13 shows the typical storage modulus and tan δ signals against the temperature. T_g and T_t of the AM specimens are found to be 110°C and 128°C, respectively. In case of HWC – 1000 specimens, T_g and T_t are reduced to 97°C and 113°C, respectively. Whereas, T_g and T_t HWC – 3000 increase marginally to 101°C and 115°C, respectively. The storage modulus plots suggest that the modulus of the conditioned and unconditioned specimens is comparable. However, the transition range shifted to the left by about 13°C. This behaviour is also comparable to the tan δ signals where there is about 15°C shift in the transition in the HWC – 1000 and HWC – 3000 specimens.

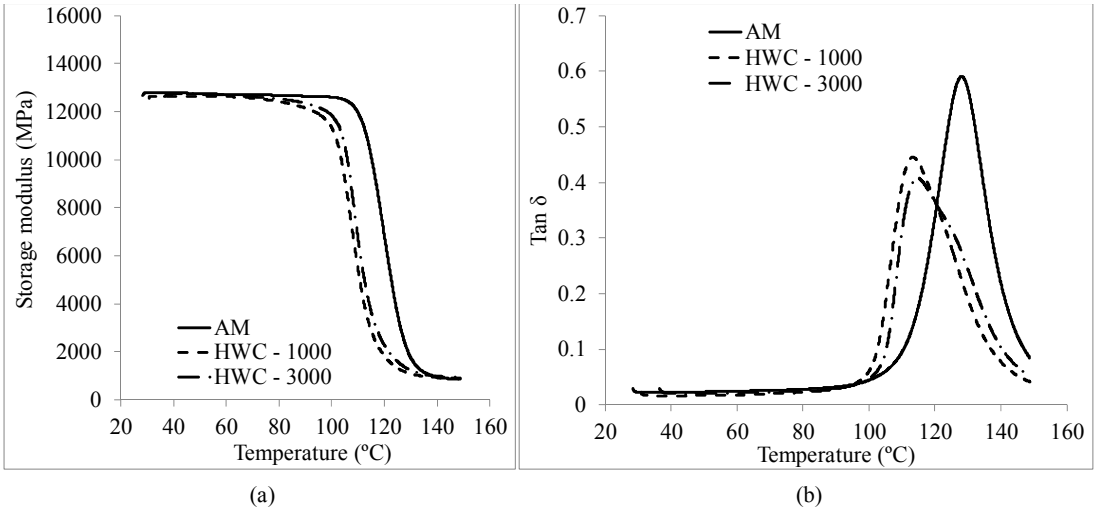

Figure 5.13 **Thermal plots for glass-reinforced composite (a) storage modulus vs temperature, and (b) Tan δ vs temperature**

5.4 Discussion

An aesthetic fading in colour from greenish white to brownish on the specimen surface was observed due to hot-wet conditioning, which can be seen from Figure 5.7 and Figure 5.8 with no apparent physical deformation. There was no formation of blisters on the specimen surface due to conditioning. The water in the water bath produced a mild odour. These phenomena were also reported in previous literature when glass fibre-reinforced composites were subjected to hygrothermal ageing (Adams & Singh 1996; Carra & Carvelli 2014; Nishizaki & Meiarashi 2002; Turvey & Wang 2007). This might be due to chemicals leaching from the resin matrix and to a reaction with the water.

5.4.1 Moisture uptake behaviour

The moisture absorption behaviour in Figure 5.4 suggests that most of the moisture is absorbed within the first 168 hours of immersion in water. The diffusion pattern can be correlated using the Fickian diffusion pattern (Crank 1975; Springer 1981), which is discussed and adopted in (Ellyin & Maser 2004; Jiang et al. 2013). It can also be seen that the moisture absorption as the function of time has maximal value of 0.22%, following which it decreases. Hence, considering this moisture content of saturation as the maximum equilibrium amount of absorption, M_∞; the moisture diffusion coefficient, D can be determined as 2.22×10^{-6} mm^2/s which are within the range of polymer composite absorption characteristics (Adams & Singh 1996; Aniskevich et al. 2012). The resulted prediction plot is also shown in Figure 5.4. This relation of moisture intake is comparable to the diffusion pattern shown by Aniskevich et al. (2012) at an elevated temperature close to the glass transition temperature. Although the conditioning temperature used in this study is below the glass transition temperature, the decrease may be attributed to the reduction of the volume content of the pores filled with water resulted from the polymer matrix after-cure.

The fact that moisture absorption does not increase beyond the maximum point indicates that polymer relaxation does not occur. Polymer relaxation is a long-term swelling phenomenon resulting in the relocation of the pores spaces. However, the reduction in moisture uptake may be due to irreversible degradation and/or leaching of low molecular weights (Chin et al. 1999). The conditioned glass composite appears to reach saturation after about 1008 hours of immersion. Similar findings were observed by Kootsookos and Mouritz (2004) wherein the glass fibre - vinyl ester composite conditioned in saline water at 30°C reached saturation at around 2000 hours (90 days). Another study suggested that the saturation of glass fibre - vinyl ester composite conditioned under saline water at a temperature range of 4 – 38°C occurred at around 3000 hours (Zhang et al. 2000). Thus, the results suggest that the moisture intake and saturation of composites are accelerated at elevated temperature which may be attributed to potential crazing, micro-cracking and other morphological changes allowing additional sorption to occur (Chin et al. 1999).

5.4.2 Effect of elevated temperature on mechanical properties

A comparison of the obtained properties is given in Table 5.3. Both the transverse tensile strength and stiffness is reduced by about 7% when the AM coupons are tested at 80°C. The transverse strength of the HWC – 1000 specimens is reduced by about 21% due to elevated temperature during test, whereas the modulus

remains the same. Hence, unconditioned specimens are less susceptible to tensile strength reduction than conditioned specimens when tested at elevated temperature. However, tensile stiffness is reduced for the AM specimens, whereas it remained similar for HWC – 1000 specimens and is increased for the HWC – 3000 specimens. This indicates that there is insignificant change in tensile stiffness due to elevated temperature for both unconditioned and conditioned specimens. A similar trend was also reported for polyester and vinyl ester based glass fibre composites where tensile strength was found to be reduced considerably than that of the modulus (Carra & Carvelli 2014). This behaviour is due to the fact that the T_g of the AM composite is found to be 110°C which is well above the conditioning temperature and hence does not plasticise the matrix. The reason of affecting the strength more than the stiffness is due to the conditioning and an associated moisture ingress mechanism is discussed in Section 5.4.3.

Both unconditioned and conditioned specimens experience a reduction in interlaminate shear strength when tested at elevated temperature. There is about a 37% reduction in the shear strength due to elevated temperature for the unconditioned AM specimens and about a 28% reduction in both HWC – 1000 and HWC – 3000 specimens. The shear modulus of AM specimens tested at elevated temperature is reduced by about 25%, whereas modulus of HWC – 1000 specimens is increased by about 71%. However, comparison is not drawn for modulus of HWC – 3000 specimens since failure in the shear specimens occurred away from the intended shear plane. Paim et al. (2013) showed that tensile strength is highly dependent on test temperature, where higher test temperature resulted in a lower tensile strength; whereas insignificant effect on modulus was observed. The reason behind increment of modulus may be the application of a protective layer of on the gauges as sealant.

Table 5.3 Summary of reduction of the mechanical properties

Properties		% Reduction						
		AM	HWC-1000	HWC-3000	RT		80°C	
		RT to 80°C	RT to 80°C	RT to 80°C	AM to HWC-1000	AM to HWC-3000	AM to HWC-1000	AM to HWC-3000
LT	Strength	12.6	-	-	-	-	-	-
	Modulus	4.9	-	-	-	-	-	-
TT	Strength	7.3	21.0	16.6	56.3	64.1	62.7	67.7
	Modulus	6.5	-0.1	-7.7	5.8	15.9	-1.2	2.9
S	Strength	37.2	27.7	27.6	66.0	69.2	60.9	64.5
	Modulus	24.6	-70.6	-	21.2	-78.3	-9.6	-

The tensile strength and stiffness of the TT specimens are reduced by about 13% and 5%, respectively when tested at 80°C. These ratios are found to be about 7% for both strength and stiffness. Study on both longitudinal and transverse direction of glass fibre composites showed that the higher variations were found in the transverse direction compared to the longitudinal direction (Carra & Carvelli 2014). It is to be noted that both the directions have got similar fibre fraction; however the LT specimens has higher fibre than the TT specimens. For that reason, despite the fact that hot-wet conditioning is carried out for the TT specimens; the comparison can also be conservatively extrapolated for the LT direction.

5.4.3 Effect of hot-wet conditioning on mechanical and thermal properties

A comparison between the AM and HWC – 1000 specimens showed that the tensile strength along the LT direction is reduced by 56% when tested at RT and by 63% when tested at 80°C. A further reduction in strength was observed for HWC – 3000 specimens as shown in Table 5.2. This implies that the hot-wet conditioning is more responsible in reducing the tensile strength than that of elevated temperature. Glass fibre – vinyl ester specimens conditioned at 75°C were found to have weaker fibres than that of unconditioned specimens which eventually suggested that hygrothermal ageing did affect the fibre properties (Ellyin & Maser 2004). Liao et al. (1999) also found the degradation of the tensile strength indicated through failure characteristics of the individual fibres due to the attachment of the water molecules to silica network (Si-O-Si bond) proposed by Michalske and Freiman (1983).

The comparison of the results also suggests that there is negligible difference in strength between HWC – 1000 and HWC – 3000 specimens. Conversely, the reduction in modulus is higher when tested at room temperature than that of at 80°C. The AM specimens have a 6% lower tensile modulus compared to HWC – 1000 specimens when tested at RT but 1% higher when tested at 80°C. The AM tensile modulus is decreased by about 16% compared to HWC – 3000 modulus when tested at elevated temperature, whereas it decreased by only about 3% when tested at 80°C. Hence, the conditioning of the glass fibre - vinyl ester composite results in a higher reduction of tensile stiffness than when tested at the elevated temperature of 80°C. It can be added that elevated temperature is found to affect the stiffness of the AM specimens. Hence, the overall percentage reduction is higher in the AM specimens at room temperature than that of elevated temperature. In case of hot-wet conditioning, the two actions can occur simultaneously: matrix plasticisation due to water sorption and stiffness increase form the loss of low molecular weight substances (Apicella et al. 1982). In the case of ageing, the strength and the failure strain is expected to decrease after the ageing process which may eventually lead to increased or decreased stiffness depending on the comparative values of these properties. However, both the strength and stiffness reduced due to hot-wet ageing and this was linked to degraded fibre-matrix bonding (Liao et al. 1999). The fact that strength and strain are reduced in contrast to an insignificant reduction in modulus, may be linked to the brittle matrix. The brittle failure of the fibre and matrix was also reported when conditioned and tested at 50°C (Ellyin & Maser 2004).

There are about a 66% and 61% decrease in the shear strength of the AM specimens compared to HWC – 1000 specimens when tested at room temperature and at 80°C, respectively. At the same time, there are about a 69% and 65% decrease in the shear strength of the AM specimens compared to HWC – 3000 specimens when tested at room temperature and at 80°C, respectively. It is to be noted that the conditioning was already carried out at the elevated temperature. The reason behind this is that possible damage imparted in the specimens in the form of matrix cracks and debonding at the interface between fibres and matrix can occur due to moisture sorption during the conditioning process (Carra & Carvelli 2014). This indicates that the hot-wet conditioning affects the interlaminate shear strength more than when tested at the elevated temperature, which also implies that once the composite goes through hot-wet conditioning the test temperature eventually has a smaller effect of the shear strength. Difference of shear strength between AM to HWC – 3000 specimens is higher than that of AM to HWC – 1000 specimens. However, the

difference is negligible compared to additional 2000 hours of conditioning. This also justifies the moisture absorption trend shown in Section 5.3.1. The increase in shear modulus for HWC – 3000 specimens suggests that the matrix becomes brittle due to hot-wet conditioning which is also evident from the reduced failure shear strain of conditioned specimens. This behaviour of attaining brittleness was also reported by Fraga et al. (2003) and Ellyin and Maser (2004) where brittle failure in fibre and matrix was found in glass fibre - vinyl ester composite conditioned at elevated temperature. However, in both the cases degradation of the matrix is indicated through the diffusion of hydrogen molecules of water to the polymer matrix. Also, the toughness of the fibre/matrix interphase to the composites was found to be affected by the water immersion (Kootsookos & Mouritz 2004). Hence, the relatively small reduction in tensile modulus and increment of shear modulus is due to the fact that the elevated temperature below glass transition temperature cause brittleness in the resin matrix and fibre-matrix interphase which results in a lower strength and failure strain. However, the relative reduction in failure strain is much lower than that of strength, thus providing a higher modulus. On the other hand, at the same time the hygrothermal ageing at the elevated temperature results in a reduction in both tensile and shear strengths due to the moisture ingress and subsequent degradation in the fibre level.

Figure 5.13b indicates that the tan δ signals reduced due to conditioning at 80°C compared to unconditioned specimens. This behaviour also indicates that the physical properties are reduced by the action of hot-wet conditioning. The T_g and T_t of HWC – 1000 specimens is found to be 97°C and 113°C, respectively. The glass transition temperature of the conditioned specimens is reduced by about 13 – 15°C when tested compared to AM specimens. However, the glass transition temperatures of HWC – 3000 specimens increased marginally by about 2 – 4°C. This is comparable to the dynamic behaviour of composites analysed by Fraga et al. (2003) wherein the T_g values exhibited insignificant variation when tested at 40°C and 80°C compared to 0°C. This also indicates that there is an insignificant difference in properties between 1000 hours and 3000 hours. Hence this composite may be used at the upper temperature limit of 80°C as per ISO/TS 24817 (2006).

5.4.4 Assessment of 1000 hours conditioning to represent long-term

Study on glass fibre / vinyl ester composite conditioned at higher temperatures of 40°C and 80°C showed that the elevated temperature accelerated the absorption rate and quickened the saturation process from about 1400 hours at 40°C to about 280 hours at 80^o (Fraga et al. 2003). Hence, it is evident that the elevated temperature used in this study has resulted in a faster achievement of saturation. Since saturation occurred within 1000 hours when conditioned at 80°C, this conditioning criterion can be considered to represent a ‘long-term’ saturation environment for the investigated composite. This consideration is valid for this particular glass / vinyl ester composite and conditioning temperature.

The glass transition and moisture uptake results suggest that the specimens are at, or close to saturation, at 1000 hrs. This indicates that the T_g of the composite is unlikely to reduce further with additional hot-wet conditioning. The mechanical results indicate that 1000 hot-wet conditioning results in a considerable reduction in tensile and shear strength. However, there is no significant change in stiffness. The reduction in strength is considered acceptable for the design application which is

governed by strain. This is because, in the case of stiffness based design, the composite can undergo significant strength reduction across its design life whilst still performing its function.

5.5 Conclusions

In this study, the mechanical, thermal and moisture absorption properties of glass fibre - vinyl ester composites subjected to hygrothermal ageing underwater for 1000 hours and 3000 hours at a temperature of 80ºC were investigated. Laminate tensile, shear and thermal properties were determined at room and at elevated temperature. The following are the main findings of the study:

- The glass fibre – vinyl ester composite absorbed moisture of 0.22% and reached saturation after 1008 hours (42 days).
- The tensile strength and modulus of the composites along the transverse direction are 427 MPa and 25 GPa, respectively. Due to the hot-wet conditioning for 1000 hours (HWC – 1000) and 3000 hours (HWC – 3000) at 80°C, strength is reduced by 68% with minimal change in stiffness.
- The interlaminate shear strength and modulus of the composites are 30 MPa and 4.2 GPa, respectively at room temperature. Due to the hot-wet conditioning, 69% strength reduction was observed with insignificant change in the modulus.
- The glass transition temperature (T_g) of the composite is 110°C. This is reduced to about 97°C after conditioning and reaching saturation indicating that the composites are suitable for pipeline repair in continuous service at 80°C.
- The hot-wet conditioning at 80°C for 1000 hours can resemble the 'long-term' service performance of the glass fibre – vinyl ester composite for pipeline repair and rehabilitation. This confirms the 1000 hours duration for the qualification test requirement suggested by ISO/TS 24817 (2006).

This chapter, along with Chapter 3 and Chapter 4, present an extensive investigation of potential components of the repair. The results point towards the high feasibility of using these materials as components of the defective pipe. A simplified finite element parametric study is performed in Chapter 6 for a range of component parameters in a grouted repair. The effective parameters are selected for full scale analysis in Chapter 7 using the material properties found from Chapter 3 and Chapter 5.

Chapter 6

Analysis of the behaviour of grouted composite repair system

6.1 Introduction

FRP repair systems of pipelines are generally divided into two types – flexible 'wet lay-up systems' and pre-cured 'layered systems' (Alexander & Francini 2006). Another development on the pre-cured system for repair of high pressure pipelines is the stand-off split sleeve where the annulus between the pipe and the FRP composite sleeve is filled with an appropriate grout to provide a continuous support for the outer shell (Palmer-Jones et al. 2011; Vu et al. 2011). In this type of repair system, the composite shell provides the major reinforcement against circumferential stresses due to internal and external loading, while the grout transfers the stress from the pipe to sleeve aside from providing a supporting bed for the composite shell. Literature related to the analysis of grouted sleeve repair systems, and especially those incorporating composite materials, are currently limited. The load distribution behaviour among these elements determines the effectiveness of a repair system (Sum & Leong 2012). Thus, it is important to investigate the effect of material and geometric properties of the grout and sleeve on the overall behaviour of a composite repair system.

Duell et al. (2008) and Freire et al. (2007) reported that a variation exists in the level of stress and strain at the steel pipe, grout and sleeve. It is essential therefore to consider the important parameters that affect the behaviour of the different structural components in a composite repair system, especially in the grout as it has considerably lower strength and stiffness than surrounding steel and composite. This is important because the grout, together with the composite sleeve, plays a critical role to keep the integrity of the whole repair system. This is in contrast with an overwrap repair system, where the composite repair is directly in contact with the steel that ensures direct load transfers. However, an infill repair contains annulus filled grout, which determined the load transfer performance of the system. The relationships among the different elements are essential for a better understanding of the overall behaviour of the repair.

The extensive investigation on the behaviour of a range of epoxy grout and glass fibre – vinyl ester composite in Chapters 3 to 5 suggests that these materials have the strength and stiffness for structural applications. Besides, the grout system experiences considerable degradation of stiffness under hot-wet conditioning which is discussed in Chapter 4. This chapter explores the potential application of these components in a grouted sleeve repair through finite element simulations. Since the repair system includes a comparatively low stiffness infill in between steel and sleeve, a parametric study through a finite element analysis is essential to determine the suitable range of grout properties that will provide an effective repair system. The effect of the thickness of the grout and the encircling sleeve was also considered. The results of this study provide essential information, which aid in the selection of optimum properties to achieve the required performance of an infilled composite sleeve repair.

6.2 Finite element modelling

This section describes the finite element modelling and non-linear analysis on the behaviour of the infilled fibre composite repair system for a steel pipeline with a particular wall thinning defect. Different grout properties and thicknesses along with varying composite sleeve thickness were investigated.

6.2.1 Repair geometry

The ASME B31G (1991) limits the maximum depth of corrosion level to 80% of the nominal pipe wall thickness for further evaluation of repair. This level of metal loss represents a worst case scenario in evaluating the behaviour of a grouted repair. The circumferential width of the repair is set at one quarter of the pipe diameter, which also conforms with defect thickness for non-leaking (Type A) defect specification by ISO/TS 24817 (2006). In the analysis, it is assumed that the repaired section is long enough in the longitudinal direction to make plane strain assumptions. A 2D plane strain finite element model was developed in this study using Strand7 (Strand7 Pty Limited 2005). Figure 6.1 shows the schematic diagram for the considered repair. The model comprises of three elements: steel pipe with a metal loss, grout and composite sleeve. Since the repair geometry is symmetrical about the vertical axis, half of the geometry is sufficient to analyse the infilled composite repair elements. The elements of the repair were modelled using 8-node *Quad8* plate elements. Figure 6.1b is a typical model used to simulate the repair system. For simplicity, the pipe-infill and infill-composite interfaces of the repair are considered perfectly bonded. The repair system is fully wrapped. The compression load along the radial direction causes the delamination in the interfaces to be less likely. The repaired system is thus considered ideal infilled close-formed and the nodes connecting the interfaces are assigned with plane-strain constraints imposed on each node.

Table 6.1 provides the values of the geometric parameters used in this study. The external diameter of the pipe is 114.3 mm with a wall thickness of 4.78 mm. Grout thicknesses of 5 to 40 mm at an interval of 5 mm were considered to observe the effect of a change in grout thickness while sleeve thicknesses of 5 to 25 mm at an interval of 5 mm were used. The maximum thickness of the grout is specified as 40 mm in the application instructions of the available grouts. From the experience of handling the grouts, it is found that grout thickness more than 40 mm produces considerable amount of heat that may induce cracks and warpage in the annulus. According to ISO/TS 24817 (2006), the circumferential extent of the repair should be more than one quarter the diameter of the pipe, which is 28.58 mm. In this study, a defect width of 31.7 mm was used. The width of the defect in the outer periphery of the pipe is two times the width at the bottom of the defect which is transitioned linearly along the pipe thickness.

6.2.2 Material properties

The mechanical properties of an API-5L-X42 pipe which were taken from Brooker (2003) and were listed in Table 6.2, while the stress-strain relation curve is given in another article by Brooker (2003). A simplified bilinear stress-strain relation was used for the steel. The moduli of grout considered were 5 and 10 GPa, which is the usual range of the modulus of elasticity of epoxy grout while investigated in Chapter 3. A modulus of 1 GPa is also considered due to the fact that grout stiffness is considerably affected by hot-wet conditioning and was found less than 1 GPa as

shown in Chapter 4. While a stiffer of grout is found to minimise the stress in steel (Sum & Leong 2013), these grouts are found difficult to mix and pour. The modulus of the carbon/epoxy composite repair was 49 GPa, which is similar to Duell et al. (2008). These results in a total 120 geometric and material combinations which are presented in a uniform sequence (X,Y,Z) and are denoted by (t_g, E_g, t_c) for any particular repair case. Table 6.2 also shows symbols to represent the different repair cases. The first number is the grout thickness (t_g) in mm, and the second is the grout modulus (E_g) in GPa followed by the sleeve thickness (t_c) in mm, which are separated by comma. The repair cases are symbolised as (X,Y,Z). For example, the repair case (25,5,15) described in Section 6.2.1 denotes repair section with a 25 mm thick layer of grout modulus of 5 GPa in the annulus under 15 mm thick sleeve. Isotropic material properties were assumed for each element of the repair.

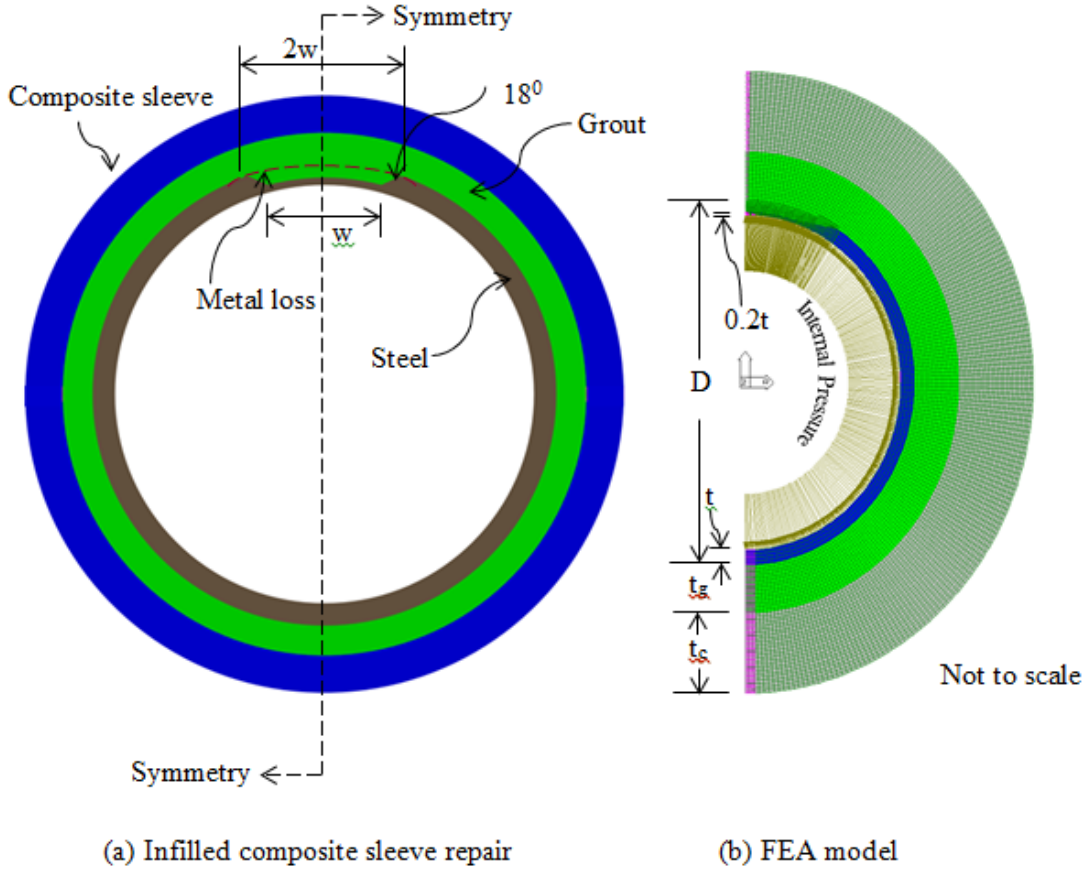

Figure 6.1 **Schematic of the composite repair and geometry**

Table 6.1 **Details of the parameters for the composite repair**

Parameters	Symbol	Description
External diameter of the pipe	D	114.3 mm
Thickness of the pipe	t	4.78 mm
Thickness of the grout	t_g	5, 10, 15, 20, 25, 30, 35, 40 mm
Thickness of the composite sleeve	t_c	5, 10, 15, 20, 25 mm
Width of the defect	w	31.7 mm

The reliability of the finite element models described in this analysis was verified though comparison to the numerical results of stress-pressure curves of a pristine pipe. No experimental verification was attempted. From the FEA simulation, the level of stresses and strains in the pristine pipe were also analysed and verified with existing literatures to identify the pressure level at which the pipe would start to yield and burst. The elastic capacity of the pristine pipe was compared to the level of pressure in which the steel pipe with composite repair starts to yield. Similarly, the burst pressure of the pristine pipe was used as a benchmark pressure to evaluate the effectiveness of the infilled composite repair system. The capacity of the corroded steel pipe in Figure 6.1 was also identified and verified with the current available practice.

Table 6.2 Material properties for the composite repair

Parameters	Symbol	Description
Yield strength of steel	σ_y	289 MPa
Ultimate strength of steel	σ_u	413 MPa
Yield strain of steel	ε_y	0.00145
Ultimate strain of steel	ε_u	0.30
Modulus of steel	E_s	200 GPa
Modulus of grout	E_g	1, 5, 10 GPa
Modulus of composite sleeve	E_c	49 GPa

The optimum number of elements was selected based on the convergence study. Figure 6.2 presents the effect of element subdivision on the maximum level of stress in a typical repair case (25,5,25) under internal pressure up to 34 MPa. The results suggested that beyond 10501 elements, the level of stress is consistent. Comparable mesh size was adopted in the critical regions for all the repair cases.

6.3 Results

From the analysis of the pipe without any defect, the burst pressure was found to be 34.0 MPa, while a pressure of 26.0 MPa is the level of pressure where the pristine pipe starts to yield. According to Det Norske Veritas (2010), the burst pressure of a pipe with 80% corrosion is 7.21 MPa, which conforms with the results of the finite element analysis. The yield will occur at 3.75 MPa.

ASME Boiler & Pressure Vessel Code (2007) provides three approaches for design against plastic collapse of pipes: (i) Elastic Stress Analysis Method, (ii) Limit Load Analysis Method, and (iii) Elastic-Plastic Stress Analysis Method. Elastic Stress Analysis incorporates yield strength as a criterion against plastic collapse of pipes, while the two other approaches suggest extending the capability of the pipe up to limit load or plastic collapse load after applying a suitable design factor. The results of this study are compared using two criteria. The first condition is when internal pressure of the pipe material reaches the yield strength. The second condition allows the pipe to be pressurised up to bursting, which results in nonlinear behaviour or plastic deformation in the steel pipe. The first condition is evaluated based on the applied internal pressure to yielding of steel, whereas, the second approach compares the level of stresses and strains in the different repair components.

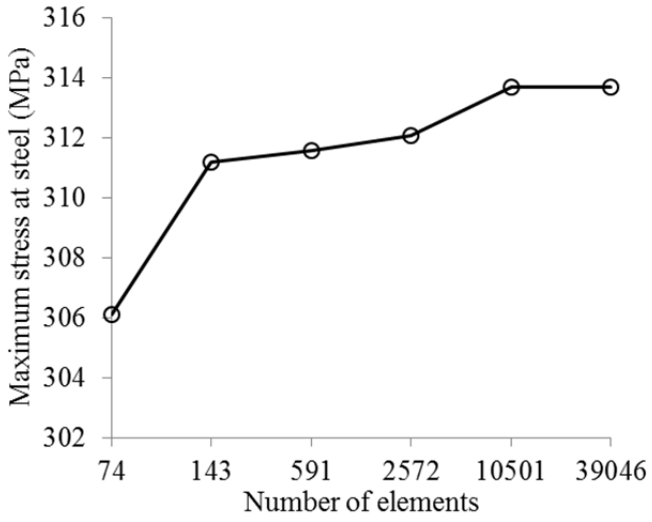

Figure 6.2 Convergence plot

6.3.1 Typical location of maximum stress

Since the pipe has a defect, the stress distribution is no longer uniform along the circumferential direction in the steel pipe, grout and sleeve even before the pipe yields as shown in Figure 6.3. This result is for the repair case with 10 mm grout layer having modulus of 5 GPa and 15 mm thick sleeve. The repaired pipe was applied with a pressure of 26 MPa, which is the internal pressure causing yielding of the pristine steel pipe (289 MPa). It can be seen from Figure 6.3b that due to change in geometry, higher stress was developed at the transition end (section B-B) of the pipe with defect. Sum and Leong (2012) also found that the transition end was the critical location under elevated temperature and internal pressure. Furthermore, Freire et al. (2007) reported failure in the steel at the transition end from the observation on the tested specimens. Their numerical investigation of repaired section also showed comparable trend of stress and strain distribution in the components along the centreline. Based on the result of the simulation, the maximum stress for sleeve occurs in the section A-A, which is the centre line of the area with defect. Hence, these locations were selected and analysed in this study to compare the level of stress and strain in the steel pipe, grout and sleeve of the infilled composite repair.

6.3.2 Pipe capacity considering yielding of steel

Figure 6.4 shows the effect of grout thickness, modulus of elasticity and thickness of sleeve on the pipe capacity. The pristine pipe capacity which is 26 MPa is shown as the upper margin and the capacity of the unrepaired pipe within elastic region of 3.75 MPa is shown as the lower margin. From the figure, it can be seen that pipe pressure capacity decreases with increasing grout thickness, decreasing grout modulus and decreasing sleeve thickness. This is due to the fact that a thicker and less stiff grout with a constant sleeve thickness allows higher radial strain in the layer which can be seen from the level of circumferential strains in grout presented later in Section 6.4.2. At the same time, a thicker sleeve thickness results in lower radial strain indicating a more effective load transfer between the layers. It is noted that there is no significant increase in the pipe pressure capacity for grout with thickness higher than 25 mm. The highest pipe capacities obtained for the repair cases with grout thickness 5 mm, sleeve thickness 25 mm and grout moduli of 10, 5 and 1 GPa,

respectively are 14.6, 12.2 and 7.8 MPa. These capacities represent 55%, 46% and 30% of the pristine pipe capacity, respectively. Similarly, the repaired pipe can withstand 3.9, 3.3 and 2.1 times the internal pressure of the unrepaired pipe, respectively. The highest pressure for each grout modulus is obtained from repair cases with 25 mm sleeve which is the thickest reinforcement layer used in this study.

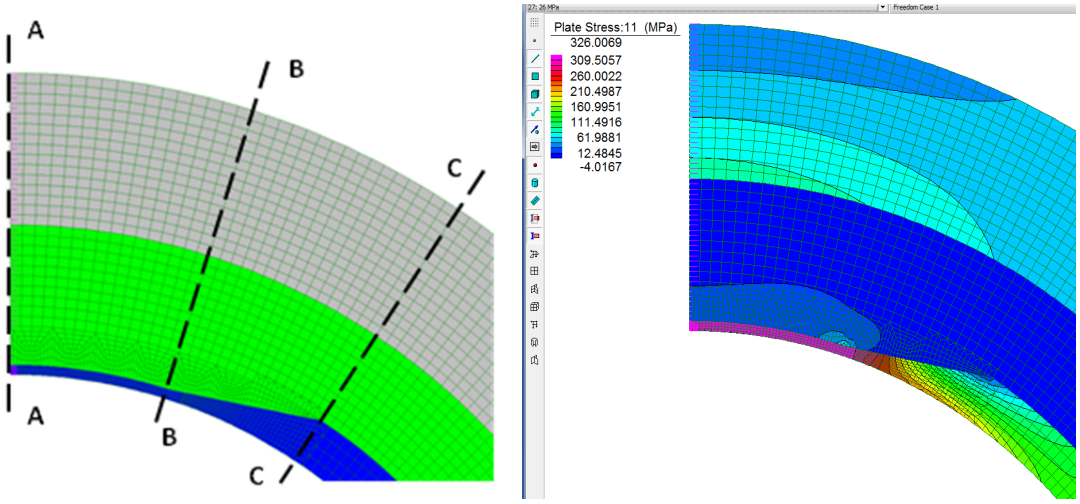

(a) Sections of the repair (b) Circumferential stresses

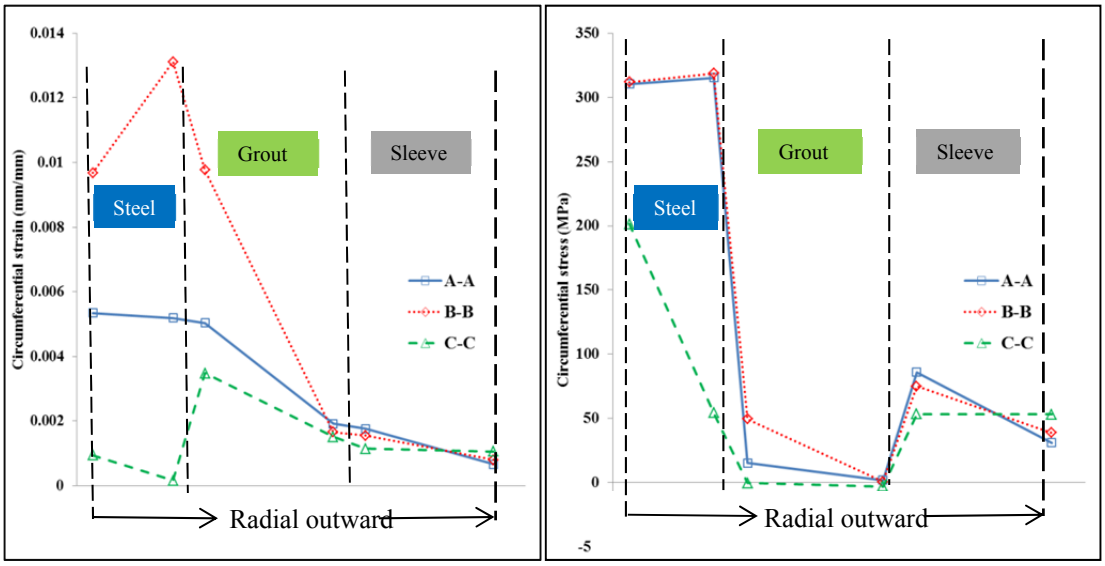

(c) Stress distribution (d) Strain distribution

Figure 6.3 Circumferential stresses and strains along the thickness of the repair at different locations for applied pressure of 26 MPa to repair case (10,5,15)

The lowest capacities of the repair cases with grout moduli 10 GPa, 5 GPa, and 1 GPa are 8.7 MPa, 6.9 MPa and 4.5 MPa which are only about 33%, 26% and 17%, respectively of the pipe capacity. However, they are about 2.3, 1.8 and 1.2 times the capacity of the unrepaired pipe, respectively. The lowest pressure among all the repair cases is found for the repair having 40 mm thick grout, modulus of 1 GPa and 5 mm thick sleeve. Repair with 1 GPa and 5 GPa grouts exhibit the lowest pressure capacity for 40 mm thick grout and thinner 5 mm sleeve. However, it is to be noted that the lowest pressure for repair cases with grout modulus of 10 GPa is obtained for 5 mm thick grout and 5 mm thick sleeve.

From the results it can be seen that pipe capacity increases with increasing sleeve thickness and increasing grout modulus. It is also observed that the pipe capacity increases with grout thickness for the repair cases (X,10,5), which is opposite to the usual behaviour of all other repair cases. The reason behind this is that the stiffer infill acts as an effective medium and provides support to the composite layer. Consequently, for constant sleeve thickness, an increased stiffer grout thickness contributes in the improvement of the pipe capacity. This indicates that a stiffer infill should be supported by sufficient layer of reinforcement to achieve higher capacity of the repair.

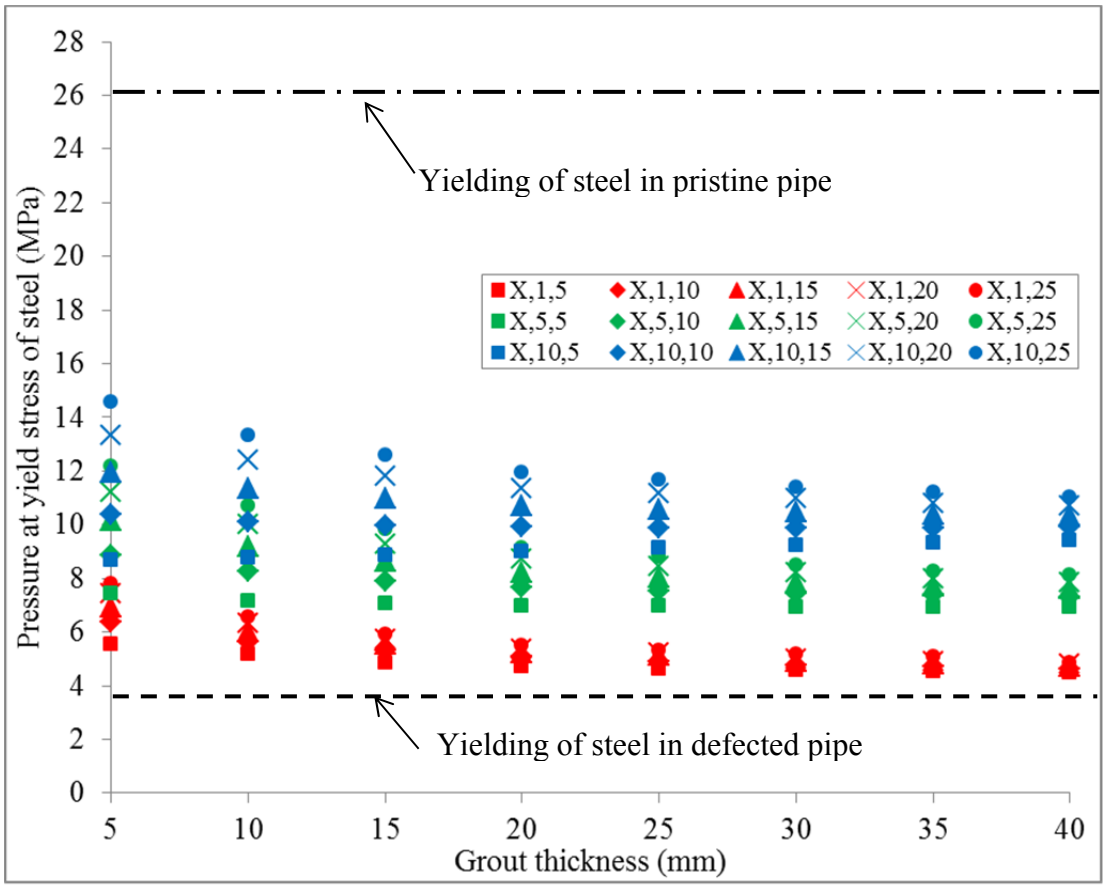

Figure 6.4 **Relation among internal pressure, grout thickness, grout modulus and sleeve thickness at yield stress of steel**

In repair cases with low grout thickness (less than 15 mm), grout and sleeve layers supplement each other. Repair with a higher modulus grout provides similar capacity with lower thickness of the sleeve. For example, (10,10,10) repair case has the same capacity as (10,5,20) repair case and (5,5,25) repair case is similar to that of capacity to (5,10,15) repair case.

6.4 Level of stress and strain in repaired pipe for burst pressure of pristine pipe

Nonlinear static analyses were conducted to determine the level of stresses and strains on the steel pipe, grout and sleeve when a pressure of 34 MPa is applied. The details of the behaviour and significant exceptions are discussed in the following sections with the results presented in charts to clearly show the effect of different repair combinations.

6.4.1 Steel

Figure 6.5 shows the distribution of circumferential stresses in steel for different repair cases under an internal pressure of 34 MPa, which is the burst pressure of pristine pipe. The circumferential stresses in the steel for the different repair combinations range from 308 to 354 MPa. It is important to note that this stress level is lower than the ultimate stress level on pristine pipe of 413 MPa suggesting the effectiveness of the repair. When compared among the repair cases with constant sleeve thickness, the repair cases with 1 GPa and 10 GPa result in the highest and the lowest circumferential and radial stresses in steel, respectively. The reason for this is that a low stiffness infill layer undergoes higher radial deformation allowing more outward expansion of the steel pipe than that of stiffer grout, causing higher stresses in steel. Circumferential stresses of the repairs cases with grout modulus of 1 GPa increase with increment of grout thickness, whereas, the stress levels are similar in the repair cases with grout moduli of 5 GPa and 10 GPa. For example, circumferential stresses for repair cases (X,1,Z), (X,5,Z), and (X,10,Z) present range from 327 to 354 MPa, 315 to 317 MPa, and 308 to 311 MPa, respectively. The compressive radial stresses are found within the range of 28.5 to 30 MPa. It is also found that the radial stress exhibits comparable behaviour for repair cases with modulus of 5 and 10 GPa with a value of -28.5 MPa. The difference between minimum and maximum radial stresses for repair cases considered in this study with grout modulus of 1 GPa is as low as 1 MPa with an average value of 30 MPa. A thicker sleeve provides a stiffer repair system and a better confinement against radial deformation of the infill grout. Hence, the circumferential stresses decreased with increment of sleeve thickness for all repair cases with constant grout thickness. However, repair cases with grout modulus of 5 and 10 GPa show negligible reduction in stresses, especially when the grout thickness is more than 20 mm.

Figure 6.6 shows the effect of repair geometry and element properties on circumferential strain of steel. The level of circumferential strains in steel is comparable and varies within 0.006 and 0.09 mm/mm. The radial strains are also found to be within -0.006 and -0.09 mm/mm. The strains for repair cases (X,1,Z), (X,5,Z), and (X,10,Z) range from 0.02 to 0.09, 0.007 to 0.02, and 0.006 to 0.013 mm/mm, respectively. The strains increased with decreased sleeve thickness and are maximum in repair cases (X,1,5). There is marginal reduction in the strain level for repair cases (X,5,Z) and (X,10,Z) when the grout thickness is more than 20 mm. This behaviour is due to the fact that stiffer grouts experience a lower strain than that of grout with lower stiffness, restraining the steel. Moreover, grout thickness of more than 20 mm is sufficient to transfer the strain towards sleeve regardless of sleeve thickness. This is evident from the level of circumferential stresses in sleeve presented later in Section 6.4.3, where a change in grout and sleeve thickness contributes to a decrease of stress in sleeve.

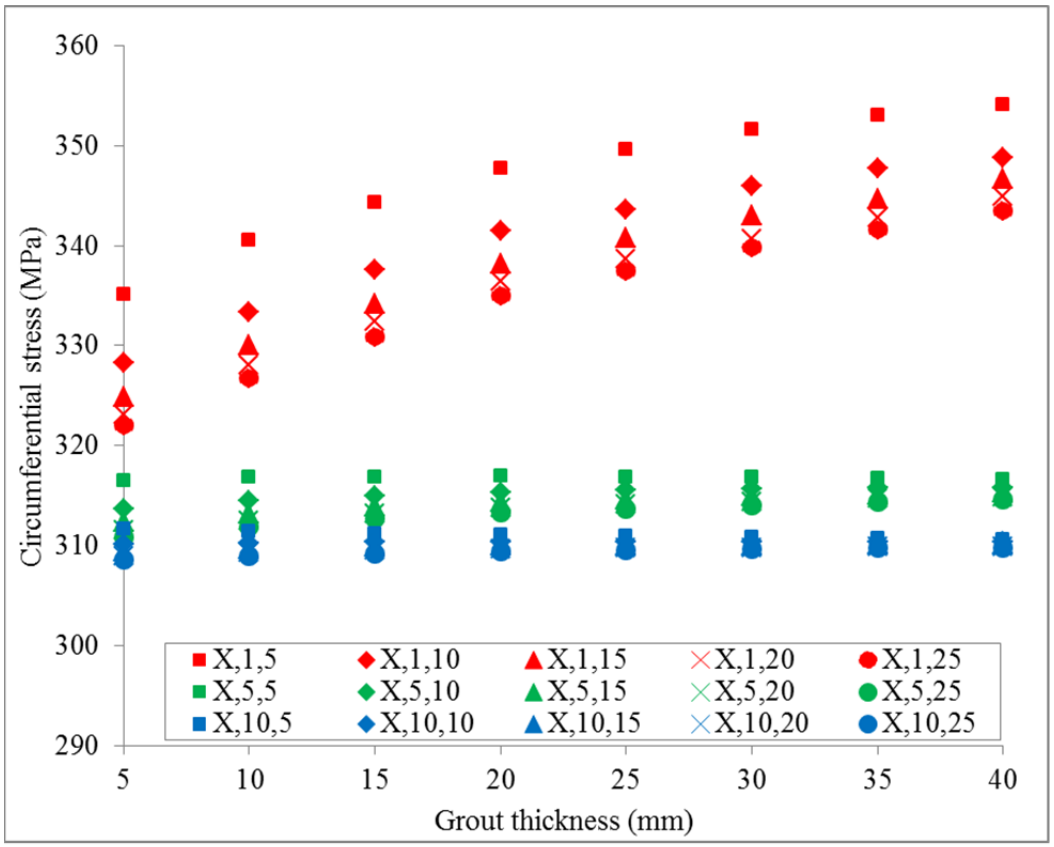

Figure 6.5 **Level of circumferential stresses in steel for different repair cases**

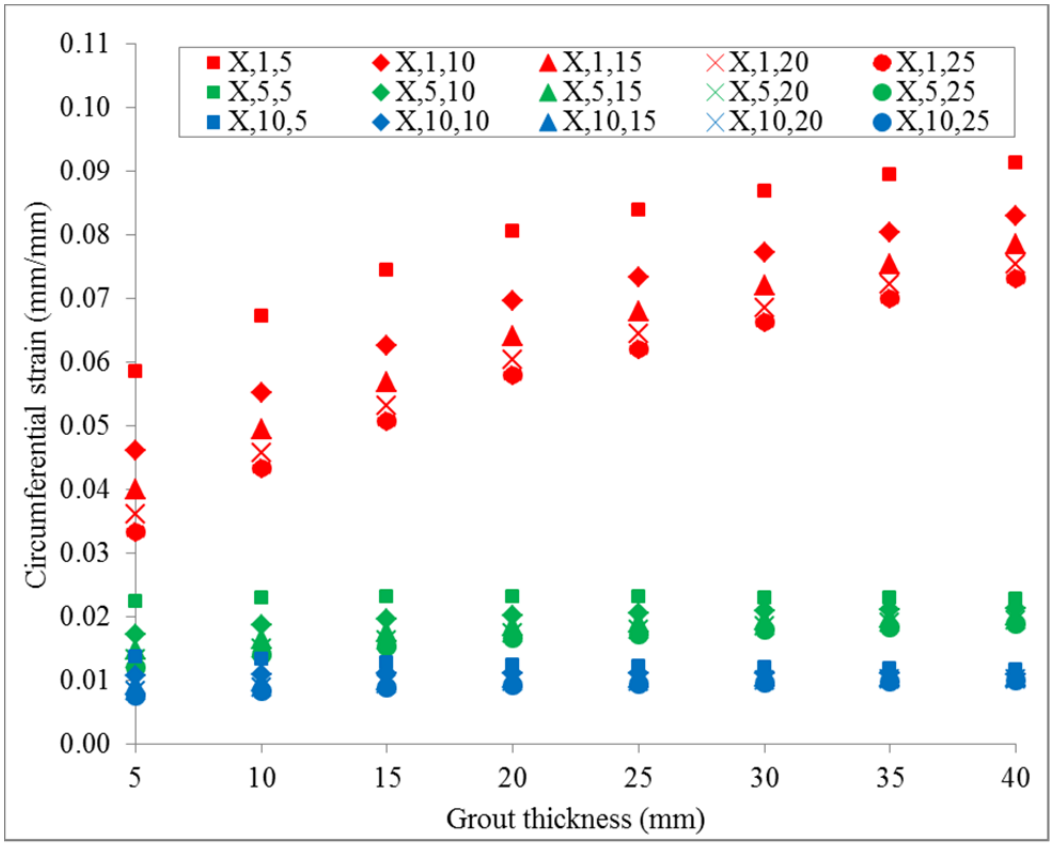

Figure 6.6 **Level of circumferential strains in steel for different repair cases**

6.4.2 Grout

Figure 6.7 presents the circumferential stresses in the grout for different repair cases under internal pressure of 34 MPa. The circumferential stresses in the grout range from 6 to 132 MPa. Circumferential stress increased with increasing grout thickness for all repair cases except for the repair cases (X,10,5) where the stress decreased with increasing grout thickness. The above mentioned repair case also results in the highest circumferential stress in the grout. In this case, a stiffer grout (10 GPa) is supported by a thinner sleeve (5 mm). It can be seen from Figure 6.8 that a stiffer grout experiences lower radial strain than low stiffness grout, which indicates that a stiffer grout is more effective in transferring radial stress toward the thinner sleeve. For constant grout thickness, a thinner sleeve undergoes higher circumferential strain. Thereby, the overall circumferential stress in the sleeve is increased. Hence, a stiffer grout should be supported by sufficient layer of reinforcement to keep the stresses lower in the grout. In general, circumferential stress decreased with increasing sleeve thickness. Circumferential stress decreased with decreasing grout thickness for repair cases with constant sleeve thickness. Again, circumferential stress increases with increasing grout modulus, at constant grout and sleeve thickness. This implies that a stiffer grout is expected to result in higher level of circumferential stress when composite reinforcement is insufficient. It is also found that the radial compressive stress ranges from 24 to 30 MPa.

Figure 6.8 shows the radial stresses in grout for various repair cases. Radial stresses in grout decrease with increasing grout thickness except for the repair cases (X,5,5) and (X,10,5) where a marginal increase in the stress is observed. The thicker the sleeve, the higher the radial resistance toward the infill layer than a thinner sleeve which eventually increases the radial compressive stresses. Hence, radial stresses increased with increasing sleeve thickness for repair cases with constant grout modulus. Radial stress decreased with increasing grout thickness for repair cases with constant sleeve thickness. This behaviour is expected as the thicker grout in between steel and sleeve can undergo more deformation and experience a higher radial strain when under compression than a thinner grout, which is evident from Figure 6.8.

Circumferential and radial strains in the grout are shown in Figure 6.9. The levels of circumferential and radial strains in grout range within 0.005 and 0.08 mm/mm, and -0.005 and -0.07 mm/mm, respectively. The circumferential strains increase with the increment of the grout thickness except for the repair case (X,10,5) where there is a marginal decrease in strain. This increment of strain is more prominent in the repair cases with grout modulus of 1 GPa and relatively marginal in repair cases with grout having higher modulus (5 and 10 GPa) and thicker grout (more than 20 mm). Higher sleeve thickness is stiffer than thinner sleeve and restricts radial deformation of the infill layer. Hence, the strains decrease with increasing sleeve thickness when compared for repair cases with constant grout modulus. As can be seen in Figure 6.10, low stiffness grout allows higher circumferential and radial deformation in the infill layer than high stiffness grout. As a result, the strains decrease with increasing grout modulus for repair cases with constant sleeve thickness.

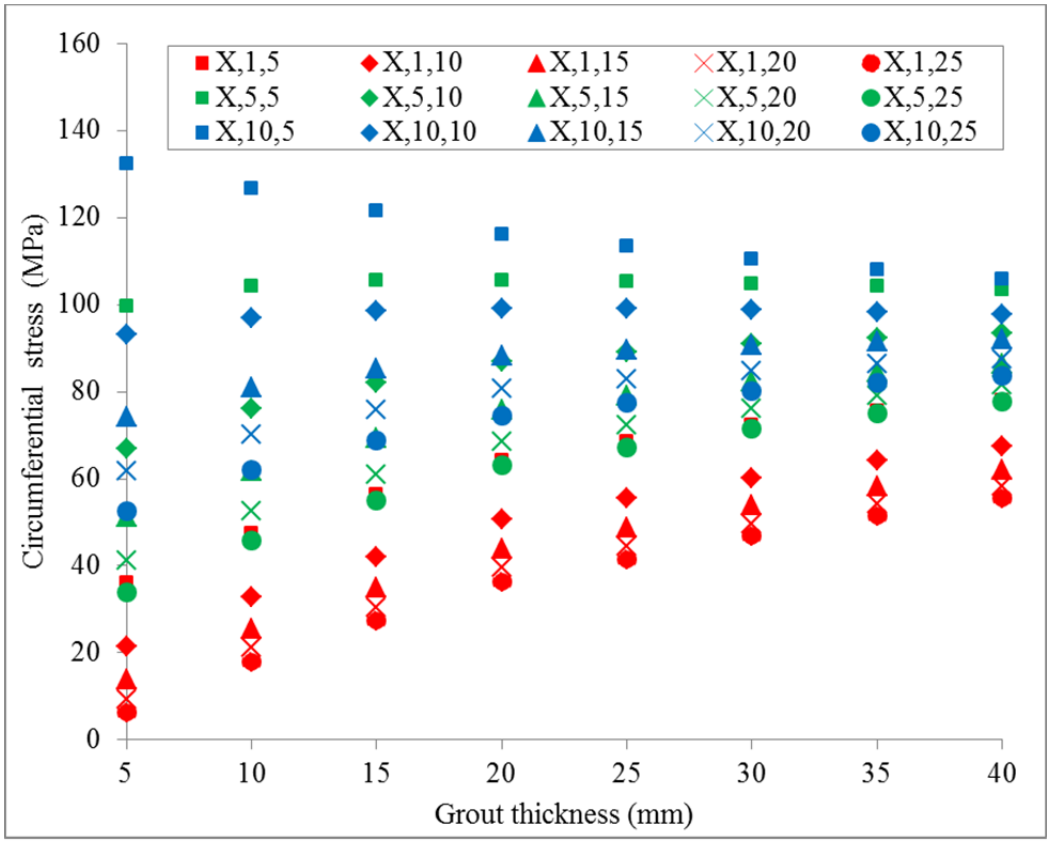

Figure 6.7 **Level of circumferential stresses in grout for different repair cases**

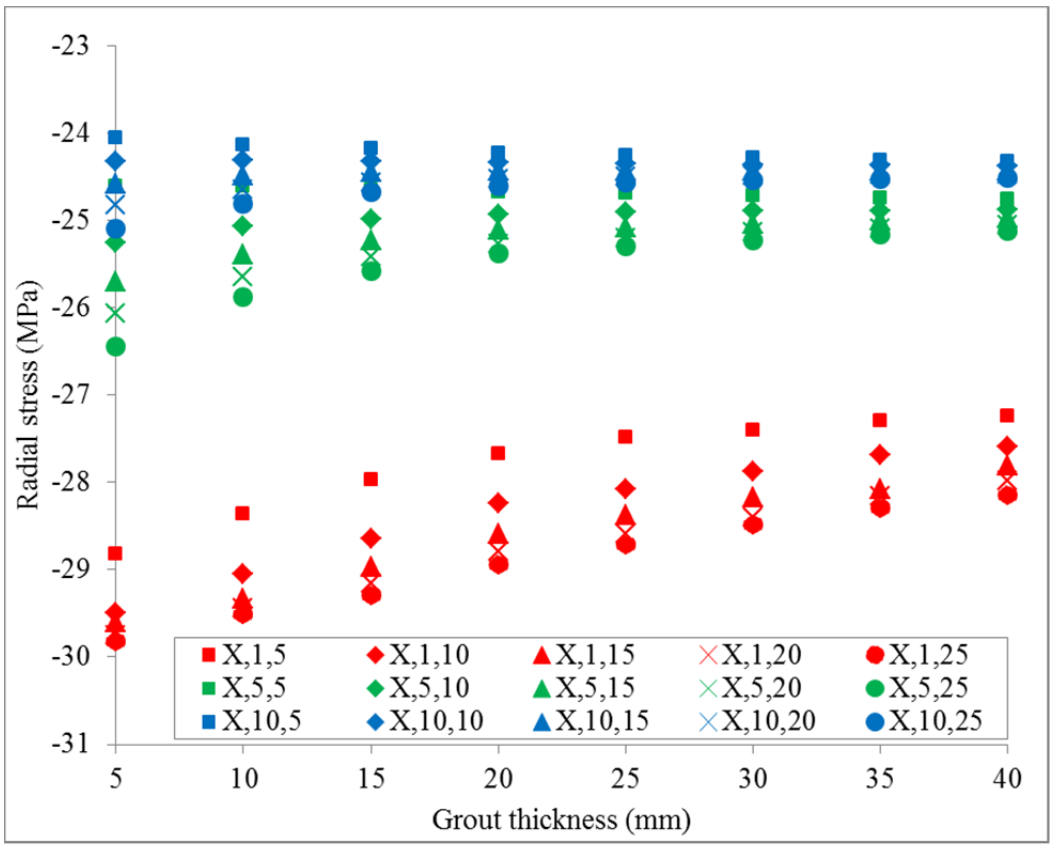

Figure 6.8 **Level of radial stresses in grout for different repair cases**

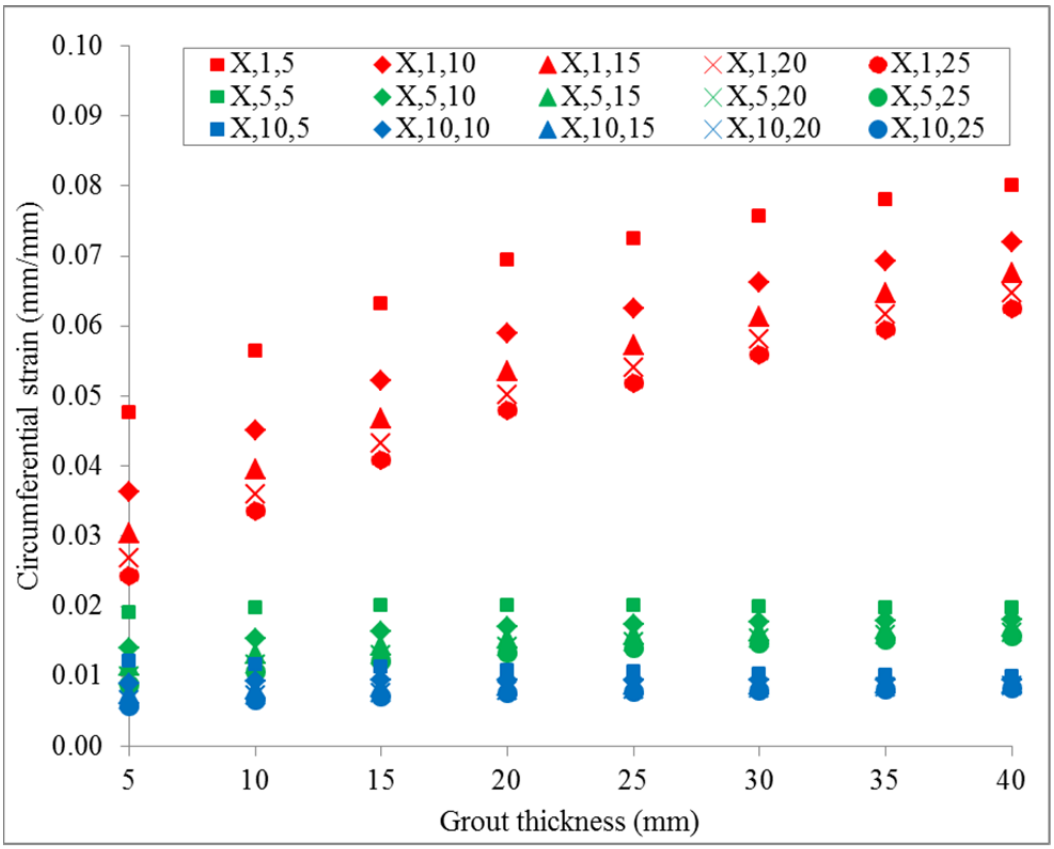

Figure 6.9 **Level of circumferential strains in grout for different repair cases**

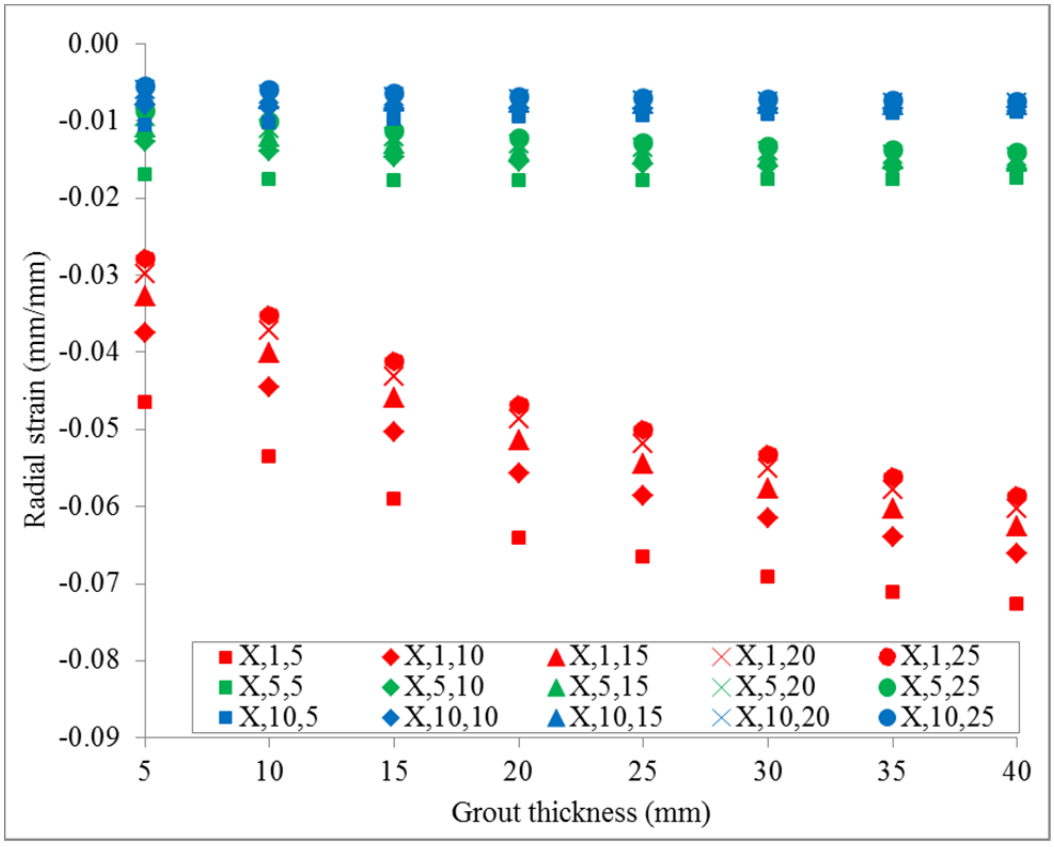

Figure 6.10 **Level of radial strains in grout for different repair cases**

6.4.3 Sleeve

Figure 6.11 shows the level of circumferential stresses in sleeve for different repair cases under bursting pressure of the pristine pipe. The range of circumferential stresses in the steel for the repair combinations are 36 to 378 MPa. The repair cases with 1 and 10 GPa grouts cause the highest and the lowest circumferential and radial stresses in steel. A thick sleeve has a lower stress than with thin sleeve due to the increased sleeve stiffness in circumferential direction. As a result, circumferential stresses decreased with increasing sleeve thickness for repair cases with constant grout modulus. Circumferential stresses of the repairs cases with modulus 5 and 10 GPa decrease with the increment of grout thickness, which is also observed for the repair case (X,1,5). On the other hand, the stresses increase up to grout thickness 15 to 20 mm and then decrease for the repair cases (X,1,10-25). It is also found that the compressive radial stresses range within 1 to 26 MPa. The highest and lowest radial stresses are found for repair cases (X,1,25) and (X,10,5), respectively. In general, radial stresses decrease with increasing grout modulus. This implies that a stiffer grout generates higher radial stresses and transfers the load towards encircling sleeve more effectively than lower stiffness grout, as can also be seen from Figure 6.8.

Figure 6.12 shows circumferential strains in sleeve for the investigated repair cases. The levels of circumferential and radial strains in sleeve vary from 0.0007 to 0.008 mm/mm, and from -0.0001 to -0.0013 mm/mm, respectively. Circumferential strains of the repairs cases with modulus 5 and 10 GPa decrease with increasing of grout thickness, which is also observed for the repair case (X,1,5). On the other hand, the strains increases when grout thickness is 15 – 20 mm and then decrease for repair cases (X,1,10-25). A thick sleeve reduces circumferential stresses and strains due to its high stiffness. Thus, the circumferential strain decreases with increasing sleeve thickness. When compared among repair cases with similar sleeve thickness, circumferential strains decrease with increasing grout modulus. It is also seen that the radial strains decrease with increasing grout thickness for all repair cases. Radial strains decrease with increasing sleeve thickness for repair cases with grout modulus of 1 GPa. This trend is also observed for repair cases grout modulus of 5 and 10 GPa at lower grout thicknesses (5 to 15 mm). Beyond this, the radial strains begin to increase with increasing sleeve thickness. This behaviour suggests that a stiffer grout causes increment in radial load towards a thicker sleeve which circumferentially sufficient to reinforce the repair system than a lower stiffness grout.

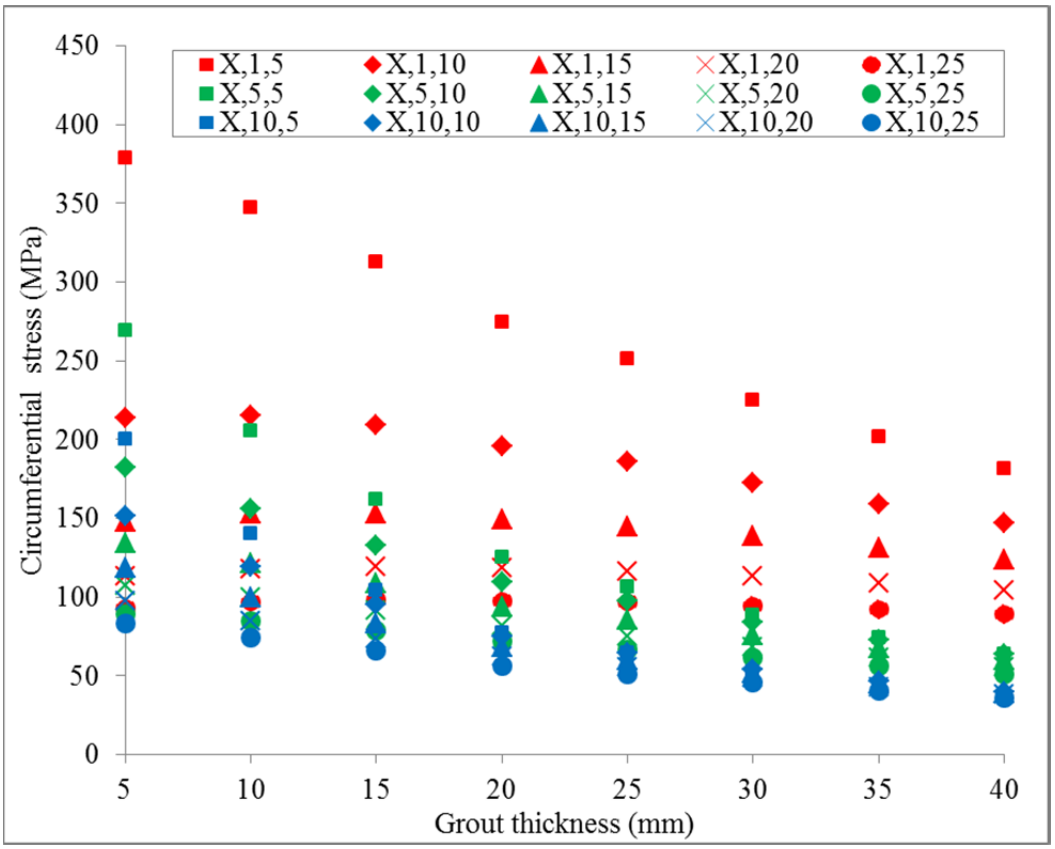

Figure 6.11 **Level of circumferential stresses in sleeve for different repair cases**

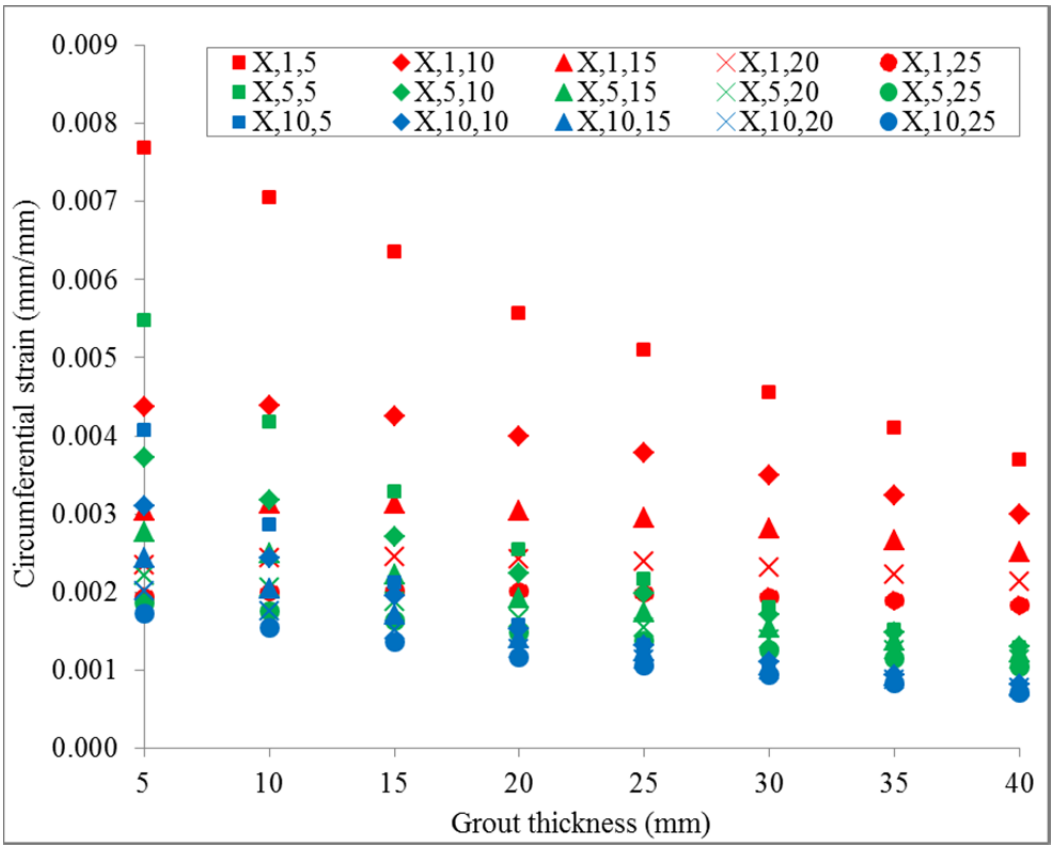

Figure 6.12 **Level of circumferential strains in sleeve for different repair cases**

6.5 Discussion

The effects of the grout and sleeve thickness as well as the grout modulus on the behaviour of the infilled composite repair are discussed in this section. An evaluation was also carried out to determine the practical range of values for elements of an infilled composite repair for steel pipelines. Table 6.3 provides a comparison of the effects of repair geometry on the levels of stress and strain, as well as the general trends on parameters. The comparison suggests that thicker reinforcement reduces the level of stress and strain in all the components of the repair. Aside from an increase in stress in itself, a higher infill layer causes lower stress and strain in the components. A thicker grout layer reduces the stress and strain in the sleeve, whereas increases the level of stress and strain in the steel and the grout. The infilled composite repair used in this study is based on the concept that the encircling composite sleeve is continuous. However, it is impractical to apply a pre-cured continuous shell around a pipe without detaching the pipe segment from the pipeline. In practice, split sleeves are used around the pipe for ease of in-situ installation. Hence, an effective joint between the split shells is necessary. The joint should also be designed to characterise the repair which is beyond the scope of this work.

Table 6.3 **Effect of repair geometry and material property on circumferential stresses and strains of the layers of the repair**

Location		Repair parameters		
		Increase in		
		t_g	E_g	t_s
Stress	Steel	Increase	Decrease	Decrease
	Grout	Increase	Increase	Decrease
	Sleeve	Decrease	Decrease	Decrease
Strain	Steel	Increase	Decrease	Decrease
	Grout	Increase	Decrease	Decrease
	Sleeve	Decrease	Decrease	Decrease

6.5.1 Effect of grout thickness

The effect of grout thickness on the level of stress in the steel is shown in Figure 6.13. The results indicate that level of stresses in steel increases for a grout with stiffness of 1 GPa. This result suggests that when a repair system is subjected to hot-wet conditioning and the stiffness of the grout is reduced, it will lead to an increment of stress in the steel. On the other hand, thinner grouts with a modulus of 5 GPa and 10 GPa reduce stress and strain in the steel. This grout exerts a higher circumferential stress and lower radial stress along with a lower circumferential and radial strain which indicates that the radial forces from the steel is effectively transferred towards the sleeve rather than a thick grout. At the same time, there is no significant reduction in the stresses and strains in steel for grout thickness more than 20 mm and grout modulus of more than 5 GPa. This is due to the fact that stiffness greater than 5 GPa with thickness more than 20 mm produces a sufficiently rigid layer to effectively transfer the load between the steel and sleeve. It is to be noted that there is a reversal of behaviour for stiffer grout and sleeve thickness of 5 mm. This implies that a stiffer grout needs a sufficient sleeve thickness to transfer the load. This behaviour is due to the fact that a grout transfers the load that is been imposed from the steel towards the sleeve. Since the grout is stiffer, it ensures a

more effective load transfer which need to be supported by a stiffer or thicker sleeve. The sleeve will experience higher stress if otherwise. The levels of circumferential stresses and strains are found to be within the range of 308 to 354 MPa, and 0.006 to 0.09 mm/mm, respectively for the different repair cases. It is apparent from the results that the stresses and strains in steel at the pressure of 34 MPa are lower than the ultimate tensile strength (413 MPa) and burst strain (0.3) of steel pipe considered for this study. Hence, the repaired section is effective and the pipe section outside the repair is expected to burst.

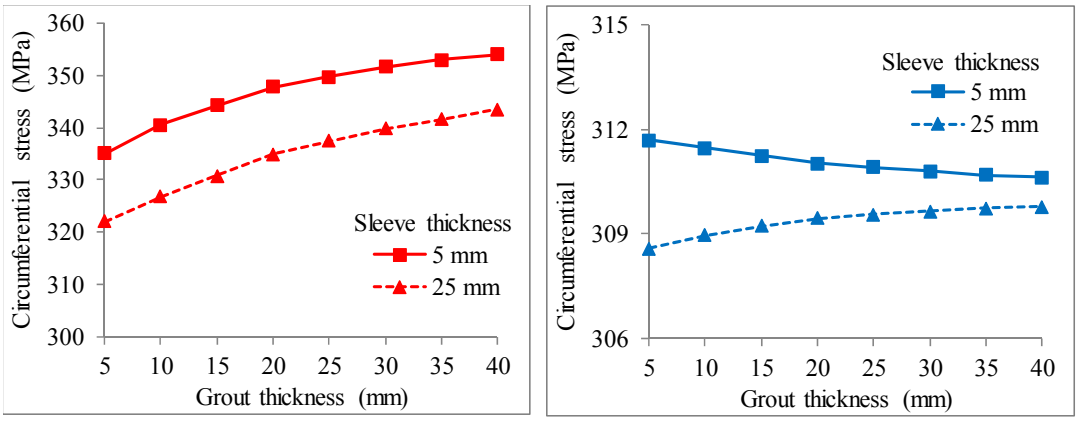

Figure 6.13 **Typical effect of grout thickness on the circumferential stress of the steel; (a) 1 GPa and (b) 10 GPa**

The effect of grout thickness on the stress of the grout is summarised in Figure 6.14. Higher circumferential stresses and strains in infill layer are expected when stiffer and thicker grouts are used. It can be seen that the sleeve thickness of more than 20 mm has a insignificant effect on the level of stresses in the 10 GPa grout. The circumferential and radial strains vary from 0.5% to 8%, and -0.5% to -7%, respectively. It can be seen from Figure 6.7 and Figure 6.9 that the radial stresses and strains are compressive in nature. It is due to the fact that outward movement of steel under internal pressure creates compressive effect on the infill layer. A fly ash and epoxy based grout with the compressive strength of 85 MPa was found suitable to repair fatigue damaged tubular joints (Thandavamoorthy et al. 2001). An epoxy-grouted hot tap fittings technology for pipeline repair was described by Vu et al. (2011), in which the tensile and compressive strengths specified were 23 and 75 MPa, respectively. Based on the findings in Chapter 3, the tensile and compressive strength of grouts ranged from 11 to 32 MPa, and 67 to 114 MPa, respectively. From the FEA results, the grouted infill layer can experience a circumferential stress of 6 to 132 MPa and radial compressive stress of 24 to 30 MPa. It can be seen from Figure 6.7 and Figure 6.14 that a grout thickness of less than 20 mm along with lower grout stiffness (1 GPa) is necessary to maintain the level of circumferential stress below 32 MPa. These results indicated that the maximum compressive stress in the infill layer is well below the compressive strength of the grouts investigated.

The effect of hot-wet conditioning can be reflected from Figure 6.14. It is evident from the trend that a stiffer grout results in higher stress in the infill layer. However, a lower stiffness grout results in lower stress in the infill layer (Figure 6.14a). The investigation of the physical properties of grouts suggests that there is a

considerable reduction in the stiffness of the grout under hot-wet conditioning. Hence, the conditioned grout will result in lower stress in the infill layer.

Figure 6.15 shows the effect of grout thickness on the circumferential stress of the sleeve. A thicker grout reduces the stress in the sleeve, however increases the stress in the steel and grout. The effect of grout thickness is more prominent in low thickness sleeve than that of the higher thickness. This is due to the infill layer that is also acting as reinforcement against circumferential stress in the steel and supplements the sleeve layer. However, it should be noted that the grout material model was assumed isotropic and able to carry load in circumferential direction that are well above the tensile strength (Figure 6.15) obtained from the experimental study, which is discussed earlier in this section. This necessitates including the actual behaviour of the materials for further analysis of the repair system. The effect of this support is more evident when a thinner layer of sleeve is used. The effect of the action of the grout layer is less visible in a system with a thicker sleeve. It is to be noted that grout thickness more than 20 – 25 mm results in a repair system with grout modulus of 10 GPa provide comparable stress in the sleeve. Furthermore, the level of circumferential stresses and strain in the sleeve layer is found to be within 36 to 378 MPa, and 0.07% to 0.8% which are well below the carbon fibre reinforced composite overwrap indicated by Toutanji and Dempsey (2001) and Duell et al. (2008). Repair system with low stiffness grout (1 MPa) results in higher stress in the sleeve than that of the repair with high stiffness grout. This implies that hot-wet conditioning is expected to increase the stress in the sleeve and is less effective in transferring the stress from the steel to the composite sleeve than the stiffer grouts.

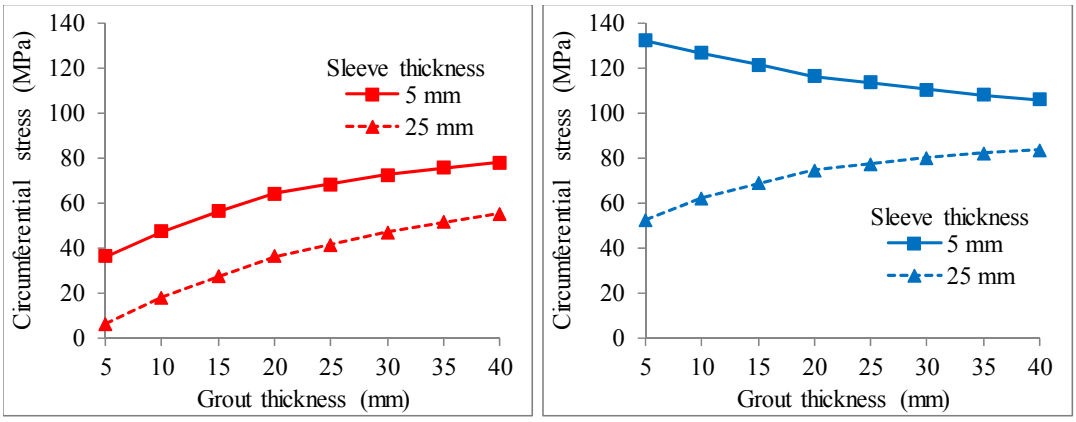

Figure 6.14 **Typical effect of grout thickness on the circumferential stress of the grout; (a) 1 GPa and (b) 10 GPa**

Thermosets like epoxies and their products go through polymerisation during curing process. The polymerisation of thermosetting composites creates internal stresses during resin cure (Ruiz & Trochu 2005). A thicker layer of grout is expected to produce high heat of hydration than that of a thinner grout. The polymer matrix has a much higher coefficient of thermal expansion and is thus more susceptible to temperature changes. Volume mismatch between sides of a product may cause thermally induced deformations and chemically induced shrinkage to occur. Residual stresses may also occur in the composite. Besides, a cracked infill layer may compromise the effectiveness of the repair system. For this reason, it is recommended to maintain a relatively thin layer of grout to reduce the heat of

polymerisation and potential formation of crack though thick enough to fill easily the space between the steel pipe and the composite sleeve. However, it is not always suitable to maintain a thin layer of annulus due to flowability of the grout. A wide annulus allows ease of placing without pressurised grouting. Besides, a thin layer of grout is found more vulnerable to hot-wet conditioning from Chapter 4. Hence, a suitable thickness should be sorted for the repair system based on the factors discussed above.

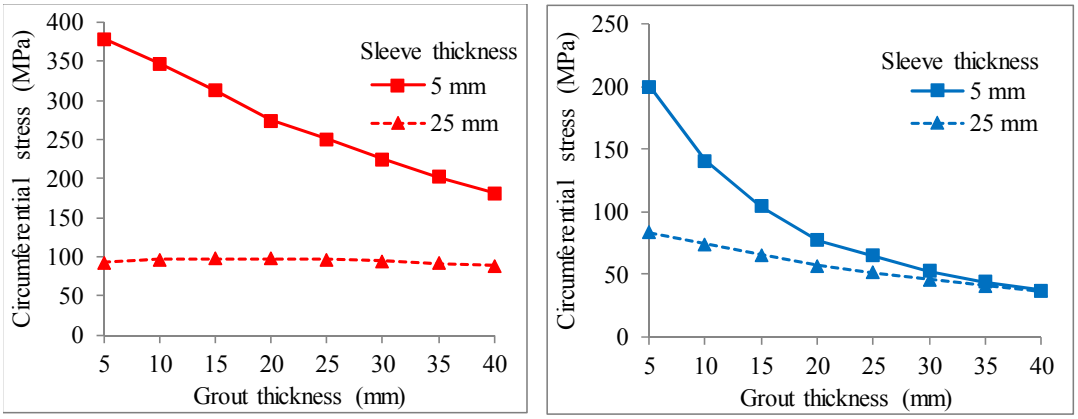

Figure 6.15 **Typical effect of grout thickness on the circumferential stress of the sleeve; (a) 1 GPa and (b) 10 GPa**

6.5.2 Effect of sleeve thickness

Figure 6.16 shows the effect of sleeve thickness on the level of stresses on the steel. Thicker sleeve results in lower level of stresses in the steel indicating that a stiffer sleeve will resist a higher load than a thinner sleeve. However, when the thickness of the sleeve is less than 10 mm and a 10 GPa grout is used, the stress in the steel with repair containing thinner grout is found to be higher than that of the thicker grout. This also confirms the effectiveness of providing a thicker than thinner sleeve which is discussed in earlier section. An increased sleeve thickness results in an increased rigidity against circumferential deformation, which also provides radial support for infill grout and steel pipe resulting in lower stresses and strains in the steel. However, the reduction of stresses in the steel due to change in sleeve thickness is more prominent when low stiffness (1 GPa) grout is used. When compared between the repair cases with 1 GPa and 10 GPa grouts, low stiffness grouts results in higher stress in the steel than that of the high stiffness grout. This also implies that hot-wet conditioning will result in increased stresses in the steel. Again, there are insignificant variations in the stresses in the steel due to increment of the grout thickness from 20 mm to 40 mm which can be seen from Figure 6.16b. This suggests that grout thickness more than 20 mm poses insignificant contribution on the stress in the steel.

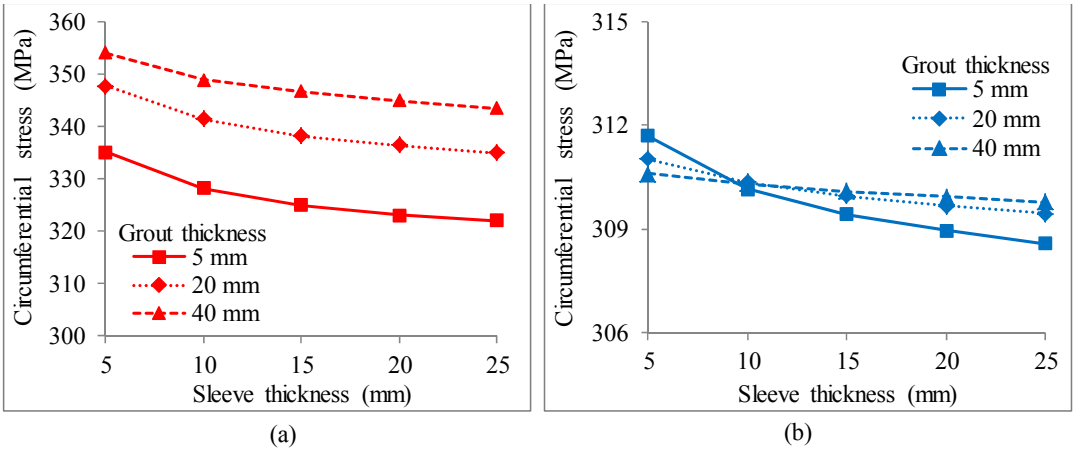

Figure 6.16 **Typical effect of sleeve thickness on the circumferential stress of the steel; (a) 1 GPa and (b) 10 GPa**

The effect of sleeve thickness on the level of stresses in the grout is given in Figure 6.17. As expected, a thicker sleeve is beneficial for reducing the stresses in the grout especially for low stiffness grout (1 GPa). The level of circumferential stresses further reduces for grout with higher modulus (5 and 10 GPa). The highest circumferential stress is observed for repair cases with 10 GPa grout supported by 5 mm sleeve. According to the results, there are negligible variations in level of stresses and strains in the components of the repair with moderate to high stiffness grout used (5 and 10 GPa) beyond sleeve thickness more than 20 mm. This implies that a stiffer grout infill should be confined by a minimum thickness of sleeve to ensure an effective reinforcement. Hence, a sleeve thickness of around 15 to 20 mm is necessary to provide a sufficient layer of reinforcement for the infilled composite repair. It is to be noted that level of stresses and strains along the layers are valid provided that the infill layer remained uncracked and act as a continuous support. Hence, further study is required to observe the behaviour of the repair components when the cracking of the grouts is considered in the analysis.

The effect of sleeve thickness on the circumferential stress of the sleeve is shown in Figure 6.18. The stress in the sleeve layer decreases with increasing sleeve thickness. However, the level of stresses in the composite sleeve is very low compared to the strength of composites indicating that a thinner composite is sufficient for the repair system considered. There is insignificant variation in the stress in the sleeve due to increment of sleeve thickness with grout thickness more than 20 mm for a repair system with higher grout modulus (10 GPa). This implies that sleeve thickness has minimum effect on a thicker stiff grout. This is due to the fact that a stiff grout thickness more than 20 mm sufficiently transfers the load to the sleeve. The results also indicate that a thicker layer of sleeve is imminent when thinner grout is used to ensure effective support to the system.

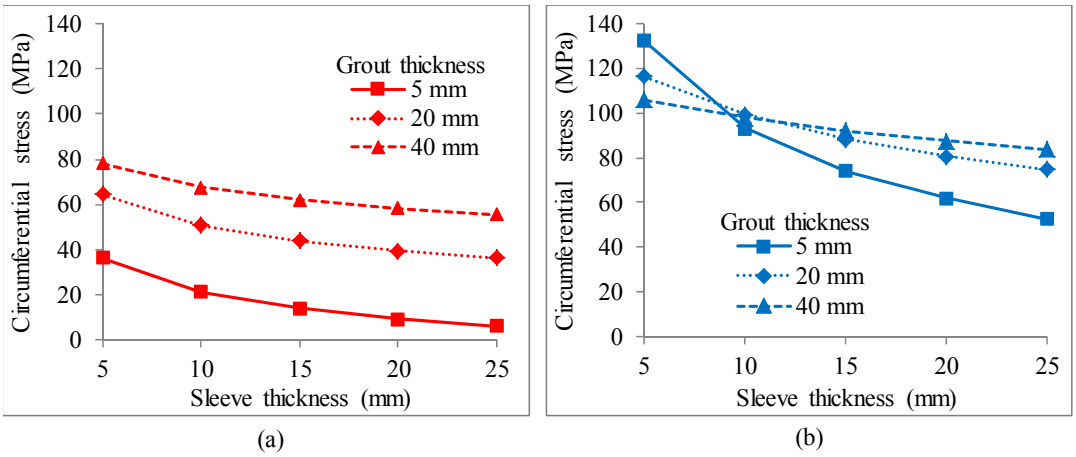

Figure 6.17 **Typical effect of sleeve thickness on the circumferential stress of the grout; (a) 1 GPa and (b) 10 GPa**

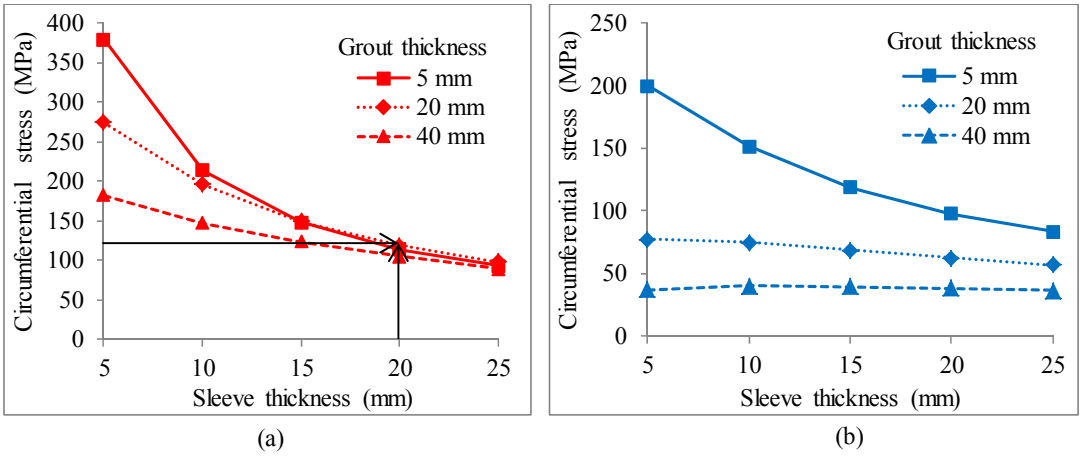

Figure 6.18 **Typical effect of sleeve thickness on the circumferential stress of the sleeve; (a) 1 GPa and (b) 10 GPa**

6.5.3 Effect of grout modulus

Infill system with the 5 to 10 GPa grout undergoes higher circumferential stress and lower radial strain as the rigid infill supports the steel pipe and effectively transfers the load from steel to sleeve. The circumferential strain of the steel decreases with the increment of the grout modulus. As a result, using a grout with higher stiffness is also expected to increase the elastic pipe capacity.

The effect of grout modulus on the level of stress in the steel is presented in Figure 6.19. Low stiffness grout results in higher stress in the steel which indicates that this grout is not effective in transferring the load from the steel to the sleeve. However, a stiffer grout (5 to 10 GPa) decreases the level of stresses in the steel but there is insignificant difference on the levels of stresses between a 5 GPa and 10 GPa grout. This is due to the fact that a stiffer grout ensures effective transfer of the stress in the repair system.

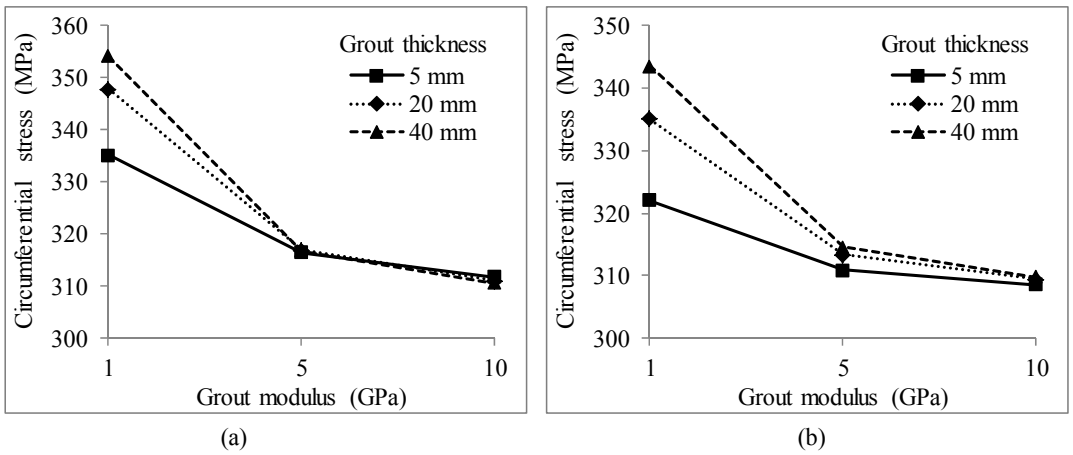

Figure 6.19 **Typical effect of grout modulus on circumferential stress of steel; (a) 5 mm and (b) 25 mm**

Figure 6.20 presents the effect of the grout modulus on the stress in the grout. Generally, higher stiffness results in a higher stress in the infill indicating that it absorbed the stresses from the steel and transfer it to the sleeve. From the results presented in Section 6.4, it is also seen that the stresses and strains in steel are less affected by the thickness of the grout when a modulus of (5 to 10 GPa) is used with a sufficient sleeve thickness. This increment of stress and strain in steel and sleeve is more prominent for a low stiffness grout that may result from hot-wet conditioning. Hence, the effect of hot-wet conditioning produces higher stress and strain, which eventually reduces pipe capacity. The low grout stiffness results in higher strain but low stress in the grout. The ranges of circumferential and radial strains in the grouted infill layer are found to be within 0.5 to 8%, and -0.5 to -7%, respectively.

According to study of the physical properties of grouts in Chapter 3, the tensile and compressive strain of grouts range from 0.1 to 1.0% and 2 to 6%, respectively. Hence, the circumferential strain developed in the infill layer is higher than the allowable strain for the grouts with modulus less than 10 GPa. This indicates that the grout will crack at an applied pressure of 34 MPa. As the selection of material properties and repair geometries should be carried out based on the performance requirement of the repair, a low stiffness grout should be used for a non-leaking repair based on the result of this study. On the other hand, a grout with modulus greater than 5 GPa should be used for a repair requiring higher capacity and where leak containment of the infill can be compromised. This implies that moderately stiffer grout will provide an effective layer that aid to minimise the stresses and strains in the steel and sleeve while the grouts with lower stiffness (1GPa) is not effective as seen by the low levels of stress and strain experienced by these grouts.

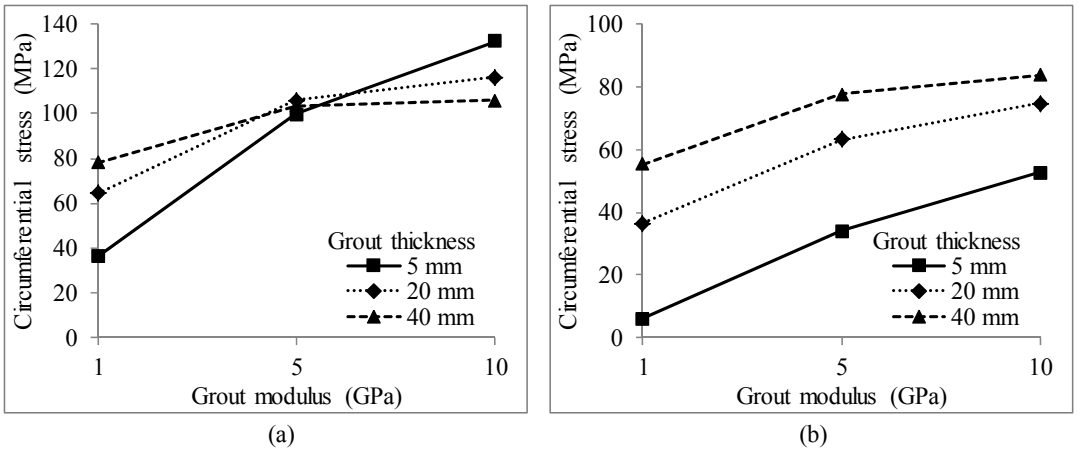

Figure 6.20 **Typical effect of grout modulus on circumferential stress of grout; (a) 5 mm and (b) 25 mm**

Figure 6.21 shows the effect of grout modulus on the stresses in the sleeve. The results indicate that using higher modulus grout reduces the stress in the sleeve. This is due to the fact that a thicker stiff grout (5 to 10 GPa) provides support for the steel and reduces the stress in the sleeve. Since, there was reduction in modulus of the grout due to hot wet conditioning (as found from Chapter 4), the stress in the sleeve increases. Although, there was negligible reduction in stiffness, considerable reduction occurred in strength in the composite due to hot-wet conditioning (as investigated from Chapter 5). Hence, the hot-wet conditioning may be proven critical for a grouted repair system susceptible to environmental degradation and optimum grout thickness is necessary to maintain the stress in the sleeve within allowable limit. Due to hot-wet conditioning, the minimum tensile strength in the composite was found to be 127 MPa. Figure 6.11 and Figure 6.18a suggest a grout thickness of at least 20 mm with modulus 1 GPa can retain that stress in a sleeve with thickness of 20 mm. It is to be noted that 1 GPa grout represents a grout that has gone under conditioning. Hence, a 20 mm grout thickness is recommended in the next investigation.

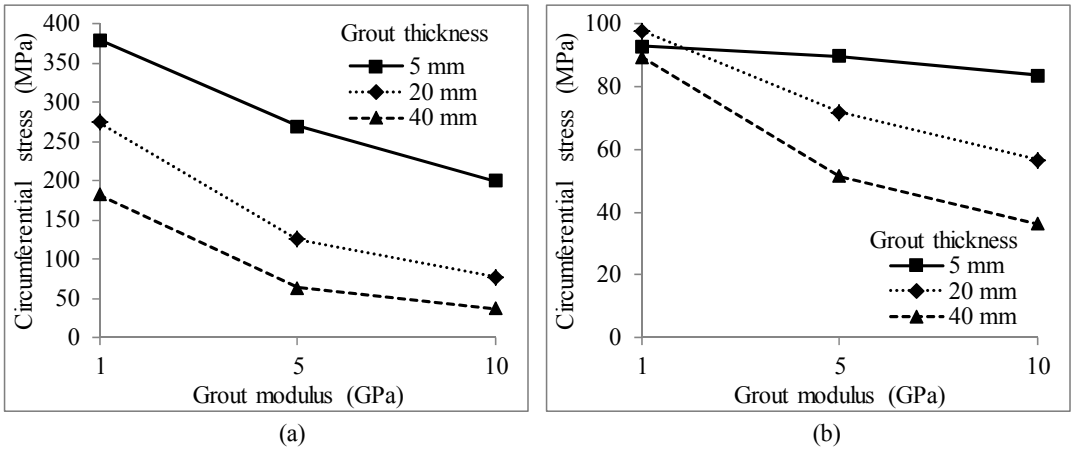

Figure 6.21 **Typical effect of grout modulus on circumferential stress of sleeve; (a) 5 mm and (b) 25 mm**

6.6 Conclusions

Finite Element Analysis (FEA) was carried out on the infilled fibre-reinforced composite repair system for steel pipe with 80% metal loss. A total of 120 repair combinations of grouted sleeve repair of steel pipe were analysed to investigate the effect of grout thickness and sleeve thicknesses and grout modulus on the effectiveness of an infilled repair. The repair system is expected to restrengthen the repaired pipe through effective load transfer among the components. The circumferential stress and strains are found critical for all the repair components. The following conclusion can be drawn for the observations of the analysis:

- A thin infill layer reduces the stresses and strains in the steel and infill grout and is found suitable to effectively transfer the stresses from the steel to the composite sleeve. However, the optimum grout thickness will also be governed by practical curing, flowability and installation considerations when used in the grouted repair system.
- Grouts with higher modulus are found to reduce the stresses and strains in all the components of the repair other than an increased stress in the infill layer itself. As a result, a grout modulus of about 5 to 10 GPa is found desirable for keeping lower strain in the steel and infill since a stiff grout can effectively transfers the load from steel to the sleeve.
- Thicker sleeve is found to reduce the level of stresses and strains in all the components of the repair. Hence, sufficient sleeve thickness is required for providing support to the layers and to improve the repair performance.
- There may be reduction in strength and modulus in the grouts, when they go under environmental degradation due to hot and humid conditions. This can result in higher stress and strain in the steel and sleeve. Again, hot-wet environment can considerably reduce the strength in the sleeve, however, negligible variation on the modulus. Hence, when grout and sleeve are selected, subsequent effect of hot-wet conditioning should also be taken into consideration. A grout and sleeve thickness of 20 mm is found appropriate to effectively transfer the load as well as reduce the stress in the sleeve subjected to conditioning within allowable limit.

The results of the analyses in this chapter provided a basis for an optimum parameters that need to be considered to have an effective grouted repair system for pipelines with defect. However, this analysis considers only the most critical level of metal loss which is 80%. Practically the actual metal loss may vary and is localised with different shapes and sizes. Hence, a 3D analysis is warranted to investigate the effectiveness of a grouted composite system in repairing a steel pipe with a localised defect. The critical design parameters obtained from this extensive numerical simulation and the cracking of the grout are considered and their effects on the behaviour of a steel pipe with localised defect and repair with a grouted composite system are investigated in the next chapter.

Chapter 7

Investigation on the effectiveness of grouted sleeve repair system with a localised defect

7.1 Introduction

Fibre-reinforced composites have proven their practicality in repairing corroded pipelines. A comprehensive literature review in Chapter 2 suggested the grouted composite sleeve as a potential repair system. Nevertheless, a number of studies on the structural performance of the grouted sleeve repair is very limited. The extensive investigation of the grout and composite materials in Chapters 3 to 5 suggests that these materials have the strength and stiffness for structural applications and also suitable for pipeline repair as compared to the previous studies (Duell et al. 2008; Freire et al. 2007; Palmer-Jones et al. 2011; Vu et al. 2011) and results of the analyses in Chapter 6.

The remaining strength of a corroded pipe is dependent on the level of metal loss (Cunha & Netto 2012). In Chapter 6, only 80% corrosion level is considered and is assumed to extend throughout the length. This justifies the need for an analysis of the effectiveness of the grouted composite sleeve for a pipeline repair with a localised metal loss. It is also essential to consider the material properties, obtained in Chapters 3 to 5, so that the effect of actual strength and stiffness of the infill and reinforcement sleeve can be investigated. This chapter focuses on three dimensional (3D) finite element analysis (FEA) of a full-scale pipe with different levels of metal loss. The results of this investigation will provide useful understanding of the behaviour of the system for design and practical application. The effectiveness of the repair system is also quantified in comparison to pipe capacity of bare pipe. The pipe capacity is determined as the internal pressure for yielding of steel at the defect of the corroded pipe.

7.2 Simulation methodology

7.2.1 Description of the FE model

A 3D finite element model and mesh consisting of *Hexa8* solid brick elements of the steel pipelines repaired with a grouted composite sleeve system was generated using the finite element software Strand7 (Strand7 Pty Limited 2005) in order to assess the stress levels in the different components of repair under internal pressure. This analysis scopes the behaviour of an externally corroded pipe with a metal loss ranging from 20% – 80%, repaired with two types of infill grouts and five sleeve thicknesses varying from 5 – 25 mm. The properties of grouts C, D and E are found to satisfy the requirement for a range of structural repair and rehabilitation works to a pipe (Duell et al. 2008; Mattos et al. 2012; Mendis 1985; Vu et al. 2011). In this study, grouts C and E are selected as the representative of fine filled and coarse filled aggregate, respectively. While Chapter 6 suggests that a thinner grout is more suitable, a grout thickness of 20 mm is adopted as it was found optimum to keep the system effective even under hot-wet environment.

The study determines the level of stresses in the components at the location of the defect. The repaired system is considered close-formed and the interfaces are

considered flawless, resembling an ideal filled repair system reinforced with fibre-reinforced sleeve. The following assumptions are considered in the finite element analysis of the repaired pipeline:

- The analysed pipe is seamless (SMLS) and free of welding in between segments.
- The pipe-infill and infill-composite interfaces of the repair are considered perfect.
- The pipe is subjected to internal pressure only and free from external pressure, bending, torsion, indentation, and other live loads.

7.2.2 Geometry of the repair

An infilled sleeve repair system applied on a pipe with a defect is already described in Figure 1.5 and Figure 6.1. The diameter and thickness of the pipe is 114.3 mm and 4.8 mm, respectively. The adopted lengths of the pipe and the repair are L = 1000 mm and L_{repair} = 400 mm, respectively. Figure 7.1 shows the dimensions of typical repaired pipe. An extended 300 mm pipe on both sides of the sleeve is introduced to investigate the level of stresses in the pipe outside the repair, and to ensure that a sufficient length of pipe provided outside the repaired area. The length of the repair provided conforms to ISO/TS 24817 (2006). The ends of the repair are not tapered in this analysis the pipe is not subjected to axial loads and the investigation of stresses is focused near the pipe section with a metal loss. The level of stress along the length shown in Figure 7.2 suggests that extended pipe is sufficient to eliminate stress concentration at the end of the composite repair due to the close-end effect and the stress level plateaus along the length. The results also suggest that the circumferential stress outside the repaired section of the pipe is expected to burst when an internal pressure of 34 MPa is applied. The yielding of steel occurs at around 26 MPa of internal pressure which is also considered as the capacity of the pipe without any defect.

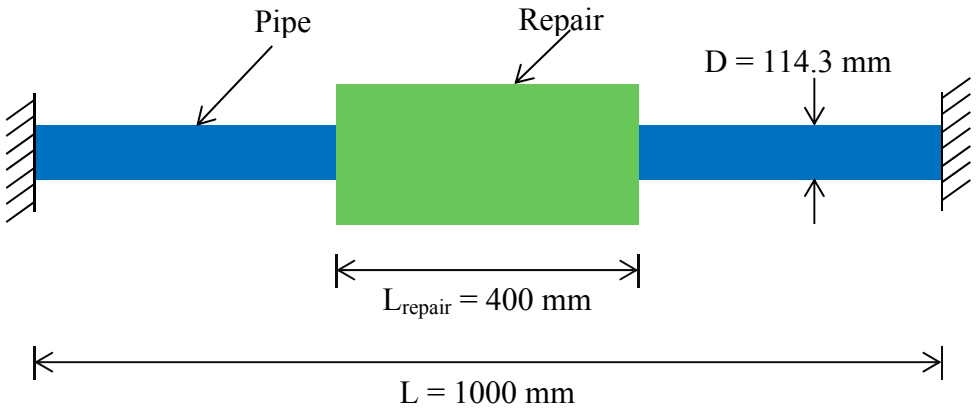

Figure 7.1 Schematic illustration of repaired pipe

Only half of the system is modelled due to the symmetry along the length and the vertical axis. Figure 7.3 shows the model along the longitudinal section of the repaired pipe. Figure 7.4a shows the details of the defect in the pipe. The parameters, l_1 and θ_1 represent half of the length and angular extent, respectively for the bottom area of the defect. Transition along the longitudinal and angular direction of the defects is defined by l_2 and θ_2, respectively. Combinations of the geometry of the

defect are given in Table 7.1. Since, only half of the model is used, the sum of $\theta_1$and $\theta_2$is half of the total angular extension and the sum of $l_1$and l_2 is half of the length of the defect. Typical mesh and metal loss are shown in Figure 7.5. Symmetry boundary conditions were applied at the appropriate faces of symmetry of the model.

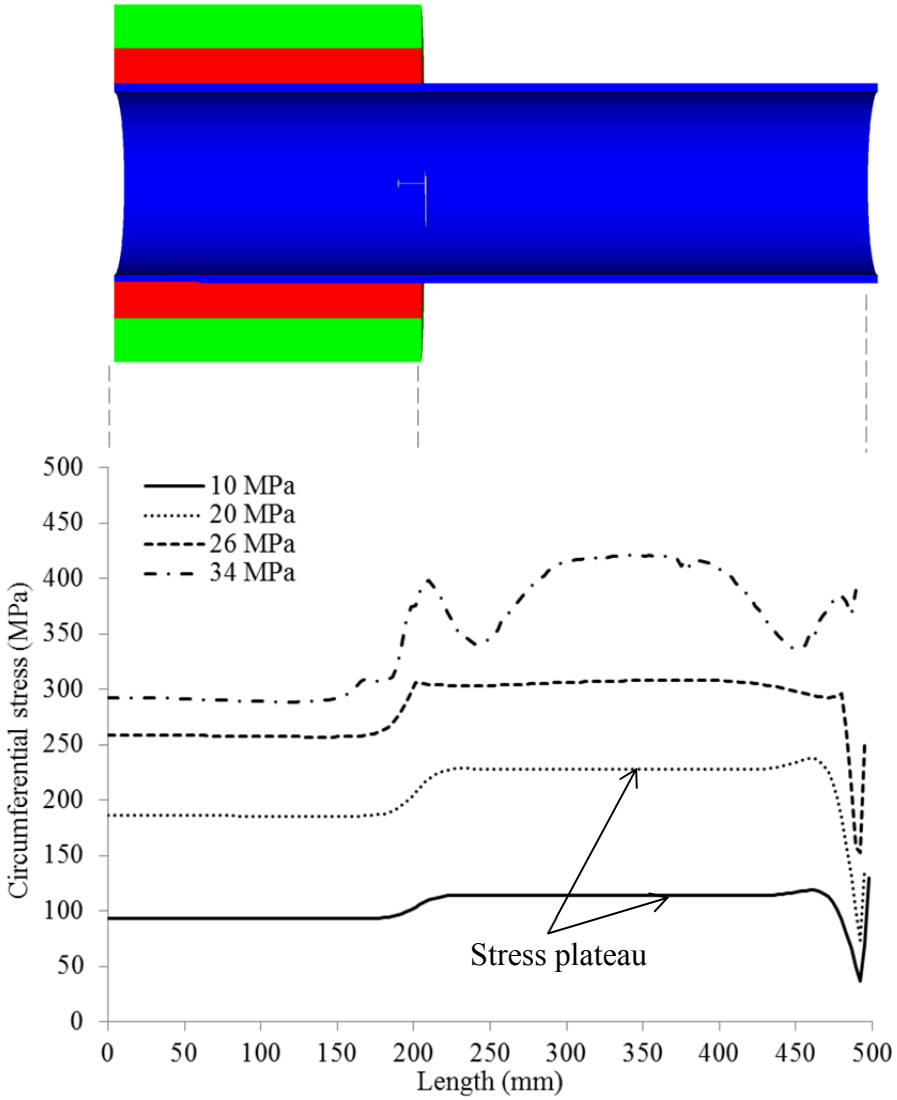

Figure 7.2 **Distribution of circumferential stress along the length of the repaired pipe**

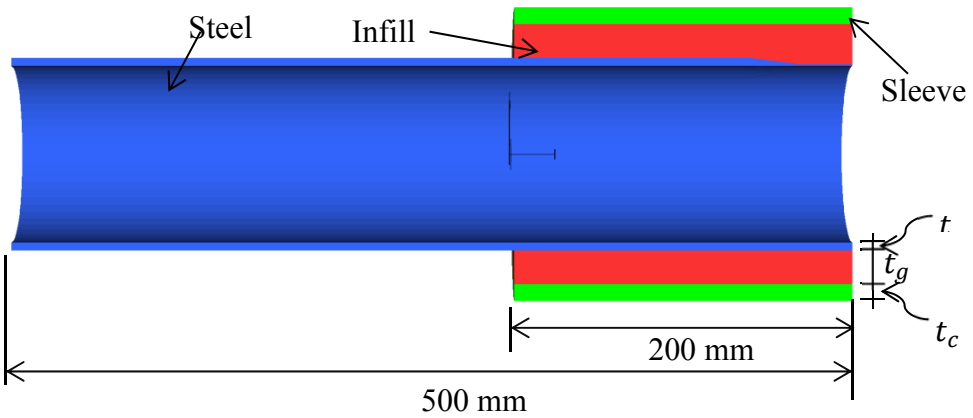

Figure 7.3 **Longitudinal section of the repair system**

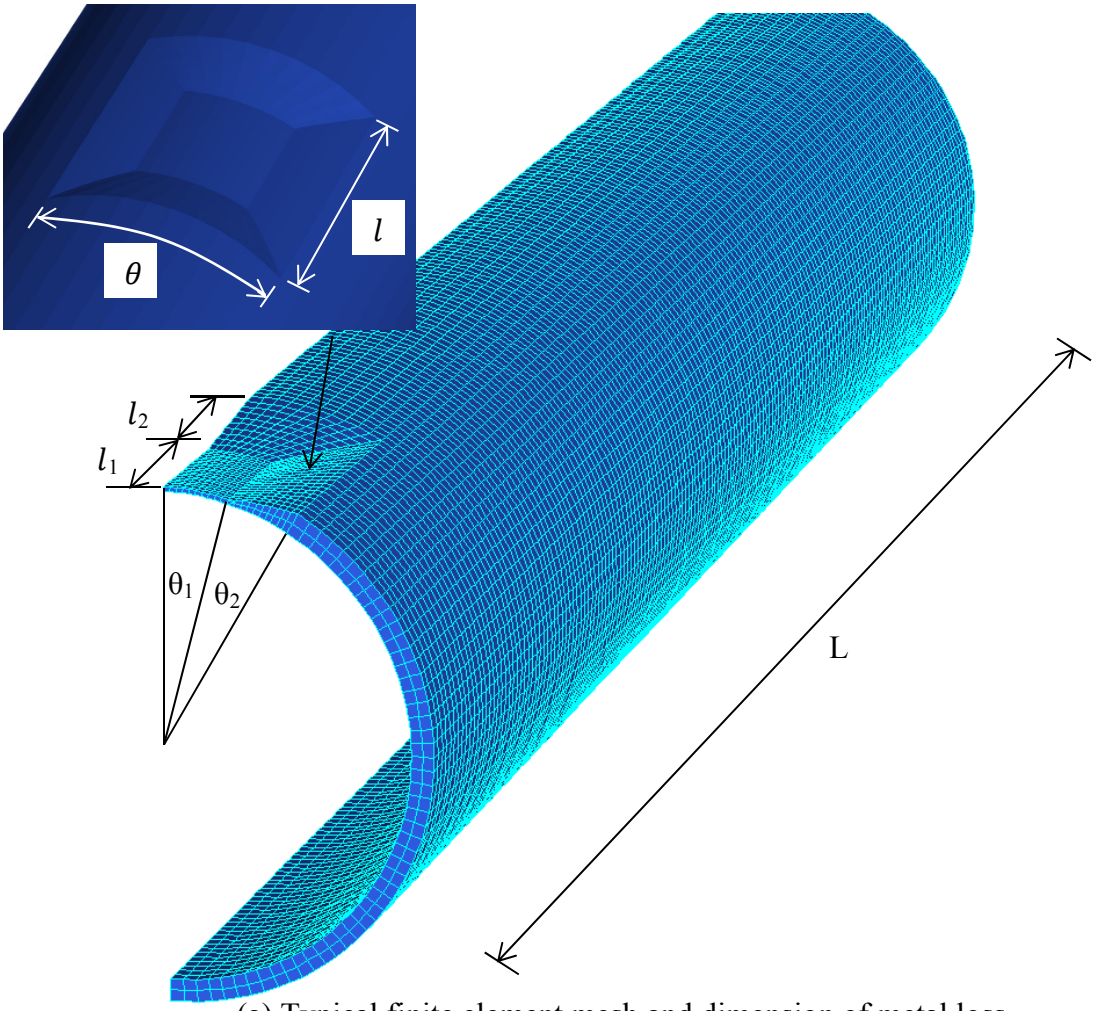

(a) Typical finite element mesh and dimension of metal loss

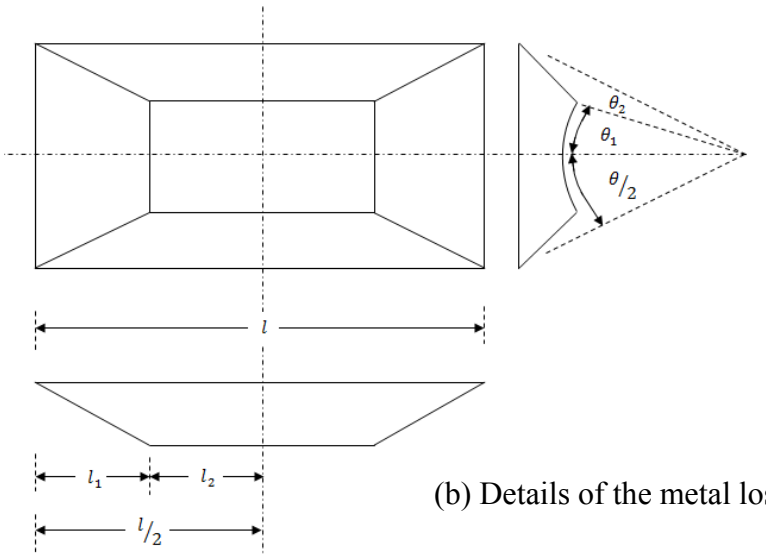

(b) Details of the metal loss

Figure 7.4 Geometry of the finite element model

Table 7.1 Distribution of geometries of the metal loss in the pipe

		d/t			
		0.8	0.6	0.4	0.2
$\theta/2$	θ_1 (deg)	15	18.75	22.5	26.25
	θ_2(deg)	15	11.25	7.5	3.75
$l/2$	l_1 (mm)	30	37.5	45	52.5
	l_2 (mm)	30	22.5	15	7.5

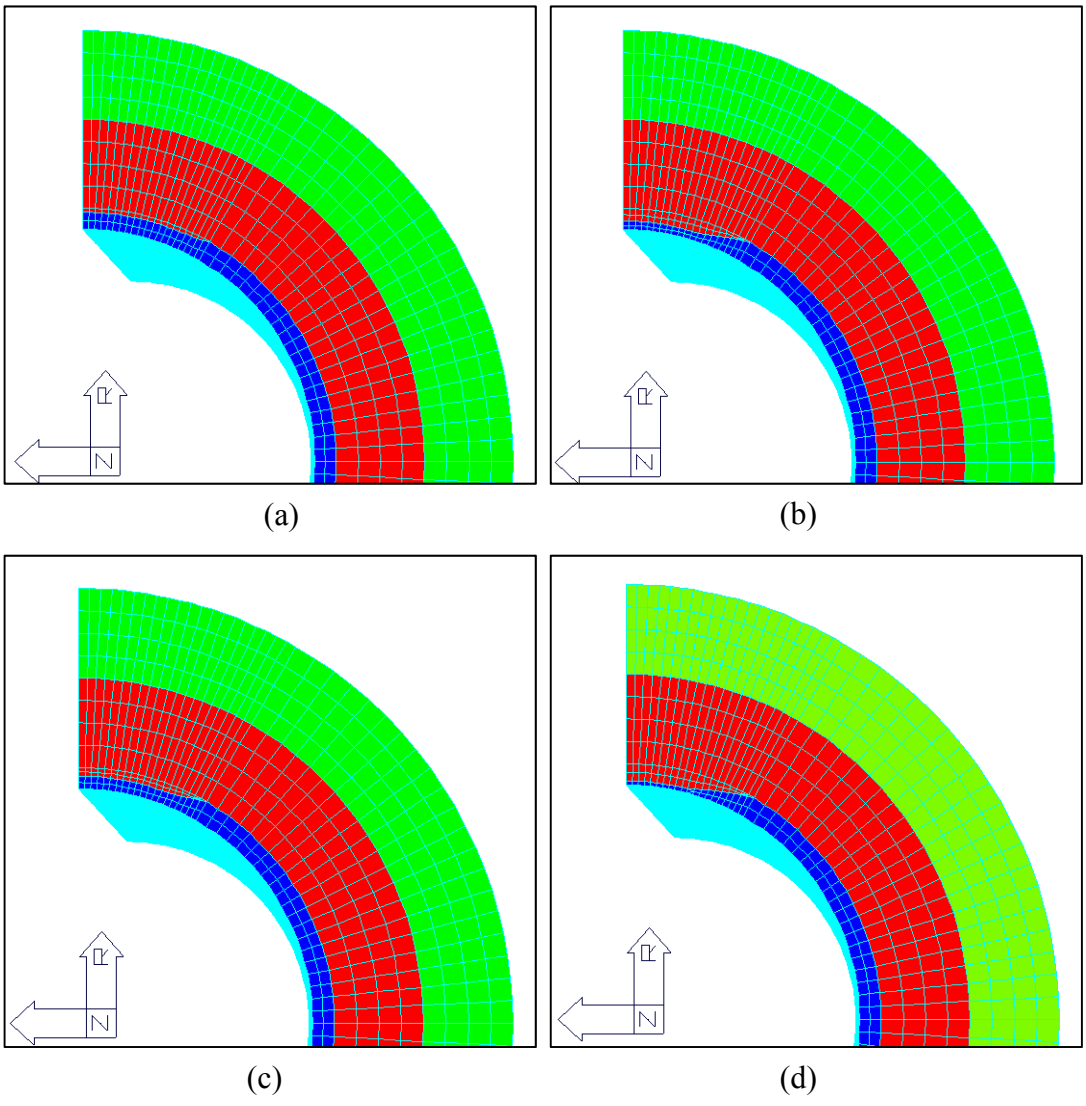

Figure 7.5 Typical finite element models for the numerical analysis of pipes with metal loss; (a) 20%, (b) 40%, (c) 60% and (d) 80%

7.2.3 Constitutive material model

The pipeline material considered is an American Petroleum Institute, API-L-X42 steel. The stress-strain curve of X42 steel is shown in Figure 7.6. This simplified stress-strain relation is adopted from Brooker (2003) wherein standardised tri-linear stress-strain behaviour of the steel is used. The Young's modulus, yield strength and ultimate tensile strength of the pipe are 200 GPa, 289 MPa and 413 MPa, respectively. The von Mises yield was adopted to model the metal plasticity model.

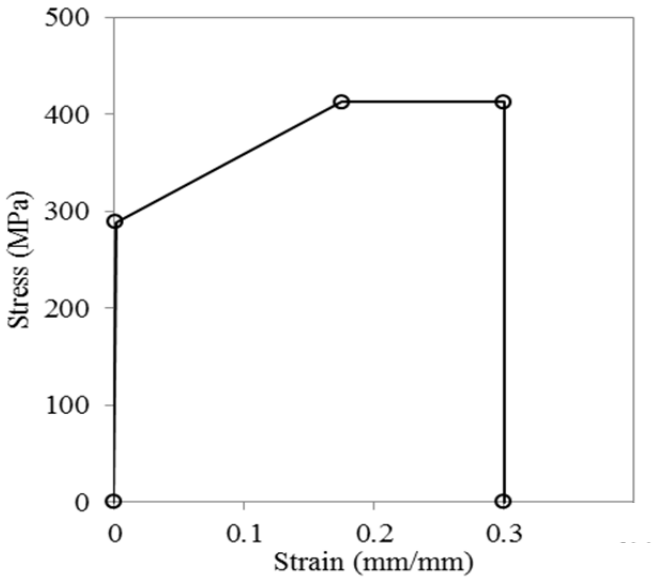

Figure 7.6 Stress-strain curve of X42 steel for the analysis

Figure 7.7 shows the actual stress-strain behaviour of grouts C and E obtained from experimental investigation in Chapter 3. This range of modulus for grout is found to be suitable for improving the performance of the repair system. These investigated grouts will easily flow in the confined annulus which is an important consideration in the repair system. Grout with higher stiffness is directly related to increased viscosity and lower workability. It is to be noted that the behaviour under compression of grout C, shows a prolonged strain with a lower stress beyond peak stress. The stress-strain behaviour is considered only up to the peak stress for simplicity.

The orthotropic material model was used for the composite sleeve. Two types of sleeve materials, Carbon Glass Fibre Reinforced Polymer (CFRP), and Glass Fibre Reinforced Polymer (GFRP), with properties listed in Table 7.2 were used. The directions 1, 2 and 3 refer to radial, circumferential and axial direction, respectively of the repair system. CFRP properties were adopted from Duell et al. (2008) while the GFRP sleeve properties were obtained from the experimental studies carried out in Chapter 5.

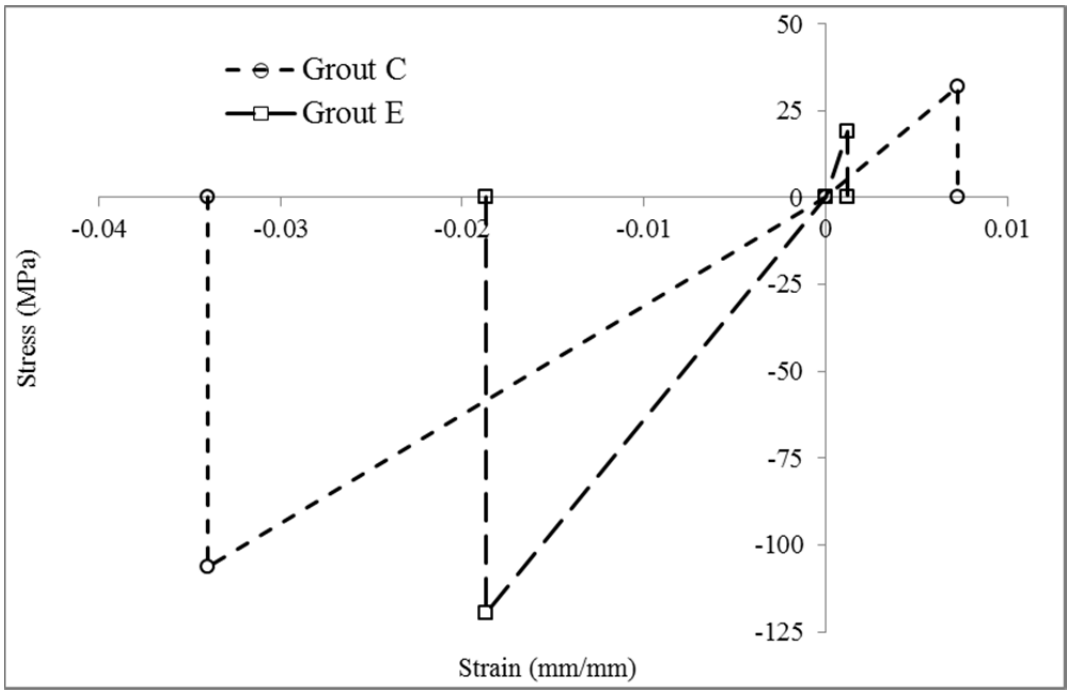

Figure 7.7 Stress-strain behaviour of infill grouts adopted for the analysis

Table 7.2 Properties of composite sleeve for the analysis

Parameter	Sleeve	
	CFRP	GFRP
E_1(GPa)	5.5	24.6
E_2(GPa)	49.0	28.0
E_3(GPa)	23.4	24.6
ϑ_{12}	0.196	0.133
ϑ_{23}	0.43	0.126
ϑ_{31}	0.43	0.133
G_{12}(GPa)	29.60	10.85
G_{23}(GPa)	0.69	12.35
G_{31}(GPa)	0.69	10.85

A total of 80 geometric and material combinations are used in this study, which are generally symbolised in a uniform sequence of $(Type\ of\ grout, {}^{d}/_{t}, Type\ of\ sleeve, t_s)$. For example: (C,20,$GL$,5) indicates a repair system using grout C on a pipe with 20% metal loss and reinforced with 5 mm thick GFRP. Table 7.3 shows the range of parameters and materials used in the analysis.

An incremental internal pressure was applied to all surface areas of the inside wall of the pipe. The level of stresses was determined for each pressure increment and was plotted against applied pressure for each repair case. According to ISO/TS

24817 (2006), the composite repair can be classified as non-leaking (Type A) and leaking (Type B). In this analysis, the type A repair system is adopted implying that the repair system is considered functioning as long as the infill grout is carrying the circumferential stress. Hence, the effectiveness of the repair system is determined from the applied pressure in which the infill layer cracks. The applied pressure was used as the pipe capacity, and subsequent comparison was drawn among the repair cases based on the results.

Table 7.3 Details of the parameters

Parameters	Symbol	Description
Thickness of the grout	t_g	20 mm
Type of the grout	C, E	Grout C, Grout E
Level of metal loss	d/t	20, 40, 60, 80%
Type of the sleeve	CA, GL	Carbon, Glass
Thickness of the composite sleeve	t_c	5, 10, 15, 20, 25 mm

7.3 FE Results and Analysis

The following sections provide the stress levels in the different components of the composite repair system due to the applied internal pressure in the pipes. These results are used to evaluate the effectiveness of the applied repair system. The effect of metal loss, grout types and sleeve thickness on the effectiveness of a grouted composite sleeve system for the repaired pipe is determined from the level of stresses in each component of the repair system.

7.3.1 Behaviour of the components of the repair

Figure 7.8a shows the typical stress distribution along the components of the repair. Figure 7.8b suggests that the critical locations of the repair occur along the transition end and Figure 7.8c shows the potential rupture line of the steel. The potential rupture line in the steel is near the transition end which was also observed experimentally by Freire et al. (2007) in a pipe repaired with composite wrap with locally applied putty. The critical locations in the steel pipe, grout and composite sleeve are also comparable to the results of the analysis in Chapter 6. The deformed shape of the model suggests that the grout restrains the radial expansion of the defected pipe when compared to pipe section outside repair cases.

A typical progressive localised crack formation in the grout is shown in Figure 7.9. Three consecutive stress fields with 0.5 MPa pressure increment are shown in this figure. It can be seen that the highest stress level is found at the transition end indicated by the red colour (Figure 7.9a). After cracking, the stress in the grout became zero (shown in blue in Figure 7.9b). Finally, the crack propagated towards the thickness of the infill layer as shown in Figure 7.9c. The changing stress field along the transition end corresponding to the applied internal pressure is recorded and plotted for analysis. Since the grout infill lies in between the steel and composite with modulus significantly higher compared to the grout, the stress in the grout is found critical for this analysis.

Figure 7.10 shows the comparison of circumferential and radial stresses in the layers of the repair system with increasing internal pressure. As expected, the tensile circumferential stress is higher than that of compressive radial stress in the grout, steel and composite sleeve. Thus, only the level of circumferential stress is

analysed in the succeeding sections as this is the governing stress in the grouted sleeve repair system. It is to be noted that there are sudden increase in the level of stresses in all the components near 19 MPa. This is due to formation of crack in the infill layer and rearrangement of stresses from one element to another. Details of this behaviour are discussed next in Section 7.3.2.

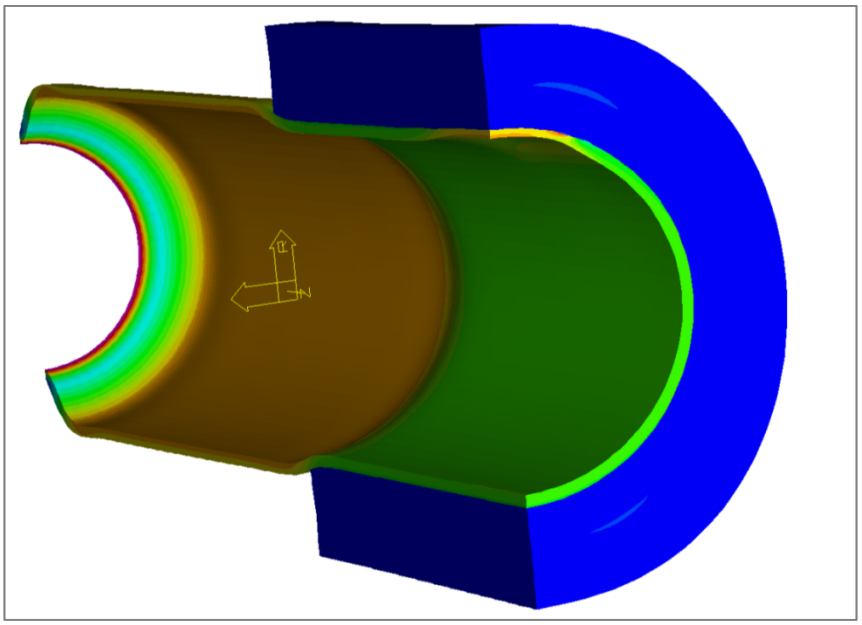

(a) Stress distribution

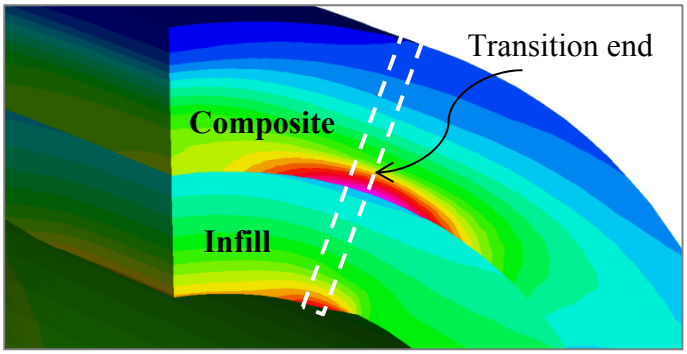

(b) Critical stress in the infill and sleeve

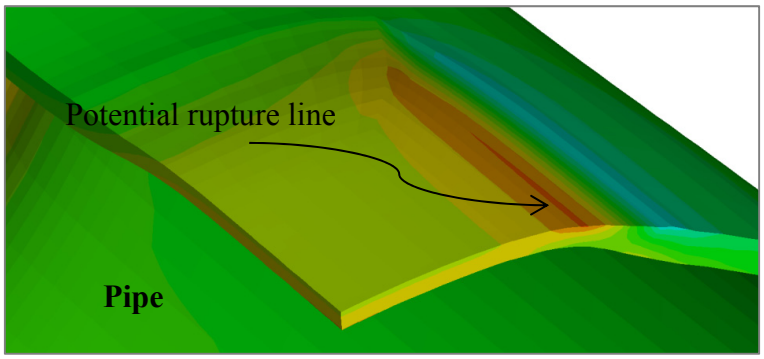

(c) Critical stress in the steel

Figure 7.8 **Typical level of circumferential stress in a full 3D model of a pipe with repair combination of (E,40,CA,25) under internal pressure of 10 MPa**

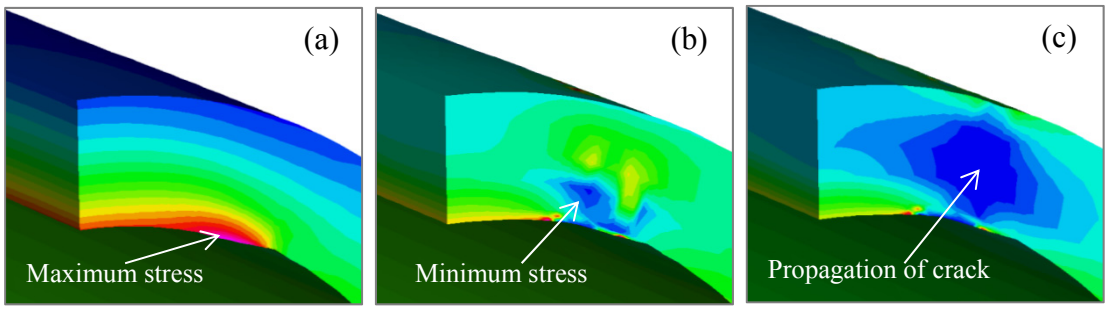

Figure 7.9 **Typical propagation of crack in the infill layer with repair combination of (E,40,CA,25) under internal pressure; (a) 18.5 MPa, (b) 19.0 MPa and 19.5 MPa**

7.3.2 Distribution of circumferential stress in the components of the repair

Figure 7.11 shows the level of circumferential stresses with increasing internal pressure in the components of the repair reinforced with the carbon sleeve reinforcement and filled with grouts C and E. The stress in steel pipe with grout C is linear until yielding but a sudden increment in the stress was observed during cracking of the grout as shown in Figure 7.11a. The stress in grout C after yielding of the steel, is higher than that of before the yielding of the steel. A magnified view of the level of stresses in the grout and sleeve is shown in Figure 7.11b and implies that upon the yielding of steel, an increased stress is experienced by the grout and the sleeve. The increment in the stress in the steel is due to the fact that there is zero circumferential stress in the grout after cracking.

The cracking of the grout states the inability of the infill layer to transfer the load since it does not provide any circumferential contribution that may restrain the expansion of the steel. The sudden increase in the stress in the steel is due to the reduced support by the grout layer which is cracked. As a result, the stress is suddenly transferred from the steel to the sleeve. The stress in the sleeve layer is also found to increase at the same time. There is sudden drop in the circumferential stress in grout C, when it reaches near 32 MPa. This is because grout C has a tensile strength of 32 MPa, which suggests the formation of crack in the grout upon reaching this level of stress. The internal pressures during the cracking of the grout are found to be 34.0 MPa and 18.5 MPa for the repair cases with grout C and E, respectively as shown in Figure 7.11b.

The stress-pressure behaviour of the elements of the repair conditions containing both carbon and glass is comparable. Figure 7.12 shows the level of circumferential stresses in the components of the repair reinforced with glass reinforcement and filled with grouts C and E. The stress-pressure behaviour is linear for the steel, grout and sleeve up to the yielding of the steel. When the tensile crack in the grout layer occurs, a sudden increment in the circumferential stress in the steel resulted. Again, the cracking in the infill layer occurs at a circumferential stresses of about 32 MPa and 19 MPa which are the tensile strengths of grout C and E, respectively. The cracking of the grout is found to occur at internal pressure of about 36.0 MPa and 19 MPa for the repair cases with grout C and E, respectively (as shown in Figure 7.12b).

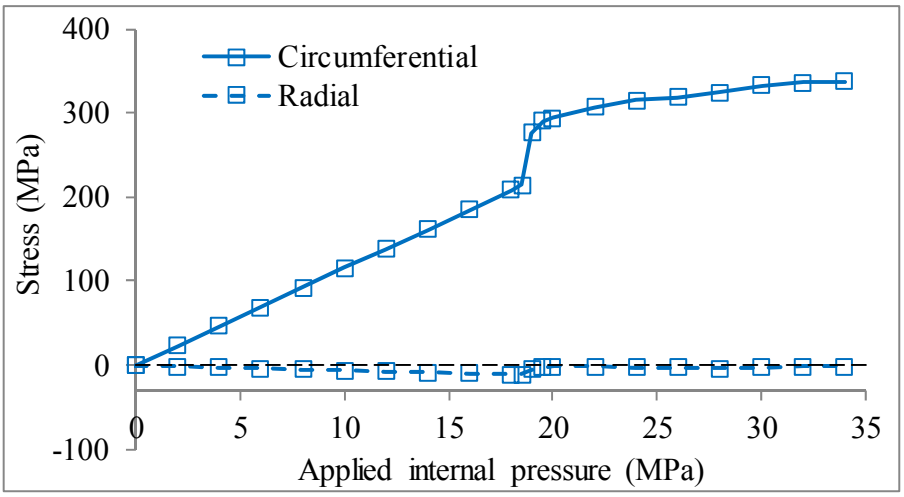

(a) Steel

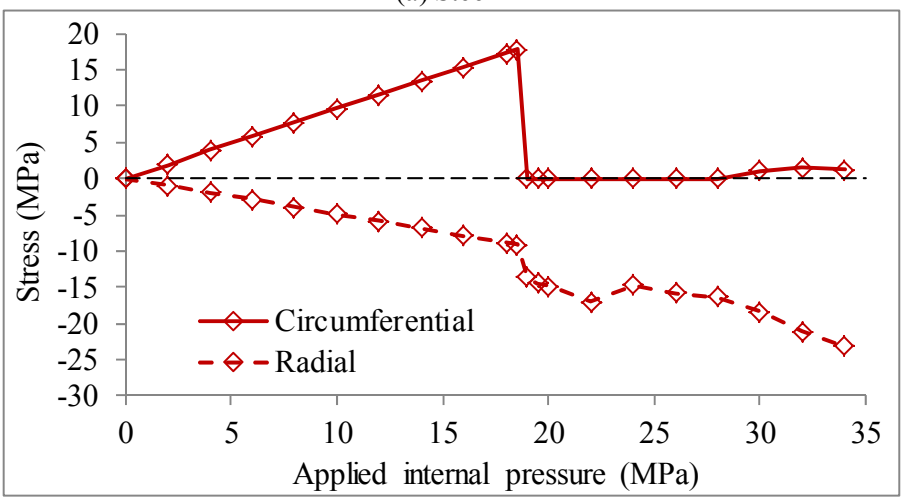

(b) Infill

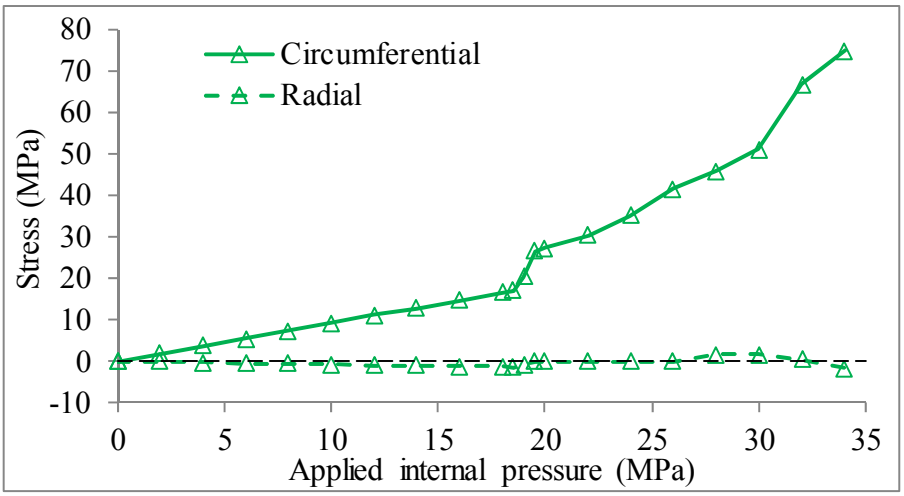

(c) Sleeve

Figure 7.10 **Level of circumferential and radial stresses in the components of the repair with combination of (E,40,CA,25)**

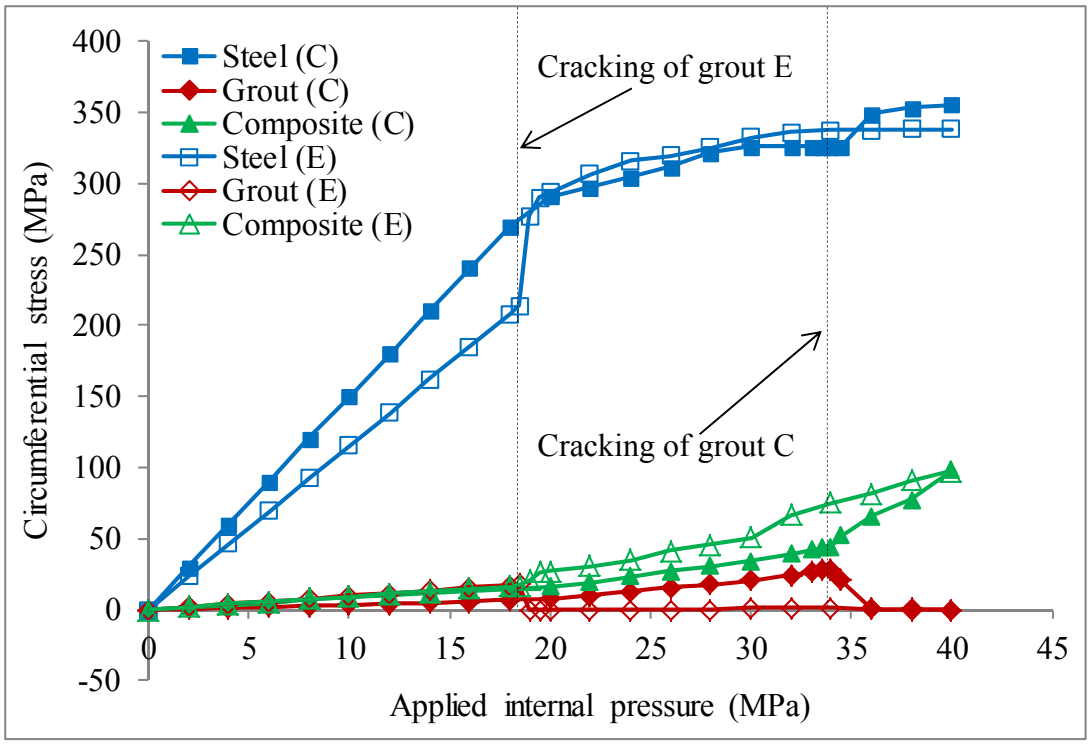

(a) Steel, grout and composite

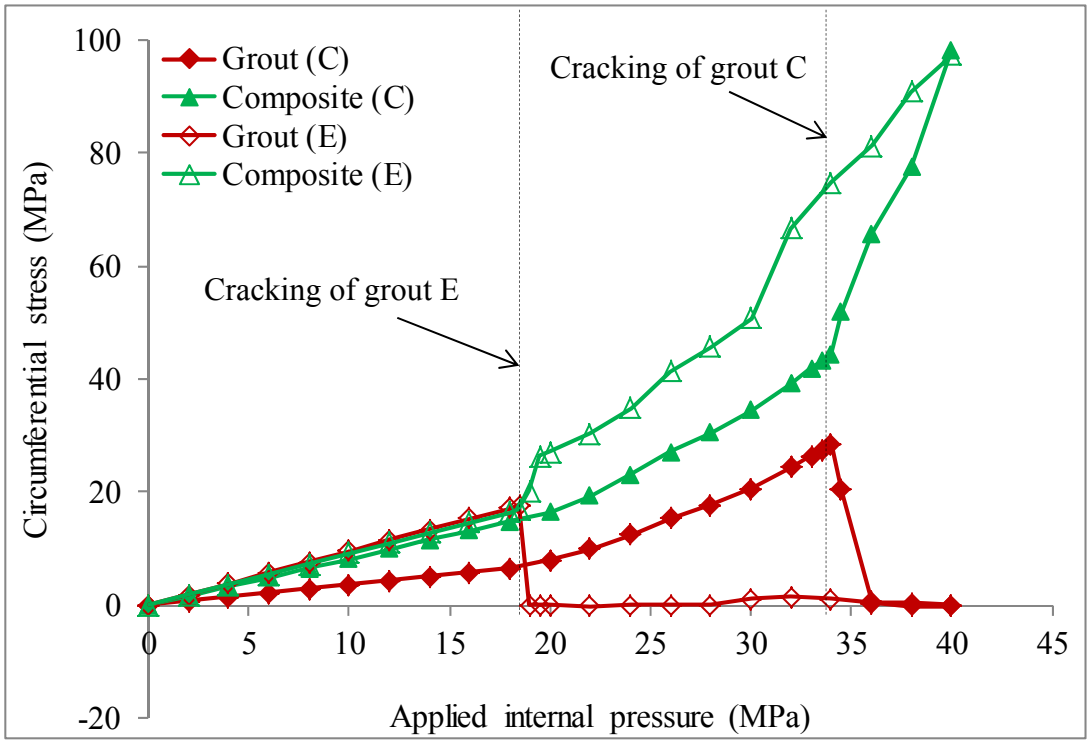

(b) Grout and composite

Figure 7.11 **Typical level of circumferential stresses in a grouted repair with combination of (C/E,40,*CA*,25)**

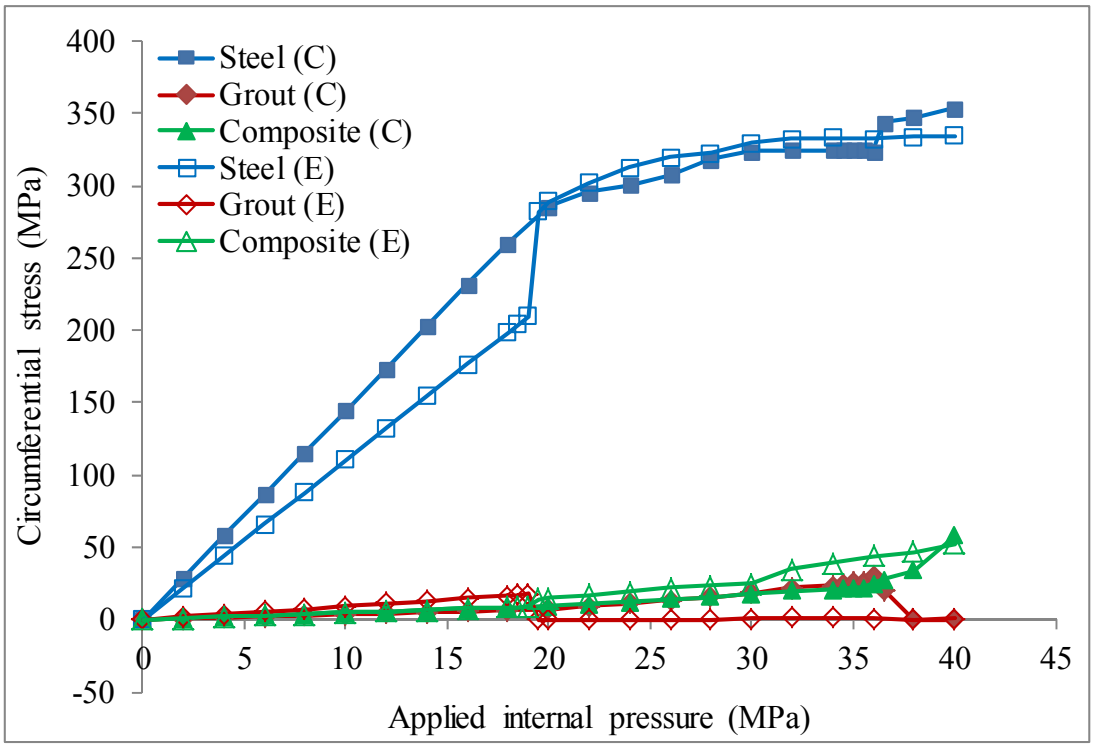

(a) Steel, grout and composite

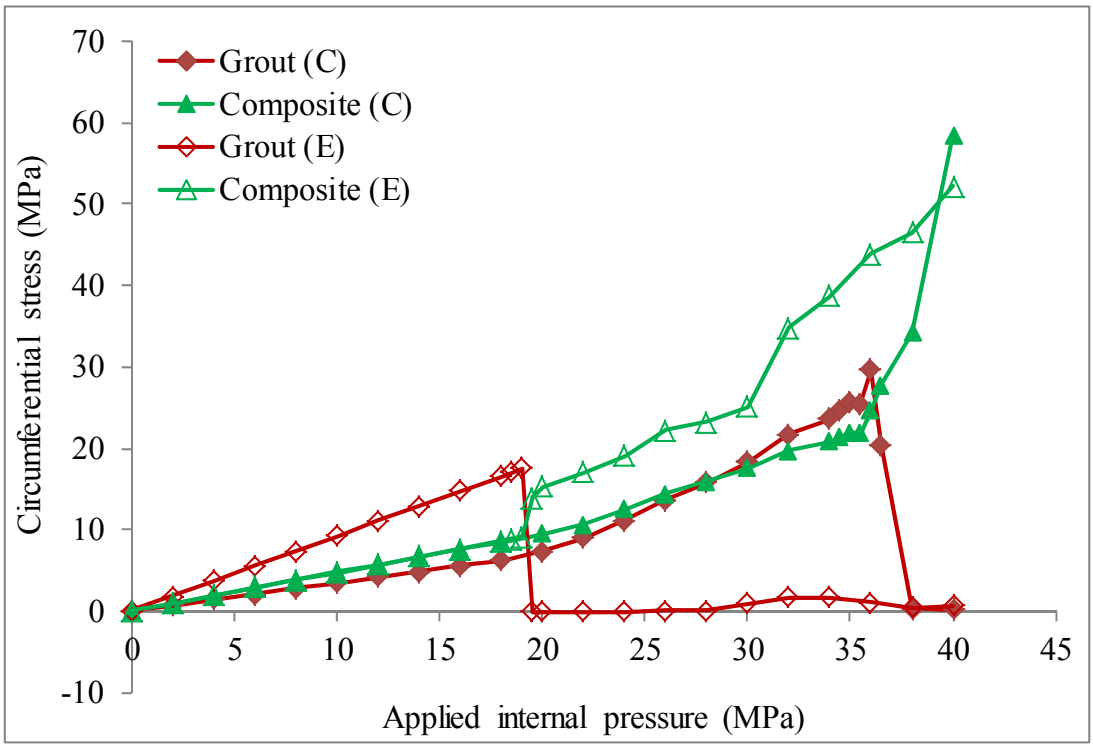

(b) Grout and composite

Figure 7.12 Typical level of circumferential stresses in a grouted repair with combination of (C/E,40,GL,25)

It is evident from the stress-pressure relationship of the repair that the steel pushes the grout and experiences higher stress when the grout fails. The sleeve experiences an increment in stress when there is an increment of stress in the steel

and grout. This implies that the infill grout provides an effective support and provides an effective transfer between the pipe and the sleeve repair before it cracks. The steel yields before crack in the grout for the repair system with grout C, whereas grout E cracks prior to yielding of steel. The results suggest that the capacity of the repaired pipeline using carbon or glass fibre reinforcement is the same for grouts C and E. The details of the pressure levels for the yielding of the steel and cracking of the grout of the repair cases are discussed in the following section.

7.3.3 Level of applied internal pressure

Figure 7.13 shows the level of internal pressure when the grout cracks and the steel yields for the repaired system with grout C and different sleeve thicknesses. The notations "CK" and "YD" refer to the cracking of the grout and yielding of the steel, respectively. The results suggest that the applied pressure at the cracking of the grout is higher than the yielding of the steel. Hence, cracking of the infill layer will occur after the yielding of the steel. The results also suggest that pressure capacity increases with increasing sleeve thickness. As expected, the pressure levels of the repaired section are found to be the highest and the lowest for the metal loss of 20% and 80%, respectively. It is to be noted that the pressure level of the repaired pipe with less than about 70% metal loss is more than 26 MPa irrespective of sleeve thickness and sleeve material. This indicates that the repair system with grout C is sufficient to reinforce the pipe up to 70% metal loss and the pipe outside the repaired section is expected to yield first.

Figure 7.14 shows the capacity of the repaired pipe during cracking of the grout and yielding of the steel against sleeve thickness for repair cases with 20 mm thick grout E with carbon and glass fibre composite sleeve. The pipe capacity increases with the increment of the sleeve thickness. It is evident from the results that, the internal pressure resulting from yielding of the steel is higher than that of the cracking of the grout. However, the difference between the yielding of the steel and the cracking of the grout for repairs with grout E is smaller than that of grout C. This indicates that the circumferential stress in the grout increases immediately after yielding of the steel. The maximum level of pipe capacity for the pipe reinforced with the metal losses considered containing carbon and glass sleeve is about 27 MPa. The results also suggest that grout E is sufficient to reinforce the pipe up to about 20% metal loss.

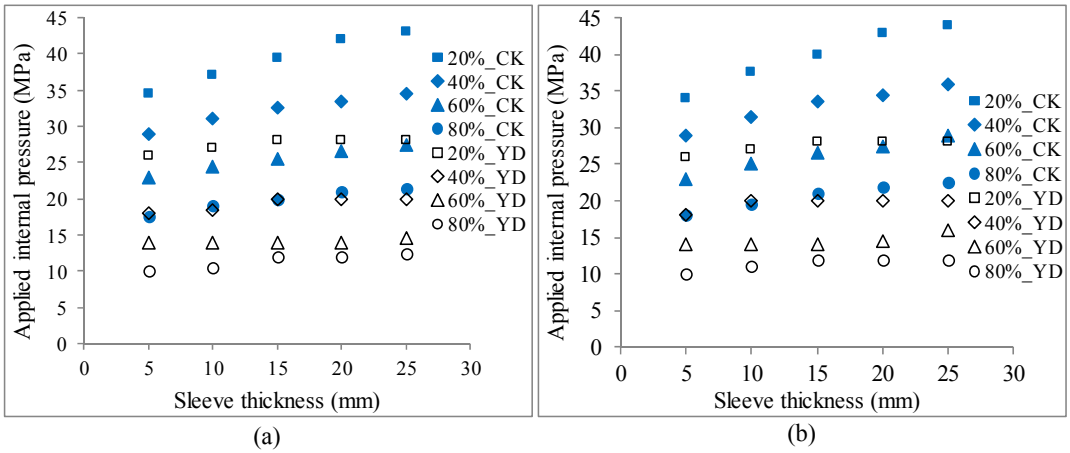

Figure 7.13 **Level of applied internal pressure considering yielding of the steel and cracking of the grout for repair cases with grout C; (a) carbon sleeve and (b) glass sleeve**

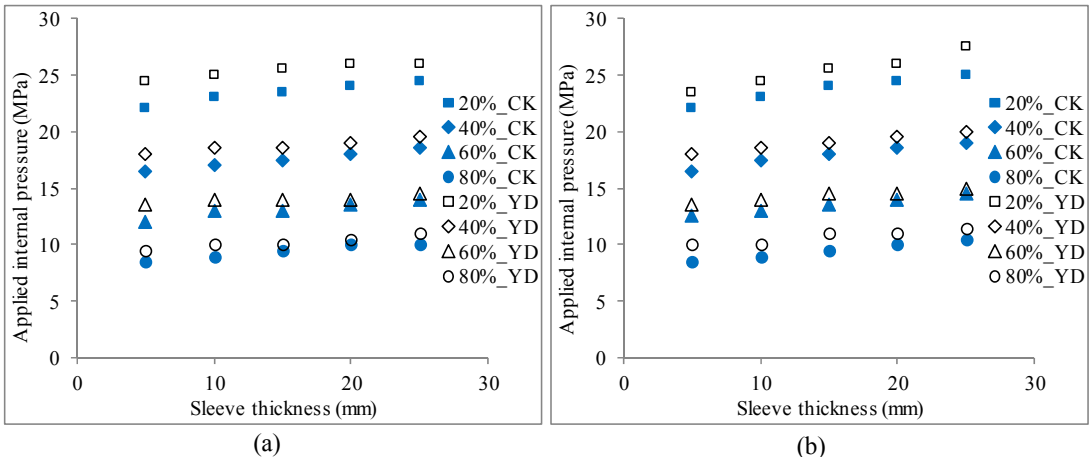

Figure 7.14 **Level of applied internal pressure considering yielding of the steel and cracking of the grout for repair cases with grout E; (a) carbon sleeve and (b) glass sleeve**

7.4 Discussion

A defective pipe experiences a reduction in capacity. Figure 7.15 shows the deformation of steel pipes without any repair for different levels of metal loss. Hence, it is evident that highest metal loss has the lowest capacity. The restoration of the pipe with the corroded pipe using the composite is thus required to increase the capacity of the steel close to the pipe without corrosion. A typical case of restoring a corroded pipe with an overwrap repair was given by Alexander (2007). In the following sections, the effect of the repair parameters on the effectiveness of the repair system is discussed.

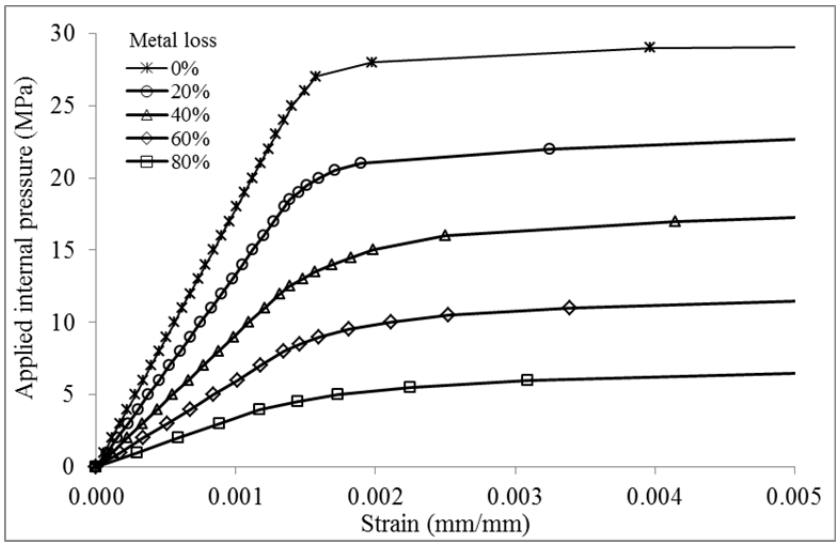

Figure 7.15 **Pressure-strain relationship of the bare pipe with defects**

7.4.1 Effect of metal loss

The variations in internal pressure in relation to metal loss for cracking of the grout in repair system with grouts C and E are shown in Figure 7.16 and Figure 7.17, respectively. The relationship is linear for the repair cases. The failure in the repair system containing grout C is due to a crack in the infill layer which follows a linear stress strain relationship under tensile load. In some cases, the pressure of the repaired pipe reaches more than the burst pressure of the pipe. This implies that the

repair system can successfully reinforce beyond the ultimate capacity of the pipe. This again warrants the necessity to impose a limit while designing a repair system. To ensure a higher capacity of the repaired pipe, the performance of the repair system again can be evaluated by the cracking of the grout. Appendix B provides design charts to determine the parameters required to achieve a certain level of pipe capacity using grouted sleeve repair. The Design charts are constructed based on the repair capacities and the maximum allowable pressure criteria. These design plots provide a guide for ease of selection of repair parameters used in this analysis. The plots, characteristics are governed by the cracking of the grout. The pipe capacity of the repaired system ranges from 9.5 to 26 MPa. The charts suggest that repair system with grout C can restore full capacity of the pipe with 70% metal loss. On the other hand the system with grout E can gain full capacity for up to 20% defect in the pipe. It is evident from the results of Chapter 6 that the repair efficiency is expected to improve when lower grout thickness is used.

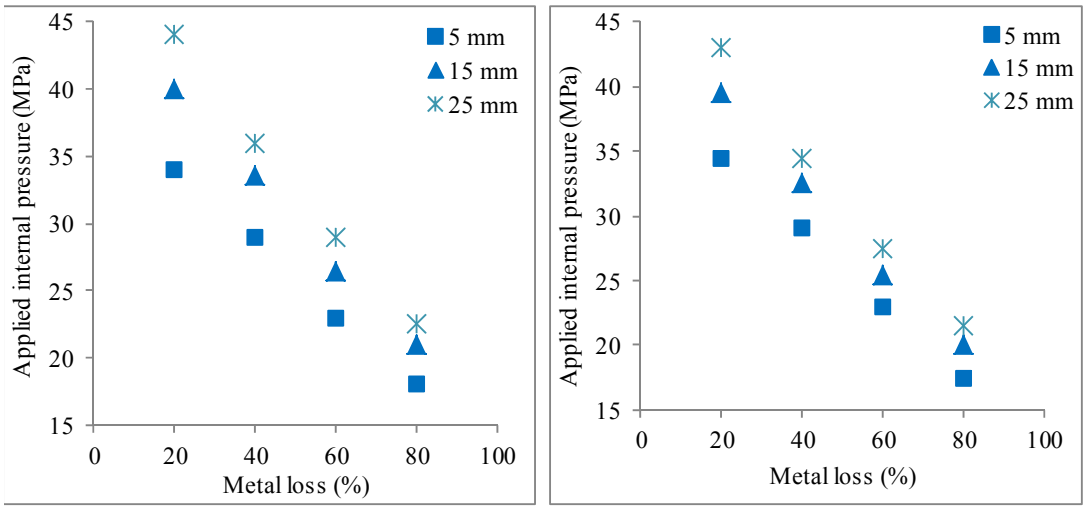

Figure 7.16 **Effect of metal loss on the internal pressure for cracking of the grout for the repair systems with grout C; (a) carbon sleeve and (b) glass sleeve**

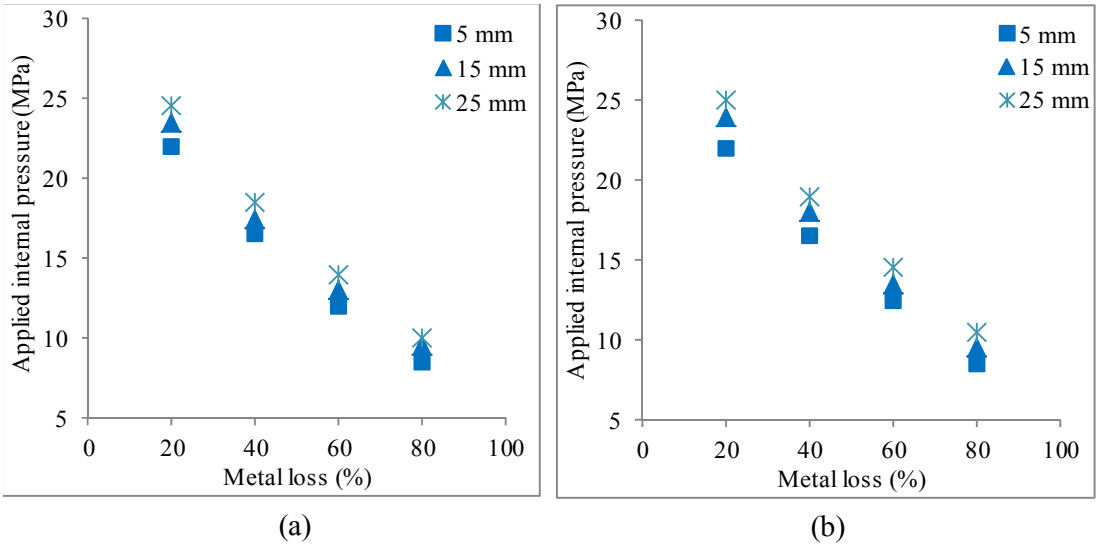

Figure 7.17 **Effect of metal loss on the internal pressure for cracking of the grout for the repair systems with grout E; (a) carbon sleeve and (b) glass sleeve**

A typical comparison of the effectiveness of the repaired system with a carbon sleeve is shown in Figure 7.18. The comparisons suggest that there are about 74 – 350% and 13 – 110% increment in the pressure level for repair cases with grout C and E, respectively in comparison to bare pipe. The pipe capacity, considering cracking of the grout in the repair with lower metal loss, is higher than that of the higher metal loss. However, the repair system provides overall much increment in a repaired pipe with higher corrosion than that of a pipe with lower corrosion. It is also evident, from the comparison that, grout E provides a lower increment than that grout C. The reason behind this behaviour is discussed in the next section. Figure 7.19 presents the effect of metal loss on the steel and grout layers. The plot suggests that the pressure-strain line becomes steeper for both the grout and the sleeve. This behaviour is also comparable to the grout layer. For a lower metal loss (20%), the steel plot is found to have a higher slope than that of the pipe without defect.

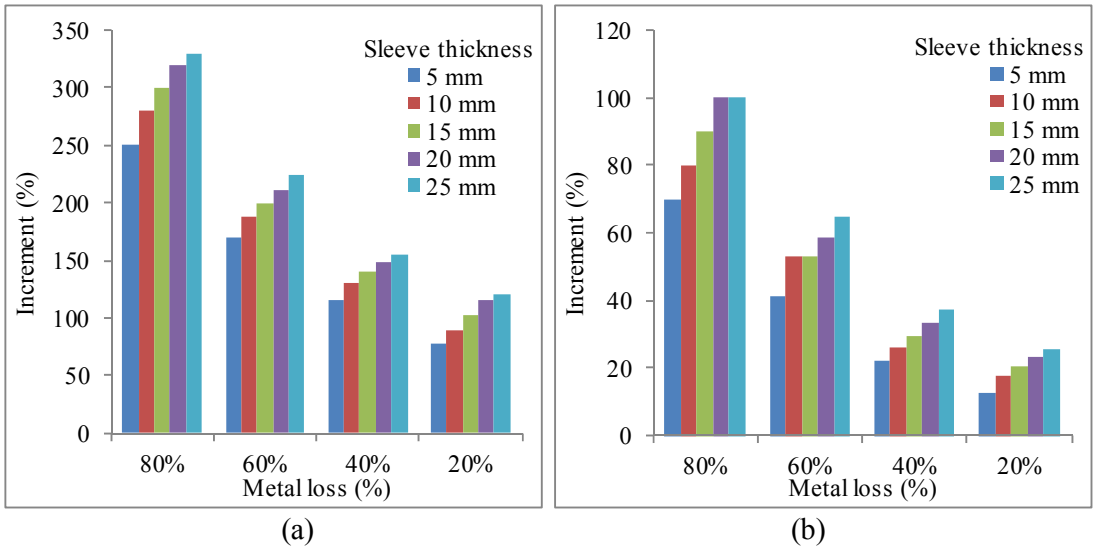

Figure 7.18 Increment of the pressure at cracking of the grout in the repaired pipe using carbon sleeve compared to the yield capacity of the bare pipe with defect; (a) grout C and (b) grout E

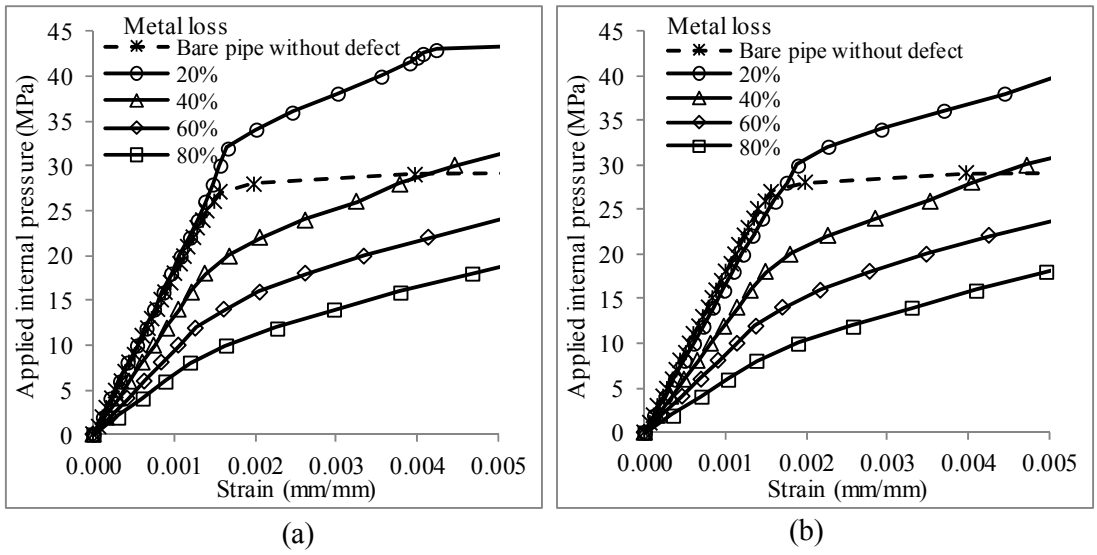

Figure 7.19 Effect of metal loss on the behaviour with repair combination of (C,20-80,*CA*,25); (a) steel and (b) composite

7.4.2 Effect of grout properties

The strength and stiffness of the grouts affect the effectiveness of the repair. Figure 7.11 shows that cracks in the infill grout layers formed at or near the value of their respective tensile strengths. The lower modulus and higher strength of grout C allows the steel to yield before the infill cracks, whereas the lower strength and higher modulus of grout E results in the cracking of the grout first before yielding of steel. At the same, the cracking in the higher stiffness grout (grout E) resulted in a sudden increase in stress in the steel. This suggests that the cracking of the grout can be identified as a governing factor in assessing the effectiveness of a grouted repair. This approach was also used by Palmer-Jones and Paisley (2000) where cracking of the grout is considered critical as the tensile strength and stiffness of the infill layer dictate the effectiveness of the grouted repair. Hence, a grout with higher tensile strength results in increased pipe capacity.

The results suggest that there are about 89 – 100% and 138 – 156% increase in the pressure within the repair section using grouts C and E, respectively from 80% to 20% metal loss. This implies that grout E is more effective in transferring the load from the steel to composite than that of grout E. Figure 7.20 shows the effect of grout modulus on the behaviour of the grouted repair system with grouts C and E. The effectiveness of the grout systems in transferring load from the steel to the composite are indicated through the slope of the pressure-stress line of the steel. The closer the line to the original pipe, the better the load transfer. Similar to the findings in Chapter 6, the stiffer grout is more effective in transferring the load from steel to sleeve. However, as grout E has a lower tensile strength than grout C, cracking occurs at a lower pressure. On the other hand, the repair system with grout C is less effective in load transfer than that of grout E, but it can lead the system to a higher capacity. It is to be noted that the steel and grout lines are closely spaced together for the repair cases with grout E than that of grout C. This is due to the fact that infill, being the intermediate layer between the steel and sleeve, determines the load transfer performance. This again confirms that grout E provides an effective load transfer.

7.4.3 Effect of sleeve properties

Figure 7.18 shows that the pressure increases with increased sleeve thickness. There are about a 19 – 25% and 24 – 29% increase in pipe capacity, corresponding to 5 – 25 mm sleeve, considering cracking of the grout for the repair cases with grout C containing carbon and glass sleeve, respectively. At the same time, the pipe capacities increase by 11 – 18% and 14 – 24% with grout E containing carbon and glass sleeve, respectively. This indicates that there is insignificant effect of sleeve thickness on the capacity of the repaired pipe. The strains in the steel and composite are more closely situated in a repair when there is direct contact between them (Freire et al. 2007). Since there is a layer of grout between the steel and sleeve, the strain levels deviate due to dissipation of energy in the infill layer which has comparatively lower stiffness than that of the other components.

Figure 7.21 shows the effect of sleeve type on the repair performance. The comparison suggests that the stiffer carbon sleeve experienced lower strain than that of the glass sleeve. However, there is negligible variation in the pressure levels in the steel pipe, which can also be seen from Figure 7.16 and Figure 7.17. This is due to the fact that the stiffness required from the sleeve to transfer the load from steel to sleeve through grout is sufficient and reflects a comparable effect on the steel.

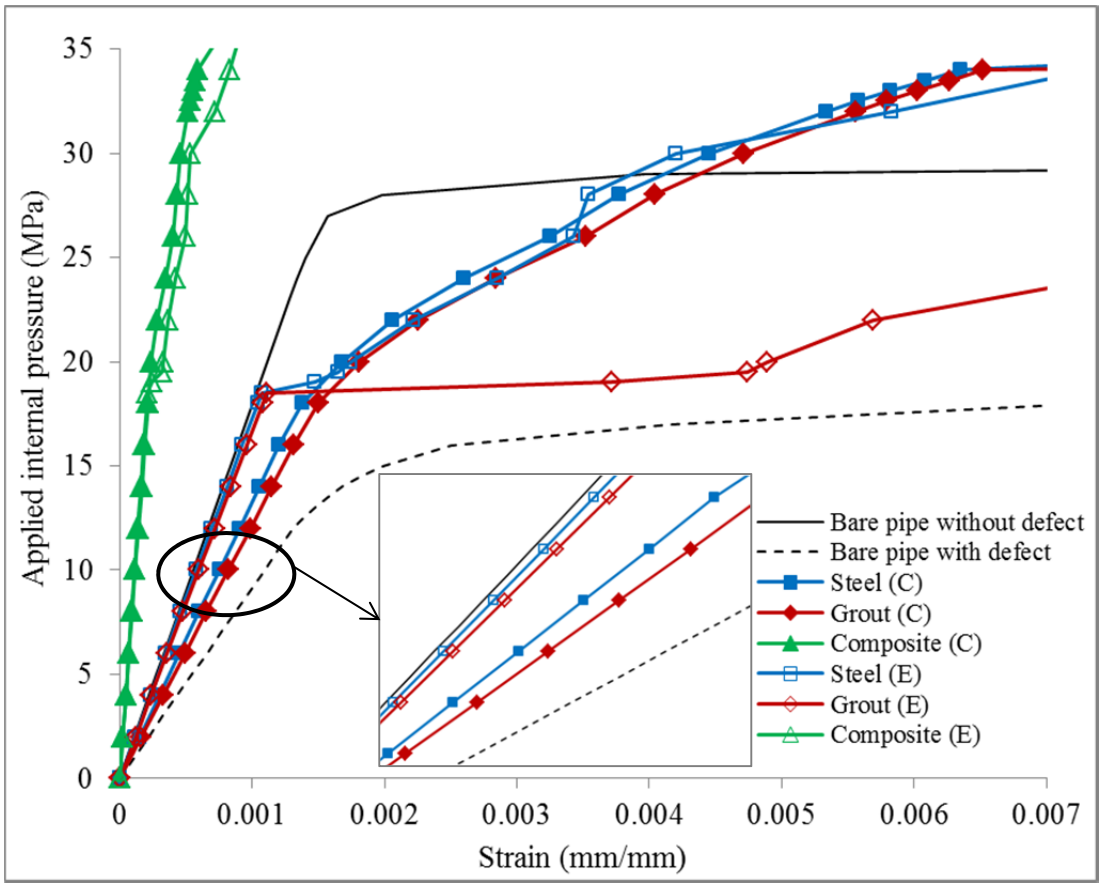

Figure 7.20 **Effect of grout modulus on the behaviour of the grouted repair with repair combination of (C/E,40,CA,25)**

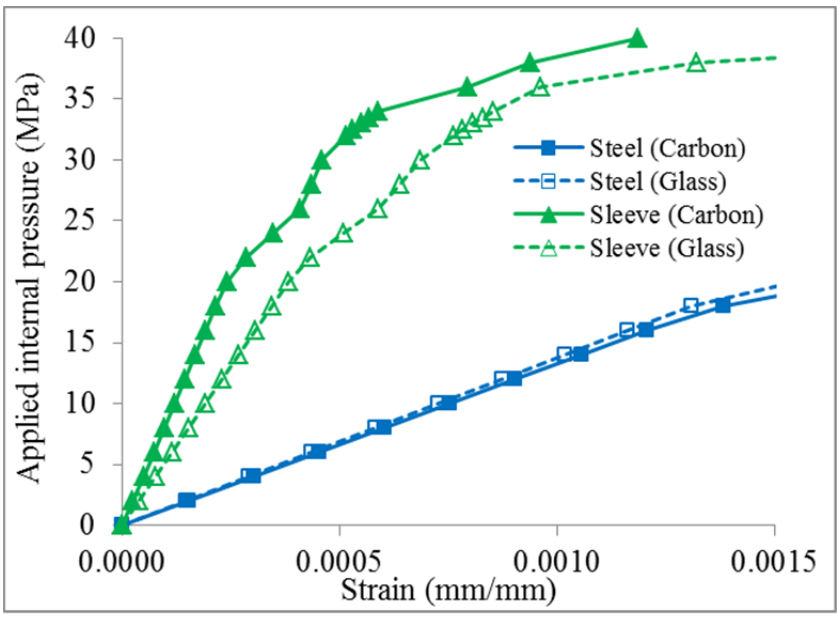

Figure 7.21 **Effect of sleeve properties on on the steel and sleeve behaviour with repair combination of (C,40,CA/GL,25)**

Figure 7.22 presents the variation of strain in the sleeve and the grout. The strain in the sleeve increases with reduced thickness of sleeve. The plot also suggests that there is a change in slope in the pressure-strain line of the sleeve during the

change in the slope in the grout and the steel due to yielding of the steel. Thus indicates that the grout transfers load to the sleeve. An ideal behaviour of an overwrap repair system suggests a comparable behaviour of the reinforcement system in response to stress transfer from the steel (Freire et al. 2007). However, the behaviour indicated in this study is comparable to another overwrap repair by Alexander (2007), where additional layer of shells were used to provide rigidity for tension and bending loads.

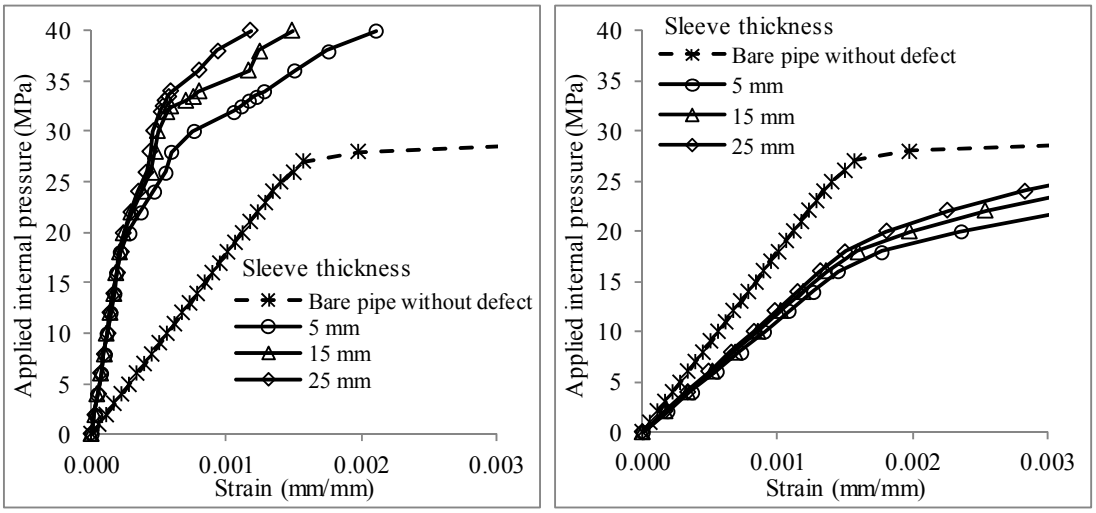

Figure 7.22 **Effect of sleeve thickness on the behaviour with repair combination of (C,40,CA,5-25); (a) composite and (b) grout**

Figure 7.21 also shows the effect of sleeve type on the level of strain in the sleeve. There is lower strain in the carbon sleeve than that of glass sleeve. This is because carbon sleeve has higher modulus than that of glass sleeve. Again, Figure 7.22 shows that thicker sleeve experiences lower strain compared to a thinner sleeve. This implies that a thinner high modulus sleeve can replace a thicker low modulus sleeve.

7.5 Design considerations

The behaviour of the grouted sleeve repair obtained from the analysis of this chapter indicated some important features, which must be taken into consideration while designing this type of repair system for defective pipes. The behaviour of the system suggested that the system is capable of increasing the capacity of the pipe for a range of metal loss. However, the components of the repair system played an important role depending on their properties and potential degradation due to elevated temperature and humid conditions.

It was evident from this study that, infill materials and their properties, primarily affected the repair performance. A stiffer infill ensured better stress transfer. Hence, grout, with modulus of 5 – 10 GPa, is effective to transfer load from the steel to sleeve. On the other hand, the performance of the repair was governed by the cracking of the grout. For this reason, a grout with higher tensile strength is expected to prevent cracking in the infill and improve capacity of the repair system. The compressive stress in the infill layer was found lower than the compressive strengths of the grouts. Therefore, compressive properties are not critical for this type of repair system. There was significant reduction in the strength and modulus of

the grouts due to hot-wet conditioning, which eventually increased stresses and strains in the steel and sleeve. This necessitates considering grout system with higher glass transition temperature to achieve improved performance by the repair system in harsh environmental conditions.

A thinner grout was found more effective transferring load in the repair system. However, handling, flowability and installation issues do not always facilitate a thin infill layer in the repair system. Moreover, under hot-wet conditioning, a thin layer allowed much water ingress than a thick layer of grout. Thus, an optimum grout thickness should be selected based on the grout performance and practical considerations. An optimum grout thickness of 20 mm could be identified in previous analysis to ensure effective load transfer in the repair system susceptible to hot-wet conditioning.

A thicker sleeve reduced stresses and strains in the components of the repair system. At the same time, a thicker sleeve attracts higher cost. A thinner sleeve, with high modulus, could replace a thicker sleeve with low modulus. Hence, a cost optimisation should be carried out prior selecting a sleeve type considering stiffness for performance requirement and cost associated with thickness.

7.6 Conclusions

Three dimensional (3D) finite element analysis (FEA) of a full-scale pipe was carried out in this chapter with different levels of metal loss and material properties. This segment also investigated the behaviour and evaluated the performance of a pipeline with a localised defect ranging from 20 – 80% metal loss and repaired by infilled composite sleeve system. The repair cases considered two grout systems C and E reinforced with carbon and glass sleeves. The following observations and conclusions are drawn:

- A grouted sleeve repair effectively restored the capacity of the pipelines with localised defects. The repair system with grout C can restore the capacity of the steel pipe with defect up to 70%. The system with grout E can restore capacity for a pipeline with 20% defect because of its low strength, although it has higher modulus. However, a grout, with similar strength as grout C and modulus as grout E, may provide higher capacity than grout C.
- Grout with higher tensile strength delivers higher pipe capacity in the repair system by permitting the steel stress beyond yielding. On the other hand, a high modulus grout provides a more effective load transfer from steel to sleeve, however, causes earlier cracking of the infill layer resulting to a lower pipe capacity. When the grout cracks, it no more contribute to the system and an increment in the stress in the steel and composite is observed due to redistribution of the load. The performance of the repair system is consequently governed by the cracking of the grout for the parameters considered. Grout with high tensile strength is thus needed to delay the cracking in the repair system.
- A thicker sleeve is expected to provide higher capacity for the repair system within the sleeve thickness considered in this study due to improved restrain to the infill layer that transfers the load from the

steel. However, a high modulus sleeve can replace a thicker sleeve. Therefore, a balanced selection is needed considering material types and cost requirements.

Chapter 8

Conclusions

8.1 Summary

Infilled composite repair system is found effective in restoring the capacity of steel pipelines with metal loss. The performance requirements for the different components are determined in this study and the effects of critical parameters on the behaviour of the repair system are investigated.

Physical and thermal properties of infill and composite materials were investigated along with the effect of hot-wet conditioning. The parametric study on a sleeve with grouted composite repair gave an insight of how the material properties and the changes in the repair geometry affect the level of stresses and strains in the different components of the repair. The behaviour of the repaired steel pipeline with localised defect was also analysed to determine the effectiveness of the system considered. The results provided a better understanding on the behaviour of a new type of composite repair system for pipelines in corrosive underwater and underground environments. The findings and conclusions gathered from the thesis will aid the future researchers, designers and pipeline owners in considering using infill and fibre composites on repairing corroded pipelines. Additional research studies are also suggested to facilitate and expedite the improvement and authentication of the grouted sleeve repair in the in-situ application.

8.2 Main conclusions from the study

8.2.1 Behaviour of epoxy grouts as infill

The physical and thermal behaviour of five epoxy grouts without and with coarse filler were investigated to determine their potential as infill material. Among these grouts, three grouts were chosen for extended study on their curing behaviour and the effect of hot-wet conditioning on their properties. The results of the study suggest the following:

- Three of the investigated epoxy grouts have properties within the acceptable range that can be used for structural rehabilitation and repair of pipelines. The thermal properties of these grouts ranged from 80 – 90^{o}C.
- An extended investigation on the compressive properties suggested that the infill grouts gained more than 90% of their properties within 7 days. Moreover introduction of coarse filler resulted in two and three times higher compressive and tensile modulus, respectively. However, strengths were reduced in grout systems due to action of the coarse aggregate as filler rather than reinforcement.
- The volumetric shrinkage of grout system with fine filler was found to be 2.72% after 7 days which could be reduced by about 2.5 times through introducing coarse filler. The post-gel shrinkage in a filled system was also reduced due to slow curing rate indicated by longer

gel time. Hence, a coarse filled grout was more appropriate for the repair system.

- There was about 90% reduction in the modulus of the grouts due to hot-wet conditioning. The failure of the grout specimens were governed by plasticisation and week aggregate matrix debonding due to hot-wet conditioning. The reduction of strength and stiffness was due to the reduction of the glass transition temperature below and close to the elevated temperature used for hot-wet conditioning. This indicated the necessity to use of a lower conditioning temperature and to explore grout system with higher glass transition temperature to achieve a higher service temperature of the repair system.

8.2.2 Behaviour of glass fibre – vinyl ester composite as sleeve

The behaviour of the glass fibre – vinyl ester composite was evaluated to determine their potential as sleeve material in the repair system. Additional study over an extended period of time was also carried out to investigate the effect in the properties. The following are the main findings of the investigation:

- The tensile strength, modulus and interlaminar shear strength of the composite was 427 MPa, 25 GPa and 30 MPa, respectively and its glass transition temperature was 110^{o}C, which were found to be suitable as sleeve in the grouted sleeve repair.
- Accelerated conditioning could be achieved for the hot-wet conditioning adopted. The composites absorbed moisture of 0.22% and reached saturation after 1008 hours. The hot-wet conditioning at for 1000 hours could resemble the 'long-term' service performance of the glass fibre – vinyl ester composite for pipeline repair and rehabilitation.
- The laminate tensile and interlaminate strength of the composite was reduced by 70% with minimal change in the modulus after hot-wet conditioning for 3000 hours. The glass transition temperature was 110°C which decreased to 97°C after conditioning and reaching saturation indicating that the composites are suitable for pipeline repair in continuous service at higher temperature. There was minor variation among the properties for 1000 hours and 3000 hours of conditioning. The reduction of strength after conditioning was attributed to moisture ingress and subsequent degradation in the fibre level in the composite.

8.2.3 Effectiveness of the grouted sleeve repair

A simplified two dimensional model was used to investigate the effect of the repair parameters on the performance of a grouted repair system. Grout modulus, grout thickness and sleeve thickness were considered for the analysis. An extensive analysis of full-scale three dimensional models was also carried out to determine the effectiveness of the repair system with a range of metal loss. The grouted sleeve repair enhanced the overall capacity by reinforcing the steel pipe with defect. The main findings of these analyses are summarised below:

- A thin infill layer was found more effective in reducing the stresses and strains in the steel and infill, indicating the necessity to facilitate a narrower annulus in between the steel and sleeve. At the same time, a thin layer was more prone to degradation under hot-wet conditions. Besides, narrow infill layer attracts flowability and installation difficulties. Therefore, a suitable thickness should be sorted considering practical considerations and service conditions.
- The tensile strength and modulus of the infill grout governed the load transfer performance and effectiveness of the repair system. A stiffer and low strength grout similar to a coarse filled system provided superior load transfer performance, however, attracted formation of crack in the grout. On the other hand, a repair system with high tensile strength grout was found effective to increase the pipe capacity by taking the stress in the steel beyond yielding. Therefore, a grout system with high tensile strength and stiffness is necessary to achieve improved repair performance.
- The materials used as a sleeve in the analysis effectively reinforced the system. A thicker sleeve improved the performance of the repair system by providing radial support for the infill grout and steel pipe, causing lower stresses and strains in the steel. At the same time, a stiffer sleeve was also found effective to support the system. An optimised choice should be sorted considering the thickness and material of the sleeve.
- The hot-wet conditioning reduced the strength and modulus of the grout, resulting higher stress and strain in the steel and sleeve. On the other hand, there was considerable reduction in the strength, however, insignificant change in the modulus of the sleeve. An optimum grout thickness of 20 mm could be selected to retain the effectiveness of the repair system even under hot-wet condition. Furthermore, the effect of hot-wet conditioning may be crucial for the grouted repair system necessitating repair components with improved thermal stability.

8.3 Recommendations for the future study

The following studies need to be further considered in more detail for an extended understanding and application of the grouted sleeve repair for repair and rehabilitation of the steel pipelines.

- This study investigates the behaviour of the repair system under internal pressure. Further evaluation of the system under other loading conditions, for example: axial and flexural loading, temperature gradient, is recommended to further assess the system for wider applicability.
- The degradation of physical and thermal properties of the investigated grout systems under hot-wet conditioning indicates further study using a lower conditioning temperature. Further exploration of other grout system with a higher glass transition temperature is also recommended.

- Experimental investigation of the steel-infill and infill-sleeve bonding resembling the adjacent annulus interfaces under both without and with hot-wet conditioning will provide improved information about the effect of interlayer bonding that governs the load transfer performance of the repair system.
- A more rigorous finite element analysis is needed to incorporate the effect of temperature variation and volumetric shrinkage of the infill and interface bonding of among the components resembling the practical limitations during installation of the repair system.
- The present study experimentally investigated glass fibre – vinyl ester composite and considered carbon fibre reinforced composite as sleeve material. The properties of carbon fibre reinforcement options along with the effect of hot-wet conditioning should be investigated to further explore the potential in field conditions.
- Full-scale performance evaluation of the repair system will provide with more realistic and reliable observations necessary to investigate actual behaviour of the system and identify potential issues before choosing suitable design factors for service factors. The cost-benefit analysis in conjunction with practical installation issues will afford optimised grout and sleeve thickness for the repair system.
- Finally, continuous research and development are necessary to develop confidence in the repair system and popularise the system in the industrial arena. The continued efforts to optimise the performance and to improve the installation technique should make the grouted composite sleeve an alternative to the existing repair system.

References

Adams, RD & Singh, MM 1996, 'The dynamic properties of fibre-reinforced polymers exposed to hot, wet conditions', *Composites Science and Technology*, vol. 56, no. 8, pp. 977-97.

AEA Technology Consulting 2001, *Temporary/permanent pipe repair-guidelines*, AEA Technology Consulting for Health and Safety Executive, Oxfordshire.

Aggarwal, LK, Thapliyal, PC & Karade, SR 2007, 'Properties of polymer-modified mortars using epoxy and acrylic emulsions', *Construction and Building Materials*, vol. 21, no. 2, pp. 379-83.

Alexander, C 2007, 'Development of a Composite Repair System for Reinforcing Offshore Risers', PhD Thesis thesis, Texas A & M University.

Alexander, C & Francini, B 2006, 'State of the art assessment of composite systems used to repair transmission pipelines', paper presented to 6th International Pipeline Conference, 25-29 September, Calgary, Alberta.

Alexander, CR 2009, 'Development of Standards for Composite Repair Systems', *Pipeline & Gas Technology Magazine*, vol. October 2009.

Alexander, CR & Wilson, FD 2000, 'Recent Test Results and Field Experience with Armor Plate® Pipe Wrap Repairing Corroded and Mechanically-Damaged Pipes', paper presented to Pigging Conference, 1-2 February, Houston, Texas.

Alshrif, ZA, Saied, RO, Abujelala, MT & Elarbi, MI 2009, 'Experimental investigation on repairing of steel pipes using composite materials: part II', *Journal of Engineering Research (Al-Fateh University)*, vol. March 2009, no. 11, pp. 1-12.

Aniskevich, K, Aniskevich, A, Arnautov, A & Jansons, J 2012, 'Mechanical properties of pultruded glass fiber-reinforced plastic after moistening', *Composite Structures*, vol. 94, no. 9, pp. 2914-9.

Apicella, A, Migliaresi, C, Nicodemo, L, Nicolais, L, Iaccarino, L & Roccotelli, S 1982, 'Water sorption and mechanical properties of a glass-reinforced polyester resin', *Composites*, vol. 13, no. 4, pp. 406-10.

Araki, W, Nemoto, K, Adachi, T & Yamaji, A 2005, 'Fracture toughness for mixed mode I/II of epoxy resin', *Acta Mater.*, vol. 53, no. 3, pp. 869-75.

American Society of Mechanical Engineers 2007, ASME Boiler and Pressure Vessel Code, ASME, Rules for Construction of Pressure Vessels, Sec. VIII, Div. 2, Alternative Rules, New York.

American Society of Mechanical Engineers 1991, Manual for determining the remaining strength of corroded pipelines, ASME B31G, New York.

The American Society of Mechanical Engineers 2006, Repair of pressure equipment and piping, ASME PCC-2, New York.

Asp, LE, Berglund, LA & Talreja, R 1996, 'A criterion for crack initiation in glassy polymers subjected to a composite-like stress state', *Compos. Sci. Technol.*, vol. 56, no. 11, pp. 1291-301.

American Society for Testing and Materials 2001, Standard test method for compressive strength of cylindrical concrete specimens, ASTM C 39, ASTM Committee C09, West Conshohocken, PA, USA.

American Society for Testing and Materials 2001, Standard test method for compressive strength of chemical-resistant mortars, grouts, monolithic surfacings, and polymer concretes, ASTM C 579, ASTM Committee C03, West Conshohocken, PA, USA.

American Society for Testing and Materials 2002, Standard test method for flexural strength and modulus of elasticity of chemical-resistant mortars, grouts, monolithic surfacings, and polymer concretes, ASTM C 580, ASTM Committee C03, West Conshohocken, PA, USA.

American Society for Testing and Materials (ASTM) 2008, Standard Test Method for Tensile Properties of Polymer Matrix Composite Materials, ASTM D3039, ASTM Committee D30, West Conshohocken, PA, USA.

American Society for Testing and Materials 2010, Standard test method for tensile properties of plastics, ASTM D 638, ASTM Committee D20, West Conshohocken, PA, USA.

American Society for Testing and Materials 1999, Standard Test Method for Gel Time and Peak Exothermic Temperature of Reacting Thermosetting Resins, ASTM D 2471, ASTM Committee, West Conshohocken, PA, USA.

American Society for Testing and Materials (ASTM) 2006, Standard Practice for Obtaining Hydrostatic or Pressure Design Basis for “Fibreglass” (Glass-Fibre-Reinforced thermosetting-Resin) Pipe and Fittings, ASTM D 2992, ASTM Committee D20, West Conshohocken, PA, USA.

American Society for Testing and Materials 1999, Standard test method for constituent content of composite materials, ASTM D 3171, ASTM Committee D30, West Conshohocken, PA, USA.

American Society for Testing and Materials 2010, Standard Test Method for Moisture Absorption Properties and Equilibrium Conditioning of Polymer Matrix Composite Materials, ASTM D 5229, ASTM Committee D30, West Conshohocken, PA, USA.

American Society for Testing and Materials 1998, Standard test method for shear properties of composite materials by the v-notched beam method, ASTM D 5379, ASTM Committee D30, West Conshohocken, PA, USA.

American Society for Testing and Materials 2009, Standard test method for assinment of the glass transition temperature by dynamic mechanical analysis, ASTM E 1640, ASTM Committee E37, West Conshohocken, PA, USA.

Standards Association of Australia 1997, Metal finishing - Preparation and pretreatment of surfaces, Method selection guide, Australian Standard Committee MT/9, AS 1627, Part:0, Homebush, NSW.

Bakis, CE, Bank, LC, Brown, VL, Cosenza, E, Davalos, F, Lesko, JJ, Machida, A, Rizkalla, SH & Triantafillou, TC 2002, 'Fibre-reinforced polymer composites for construction - state-of-the-art review', *Journal of Composites for Construction*, vol. 6, no. 2, pp. 73-87.

Béland, S 1990, *High Performance Thermoplastic Resins and Their Composites*, Noyes Publications, New Jersey.

Biel, RC & Alexander, C 2005, 'Applications of limit load analyses to assess the structural integrity of pressure vessels', paper presented to ASME Pressure Vessels and Piping Division Conference, 17-21 July, Denver.

Brooker, DC 2003, 'Numerical modelling of pipeline puncture under excavator loading. Part II: parametric study', *International Journal of Pressure Vessels and Piping*, vol. 80, no. 10, pp. 727-35.

Brooker, DC 2003, 'Numerical modelling of pipeline puncture under excavator loading. Part I. Development and validation of a finite element material failure model for puncture simulation', *International Journal of Pressure Vessels and Piping*, vol. 80, no. 10, pp. 715-25.

Carbas, RJC, da Silva, LFM, Marques, EAS & Lopes, AM 2013, 'Effect of post-cure on the glass transition temperature and mechanical properties of epoxy adhesives', *Journal of Adhesion Science and Technology*, vol. 27, no. 23, pp. 2542-57.

Carra, G & Carvelli, V 2014, 'Ageing of pultruded glass fibre reinforced polymer composites exposed to combined environmental agents', *Composite Structures*, vol. 108, no. 0, pp. 1019-26.

Cercone, L & Lockwood, JD 2005, 'Review of FRP Composite Materials for Pipeline Repair', in *Pipelines*, pp. 1001-13.

Chekanov, YA, Korotkov, VN, Rozenberg, BA, Dhzavadyan, EA & Bogdanova, LM 1995, 'Cure shrinkage defects in epoxy resins', *Polymer*, vol. 36, no. 10, pp. 2013-7.

Chen, W, Lu, F & Cheng, M 2002, 'Tension and compression tests of two polymers under quasi-static and dynamic loading', *Polym. Test.*, vol. 21, no. 2, pp. 113-21.

Chin, JW, Nguyen, T & Aouadi, K 1999, 'Sorption and diffusion of water, salt water, and concrete pore solution in composite matrices', *Journal of Applied Polymer Science*, vol. 71, no. 3, pp. 483-92.

Chow, TS 1991, 'Prediction of stress-strain relationships in polymer composites', *Polymer*, vol. 32, no. 1, pp. 29-33.

Crank, J 1975, *The Mathematics of Diffusion*, Clarendon Press, Oxford.

Cunha, SB & Netto, TA 2012, 'Analytical solution for stress, strain and plastic instability of pressurized pipes with volumetric flaws', *International Journal of Pressure Vessels and Piping*, vol. 89, no. 0, pp. 187-202.

Det Norske Veritas (DNV) 2010, Corroded Pipelines, Det Norske Veritas, Recommended Practice DNV-RP-F101.

Djukic, LP, Leong, AY, Falzon, PJ & Leong, K 2013, 'Qualification of a composite system for pipeline repairs under dry, wet, and water-submerged conditions', *Journal of Reinforced Plastics and Composites*, p. 0731684413505009.

Duell, JM, Wilson, JM & Kessler, MR 2008, 'Analysis of a carbon composite overwrap pipeline repair system', *International Journal of Pressure Vessels and Piping*, vol. 85, no. 11, pp. 782-8.

Ehsani, M 2009, 'FRP super laminates present unparalleled solutions to old problems', *Reinforced Plastics*, vol. 53, no. 6, pp. 40-5.

Ehsani, M 2010, 'Superlaminate: The Next Generation of Carbon FRP Products for Repair of Pipelines', paper presented to Climbing New Peaks to Infrastructure Reliability-Renew, Rehab, and Reinvest, 28 August - 1 September, Keystone, Colorado, USA.

Ellyin, F & Maser, R 2004, 'Environmental effects on the mechanical properties of glass-fiber epoxy composite tubular specimens', *Composites Science and Technology*, vol. 64, no. 12, pp. 1863-74.

Engindeniz, M & Zureick, A 2008, 'Deflection Response of Glass Fiber-Reinforced Pultruded Components in Hot Weather Climates', *Journal of Composites for Construction*, vol. 12, no. 3, pp. 355-63.

Farshad, M & Necola, A 2004, 'Effect of aqueous environment on the long-term behavior of glass fiber-reinforced plastic pipes', *Polymer Testing*, vol. 23, no. 2, pp. 163-7.

Fitzer, E & Weiss, R 1987, 'Effect of surface treatment and sizing of c-fibres on the mechanical properties of cfr thermosetting and thermoplastic polymers', *Carbon*, vol. 25, no. 4, pp. 455-67.

Fraga, AN, Alvarez, VA, Vazquez, A & de la Osa, O 2003, 'Relationship between Dynamic Mechanical Properties and Water Absorption of Unsaturated Polyester and Vinyl Ester Glass Fiber Composites', *Journal of composite materials*, vol. 37, no. 17, pp. 1553-74.

Francis, R 1994, 'Galvanic corrosion of high alloy stainless steel in sea water', *British Corrosion Journal*, vol. 29, no. 1, pp. 53-7.

Frankel, GS 1998, 'Pitting Corrosion of Metals A Review of the Critical Factors', *Journal of the Electrochemical Society*, vol. 145, no. 6, pp. 2186-98.

Freire, JLF, R D Vieira, Diniz, JLC & Meniconi, LC 2007, 'Effectiveness of composite repairs applied to damaged pipeline', *Experimental Techniques, Society for Experimental Mechanics*, vol. September/October 2007, pp. 59-66.

Fridleifsson, IB 2003, 'Status of geothermal energy amongst the world's energy sources', *Geothermics*, vol. 32, pp. 379-88.

Geraghty, M, Pridmore, A & Sanchez, J 2011, 'Transitioning from Leak Detection to Leak Prevention: Proactive Repair of Steel Pipelines Using Fiber Reinforced Polymer (FRP) Composites', in *Pipelines*, pp. 100-7.

Giancaspro, JW, Papakonstantinou, CG & Balaguru, PN 2010, 'Flexural response of inorganic hybrid composites with E-glass and carbon fibres', *J of Engg Mat and Tech*, vol. 132, pp. 1-8.

Gibson, AG 2003, *The cost effective use of fibre reinforced composites offshore*, Research report 039, University of Newcastle Upon Tyne, Norwich (UK).

Gibson, AG, Linden, JM, Elder, D & Leong, KH 2011, 'Non-metallic pipe systems for use in oil and gas', *Plastics, Rubber and Composites*, vol. 40, no. 10, pp. 465-80.

Goertzen, WK & Kessler, MR 2007, 'Dynamic mechanical analysis of carbon/epoxy composites', *Composites Part B*, vol. 38, pp. 1-9.

Golestaneh, M, Amini, G, Najafpour, GD & Beygi, MA 2010, 'Evaluation of mechanical strength of epoxy polymer concrete with silica powder as filler', *World Applied Sciences J.*, vol. 9 no. 2, pp. 216-20.

Green Cleaning Ideas 2011, *Seawater Corrosion*, 08-12-2011, <http://www.greencleaningideas.com/2009/03/eco-tech-%E2%80%98biological-coating%E2%80%99-could-prevent-metal-corrosion-in-seawater/>.

Green, M 2010, *Fiberglass repair systems give corrosion, impact protection to pipelines and risers*, 09-06-2011, <http://www.offshore-mag.com/articles/print/volume-70/issue-10/flowlines-__pipelines/composites-offer-effective-offshore-pipe-repair-alternative.html>.

Haider, M, Hubert, P & Lessard, L 2007, 'Cure shrinkage characterization and modeling of a polyester resin containing low profile additives', *Composites Part A: Applied Science and Manufacturing*, vol. 38, no. 3, pp. 994-1009.

Hamerton, I 1996, *Recent developments in epoxy resins*, Rapra Technology Limited, Shawbury.

Hausrath, RL & Longobardo, AV 2011, 'High-Strength Glass Fibers and Markets', in FT Wallenberger & PA Bingham (eds), *Fiberglass and Glass Technology: Energy-Friendly Compositions and Applications*, Springer, New York.

Heldt, T, McGuffin, J, Marsh, R, Youngberry, M & Carse, A 2005, *FRP rehabilitation of ASR affected piles underwater*, 3, John Wiley & Sons Ltd., 1528-2716, <http://dx.doi.org/10.1002/pse.199>.

Hille, GM & Romer, AE 2004, 'Fiberglass Pipe Design for Water Mains', paper presented to Pipeline Engineering and Construction : What's on the Horizon?, 1-4 August, San Diego, California, United States.

Horii, H & Nemat-Nasser, S 1985, 'Compression-Induced microcrack growth in brittle solids' axial splitting and shear failure', *J. Geophys. Res.*, vol. 90, no. March 10, pp. 3105-25.

Hossain, M, Possart, G & Steinmann, P 2009, 'A small-strain model to simulate the curing of thermosets', *Computational Mechanics*, vol. 43, no. 6, pp. 769-79.

Integ Pipeline Services 2011, *StrongBack system overview*, 17-06-2011, <http://www.integpipelineservices.com/skins/integ/homepage.aspx?elid=298&SkipFlip=298 >.

International Organization for Standardization (ISO) 1997, Plastics - Unsaturated polyesters and epoxy - Determination of overall volume shrinkage, ISO 3521, Switzerland.

International Organization for Standardization (ISO) 1988, Preparation of steel substrates before application of paints and related products - Visual assessment of surface cleanliness - Part 1: Rust grades and preparation grades of uncoated steel substrates and of steel substrates after overall removal of previous coatings, ISO 8501-1, Switzerland.

International Organization for Standardization (ISO) 2006, Petroleum, petrochemical and natural gas industries - composite repairs of pipework - qualification and design, installation, testing and inspection, ISO/TS 24817, London.

Jang, SS & Jo, WH 1999, 'Analysis of the mechanical behavior of poly (trimethylene terephthalate) in an amorphous state under uniaxial extension–compression condition through atomistic modeling', *J. Chem. Phys.*, vol. 110, p. 7524.

Jiang, X, Kolstein, H & Bijlaard, FSK 2013, 'Moisture diffusion in glass–fiber-reinforced polymer composite bridge under hot/wet environment', *Composites Part B: Engineering*, vol. 45, no. 1, pp. 407-16.

Jianghong, X 2006, 'A non-linear finite-element analysis of buckle propagation in subsea corroded pipelines', *Finite Elements in Analysis and Design*, vol. 42, no. 14-15, pp. 1211-9.

Joshi, SV, Drzal, LT, Mohanty, AK & Arora, S 2004, 'Are natural fiber composites environmentally superior to glass fiber reinforced composites?', *Composites Part A: Applied Science and Manufacturing*, vol. 35, no. 3, pp. 371-6.

Jupiter, T, Rashidi, AH & Ismail, I 2010, 'Effect of seawater on the properties of Epoxy Modified Concrete', *UNIMAS E-Journal of Civil Engineering*, vol. 1, no. 2, <http://www.feng.unimas.my/ujce/images/article/vol1issue2/3874-0410-03.pdf>

Kang, LS & Hussin, MW 2008, 'Effect of filler on strength development of epoxy grout', *Malaysian J. of Civil Engineering*, vol. 20, no. 1, pp. 38-46.

Keller, MW, Jellison, BD & Ellison, T 2013, 'Moisture effects on the thermal and creep performance of carbon fiber/epoxy composites for structural pipeline repair', *Composites Part B: Engineering*, vol. 45, no. 1, pp. 1173-80.

Kelsey, R & Biswas, M 1993, 'Thermomechanical Properties of Epoxy Mortars', *Journal of Materials in Civil Engineering*, vol. 5, no. 2, pp. 187-97.

Kennedy, JL 1993, *Oil and Gas Pipeline Fundamentals*, 2nd edn, PennWell Publishing Company, Tulsa, Oklahoma.

Khoun, L & Hubert, P 2010, *Characterizing the cure shrinkage of an epoxy resin in situ*, Society of Plastics Engineers, 18 October 2012, <http://www.4spepro.org/pdf/002583/002583.pdf>.

Kim, J-K, Yi, S-T, Park, C-K & Eo, S-H 1999, 'Size effect on compressive strength of plain and spirally reinforced concrete cylinders', *ACI Struct. J.*, vol. January-February, pp. 88-96.

Kin-tak, L & Li-min, Z 2001, 'The mechanical behaviour of composite-wrapped concrete cylinders subjected to uniaxial compression load', *Composite Structures*, vol. 52, no. 2, pp. 189-98.

Kneuer, RL & Meyers, M 1991, 'Strengths and limitations of epoxy grouts', *Concrete International*, vol. March, pp. 54-6.

Kootsookos, A & Mouritz, AP 2004, 'Seawater durability of glass- and carbon-polymer composites', *Composites Science and Technology*, vol. 64, no. 10–11, pp. 1503-11.

Kopeliovich, D 2009, *Pitting corrosion*, 07/12/2011, <http://www.substech.com/dokuwiki/doku.php?id=pitting_corrosion>.

Köpple, MF, Lauterbach, S & Wagner, W 2013, 'Composite repair of through-wall defects in pipework – Analytical and numerical models with respect to ISO/TS 24817', *Composite Structures*, vol. 95, no. 0, pp. 173-8.

Kou, J & Yang, W 2011, 'Application Progress of Oil and Gas Pipeline Rehabilitation Technology', paper presented to ICPTT 2011, 26-29 October, Beijing, China.

Lassila, LVJ, Nohrström, T & Vallittu, PK 2002, 'The influence of short-term water storage on the flexural properties of unidirectional glass fibre-reinforced composites', *Biomaterials*, vol. 23, pp. 2221-9.

Lee, C-H & Park, J-J 2010, 'The properties of DSC and DMA for epoxy nano-and-micro mixture composites', *Trans. Electr. Electron Mater.*, vol. 11, no. 2, pp. 69-72.

Lees, WA (ed.) 1989, *Adhesives and the engineer: A review of the role of modern adhesives in the structural and mechanical engineering industries*, Mechanical Engineering Publications, London.

Leong, AYL, Leong, KH, Tan, YC, Liew, PFM, Wood, CD, Tian, W & Kozielski, KA 2011, 'Overwrap composite repairs of offshore risers at topside and splash zone', paper presented to International Conference on Composite Materials (ICCM-18), 21-26 August, Jeju Island, Korea

Leong, KH, Leong, AYL, Ramli, SH, Tan, YC, Johar, RM, Chia, MT & Hassan, HA 2009, 'Testing grouted sleeve connections for pipelines repairs', paper presented to 3rd International Conference on Integrity, Reliability and Failure, 20-24 July, Porto, Portugal.

Li, C, Potter, K, Wisnom, MR & Stringer, G 2004, 'In-situ measurement of chemical shrinkage of MY750 epoxy resin by a novel gravimetric method', *Composites Science and Technology*, vol. 64, no. 1, pp. 55-64.

Li, G, Lee-Sullivan, P & Thring, R 2000, 'Determination of activation energy for glass transition of an epoxy adhesive using dynamic mechanical analysis', *J. Therm. Anal. Calorim.*, vol. 60, no. 2, pp. 377-90.

Liao, K, Schultheisz, CR & Hunston, DL 1999, 'Effects of environmental aging on the properties of pultruded GFRP', *Composites Part B: Engineering*, vol. 30, no. 5, pp. 485-93.

Littell, J, Ruggeri, C, Goldberg, R, Roberts, G, Arnold, W & Binienda, W 2008a, 'Measurement of Epoxy Resin Tension, Compression, and Shear Stress–Strain Curves over a Wide Range of Strain Rates Using Small Test Specimens', *Journal of Aerospace Engineering*, vol. 21, no. 3, pp. 162-73.

---- 2008b, 'Measurement of epoxy resin tension, compression, and shear stress–strain curves over a wide range of strain rates using small test specimens', *J. Aerospace Eng.*, vol. 21, no. 3, pp. 162-73.

Lixin, W, Suong, VH, Minh-Tan & Ton-That 2004, 'Effects of water on the curing and properties of epoxy adhesive used for bonding FRP composite sheet to concrete', *Journal of Applied Polymer Science*, vol. 92, no. 4, pp. 2261-8.

Lopez-Anido, R, Michael, AP, Sandford, TC & Goodell, B 2005, 'Repair of Wood Piles Using Prefabricated Fiber-Reinforced Polymer Composite Shells', *Journal of Performance of Constructed Facilities*, vol. 19, no. 1, pp. 78-87.

Lukács, J, Nagy, G, Török, I, Égert, J & Pere, B 2010, 'Experimental and numerical investigations of external reinforced damaged pipelines', *Procedia Engg*, vol. 2, pp. 1191-200.

Mableson, AR, Dunn, KR, Dodds, N & Gibson, AG 2000, 'Refurbishment of steel tubular pipes using composite materials', *Plast. Rubber Compos.*, vol. 29, no. 10, pp. 558-65.

Magniez, K, Vijayan, A & Finn, N 2012, 'Apparent volumetric shrinkage study of RTM6 resin during the curing process and its effect on the residual stresses in a composite', *Polymer Engineering & Science*, vol. 52, no. 2, pp. 346-51.

Mattos, HSdC, Paim, LM & Reis, JML 2012, 'Analysis of burst tests and long-term hydrostatic tests in produced water pipelines', *Eng. Fail. Anal.*, vol. 22, no. 0, pp. 128-40.

Mattos, HSdC, Reis, JML, Sampaio, RF & Perrut, V 2009, 'An alternative methodology to repair localized corrosion damage in metallic pipelines with epoxy resins', *Mater. Des.*, vol. 30, pp. 3581-91.

McBagonluri, F, Garcia, K, Hayes, M, Verghese, KNE & Lesko, JJ 2000, 'Characterization of fatigue and combined environment on durability performance of glass/vinyl ester composite for infrastructure applications', *International Journal of Fatigue*, vol. 22, no. 1, pp. 53-64.

McCullouch, BG 1991, *Repair/Rehabilitation of Deteriorated Drainage Pipe*, Indiana Department of Transportation and Purdue University, West Lafayette.

Mendis, P 1985, 'Commercial applications and property requirements for epoxies in construction', *ACI Special Publication*, vol. SP, no. 89-7, pp. 127-40.

Michalske, TA & Freiman, SW 1983, 'A molecular mechanism for stress corrosion in vitreous silica', *Journal of the American Ceramic Society*, vol. 66, no. 4, pp. 284-8.

Nawab, Y, Shahid, S, Boyard, N & Jacquemin, F 2013, 'Chemical shrinkage characterization techniques for thermoset resins and associated composites', *Journal of Materials Science*, no. (April, pp. 1-23.

Newberry, AL, Bakhshaliyev, R & Garnish, M 2008, 'World's largest high pressure, large diameter GRP pipe project', *Reinforced Plastics*, vol. September 2008,

Nishizaki, I & Meiarashi, S 2002, 'Long-Term Deterioration of GFRP in Water and Moist Environment', *Journal of Composites for Construction*, vol. 6, no. 1, pp. 21-7.

Niu, L & Cheng, YF 2007, 'Corrosion behavior of X-70 pipe steel in near-neutral pH solution', *Applied Surface Science*, vol. 253, no. 21, pp. 8626-31.

Ochola, RO, Marcus, K, Nurick, GN & Franz, T 2004, 'Mechanical behaviour of glass and carbon fibre reinforced composites at varying strain rates', *Composite Structures*, vol. 63, no. 3–4, pp. 455-67.

Paim, LM, Reis, JMLd & Mattos, HSdC 2013, 'Behaviour model for glass fibre reinforced polyurethane at different temperatures for corroded pipeline repair systems', paper presented to 22nd International Congress of Mechanical Engineering (COBEM 2013), November 3-7, Ribeirão Preto, SP, Brazil.

Palmer-Jones, R & Paisley, D 2000, 'Repairing Internal Corrosion Defects in Pipelines - A Case Study', paper presented to 4th International Pipeline Rehabilitation and Maintenance Conference, 4-8 September, Prague, Czech Republic.

Palmer-Jones, R, Paterson, G & Nespeca, GA 2011, 'The flexible grouted clamp-a novel approach to emergency pipeline repair', paper presented to Rio Pipeline Conference & Exposition 2011, 20-22 September, Rio de Janeiro, Brazil.

Patrick, AJ 2004, *Composites - case studies of pipeline repair applications*, 04-11-2011, <http://www.ppsa-online.com/papers/2004-London-8-Patrick.pdf>.

Peck, JA, Li, G, Pang, S-S & Stubblefield, MA 2004, 'Light intensity effect on UV cured FRP coupled composite pipe joints', *Composite Structures*, vol. 64, no. 3–4, pp. 539-46.

Peck, JA, Jones, RA, Pang, S-S, Li, G & Smith, BH 2007, 'UV-cured FRP joint thickness effect on coupled composite pipes', *Composite Structures*, vol. 80, no. 2, pp. 290-7.

PETRONAS-CSIRO *PIPEASSURE™ - a repair solution for subsea pipelines*, 11-10-2012, <http://www.iossb.com.my/lz_images/pdf/PipeAssure_A4.pdf>.

Pfennig, A & Kranzmann, A 2009, 'Effects of saline aquifere water on the corrosion behaviour of injection pipe steels 1.4034 and 1.7225 during exposure to CO2 environment', *Energy Procedia*, vol. 1, no. 1, pp. 3023-9.

Pfennig, A, Linke, B & Kranzmann, A 2011, 'Corrosion behaviour of pipe steels exposed for 2 years to CO2 -saturated saline aquifer environment similar to the CCS-site Ketzin, Germany', *Energy Procedia*, vol. 4, no. 0, pp. 5122-9.

Picard, D, Hudson, W, Bouquier, L, Dupupet, G & Zivanovic, I 2007, 'Composite carbon thermoplastic tubes for deepwater applications', paper presented to Offshore Technology Conference, 30 April-3 May, Houston, Texas.

PLIDCO Split+Sleeve 2012, *Permanently repairs a variety of pipelines*, 12-01-2012, <http://plidco.com/public/products/split_sleeve.php>.

Presser, M & Geiss, PL 2011, 'Experimental investigation of the influence of residual stress due to curing shrinkage on the interphase formation in adhesively bonded joints', *Procedia Engineering*, vol. 10, no. 0, pp. 2743-8.

Prolongo, SG, del Rosario, G & Ureña, A 2006, 'Comparative study on the adhesive properties of different epoxy resins', *Int. J. Adhes. Adhes.*, vol. 26, no. 3, pp. 125-32.

Ray, BC 2006, 'Temperature effect during humid ageing on interfaces of glass and carbon fibres reinforced epoxy composites', *Journal of Colloid and Interface Science*, vol. 298, pp. 111-7.

Ruiz, E & Trochu, F 2005, 'Numerical analysis of cure temperature and internal stresses in thin and thick RTM parts', *Composites Part A: Applied Science and Manufacturing*, vol. 36, no. 6, pp. 806-26.

Saeed, N, Ronagh, HR, Virk, A & Ashraf, M 2012, 'Investigating the effects of pipe live pressure on the design of composite overwrap repairs', paper presented to Australasian Structural Engineering Conference, 11-13 July, Perth.

Sala, G 2000, 'Composite degradation due to fluid absorption', *Composites Part B: Engineering*, vol. 31, no. 5, pp. 357-73.

Schoch Jr, KF, Panackal, PA & Frank, PP 2004, 'Real-time measurement of resin shrinkage during cure', *Thermochimica Acta*, vol. 417, no. 1, pp. 115-8.

Sciolti, M, Frigione, M & Aiello, M 2010, 'Wet Lay-Up Manufactured FRPs for Concrete and Masonry Repair: Influence of Water on the Properties of Composites and on Their Epoxy Components', *Journal of Composites for Construction*, vol. 14, no. 6, pp. 823-33.

Seica, VM & Packer, AJ 2007, 'FRP materials for the rehabilitation of tubular steel structures, for underwater applications', *Comp Struct*, vol. 80, pp. 440-50.

Sen, R & Mullins, G 2007, 'Application of FRP composites for underwater piles repair', *Comp: Part B*, vol. 38, pp. 751-8.

Shah, DU & Schubel, PJ 2010, 'Evaluation of cure shrinkage measurement techniques for thermosetting resins', *Polymer Testing*, vol. 29, no. 6, pp. 629-39.

Shamsuddoha, M, Islam, MM, Aravinthan, T, Manalo, A & Lau, KT 2013, 'Effectiveness of using fibre-reinforced polymer composites for underwater steel pipeline repairs', *Composite Structures*, vol. 100, no. June, pp. 40-54.

Shouman, A & Taheri, F 2011, 'Compressive strain limits of composite repaired pipelines under combined loading states', *Composite Structures*, vol. 93, no. 6, pp. 1538-48.

Sirimanna, CS, Islam, MM & Aravinthan, T 2010, 'Preliminary development of polymer based filler materials for GFRP tubular connector', paper presented to Incorporating Sustainable Practice in Mechanics of Structures and Materials (ACMSM 21), 7-10 Dec, Melbourne, Australia.

Sirimanna, CS, Islam, MM & Aravinthan, T 2011, 'Polymer Based Filler Materials as Infill for GFRP Pile Connector', *Key Engineering Materials*, vol. 471-472, pp. 763-8.

Sirimanna, CS, Lokuge, W, Islam, MM & Aravinthan, T 2012, 'Compressive strength characterization of polyester based fillers', *Advanced Materials Research*, vol. 410, pp. 32-5.

Siviour, CR, Walley, SM, Proud, WG & Field, JE 2005, 'The high strain rate compressive behaviour of polycarbonate and polyvinylidene difluoride', *Polymer*, vol. 46, no. 26, pp. 12546-55.

Sleeper, B, Arnold, S, Carr, H & Pridmore, A 2010, 'Carbon Fiber Reinforced Polymer (CFRP) As a Long Term Repair Solution', in *Pipelines*, pp. 1133-42.

Smith, GE 2005, 'Bond characteristics and qualifications of adhesives for marine applications and steel pipe repair [MSc Thesis]', North Carolina State University.

Springer, GS 1981, *Environmental effects on composite materials*, vol. 1, Technomic Pubnishing Company, Lancaster (PA).

Strand7 Pty Limited 2005, *Strand7 Software: Finite element analysis system*, Strand7 Pty Limited, Sydney, Australia.

Strong, AB 2008, *Fundamentals Of Composites Manufacturing: Materials, Methods and Applications* Society of Manufacturing Engineers, Michigan.

Sum, WS & Leong, KH 2012, 'Parametric finite element study of grouted composite sleeves for pipeline repairs', paper presented to 8th Asian-Australasian Conference on Composite Materials (ACCM-8), 6-8 November, Kuala Lumpur, Malaysia.

Sum, WS & Leong, KH 2013, 'Numerical study of annular flaws/defects affecting the integrity of grouted composite sleeve repairs on pipelines', *Journal of Reinforced Plastics and Composites*,

Suwanprateeb, J 2000, 'Calcium carbonate filled polyethylene: correlation of hardness and yield stress', *Compos Part A: Appl S*, vol. 31, no. 4, pp. 353-9.

Szary, T 2006, 'The Finite Element Method Analysis for Assessing the Remaining Strength of Corroded Oil Field Casing and Tubing [PhD Thesis]', Geotechnik und Bergbau der Technischen Universität Bergakademie.

T. D. Williamson Inc 2007, *Steel Repair Sleeves*, 14-09-2012, <http://www.tdwilliamson.com/en/Products/RehabilitationProducts/SteelRepairSleeves/Documents/Steel%20Repair%20Sleeves.pdf>.

T. D. Williamson Inc. 2008, *RES-Q Composite Wrap*, Oklahoma, 14-09-2012, <http://www.tdwilliamson.com/en/Products/RehabilitationProducts/CompositeWrap/Documents/RESQ.pdf>.

Tanaka, K, Minoshima, K, Grela, W & Komai, K 2002, 'Characterization of the aramid/epoxy interfacial properties by means of pull-out test and influence of water absorption', *Composites Science and Technology*, vol. 62, no. 16, pp. 2169-77.

Tavakkolizadeh, M & Saadatmanesh, H 2001, 'Galvanic corrosion of carbon and steel in aggressive environments', *J of comp for constr*, vol. 5, no. 3, pp. 200-10.

Thandavamoorthy, TS, Madhava Rao, AG & Santhakumar, AR 2001, 'Development of a fly ash and epoxy based high-performance grout for the repair of offshore platforms', *ACI Special Publication*, vol. 199, no. SP199-14, pp. 239-58.

ASME 2006, Repair of pressure equipment and piping, The American Society of Mechanical Engineers, ASME PCC-2-2006, New York.

The Clock Spring Company 2011, *Clock Spring*, Houston, 14-09-2012, <http://www.clockspring.com/wp-content/uploads/2011/12/brochure1.pdf>.

Thompson's Welding Services, I *Surface preperation standards cross reference*, http://www.thompsonswelding.com, 11-10-2012, <http://www.thompsonswelding.com/useful_info/surface_prep_cross.pdf>.

Torabizadeh, MA & Fereidoon, A 2013, *Progressive Failure Analysis of Glass/Epoxy Composites at Low Temperatures*, Materials Science - Advanced Topics. <http://www.intechopen.com/books/materials-science-advanced-topics/progressive-failure-analysis-of-glass-epoxy-composites-at-low-temperatures>.

Toutanji, H & Dempsey, S 2001, 'Stress modelling of pipelines strengthened with advanced composites materials', *Thin-Walled Struct*, vol. 39, pp. 153-65.

Turvey, GJ & Wang, P 2007, 'Failure of pultruded GRP single-bolt tension joints under hot–wet conditions', *Composite Structures*, vol. 77, no. 4, pp. 514-20.

University of Southern Queensland *Pile rehabilitation*, 10-10-2012, <http://www.usq.edu.au/ceefc/research/past/project2>.

Vanlandingham, MR, Eduljee, RF & Gillespie, JW 1999, 'Moisture diffusion in epoxy systems', *Journal of Applied Polymer Science*, vol. 71, no. 5, pp. 787-98.

Vipulanandan, C & Paul, E 1990, 'Performance of epoxy and polyester polymer concrete', *ACI Mater. J.*, vol. 87, no. 3, pp. 241-51.

Vipulanandan, C & Paul, E 1993, 'Characterization of polyester polymer and polymer concrete', *J. Mater. Civ. Eng.*, vol. 5, no. 1, pp. 62-82.

Vu, D, Glennie, A & Booth, P 2011, 'Pipeline repairs and hot tapping technologies using epoxy based grouted technology', paper presented to 6th International Offshore Pipeline Forum (IOPF 2011), 19-20 October, Houston, Texas, USA.

Wang, X, Wang, C, Jia, Y, Luo, L & Li, P 2012, 'Cure-volume-temperature relationships of epoxy resin and graphite/epoxy composites', *Polymer*, vol. 53, no. 19, pp. 4152-6.

Wolfrum, J, Ehrenstein, G & Avondet, M 2000, 'Dynamical mechanical thermo analysis of high performance composites-influences and problems', *J. Compos. Mater.*, vol. 34, no. 21, pp. 1788-807.

Wonderly, C, Grenestedt, J, Fernlund, G & Cêpus, E 2005, 'Comparison of mechanical properties of glass fibre/vinyl ester and carbon fibre/vinyl ester composites', *Comp: Part B*, vol. 36, pp. 417-26.

Worth, F 2005, *Analysis of Aquawrap® for Use in Repairing Damaged Pipeline: Environmental Exposure Conditions, Property Testing Procedures, and Field Testing Evaluations*, Air Logistics Corporation, California, 14-09-2012, <http://pipingrepairtechnologies.com/wp-content/uploads/2009/04/analysis-of-aquawrap-for-use-in-repairing-damaged-pipelines.pdf>.

WrapMaster *WeldWrap*™, Texas, 14-09-2012, <http://www.wrapmaster.us/weldwrap%20brochure%2004.12.pdf>.

Yu, HN, Kim, SS, Hwang, IU & Lee, DG 2008, 'Application of natural fiber reinforced composites to trenchless rehabilitation of underground pipes', *Composite Structures*, vol. 86, no. 1–3, pp. 285-90.

Yu, Y, Ashcroft, IA & Swallowe, G 2006, 'An experimental investigation of residual stresses in an epoxy–steel laminate', *International Journal of Adhesion and Adhesives*, vol. 26, no. 7, pp. 511-9.

Zarrelli, M, Skordos, AA & Partridge, IK 2002, 'Investigation of cure induced shrinkage in unreinforced epoxy resin', *Plastics, Rubber and Composites Processing and Applications*, vol. 31, no. 9, pp. 377-84

Zhang, S, Karbhari, VM, Mai, L-Y & Mai, Y-W 2000, 'Evaluation of Property Retention in E-Glass/Vinylester Composites after Exposure to Salt Solution and Natural Weathering', *Journal of Reinforced Plastics and Composites*, vol. 19, no. 9, pp. 704-31.

Zhou, J & Lucas, JP 1999, 'Hygrothermal effects of epoxy resin. Part II: variations of glass transition temperature', *Polymer*, vol. 40, no. 20, pp. 5513-22.

Appendix A: Volumetric shrinkage investigation

Volumetric shrinkage test details

Pychnometer can be used to measure the volumetric shrinkage (Nawab et al. 2013). A Quantacrome Instruments Multipycnometer was used to measure the volume of the grouts. Freshly mixed grout was poured into a 75 cm^3 plastic containers. The container was filled with 73.5 cm^3 grout as a controlled volume. Density was then calculated from the controlled volume and weight. The shrinkages were calculated based on this initial density. The shrinkage quantification approach, expressed mathematically in Equation A.1 as suggested by ISO 3521 used to determine the shrinkage of the grout, where ρ_c is the density of grout for a certain time, and $\rho_o$is the initial density of grout (ISO 3521 1997). The test apparatus and test samples of the shrinkage tests are shown in Figure A. 1. A minimum of three samples of the grouts were tested. Measurements were taken to determine the curing performance over 1, 3, 7, 14 and 28 days. Volumetric shrinkage was also determined over a 24 hour period along with gel time for each of the grouts. The gel time was determined as per ASTM D2471 (1999).

$$\Delta V = \frac{\rho_c - \rho_o}{\rho_c} \qquad \text{(A. 1)}$$

Figure A. 1 Shrinkage test apparatus and grout samples

Overall volumetric shrinkage of grouts

Table A. 1 shows the key summary of the volumetric shrinkage along with gel times. The range of shrinkage found from the literature for epoxy resins is 2-7% (Khoun & Hubert 2010; Schoch Jr et al. 2004; Shah & Schubel 2010). Thus, good agreement is found for the obtained values. From the results, it is apparent that the early curing governs the rate of shrinkage in the grouts. Higher exotherm temperature was also observed for grout C. The total shrinkages over 28 days were found to be 2.77% and 1.09% for grout C and E, respectively. The dominant period contributing to the major shrinkage was found to be 1 day. About 96% and 83% of the 28 day shrinkage of grouts C and E, respectively, occurred within the first 24 hours of mixing, whereas about 98% and 92% of the 28 day shrinkage of grouts C and E, respectively, occurred within the first 7 days. The gel times for grout C and E found to be 105 and 165 minutes, respectively.

Table A. 1 Summary of the volumetric shrinkage

Grout	Gel time (min)	Duration				
		1-day	3-day	7-day	14-day	28-day
A	105	2.651 (0.337)	2.670 (0.250)	2.716 (0.361)	2.742 (0.238)	2.767 (0.268)
B	165	0.899 (0.479)	0.927 (0.490)	1.005 (0.452)	1.079 (0.444)	1.091 (0.443)

The Pycnometer is a high precision instrument and determines the volume using Boyle's Law, which assumes the temperature as a constant (Shah & Schubel 2010). Grout E exhibited a higher standard deviation than that of grout C. It is noted that during measurement the samples were still curing. Hence, the temperature can marginally affect the readings. Another reason for the difference between grouts C and E is that air bubbles that were entrapped in the high viscous paste during mixing in the case of grout E. The bubbles can cause deviation in the obtained volume of the grout from Pycnometer.

Post-gel shrinkage of grouts

Figure A. 2 shows the average shrinkage distribution over the 28 days periods. The gel time shrinkages are also shown as dotted lines. The results suggested that grout C experienced more shrinkage than that of grout E at the early stage of curing. After 24 hours of mixing, the average shrinkages that may contribute to post-gel stress in grout C and E are approximately 2.53% and 0.21%, respectively, whereas the 28 day post-gel shrinkages are about 2.65% and 0.41%, respectively. The shrinkage occurred fastest within the first 3 hours of mixing for both grouts. Although, gel time of grout C is lower than grout E, grout C experienced higher post-gel shrinkage than that of grout E. This implies that grout C undergoes shrinkage over a prolonged period compared to grout E.

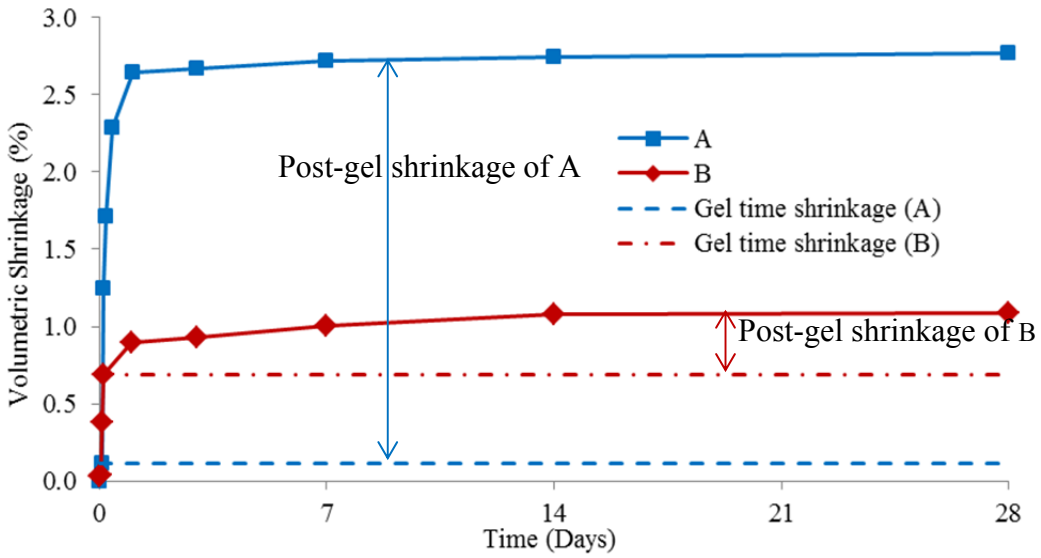

Figure A. 2 Volumetric shrinkage of grouts

Effect of filler on shrinkage properties

Inclusion of coarse filler in grout C system in the ratio of 1:1 by weight considerably reduces the volumetric shrinkage. This also results in prolonged gel time for grout E. It implies that grout C exhibits faster curing at the early stage of mixing. It is evident that filled system undergone less shrinkage. The 1 day

shrinkage of grout C is about 3 times higher than that without aggregate filler. This ratio between shrinkage of the two grouts is approximately maintained up to 28 days, where shrinkage of grout C is about 2.5 times higher than that of grout E. The reduced shrinkage of grout E compared to C is due to the inclusion of aggregate filler that occupied approximately 44% of its volume (50% by weight). By weight, approximately 37% of grout C is epoxy resin and hardener, which reduces to half when filler is added in the case of grout E. The inclusion of inert coarse filler along with reduction of total resin and hardener content has also resulted in reduction of shrinkable content in grout E. The post-gel shrinkage is also found to be higher in grout C than grout E. This also indicates that grout C goes under higher volumetric shrinkage even after gel time. The post-gel shrinkages of grout C and E reduce to about 96% and 37%, respectively, of their total 28 day shrinkages. Hence, the shrinkage is influenced by inclusion of filler and has considerable effect on the grout system.

Appendix B: Design charts of the grouted repair

Design limit

From the results of Section 7.3, it can be decided that the system can be assumed functioning as long as the infill layer is carrying out circumferential stress i.e. the grout has not cracked yet whether the steel has yielded or not. Figure 7.13 and Figure 7.14 demonstrate interrelation among pipe capacity, defect and sleeve thickness. It can also be seen that some of the level of stresses of the repaired section is higher than 26 MPa, which is the applied pressure to yield the undamaged pipe. A typical formulation of design chart of the repairs containing grout C is given in Figure B. 1. It is evident from the results that the repair capacity may go beyond 26 MPa. Hence, a limit is applied at 26 MPa in the design lines. The inflection point is identified from the intersection of the 26 MPa capacity line and the capacity-loss line. Finally, a design line is drawn as shown in Figure B. 1b. The point of inflection provides an indication of the level of corrosion below which a minimum level of reinforcement is required.

Design plots

Figure B. 2 and Figure B. 3 show design plots for the repaired pipe containing 20 mm thick grout C with carbon and glass sleeve, respectively. A typical demonstration of the data extraction is shown in the figure. For example: a 5 mm sleeve thickness is required to achieve a capacity of 23 MPa for a pipe with 60% metal loss. The charts suggest that it is feasible to achieve the full capacity of the pipe with metal loss less than 70% reinforced with a range of 5 – 25 mm composite sleeve. A pipe having less than 50% metal loss needs 5 mm thick sleeve to restore the full capacity of the pipe. An additional line defining the capacity of the pipe with defect is also shown in the design plots. The lines can be used to determine the amount of gain in the pressure capacity through applying a certain repair case on a pipe with defect.

The relationship also follows linear trend for repair cases with grout E. Figure B. 4 and Figure B. 5 show design plots for the repaired pipe containing 20 mm thick grout E with carbon and glass sleeve, respectively. These plots suggests that a pipe having less than about 20% metal loss needs minimum 5 mm thick sleeve to restore the full capacity of the pipe. Additionally, the charts suggest that sleeve thickness with grout E possesses insignificant contribution in the pipe capacity compared to the repair system containing grout C. It is to be noted that the repair capacity of the repaired pipe and the capacity of the pipe without any repair maintained a constant increment of about 5 MPa for 5 mm sleeve thickness. This is due to the fact that both these capacities are determined based on the yielding of the steel and cracking of the grout that occur within a small pressure variation.

This charts generated with a constant grout thickness of 20 mm which was adopted to effectively transfer the load in the repair system and due to application considerations. Any grout thickness less than 20 mm is expected to improve the repair capacity according to the results of Chapter 6. Hence, the design curves presented in this chapter are the most conservative ones and will shift towards the right increasing the repair efficiency.

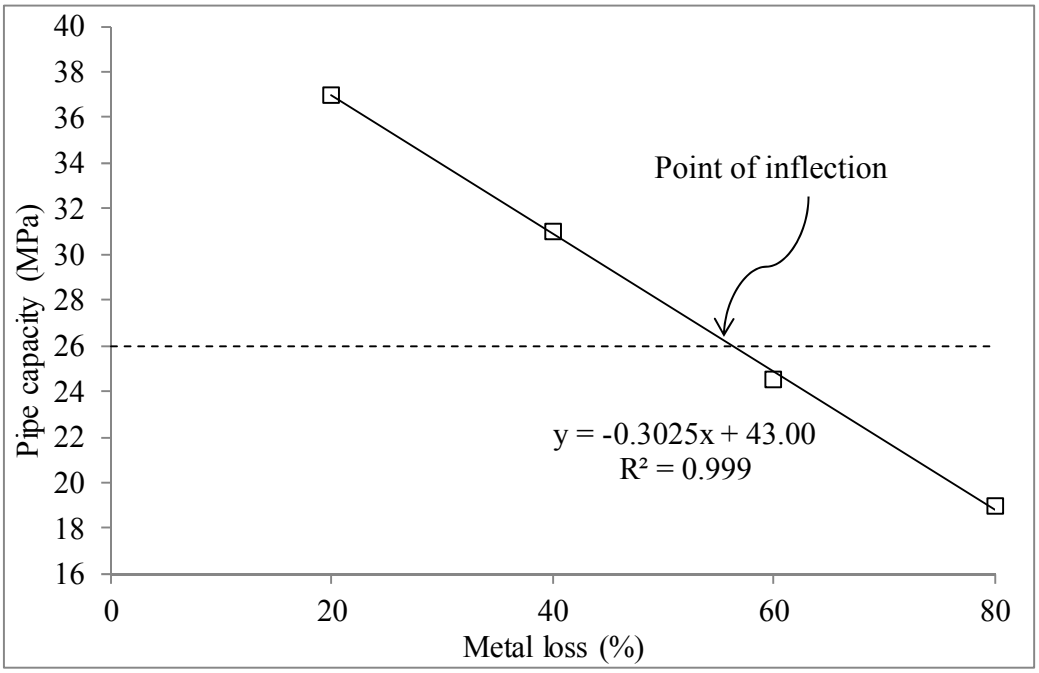

(a)

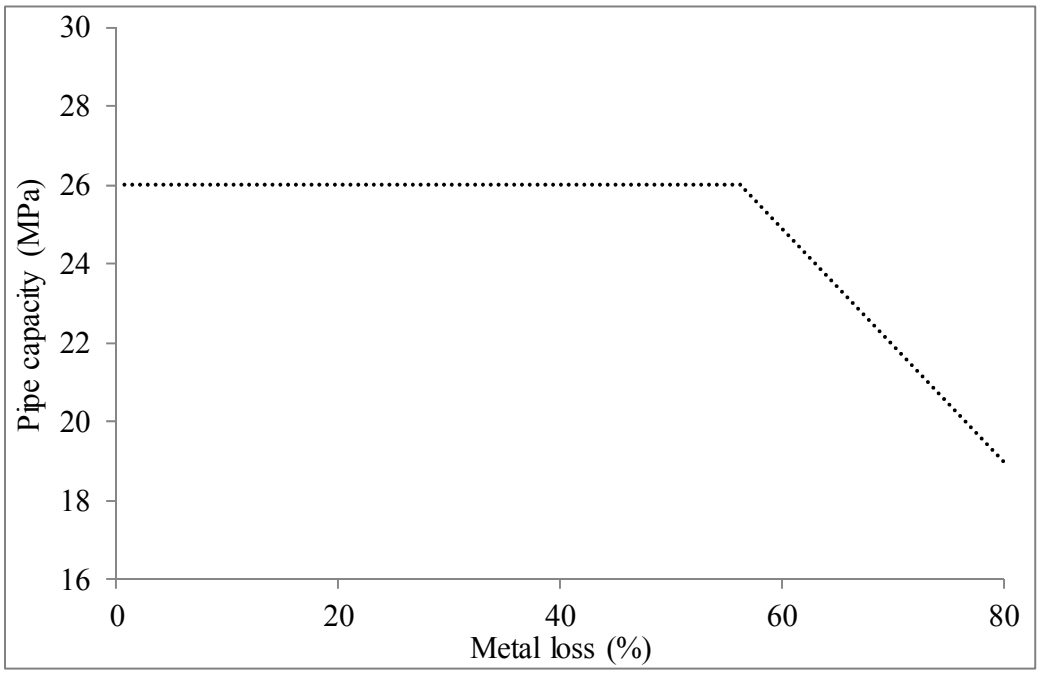

(b)

Figure B. 1 **Typical standardisation of design chart for repair case with 20 mm thick grout C and 10 mm thick carbon sleeve**

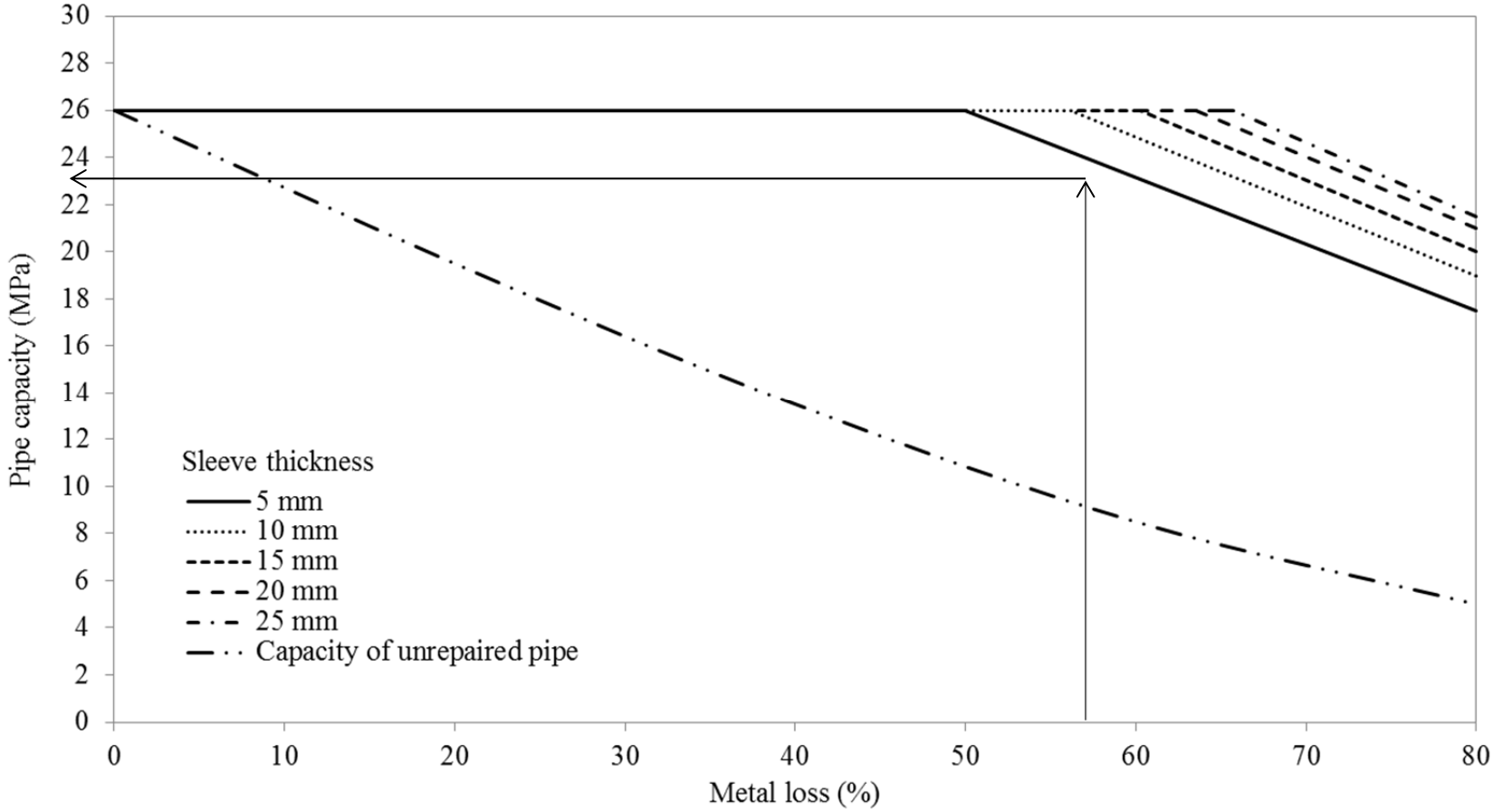

Figure B. 2 Design chart for grouted repair with 20 mm thick grout C and carbon sleeve

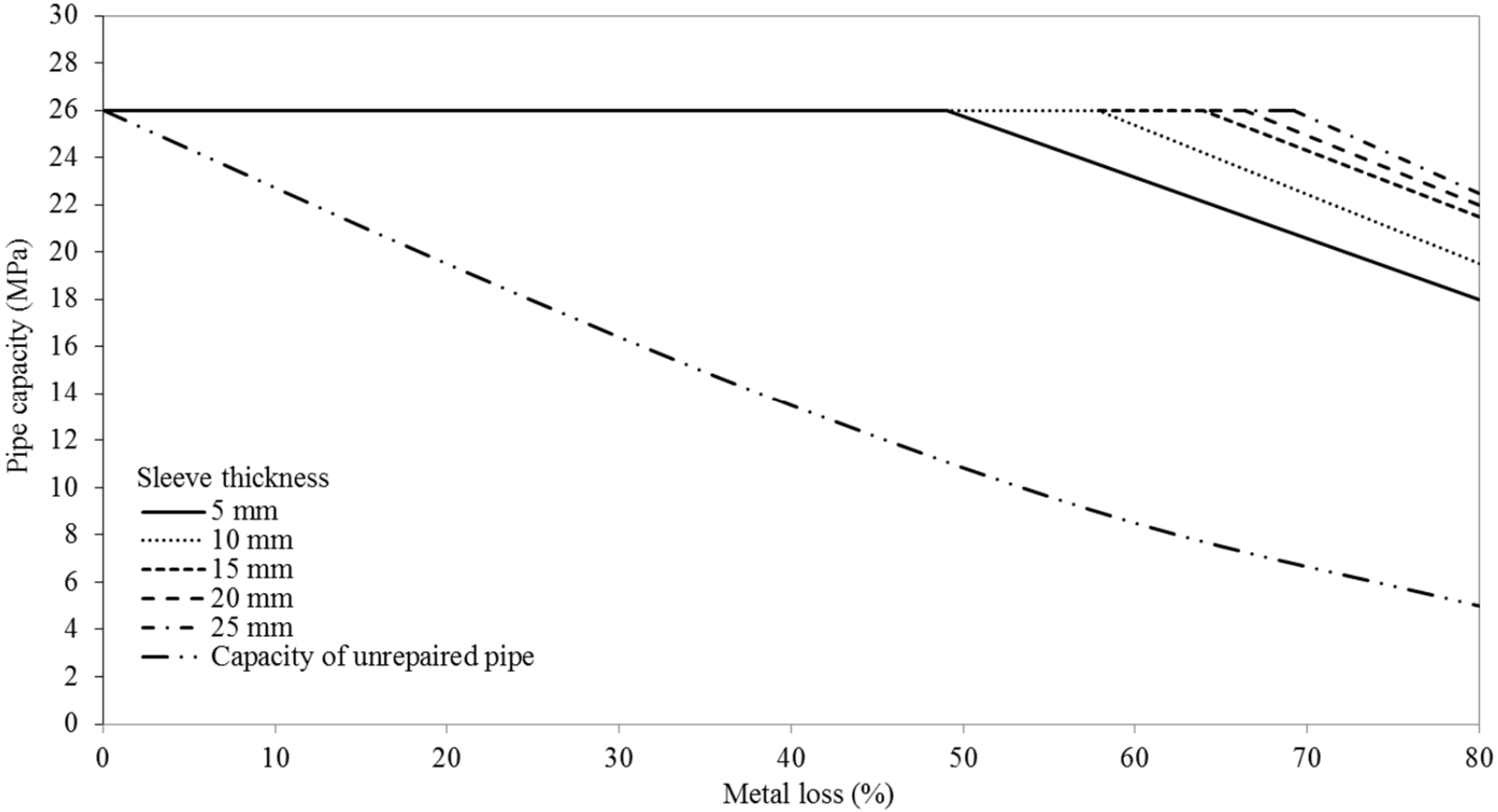

Figure B. 3 Design chart for grouted repair with 20 mm thick grout C and glass sleeve

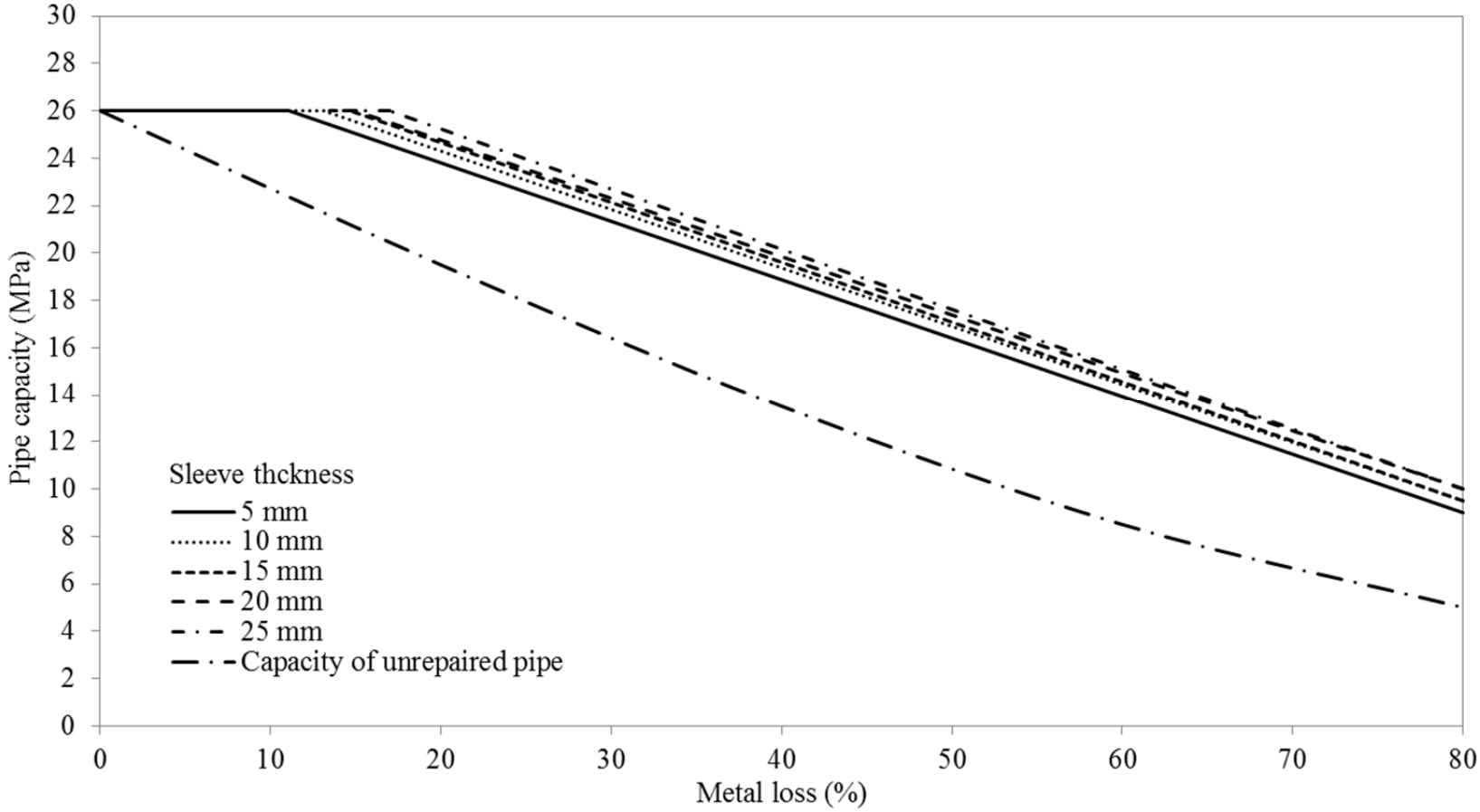

Figure B. 4 Design chart for grouted repair with geout E and carbon sleeve

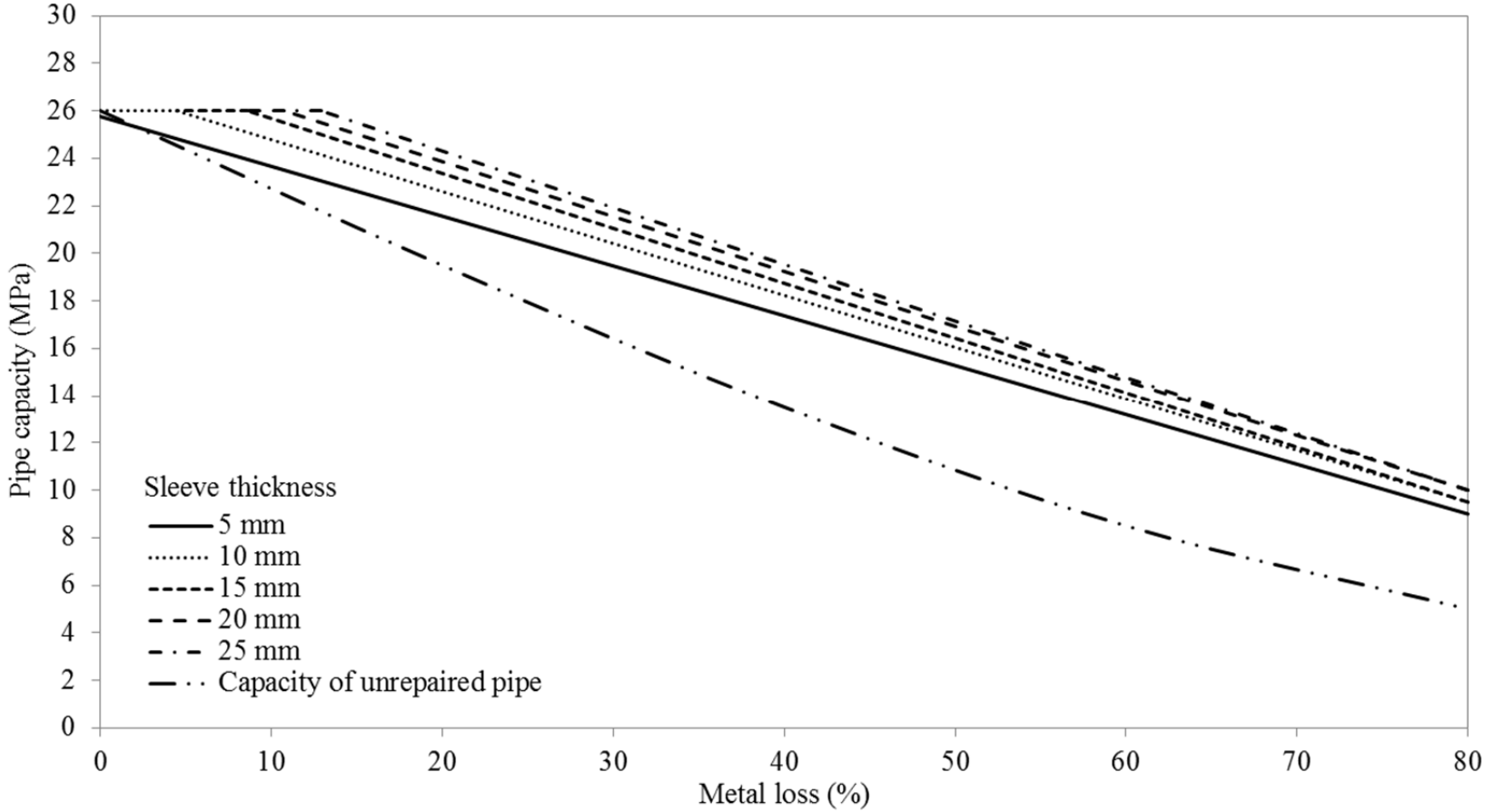

Figure B. 5 Design chart for grouted repair with geout E and glass sleeve